Air Charge Estimation in Turbocharged Spark Ignition Engines

Per Andersson

Department of Electrical Engineering
Linköping University, SE–581 83 Linköping, Sweden

Linköping 2005

Air Charge Estimation in Turbocharged Spark Ignition Engines

peran@isy.liu.se
http://www.fs.isy.liu.se/
Department of Electrical Engineering,
Linköping University,
SE–581 83 Linköping,
Sweden.

To Ulrika

Abstract

Turbocharged (TC) spark-ignited (SI) engines are popular as they combine high power output with good fuel economy. Furthermore, their emissions can be successfully reduced using a three way catalyst (TWC) provided that the air-fuel ratio is precisely controlled. As the air-fuel ratio depends on the precision of the air charge estimate, this thesis is devoted to the systematic improvement of the cylinder air charge (CAC) estimation on TC SI engines. A second objective is to provide the design engineer with a flexible framework for CAC estimation that easily can be adapted to various engines.

The CAC is not measurable and it is therefore estimated using a model. Part I concentrates on stationary conditions and examines existing air charge estimation methods using engine experiments where the wastegate is opened and closed. Measurements show that the existing methods are insufficient for TC SI engines since the CAC depends on exhaust backpressure and charge cooling from evaporating fuel. A new 2-parameter CAC model which accounts for these effects is developed and the validation shows that the error is reduced from 10% to 3%.

Part II deals with transient conditions and a dynamical component-based model is developed for the gas flow systems of TC SI engines. The physical structure of different TC SI engines is similar and these similarities are exploited in the developed model. The division into components provides the basis for a flexible framework that enables a straightforward adaption to various engines. It is described how the model parameters are systematically fitted using an engine map and maps from the turbocharger manufacturer. The accuracy of the model is good and the stationary error is less than 10% on the intake side.

An observer that estimates the CAC, given available measurements, is suggested. It is shown that the system is locally structurally observable from arbitrarily measured model states. Further, a specific combination of signals that is most suitable for CAC estimation is pointed out. The developed observer is based on the constant gain extended Kalman filter (CGEKF) and a systematic method for selecting the design parameters in CGEKF filters is proposed. The method only requires an engine map and the variance of the signals considered for observer feedback. Several different combinations of observer feedback signals are studied and it is shown that the observer is capable of estimating the model states. The design method is successfully tested on two different engines.

Finally, the developed model and observer is used for model-based air-fuel ratio control. A TC SI engine is controlled by the proposed controller in real-time and the transient deviations from $\lambda = 1$ are less than 7% in very rapid throttle transients.

ii

Acknowledgments

This work has been performed at Vehicular Systems and I am very grateful to professor Lars Nielsen for letting me join his excellent group and for all the support, discussions, and encouragement he has provided during this work.

First I would like to thank my supervisor Dr. Lars "Lasse" Eriksson, who is greatly acknowledged for guiding me into the research field of mean value models and for all careful proofreadings of research papers and this thesis. Thank you Lasse for your patient guidance and encouragement during the project! Then, I thank Dr. Erik Frisk for his help with LaTeX and Emacs and for the interesting discussions and proofreadings especially around the structural analysis, and observer design chapters. Marcus Klein and Ylva Nilsson were kind to proofread early versions of the manuscript.

This work would not have been possible without all the help from our research engineers over the years Andrej Perkovic, Jan Brugård, Mats Karlsson, and Martin Gunnarsson who take good care of our research laboratory. Erik Sunnegårdh, Per Öberg, and Christer Rosenquist are also acknowledged as they all have contributed in the development of our successful real-time control environment. I thank Kristin Wiberg and Carolina Fröberg as they made sure that the administrative work always went smoothly. The staff of Vehicular Systems is also acknowledged for creating a nice research atmosphere and amusing coffee breaks.

I also thank GM-POWERTRAIN SWEDEN AB and MECEL AB for showing great interest, for the hardware supply, and support during the project. The Swedish Agency for Innovation Systems (VINNOVA) is acknowledged for their support through the center of excellence ISIS (Information Systems for Industrial Control and Supervision).

Finally I thank my mother Karin, father Ragnar, and my brother Ulf for their support and encouragement.

Linköping, November 2005

Per Andersson

iv

CONTENTS

x

1

INTRODUCTION

Today, everyone want cars that are less harmful to the environment and have better fuel economy. As a small engine use less fuel, it is easy to save fuel by making the engine smaller. However, a small engine does not meet the power expectation of the driver during e.g. overtakings. The maximum power of the engine depends on the amount of fuel it can burn and this in turn depends on the availability of air. Thus, more air is necessary to increase the engine power. One way to increase the air to the engine is to add a turbocharger (TC) that simply raise the pressure of the air. Hence, it is possible to combine the fuel economy of the small engine with the maximum power of a bigger engine and this concept is called downsizing supercharging (Guzzella et al., 2000).

Here spark ignition (SI) engines are considered as the emissions of carbon monoxide (CO), hydro-carbons (HC), and nitrogen oxide (NO_x) can be successfully reduced using a three way catalyst (TWC). Thus, downsized and supercharged SI engines is a promising concept that gains a lot of attention in Europe. For the TWC to be efficient it is necessary to accurately control the ratio of air and fuel. The air-fuel ratio is the ratio of air-mass and fuel-mass in the cylinder when the valves are closed. The mass of air inside the cylinder, the cylinder air charge (CAC), is influenced by the driver pressing the accelerator. The fuel is injected by electronically controlled valves, so called injectors, that are located close to the intake valve. An electronic control unit (ECU) determines the mass of fuel to inject by first estimating the expected CAC. Hence, a *key component* for precise air-fuel ratio control and thus lower emissions is *precise cylinder air-charge estimates*. Improving the CAC estimates is not an easy task and therefore the topic of this thesis.

Emission Limits
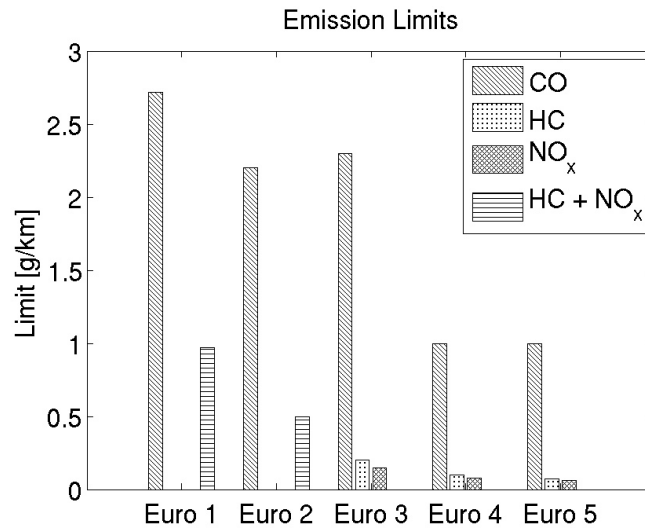
Figure 1.1: The maximum allowed emissions for gasoline powered passenger cars in Europe. From EURO-1 (1992) to EURO-5 (proposed, 2008) the maximum allowed emissions have been more than halved, which requires more accurate engine control systems. Note that for Euro 1 and Euro 2, the limit is on the sum of the HC and NO_x, while there are separate limits for HC and NO_x from Euro 3 and on .

1.1   Precise Air-Fuel Ratio Control is Necessary

Over the last decade the maximum allowed emissions have been halved, see Figure 1.1, and future legislation will require even lower emissions. Below the introduction years of the European emission legislations are summarized.

Emission Standard	Introduction
Euro 1	1992
Euro 2	1996
Euro 3	2000
Euro 4	2005
Euro 5	Proposition to 2008

To reach these low emissions, a three way catalyst (TWC) is used. Since the TWC is only highly efficient in a narrow air-fuel ratio band, as shown in Figure 1.2, accurate air-fuel ratio control is necessary. In Figure 1.2 the TWC efficiency is shown as a function of normalized air-fuel ratio λ. When there is just enough air to fully oxidize all of the fuel λ is equal to one. If the mixture is rich $\lambda < 1$, there are excess fuel and carbon monoxide is formed since there is not enough oxygen to fully oxidize the fuel to carbon dioxide. On the other side, for lean mixtures $\lambda > 1$, undesirable nitrogen oxides are instead formed. Therefore, accurate air-fuel ratio control is essential (Heywood, 1988; Bauer et al., 1996; Kiencke and Nielsen, 2000; Mondt, 2000).
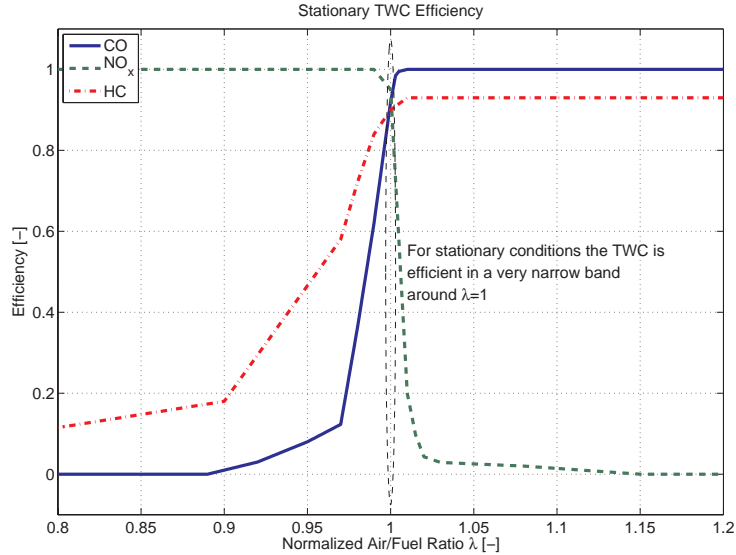
Figure 1.2: The TWC conversion efficiency for stationary λ. *Top*: The conversion efficiency is high only in a very narrow band around $\lambda = 1$. Especially the NO_x conversion efficiency drops rapidly for lean conditions.

1.2 Air-Fuel Ratio Control Challenges

To reach the required precision of the air-fuel ratio there are several design challenges to overcome and here two important topics are highlighted.

1.2.1 Feedback and Feedforward Control is Necessary

It is impossible to accomplish the necessary accuracy of the air-fuel ratio using an open-loop controller as for example the fuel composition changes over time. Feedback from a measured air-fuel ratio is therefore used to achieve the necessary accuracy for stationary conditions. As the sensor is located in the exhaust system, there is a non-negligible time delay between injector (actuator) and sensor. Long time delays result in low bandwidth of the feedback controller (Chevalier et al., 2000) and therefore a predicting feedforward component is necessary for transient control. An important component is the design of the feedforward component, which includes modeling of the air-system on TC SI-engines.

1.2.2 Desired Properties: Low Cost and Fast Calibration

The automotive industry is very cost sensitive and a short time to market is essential. As the physical structure of different TC SI engines is similar, considerable time can be saved if these similarities could be better exploited

already during the design phase. Thus, it is important to develop methods that
can help the design engineer to cut the development time.

1.3   Problem Formulation and Solution Outline

The studied problem is to improve the air-fuel ratio control by improving the
CAC estimates. A second objective is to provide the design engineer with a
flexible framework for control and diagnosis system design that easily can be
adopted to various engines. The proposed solution is a control and diagnosis
oriented model of TC SI engines' air-system with the primary focus on cylinder
air charge estimation for air-fuel ratio control. To better understand how to
estimate the CAC one must first gather knowledge of the air system on tur-
bocharged SI-engines. This is done for stationary conditions in Part I, and then
for transient conditions in Part II.

Part I starts by examining existing air charge estimation methods using
engine experiments where the wastegate is opened and closed. In Chapter 3
measurements show that the existing methods do not give correct CAC esti-
mates since the CAC depends on the exhaust backpressure. A CAC model
with explicit exhaust pressure dependency is therefore developed in Chapter 4.
Furthermore, the CAC is influenced by the air-fuel ratio for rich conditions at
high loads. A charge density increase caused by the evaporating fuel at rich
mixtures is thus included in the developed CAC model.

Part II deals with transient conditions and a component based mean value
model of the air-system is developed in Chapter 6. As the proposed CAC model
depends on several states in the engine model, it is necessary to estimate the
model's state using an observer. When an observer is developed two questions
arise: First, is the system observable and second what measured signals should
be used for observer feedback. In Chapter 7 these questions are answered and
applied in Chapter 8, where the observer feedback gains are systematically
designed using extended Kalman theory.

The final step is to show the accuracy of the developed model and observer
by applying it for model-based control. Using the model, an air-fuel ratio con-
troller is developed in Chapter 9. The accuracy of the model and observer is
shown in Figure 1.3 as the resulting controller is able to maintain stoichiometric
conditions during a rapid throttle transient.

1.4   List Of Publications

This thesis is based on the following publications:

- Per Andersson and Lars Eriksson. Air-to-Cylinder Observer on a Tur-
  bocharged SI-Engine with Wastegate. In *Electronic Engine Controls*, SP-
  1585, pages 33–40. SAE 2001 World Congress, March 2001, Detroit, MI,
  USA, March 2001. SAE Technical Paper No. 2001-01-0262.
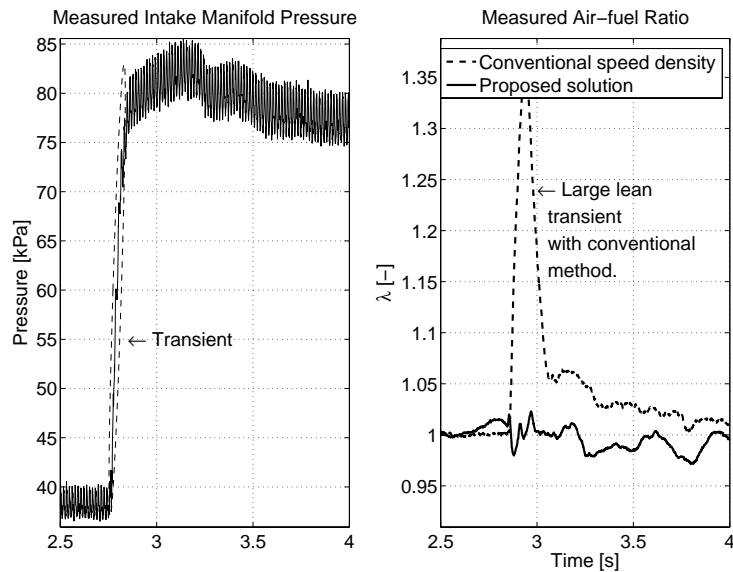
Figure 1.3: Measured air-fuel ratio at constant engine speed using a rapid step in throttle where the CAC more than doubles. Two different controllers are used, one conventional and the suggested controller from Chapter 9. Using the proposed model-based controller the deviations from $\lambda = 1$ are negligible.

- Per Andersson and Lars Eriksson. Cylinder Air Charge Estimator in Turbocharged SI-Engines. Society of Automotive Engineers, 2004. SAE Technical Paper No. 2004-01-1366.

- Per Andersson and Lars Eriksson. Exhaust Manifold Pressure Estimation on a turbocharged SI-engine with Wastegate. In *IFAC Workshop - Advances in Automotive Control; Karlsruhe, Germany*, pages 395–400, March 2001.

- Lars Eriksson, Lars Nielsen, Jan Brugård, Johan Bergström, Fredrik Pettersson, and Per Andersson. Modeling of a Turbocharged SI Engine. *Annual Reviews in Control*, 26(1):129–137, October 2002.

- Per Andersson. A Component Based Mean Value Engine Model of a Turbocharged SI-Engine. Technical report, Vehicular Systems, Department of Electrical Engineering, Linköpings Universitet, 2005.

- Per Andersson, Erik Frisk, and Lars Eriksson. Sensor Selection for Observer Feedback in Turbocharged Spark Ignited Engines. Prague, 2005. IFAC Wold Congress.

- Per Andersson and Lars Eriksson. Mean-value Observer for a Turbocharged SI-Engine. IFAC Symposium on Advances in Automotive Control, pages

146–151, Salerno, Italy, 2004a.

- Per Andersson and Lars Eriksson. Observer Based Feedforward Air-Fuel Control of Turbocharged SI-Engines. Prague, 2005. IFAC Wold Congress.

1.5   Contributions

Chapter 3 It is shown using measurements that the volumetric efficiency can change up to 5% when the wastegate is opened on a TC SI engine. An observer is proposed and deals with the varying volumetric efficiency that estimates stationary correct CAC for different wastegate settings.

Chapter 4 A CAC model for TC SI engines is proposed which captures the varying exhaust back pressure. Using the model, it is shown that the CAC is most sensitive to exhaust backpressure changes at part load. The model also includes the charge cooling effect during during fuel enrichment, which reduce the CAC error from 10% down to only 3%.

Chapter 5 A new exhaust manifold pressure estimation method for TC SI engines is developed that only uses sensors on the intake side. The method is able to describe the exhaust manifold pressure changes even when the wastegate setting is changed.

Chapter 6 A component based mean value engine model for a turbocharged SI-engine is developed and it is described how the model parameters can be systematically determined. The throttle flow equation is improved for a better fit to measured data, by showing that the discharge coefficient can be split into two factors: one that depends on the throttle area and one that depends on the pressure ratio over the throttle.

Chapter 7 It is shown that the mean value engine model from Chapter 6 is locally structurally observable using feedback from an arbitrarily measured state. It is also shown that when 3 feedback signals are used then there are only 6 out of 680 combinations that best observe the necessary states for cylinder air charge estimation.

Chapter 8 A systematic and automatic method is proposed for TC SI engine observer design based on the model in Chapter 6. Design examples show how the observer estimates states necessary for CAC estimation.

Chapter 9 A model based prediction feedforward air-fuel controller is proposed that is tested using rapid tip-ins where the air-fuel ratio error is less than 7%. The small error shows the accuracy of the mean value model, CAC-model, and designed observer.

2

BACKGROUND

This chapter has several objectives: Motivate why the focus is on air charge estimation, describe the additional air estimation challenges on turbocharged (TC) engines, and introduce common air-estimation methods. Last, this work is placed among others in a selection of recent related research.

2.1 Why Focus on Air Estimation?

Knowledge of both air-mass and fuel-mass in the cylinder are required to determine the air-fuel ratio[1]. It would be easy to control the air-fuel ratio if the port air-mass flow and the port fuel-mass flow were measurable for stationary conditions, but in a real application they are not. It is only possible to measure the air-mass flow at a location some distance away from the port, which makes the port air-mass flow indirectly measurable. Since there are considerable non-linear dynamics between actuators and sensors on the engine, transient air and fuel estimation are difficult tasks.

In this thesis the focus is given to air estimation for the following reasons:

Additional air estimation challenges on TC-engines For naturally aspirated engines the air path has been a thoroughly studied topic. Additional research on the air system of TC SI-engines is motivated by their more complex intake system. Further, there are couplings between the intake and exhaust side that influence the cylinder air charge. For more details see Section 2.1.1 and Section 2.4.2.

---

[1]For a detailed description of the air-fuel ratio definition, please consult Appendix B.

Necessity of CAC prediction In Section 2.1.2 it is motivated why port in-
jected SI engines require CAC prediction and since the air system on TC
engines is more complex it is harder to achieve CAC prediction compared
to NA-engines.

Diagnosis of sensors and leaks The emission legislations require that all
emission related components should be monitored (OBD, 1993). When
the air and fuel system is studied on a turbocharged production engine it
is clear, that most sensors are located on the intake side. To detect errors,
diagnosis methods based on mean value models have been shown very ef-
fective, see e.g. Weeks and Moskwa (1994); Nyberg (1999). This further
motivates research on the intake system of turbocharged SI-engines.

In the intake manifold there is also fuel dynamics present. However, as the fuel
dynamics on a port injected engine is similar regardless of whether the engine
has a turbocharger or not; thus it is natural to focus on the air path where
there are differences. In addition, it has been argued that the air-dynamics has
a more significant influence on the air-fuel ratio than the fuel dynamics (Powell
et al., 1998b).

2.1.1   Couplings Between Intake and Exhaust Side

On TC engines there is a device called wastegate (Watson and Janota, 1982;
Heisler, 1997), which is located in the turbocharger, on the exhaust side, with
the purpose to control the power to the turbine. It has been shown that the
engine efficiency increases when the wastegate is opened at part load as the
engine pumping losses are reduced (Eriksson et al., 2002a). Therefore, it is
desirable to use active wastegate control to improve fuel economy. A side ef-
fect of opening the wastegate is that the exhaust backpressure drops and this
influences the inducted CAC (Andersson and Eriksson, 2001), which is further
described in Section 2.4.2. Additionally the intake side and the exhaust side of
the engine are coupled through the turbine shaft. These two couplings make
CAC estimation on TC engines a complex task.

2.1.2   The Necessity of CAC Prediction

The amount of air in the cylinder depends among others on the throttle plate
angle which in turn is influenced by the driver's pedal position; and for the ECU
it then remains to determine the mass of fuel to inject. The mass of fuel to inject
depends on the inducted cylinder air charge (CAC) at intake valve closing (IVC).
Here port injected engines are considered which means that the fuel is injected
in the intake manifold close to the intake valve. To reduce the emissions of
hydrocarbons and carbon monoxide on port injected engines the injection has
to be finished around intake valve opening, see e.g. Bouza and Caserta (2003).
This means that the fuel is injected before the induction stroke starts and thus
the CAC at IVC is only known for stationary conditions. However for the ECU
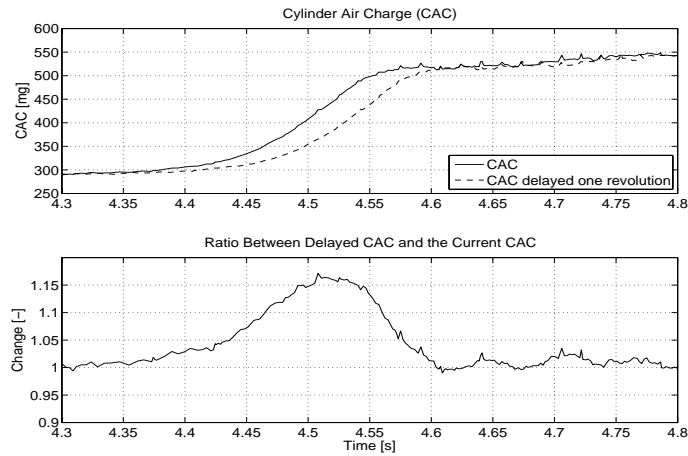
Figure 2.1: In this measured throttle step (tip-in) at a constant engine speed of 1800 RPM the CAC (solid) is compared to the same CAC delayed one revolution. The deviation from one is the resulting air-fuel ratio error if no prediction is used when the fuel-mass is determined. Without prediction, there would be a 15% error in λ in this case!

the important quantity is the CAC at intake valve closing. This means that there is an inherent delay that is constituted by the computation time, the injection time, and the duration of the intake stroke. Typically this delay is around one revolution.

During transients this time-delay becomes an issue and it is necessary to predict the CAC. Here an example is used to show that the lack of prediction results in large errors already for small throttle steps. To estimate the expected air-fuel ratio error due to the delay, the CAC is compared to a one revolution delayed CAC. The expected error in air-fuel ratio, if no prediction is used, is the deviation from one in the calculated ratio. In this example, the expected error is 15%, shown in Figure 2.1, but considerably larger errors occur for faster transients or at lower engine speeds where longer prediction times are necessary.

2.2   Air Charge Estimation Methods

The air estimation problem is a well studied topic, especially for naturally aspirated engines. In the following sections, a brief summary of two common methods are given:

- Cylinder air charge can be estimated using an air-mass flow sensor and divide the measurement by the engine speed. This strategy is particular suitable for naturally aspirated engines with central fuel injection where the fuel is injected at the throttle (Aquino, 1981).

- Speed-density methods, where mainly intake manifold pressure and engine

speed is used to determine cylinder air charge. On port injected engines this method estimates air-mass at the same location as the fuel injectors are located, which improves the accuracy of the air-fuel ratio.

Next, these air estimation principles are described with emphasis on the conditions in port-injected TC-engines, and in Section 2.5 it is motivated why speed-density methods are preferred. For a description of symbols and abbreviations, please consult the nomenclature in Appendix A.

2.3 Measured Air-Mass Flow Principle

The air-mass flow sensor, W_a, is typically located close to the air filter and thus far from the cylinders. Consequently, there is a large volume consisting of hoses, intercooler, and intake manifold separating the air-mass flow sensor from the cylinders. The volumes introduce a non-negligible filling and emptying dynamics, which means that the mass-flow measured by the sensor at the entrance of the volume will not be the same as the exiting mass-flow at the cylinders. The effect is illustrated by the following simulation, using the model developed in Chapter 6, where there is a step in throttle angle while the engine speed is constant. The result is shown in Figure 2.2 where the bottom plot shows that the difference between air-mass flow at the throttle and at the port is 30%. The resulting error in the air-fuel ratio would thus be 30%, if the measured air-mass flow is used to calculate the mass of fuel to inject.

Normally a change in the air-mass flow to the engine is caused by a change in throttle plate angle or engine speed, but a change in air-mass flow can also be caused by a change in wastegate opening. This is illustrated later in Figure 2.5.

As there are large transient errors when this method is used for CAC estimation on port injected engines, various transient compensations have been proposed. For naturally aspirated engines, improvements have been shown by inverting the mass flow sensor dynamics and the filling/emptying dynamics in the intake manifold (Grizzle et al., 1994). On TC engines it is harder to form the transfer function between the sensor and the cylinder, as there are more components that exhibit dynamics. Inversion of the air-mass flow sensor dynamics is further complicated as it has been argued that it exhibits different dynamics depending on the air-mass flow step size and direction (Hendricks et al., 1994).

2.4 Speed-Density Principles

When the measured air-mass flow was used the estimated CAC was deteriorated by the dynamics in the volumes between the air-mass flow sensor and the cylinder. Fortunately, this is not a problem for speed-density methods. These rely only on sensors in the intake manifold, namely the intake manifold pressure and temperature. Using those sensors together with the engine speed and the
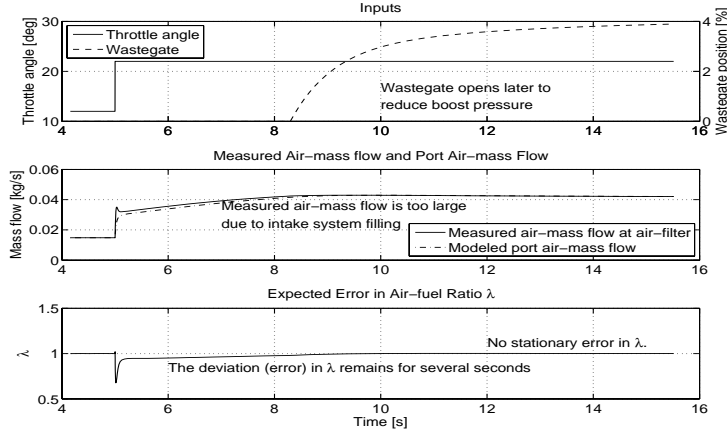
Figure 2.2: Simulated step response in throttle at a constant speed of 2000 RPM. *Top:* Throttle is opened at 5 seconds and the wastegate opens slightly a few seconds later. *Center:* Air-mass flow measured at the throttle compared to the port air-mass flow. During the transient, the air-filter mass-flow is considerably larger due to the intake system filling. *Bottom:* The ratio between the air-flow at the air-filter and at the port. If this measured air-mass flow would be used to determine injected fuel-mass, the error in λ would be 30% and the error remains at a high level for several seconds.

volumetric efficiency, the cylinder air charge is estimated as:

$$\text{CAC} = \eta_{\text{vol}}(N, p_{\text{im}}) \frac{p_{\text{im}} V_d}{R_{\text{im}} T_{\text{im}}} \tag{2.1}$$

Thus, speed-density methods are independent of the filling/emptying dynamics between the sensor and the cylinder.

The parameter volumetric efficiency, η_{vol} in Eq. (2.1), is calculated from stationary measurements using the fact that the stationary port-air mass flow is equal to the measured air-mass flow W_{a}. The port air-mass flow is determined as the product of CAC and the engine speed:

$$W_{\text{cyl}} = \text{CAC} \frac{N}{n_r} \tag{2.2}$$

For stationary conditions $W_{\text{a}} = W_{\text{cyl}}$ and solving for η_{vol} results in:

$$\eta_{\text{vol}} = \frac{W_{\text{a}} R_{\text{im}} T_{\text{im}} n_r}{p_{\text{im}} V_d N} \tag{2.3}$$

Given the stationary volumetric efficiency, a standard method to represent it is a two-dimensional map in engine speed and intake manifold pressure. Another common method is to fit a polynomial in engine speed and intake manifold pressure to the volumetric efficiency (Servati and DeLosh, 1986; Hendricks and Sorensen, 1990) e.g. :

$$\eta_{\text{vol}} = a_0 + a_1 N + a_2 N^2 + a_3 p_{\text{im}} \tag{2.4}$$

2.4.1   Filtering and Sensor Dynamics

Speed-density methods rely mainly on intake-manifold pressure, engine speed, and intake manifold temperature. When speed-density methods are used, there are two challenges that are illustrated using an engine experiment. The experiment is a rapid tip-in at constant engine speed where the measured intake manifold pressure and temperature are shown in Figure 2.3. The two challenges are:

- Filtering of the intake manifold pressure is necessary since it is subjected to noise and this propagates directly to the CAC estimate through Eq. (2.1). Unfortunately, the introduction of a filter results in a pressure phase lag, which is undesirable in speed density methods. In the example, the phase lag causes an error of more than 5% during the transient.

- Temperature sensors are too slow to capture the fast temperature dynamics during rapid throttle changes (Chevalier et al., 2000). If the measured temperature in Figure 2.3 is used in a speed-density method it would result in a 5% CAC error during the transient.
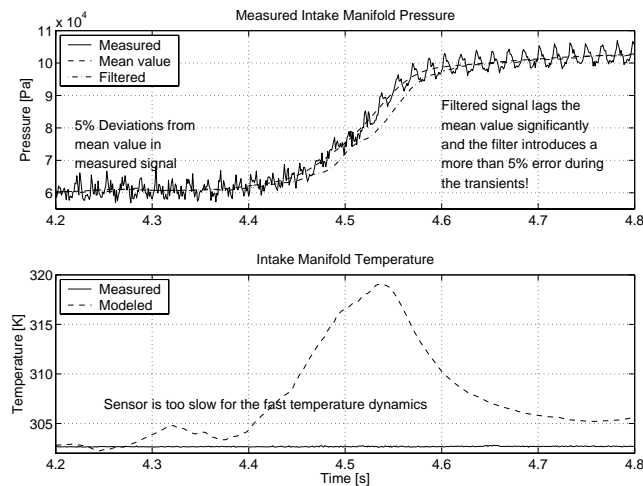
Figure 2.3: Rapid tip-in at a constant speed of 1800 RPM. *Top:* Measured intake manifold pressure is subjected to noise caused by engine pumping and electronics. When the noise is attenuated using a filter, the filtered signal lags the mean-value significantly. *Bottom:* Measured and modeled intake manifold temperature during the transient. As the sensor has a time constant of approximately 20 seconds, it misses the fast temperature rise captured by the model.

2.4.2   Side Effects of the Wastegate

Yet another challenge is present on TC-engines using speed-density methods is that the volumetric efficiency changes with wastegate setting. In Figure 2.4 the

mapped volumetric efficiency is shown together with the estimated volumetric efficiency from measurements. When the wastegate is opened and closed the exhaust manifold pressure changes rapidly and with it the residual gas mass. For open wastegate, this means that more air can enter the cylinder and thus the volumetric efficiency increases. In the lower plot of Figure 2.4 a 5% stationary increase in η_{vol} is present as the conditions stabilize at 14 and 37 seconds. A noticeable effect here is that the mapped volumetric efficiency decreases while the calculated increases! This phenomenon is addressed for stationary conditions in Chapter 3 and a more general solution is proposed in Chapter 4.

2.5 Cylinder Air Charge Estimation Principle Selection

Which of the methods two methods, measured air-mass flow or the speed-density method, is most suitable for CAC estimation? To compare the methods a simulated step in wastegate is used. Using simulated values, it is easy to show the differences between different port air-mass flow estimation methods. During the simulation the engine speed is kept constant and a controller maintains constant air-mass flow. Simulation results are shown in Figure 2.5. It is clear that the speed-density method gives the smallest transient error even though a small stationary error remains. As the error is small and constant, it is easily corrected using feedback from measured air-fuel ratio. Of the two air charge estimation methods, the speed-density principle is chosen for CAC-estimation as it:

- Gives smaller transient error for tip ins/outs. See Figure 2.2.

- Gives smaller transient error when the wastegate is opened. See Figure 2.5.

- Has been shown to give valid transient cylinder air charge estimates on NA-engines (Smith et al., 1999; Chevalier and Müller, 2000).

Further, introducing a pressure and temperature observer can solve the speed-density method's problems with noisy signals and slow sensors.

2.6 Related Work

Air-fuel control has been a studied topic since the SI-engine was invented. One of the first open-loop air-fuel controllers was the carburetor, invented by Wilhelm Maybach in 1892 (Cummins, 2000, pp. 240). A lot has then been written about air-fuel ratio control and here only a brief selection of relevant papers from the last decades are made.
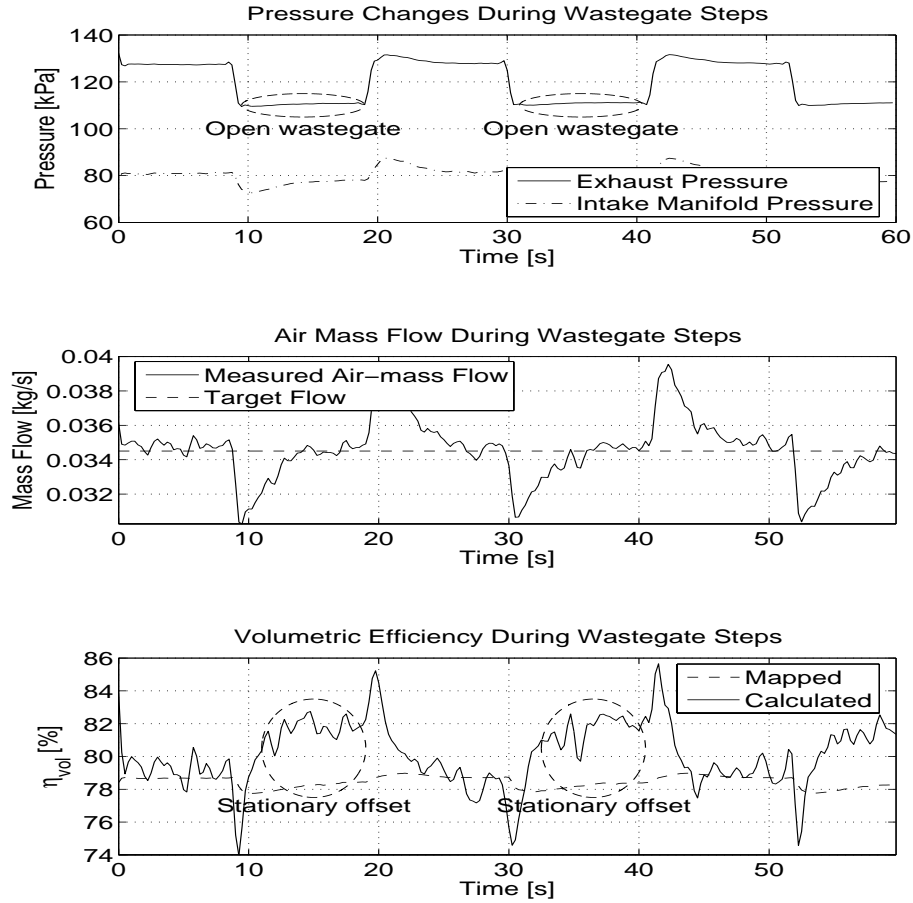
Figure 2.4: An engine experiment at constant speed and air-mass flow, which shows that the wastegate setting influences the volumetric efficiency. *Top:* Exhaust and intake manifold pressure during opening/closing of the wastegate. Wastegate is opened at 9, 30, and 52 seconds. *Center:* Measured air-mass flow, W_a. A throttle controller tries to maintain a constant reference air-mass flow (dashed). As the wastegate is opened, the air-mass flow decreases momentarily until the air-mass controller has opened the throttle. *Bottom:* Calculated and estimated volumetric efficiency. Eq. (2.4) determines the estimated volumetric efficiency and the calculated is determined using Eq. (2.3). There is a stationary offset between the mapped and estimated volumetric efficiency when the wastegate is open.
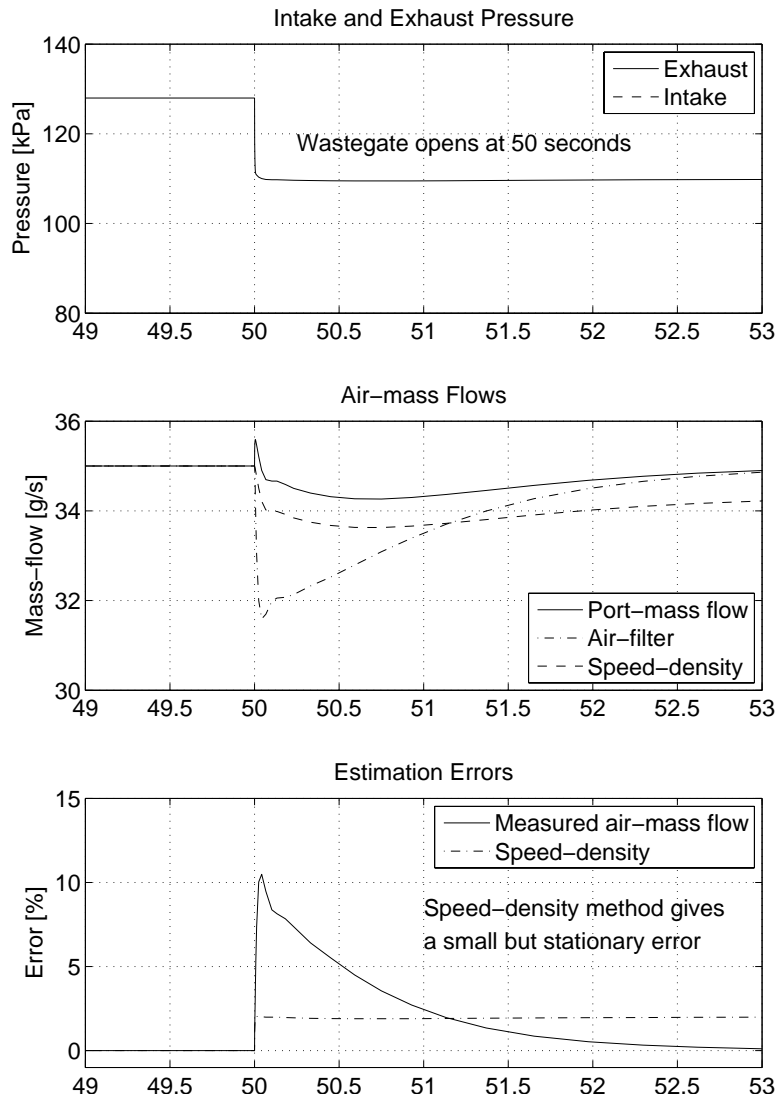
Figure 2.5: Simulated wastegate step at constant engine speed and the throttle controlled to maintain constant air-mass flow. The engine model from Chapter 6 is used and the speed-density air-mass flow is estimated using Eq. (2.2). *Top:* The wastegate opens at 50 seconds. *Center:* The speed-density method captures the dynamics of the port air-mass flow well while the measured air-mass flow underestimates the flow. *Bottom:* For the measured air-mass flow, at the air-filter, the error is almost 15% while the speed-density principle gives an error of only 2%.

2.6.1 Mean Value Engine Models

A key tool in this thesis is the mean value engine model and one of the first mean value engine model of an SI-engine was described in Hendricks and Sorensen (1990). Later the models were extended to include a turbocharger, see e.g. Jensen et al. (1991); Müller et al. (1998); Moraal and Kolmanovsky (1999). Here also some of the compressor modeling concepts from (Guzzella and Amstutz, 1998) has been adopted in a modified form. In Chapter 4 the modeling strategy with control volumes between restrictions from Eriksson et al. (2002b) is adopted. This strategy has also successfully been used for engine torque modeling and control in Frei (2005).

Cylinder Air Charge Modeling

Different approaches have been suggested for cylinder air charge estimation. In Grizzle et al. (1994) it is modeled by inverting the transfer function from measured air-mass flow to the port air-mass flow. Another very accurate model for CAC estimation on NA-aspirated engines is proposed in Hendricks et al. (1996) using an affine function in the intake manifold pressure.

In Powell et al. (1998b) an interesting approach is taken where the cylinder air-mass flow is modeled as a state instead of the intake manifold pressure. Further, the measured cylinder pressure has been used in miscellaneous methods to estimate cylinder air charge (Hart et al., 1998; Mladek, 2003).

An inspiring source to the cylinder air charge model used in this thesis is found in Fox et al. (1993). There a simple model for the residual gas fraction is described which was reformulated in Eriksson et al. (2002a) and adopted here after some additional development.

Throttle Flow Modeling

Several references have studied throttle flow modeling and noticed that the critical pressure does not occur where the compressible flow equation predicts it. In Pursifull et al. (2000) this is dealt with by introducing a throttle angle dependent discharge coefficient. Another approach is taken in Hendricks et al. (1996) where a revised flow equation is proposed. In Chapter 6 a similar approach has been followed. In Blair (1999) and Arsie et al. (1996) other methods for throttle flow modeling are employed.

Fuel Dynamics

One factor that influences the air-fuel ratio significantly especially for cold engine conditions is fuel dynamics or fuel puddles. Extensive research on the fuel dynamics has been performed, where it is commonly described as a two-path flow (Aquino, 1981; Fozo and Aquino, 1988; Onder et al., 1998; Locatelli et al., 2004). One part of the fuel from the injector enters the cylinder immediately and the remaining part of the fuel is stored in a fuel film or a fuel puddle.

From the puddle, some of the fuel evaporates and enters the cylinder together with the fuel from the first part. It has also been argued that the identified dynamics parameters are very sensitive to unknown time-delays, such as the exact injection time (Henriksson and Nielsen, 1998).

2.6.2 Measuring Air-Fuel Ratio

Traditionally the air-fuel ratio is measured using a sensor in the exhaust system. The characteristics of the oxygen sensor in the exhaust system are described in Auckenthaler et al. (2002). In this work a wide-band oxygen sensor placed in front of the TWC has been used.

Several methods to extract the air-fuel ratio from the cylinder pressure are described in Powell (1993). Another in-cylinder air-fuel ratio estimation method is to use the ion-current, which has been demonstrated in e.g. Wickström and Byttner (2005).

2.6.3 Observers and Air-Fuel Ratio Control Aspects

In this thesis gain switched extended Kalman filters are used for state estimation along the air-path. This methodology are also used in Hendricks et al. (1992); Jensen et al. (1997); Maloney and Olin (1998). A different kind of observer for air-mass flow estimation and diagnosis is also suggested for use in a natural gas engine in Weeks and Moskwa (1994). The difference lies in that the intake manifold pressure state is estimated by applying the observer error multiplicatively to the estimated mass flow through the throttle rather than to the intake manifold pressure state itself.

In Tseng and Cheng (1999) an observer for CAC estimation is suggested that deals with small errors in the volumetric efficiency. This work inspired to the observer structure in Chapter 3 where an cylinder air-mass offset is estimated instead of an offset in the volumetric efficiency. Compared to the work by Tseng and Cheng (1999) the suggested observer structure uses feedback to both the pressure state and the estimated cylinder air-mass offset.

Observers for air-fuel control using only feedback from measured air-fuel ratio have been proposed in Powell et al. (1998b). This observer is also run entirely in the event domain. Further research on air-fuel ratio control is also described in Onder and Geering (1993); Onder et al. (1997); Mladek (2003).

The need for prediction has been addressed in e.g. Chevalier et al. (2000) where a predictive observer for the air-fuel ratio control is proposed for a naturally aspirated engine. Prediction has also been discussed in Jankovic and Magner (1999) where a NA-engine with EGR is considered. When prediction is used, there are always prediction errors and an algorithm to compensate for errors in cylinder air charge estimates is demonstrated in Kotwick and Russell (2000).

TWC Control

Recent research shows that emissions can be further reduced using the fact that
the TWC can store a certain amount of oxygen to be used later in the emission
reduction (Brandt et al., 2000; Jones et al., 2000; Yasui et al., 2000; Jones,
2003; Auckenthaler, 2003; Balenovic et al., 2004). By utilizing knowledge of
the oxygen storage capacity together with active control of the oxygen entering
the TWC an HC reduction of over 30% and a 60% reduction of NO_x has been
shown (Miyamoto et al., 2002). As the air contains oxygen, knowledge of the
air-fuel ratio and the air-mass flow into the TWC is important to describe the
oxygen level.

2.6.4   Time Domain versus Crank Angle Domain

Engine controllers are executed either in the time-domain or in the crank angle
domain. It has been argued that all dynamics, except for fuel dynamics, varies
less in the crank angle domain (Chin and Coats, 1986). A challenge using event
based sampling is that the Nyquist criterion is not fulfilled for low engine speeds
(Hendricks et al., 1994).

Observers and engine models operating in the crank angle domain have been
developed for NA-engines in Fekete et al. (1995); Chang et al. (1993); Powell
et al. (1998b). In their proposed observer, structure there is a steady state
adaption table to compensate for model errors. The table is similar to the in
cylinder air-mass offset estimated in Chapter 3 but with a considerably slower
adaption.

Part I

Stationary

SPEED-DENSITY METHODS AND DIFFERENT WASTEGATE SETTINGS

Knowledge of port air-mass flow is important for accurate air/fuel ratio control on port injected SI-engines. Unfortunately it is not directly measurable and therefore several strategies to estimate it have been proposed, see for example Hendricks et al. (1992); Chang et al. (1993); Shio and Moskwa (1996); Tseng and Cheng (1999); Kotwick et al. (1999); Jankovic and Magner (1999). In Chapter 1 it was established that speed-density methods are suitable for port air-mass flow estimation. For speed-density methods accurate knowledge of the intake manifold pressure is crucial and therefore several methods to estimate it have been proposed.

Intake manifold pressure estimation is a well-studied topic for NA-engines. On TC-engines there is an additional challenge as the turbocharger couples the intake side and exhaust side and causes the volumetric efficiency to change when the wastegate is operated, which was shown in Section 2.1.1. It is desirable to open the wastegate at part load to reduce the pumping losses and thereby improve fuel economy (Eriksson et al., 2002a). Changes in wastegate opening will act as a non-measurable disturbance that influence the estimated intake manifold pressure. Thus, this chapter focuses on estimation of intake manifold pressure and port air-mass flow for different wastegate settings. In this case only stationary conditions are considered as the port-air mass flow then can be validated using any known flow in the intake system, such as a measured air-mass flow or a modeled flow through a restriction. Here a model of a restriction, the throttle, is used instead of an expensive air-mass flow meter to determine the air-mass entering the intake manifold. An additional advantage of the throttle model is that it estimates the mass-flow at the entry of the

intake manifold, compared to the air-mass flow sensor that is located far from the intake manifold.

The port air-mass estimation problem is addressed in the following steps. First two different port-air mass flow models based on the speed-density principle from literature are described and then a third speed-density based model, which combines the two previous models is presented. To each of the three models an observer is developed. For the first two observers, solutions from the literature have been used:

1. A nonlinear observer using proportional feedback from the estimation error (Hendricks et al., 1992).

2. A nonlinear observer using integration of the estimation error (Tseng and Cheng, 1999).

3. Using a new port-air mass flow model and by combining the advantages of the observers above; a third observer is developed that better suits the conditions in a TC SI-engine with wastegate.

In the evaluation of the observers, the estimated port air-mass flow and the estimated intake manifold pressure are compared to measured data at steady-state. Thus, the strategy for port air-mass flow estimation relies on:

- A fast pressure sensor in the intake manifold p_{im}. A fast sensor has a higher bandwidth than in this case the intake manifold pressure dynamics. Here a fast Kristal 4295A2 pressure sensor is used which has a cut off frequency of 2 kHz (Kri, 1997).

- Measured intake manifold temperature T_{im}, pressure p_{ic} and temperature T_{ic} before the throttle.

- Throttle plate angle α.

- Measured engine speed N.

- Models of parts of the intake system.

For a description of the subscripts and symbol names, please see the nomenclature in Appendix A.

3.1   Air Intake System Modeling

The observer estimates the intake manifold pressure and relies on an intake system model. The intake system model is described in three steps starting with the intake manifold pressure dynamics. To describe the intake manifold pressure dynamics models of the flows into and out of the manifold are required. A throttle model in Section 3.1.2 describes the flow into the intake manifold and a port air-mass flow model describes the mass flow out of the manifold. Here

three different port air-mass flow models will be described in Section 3.1.3. Each of the models are then used in the observer design and the observers capability of describing port air-mass flow and intake manifold pressure for different settings of the wastegate are investigated.

3.1.1 Intake Manifold Pressure Dynamics

The following standard assumptions are made when the intake manifold pressure dynamics is modeled: Ideal gas, no temperature dynamics, and mass conservation in the intake manifold. The pressure change inside the volume (V_{im}) of the intake manifold is expressed using mass balance, with $K_{im} = \frac{R_{im}T_{im}}{V_{im}}$, as

$$\frac{dp_{im}}{dt} = K_{im} \left(W_{at} \left(\alpha, p_{im}, p_{ic}, T_{ic} \right) - W_{cyl} \right) \tag{3.1}$$

The port air-mass flow W_{cyl} is described by one of the models in Equations (3.3, 3.4, 3.5). The flow into the manifold is described by the throttle model, Eq. (3.2).

Temperature dynamics is also present in the intake manifold during large pressure transients (Chevalier et al., 2000). In this study, temperature dynamics is neglected as the focus is on stationary conditions and stationary effects.

3.1.2 Air-Mass Flow Into the Intake Manifold

In the pressure dynamics, Eq. (3.1), the air-mass flow into the intake manifold W_{at} is required. The easiest method to access W_{at} would be to measure it, but on the modeled engine the air-mass flow sensor is located after the air filter and there are several large volumes between the intake manifold and the sensor. Each volume introduces filling and emptying dynamics, which distort the measurement. One method to deal with these volumes is to model the system between the sensor and the intake and invert its dynamics. On naturally aspirated engines, this approach has been applied in Grizzle et al. (1994). Unfortunately, this is harder to implement on turbocharged engines as several of the components are complex such as the compressor and the intercooler. Instead of modeling the dynamics between the sensor and the throttle, only a model of the throttle is used to estimate air-mass flow into the intake manifold W_{at}:

$$W_{at} \left(\alpha, p_{im}, p_{ic}, T_{ic} \right) \quad = \quad \frac{p_{ic}}{\sqrt{R_{im}T_{ic}}} A_{eff} \left(\alpha \right) \Psi \left(\Pi \right) \tag{3.2a}$$

$$\Pi \quad = \quad \frac{p_{im}}{p_{ic}} \tag{3.2b}$$

$$A_{eff} \left(\alpha \right) \quad = \quad A \left(\alpha \right) C_d \left(\alpha \right) = e^{c_2 \alpha^2 + c_1 \alpha + c_0} \tag{3.2c}$$

$$\Psi\left(\Pi\right) \quad = \quad \begin{cases} \sqrt{\frac{2\gamma}{\gamma-1}\left(\Pi^{\frac{2}{\gamma}} - \Pi^{\frac{\gamma+1}{\gamma}}\right)} & \text{for } \Pi > \left(\frac{2}{\gamma+1}\right)^{\frac{\gamma}{\gamma-1}} \\ \sqrt{\frac{2\gamma}{\gamma-1}\left(\left(\frac{2}{\gamma+1}\right)^{\frac{2}{\gamma-1}} - \left(\frac{2}{\gamma+1}\right)^{\frac{\gamma+1}{\gamma-1}}\right)} & \text{otherwise} \end{cases} \quad (3.2d)$$

The flow through the throttle depends not only on the effective area A_{eff} but also on the pressure ratio Π through Eq. (3.2d). The effective area $A_{\text{eff}}\left(\alpha\right)$ is a product of the area $A\left(\alpha\right)$ and discharge coefficient $C_d\left(\alpha\right)$. Here, this product is modeled as in Nyberg and Nielsen (1997) but using a different parameterization. The parameters in Eq. (3.2c) are fitted in a least squares sense to mapped engine data. In the left column of Figure 3.1 the result of the modeled $A_{\text{eff}}\left(\alpha\right)$ is shown. A systematic relative error is present in the bottom left plot of Figure 3.1. The relative error is positive for large Π which indicates that $A_{\text{eff}}\left(\alpha\right)$ could be slightly improved by including Π, which is supported in Krysander (2000). This is further addressed in Chapter 6.

In the lower right plot of Figure 3.1 it is shown that the stationary air-mass flow into the intake manifold is the same as the measured air-mass flow $\pm 6\%$ for most points. To decrease the effect of throttle model errors, observers for throttle air-mass flow have been proposed in e.g. Jensen et al. (1997). Here no throttle air-mass observer has been added as the focus is on the behavior when the wastegate is operated.
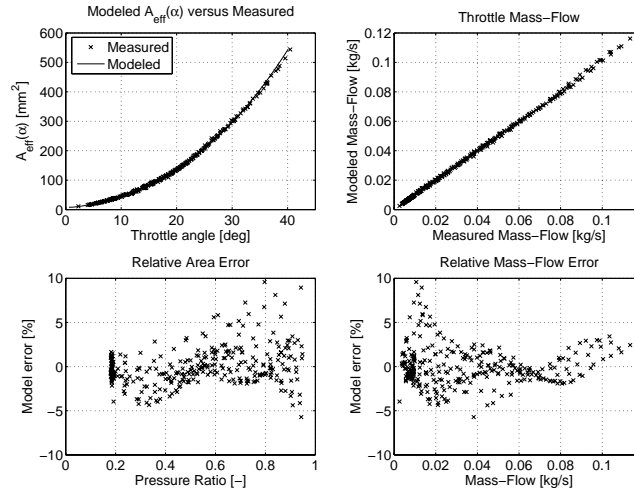
Figure 3.1: Throttle model validation. *Left column*: Comparison of measured and calculated $A_{\text{eff}}\left(\alpha\right)$. The fit is within 5% for most points. *Right column*: Validation of the throttle mass-flow. For flows larger than 20 g/s the error is less than 6%.

When throttle air-mass flow is determined through Eq. (3.2a) both the pressure p_{ic} and the temperature T_{ic} before the throttle are required. Fortunately,

measurements can be used as the dynamics of p_{ic} and T_{ic} are considerably slower than p_{im}, due to the substantially larger volume of the system before the throttle and to the slower dynamics of the turbocharger. The measurements of p_{ic} and T_{ic} are also subjected to less pumping noise.

3.1.3 Port Air-mass Flow

First a standard method from the literature is presented to model port air-mass flow based on Heywood (1988); Taylor (1994) followed by an augmented model based on Tseng and Cheng (1999). By combining these models a new interpretation of port air-mass flow is presented at the end.

Port Air-mass Flow Using Mapped Volumetric Efficiency

A standard model to describe port air-mass flow is to use the volumetric efficiency of the engine η_{vol} (Heywood, 1988; Taylor, 1994). The port air-mass flow is then given by

$$W_{\text{cyl}_{std}}\left(N, p_{\text{im}}, T_{\text{im}}\right) = \eta_{\text{vol}}\left(N, p_{\text{im}}\right) \frac{p_{\text{im}} V_d}{R_{\text{im}} T_{\text{im}}} \frac{N}{n_r} \tag{3.3}$$

The volumetric efficiency is described at steady-state, for a nominal setting of the wastegate, as a function of engine speed N and mean intake manifold pressure p_{im} using the model given by Eq. (2.4), which was proposed in Hendricks and Sorensen (1990). As all port air-mass flow models includes $W_{\text{cyl}_{std}}\left(N, p_{\text{im}}, T_{\text{im}}\right)$ that relies on the accuracy of the modeled volumetric efficiency; a separate validation of the modeled parameter volumetric efficiency is made. The result is shown in Figure 3.2, where the error in the modeled volumetric efficiency is less than 6% for operating points above 50 kPa intake manifold pressure.

Port Air-mass Flow with Modeled Offset in η_{vol}

A day-to-day variation in η_{vol} of a few percent is reported in Tseng and Cheng (1999). Their solution to the problem is to introduce an additive offset to the volumetric efficiency called $\Delta\eta_{\text{vol}}$. The port air-mass flow then becomes:

$$W_{\text{cyl}_{\text{ts}}}(N, p_{\text{im}}, T_{\text{im}}, \Delta\eta_{\text{vol}}) = (\eta_{\text{vol}}\left(N, p_{\text{im}}\right) + \Delta\eta_{\text{vol}}) \frac{p_{\text{im}} V_d}{R_{\text{im}} T_{\text{im}}} \frac{N}{n_r} =$$
$$\underbrace{\eta_{\text{vol}}\left(N, p_{\text{im}}\right) \frac{p_{\text{im}} V_d}{R_{\text{im}} T_{\text{im}}} \frac{N}{n_r}}_{W_{\text{cyl}_{std}}} + \Delta\eta_{\text{vol}} \frac{p_{\text{im}} V_d}{R_{\text{im}} T_{\text{im}}} \frac{N}{n_r} \tag{3.4}$$

The original purpose of the additive offset $\Delta\eta_{\text{vol}}$ was to compensate for slow day-to-day variations and it is therefore assumed to be more slowly varying than other dynamics. By proper selection of $\Delta\eta_{\text{vol}}$ this approach is suited to adapt to
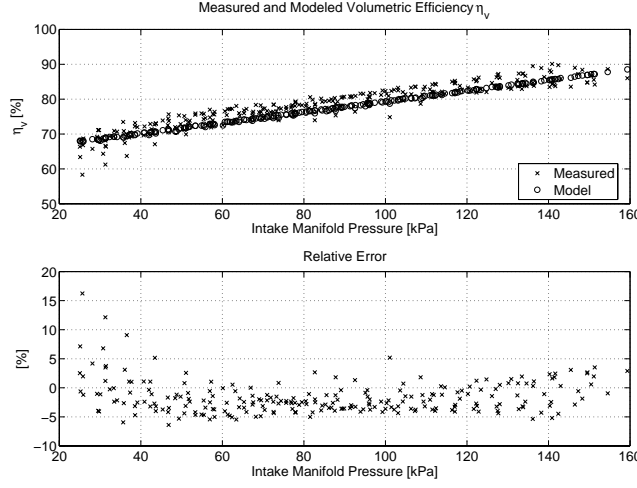
Figure 3.2: Validation of modeled volumetric efficiency.

the changing volumetric efficiency for different wastegate settings. Here $\Delta\eta_{\text{vol}}$ is estimated using an observer.

Port Air-mass Flow With Air-mass Offset

For nominal wastegate position the expected port air-mass flow is well described by the model in Eq. (3.3). However, changes in wastegate setting influences the exhaust manifold pressure and in turn the volumetric efficiency. The change in volumetric efficiency is a result of a *change in residual gas mass* when the exhaust manifold pressure changes. One way to deal with this change is to introduce an offset in the volumetric efficiency $\Delta\eta_{\text{vol}}$ as in Eq. (3.4). Another way is to keep the physical interpretation of a change or an offset in inducted air mass called ΔCAC. The in-cylinder air-mass-offset ΔCAC, is the difference between the expected air-mass Eq. (3.3) and the current port air-mass flow.

$$W_{\text{cyl}_{\text{ts}}} = \underbrace{\eta_{\text{vol}}\left(N, p_{\text{im}}\right) \frac{p_{\text{im}} V_d}{R_{\text{im}} T_{\text{im}}} \frac{N}{n_r}}_{W_{\text{cyl}_{std}}} + \underbrace{\Delta\eta_{\text{vol}} \frac{p_{\text{im}} V_d}{R_{\text{im}} T_{\text{im}}}}_{\Delta\text{CAC, Air-mass offset}} \frac{N}{n_r} \qquad (3.5)$$

If ΔCAC can be estimated using for example an observer, the port air-mass flow can be written as a sum of the air-mass expected from Eq. (3.3) and the in-cylinder air-mass offset ΔCAC.

$$W_{\text{cyl}_{\Delta\text{CAC}}}\left(N, p_{\text{im}}, T_{\text{im}}, p_{\text{em}}, (A/F), \ldots\right) =$$
$$W_{\text{cyl}_{std}}\left(N, p_{\text{im}}, T_{\text{im}}\right) + \Delta\text{CAC}\left(p_{\text{em}}, p_{\text{im}}, (A/F), \ldots\right) \frac{N}{n_r} \quad (3.6)$$

In Eq. (3.6) the in-cylinder air-mass-offset ΔCAC is sensitive to factors that cause deviations from the expected cylinder air charge. Examples of such factors are the exhaust manifold pressure, the air/fuel ratio, and the dots in Eq. (3.6) represent other influences including model errors.

3.2 Intake Manifold Pressure Observers

Here three different intake manifold pressure observers are investigated. The observers are based on the intake manifold pressure model presented in Section 3.1.1. Their differences lie in the port air-mass flow model, the number of states, and how the feedback from the fast intake manifold pressure sensor is used. The observer equations are given in Section 3.3 to Section 3.5 and Table 3.1 gives an overview.

Described in	States(s)	$W_{\mathbf{cyl}}$-model	$W_{\mathbf{at}}$-model	Feedback
Section 3.3	$\hat{p}_{im}$	Eq. (3.3)	Eq. (3.2)	Acts on $\hat{p}_{im}$
Section 3.4	$\hat{p}_{im}, \Delta\hat{\eta}_{vol}$	Eq. (3.4)	Eq. (3.2)	Acts only on $\Delta\hat{\eta}_{vol}$
Section 3.5	$\hat{p}_{im}, \widehat{\Delta CAC}$	Eq. (3.6)	Eq. (3.2)	Acts on both states

Table 3.1: The table shows the different observer configurations with states, port air-mass flow model, and which state(s) that are affected by the feedback.

The following measurement signals are used by the observers: Engine speed N, pressure before the throttle p_{ic}, temperature before the throttle T_{ic}, throttle plate angle α, intake manifold pressure p_{im}, and intake manifold temperature T_{im}.

Next, the validation method is described together with the test case that is used for validation. Then the three observers are described and evaluated in Sections 3.3, 3.4, and 3.5.

3.2.1 Port Air-mass Flow Estimation from Observed Intake Manifold Pressure

When the intake manifold pressure is estimated using the observers described in Table 3.1 the port air-mass flow is determined by substituting p_{im} for $\hat{p}_{im}$ in the port air-mass flow models. This port air-mass flow is one of the sought outputs of the observers.

3.2.2 Port Air-mass Flow Validation

To validate the estimated port air-mass flow from observed intake manifold pressure, for stationary conditions, the estimated throttle air-mass flow is used. As the throttle mass-flow depends on the *observed intake manifold pressure*, it is not likely that the estimated throttle air-mass flow is correct unless the observer converges to the measured intake manifold pressure. A sensitivity

analysis, based on the throttle mass-flow Eq. (3.2a), is therefore made to determine whether the observed intake manifold pressure can be used or not to determine the throttle air-mass flow.

$$
S\left(\frac{p_{\mathrm{im}}}{p_{\mathrm{ic}}}\right) \;=\; \frac{\frac{\partial W_{\mathrm{at}}(\alpha,p_{\mathrm{im}},p_{\mathrm{ic}},T_{\mathrm{ic}})}{\partial p_{\mathrm{im}}}}{\frac{W_{\mathrm{at}}(\alpha,p_{\mathrm{im}},p_{\mathrm{ic}},T_{\mathrm{ic}})}{p_{\mathrm{im}}}} \;=\; \frac{-2\left(\frac{p_{\mathrm{im}}}{p_{\mathrm{ic}}}\right)^{\frac{2}{\gamma_a}} + \left(\frac{p_{\mathrm{im}}}{p_{\mathrm{ic}}}\right)^{\frac{\gamma_a+1}{\gamma_a}}(\gamma_a+1)}{2\gamma_a\left(-\left(\frac{p_{\mathrm{im}}}{p_{\mathrm{ic}}}\right)^{\frac{2}{\gamma_a}} + \left(\frac{p_{\mathrm{im}}}{p_{\mathrm{ic}}}\right)^{\frac{\gamma_a+1}{\gamma_a}}\right)}
$$

As the sensitivity only depends on the pressure ratio $\frac{p_{\mathrm{im}}}{p_{\mathrm{ic}}} = \Pi$ means that S is reformulated into a function of the pressure ratio Π.

$$
S(\Pi) = \frac{(\gamma_a+1)\,\Pi^{\frac{\gamma_a+1}{\gamma_a}} - 2\Pi^{\frac{2}{\gamma_a}}}{2\gamma_a\left(\Pi^{\frac{\gamma_a+1}{\gamma_a}} - \Pi^{\frac{2}{\gamma_a}}\right)} \tag{3.7}
$$

Eq. (3.7) is valid for pressure ratios above the critical pressure Π_{crit}:

$$
\Pi_{\mathrm{crit}} \geq \left(\frac{2}{\gamma+1}\right)^{\frac{\gamma}{\gamma-1}}
$$

For pressure ratios below Π_{crit} the sensitivity function is constant and zero which means that the throttle air-mass flow is insensitive to changes in intake manifold pressure. Thus the observed intake manifold pressure can only be used to determine the air-mass flow into the intake manifold for pressure ratios below Π_{crit}. Figure 3.3 shows $S(\Pi)$ and it can be seen that $|S(\Pi)| > 1$ for pressure ratios $\Pi > 0.75$. This means that even small errors in the observed intake manifold pressure results in a biased Π; if $\Pi > 0.75$ where $|S(\Pi)| > 1$ and thus the error in the estimated throttle air-mass flow increase! Therefore, the observed intake manifold pressure is not suitable to determine the throttle air-mass flow *unless* it converges to the measured intake manifold pressure. In addition, when the observers are validated, the stationary error in estimated port air-mass flow is determined

$$
\hat{W}_{\mathrm{cyl}}(N,\hat{p}_{\mathrm{im}},T_{\mathrm{im}},\ldots) - W_{\mathrm{at}}(\alpha,p_{\mathrm{im}},p_{\mathrm{ic}},T_{\mathrm{ic}})
$$

the *measured* intake manifold pressure is used to calculate W_{at}. This guarantees an observer independent validation of the stationary port air-mass flow error.

3.2.3   Observer Test Case Description

For stationary conditions the port air-mass flow W_{cyl} is the same as the throttle air-mass flow, W_{at}, and this is used to evaluate steady-state port air-mass flow estimates for the observers in Sections 3.3, 3.4, and 3.5. The same experiment is used to validate all observers and the performed experiment is to open and close the wastegate with a constant reference air-mass flow and a constant engine
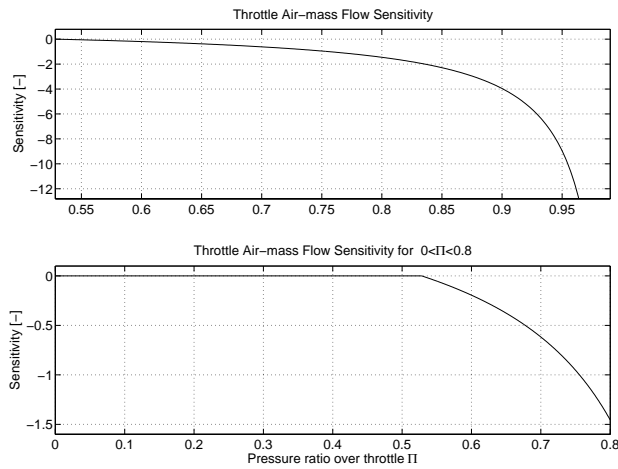
Figure 3.3: Throttle air-mass flow sensitivity to intake manifold pressure for different pressure ratios $\Pi = \frac{p_{im}}{p_{ic}}$. *Top*: For high pressure ratios the throttle air-mass flow is very sensitive to intake manifold pressure errors. *Bottom*: For low pressure ratios, below $\Pi = 0.53$, the flow is insensitive to changes in intake manifold pressure as $S(\Pi) = 0$.

speed. The test data, shown in Figure 3.4, is measured at 3100 RPM and at BMEP=5.3 bar. This operating point represents a medium engine speed at part load where the pumping losses are reduced when the wastegate is opened. In addition, all data have been low-pass filtered using a zero-phase filter to suppress noise. During the experiment the air-mass flow is held constant by a throttle controller. This is clearly visible in the center of Figure 3.4.

Wastegate steps of high amplitude are achieved using a manual control device instead of the production vacuum actuator. When the wastegate is opened and closed there are air-mass flow transients at 5 seconds and 21 seconds. What is furthermore interesting is that the mapped volumetric efficiency does not match the calculated when the wastegate is open. This shows up as a 5% steady-state difference between the mapped and measured volumetric efficiency in the bottom of Figure 3.4. The cause is that the volumetric efficiency is sensitive to changes in residual gas mass, which depends on the pressure ratio $\frac{p_{im}}{p_{em}}$ (Heywood, 1988; Taylor, 1994).

3.3 Observer with Proportional Feedback

To observe the intake manifold pressure Hendricks et al. (1992) suggest a constant gain extended Kalman filter (CGEKF) (Safanov and Athans, 1978). It uses proportional feedback from the intake manifold pressure estimation error.
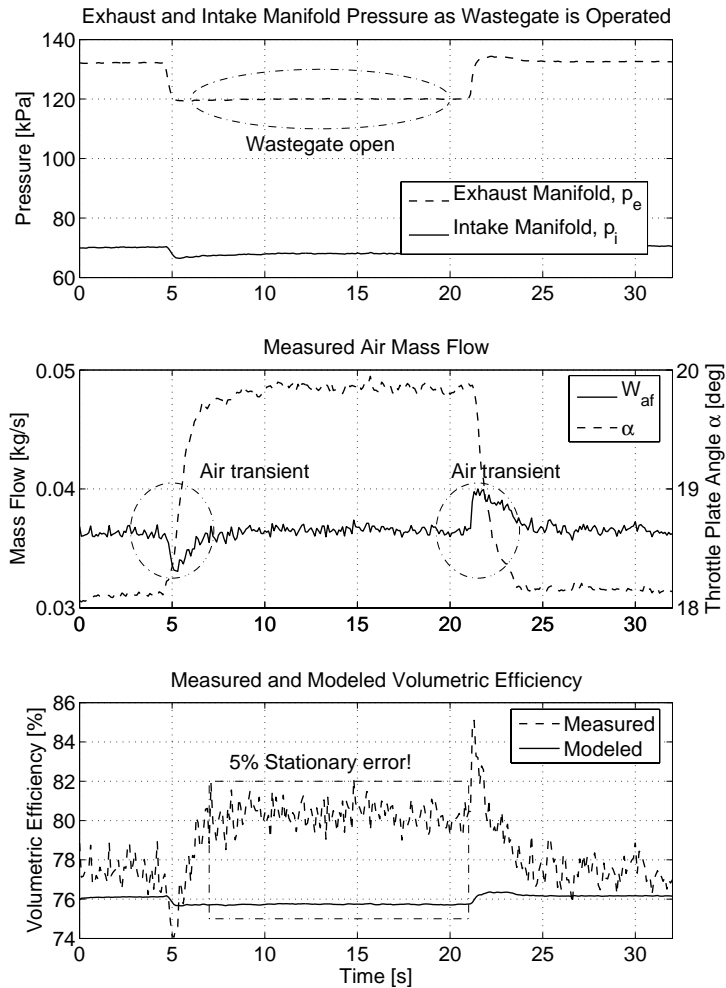
Figure 3.4: For observer validation the following measured engine data is used: Wastegate opening and closing at constant air-mass flow, constant speed 3100 RPM, and 5.3 bar brake mean effective pressure. *Top:* Exhaust pressure drops when the wastegate is opened at time 5 and it increases again when the wastegate is closed at time 21 seconds. *Center:* Air-mass flow is controlled to a constant value by changing the throttle plate angle and transients in the air-mass flow are only present after wastegate setting changes. *Bottom:* The volumetric efficiency increases for open wastegate. At most there is a 5% steady-state error, compared to the mapped value.

In Eq. (3.1) the port air-mass flow W_{cyl}

$$W_{\text{cyl}} = W_{\text{cyl}_{\text{std}}}\left(N, \hat{p}_{\text{im}}, T_{\text{im}}\right) = \eta_{\text{vol}}\left(N, \hat{p}_{\text{im}}\right) \frac{\hat{p}_{\text{im}} V_d}{R_{\text{im}} T_{\text{im}}} \frac{N}{n_r} \tag{3.8}$$

is given by Eq. (3.3), and the mass flow into the intake manifold is given by Eq. (3.2a). The resulting observer is then:

$$\frac{\mathrm{d}\hat{p}_{\text{im}}}{\mathrm{d}t} = K_{\text{im}}\left(W_{\text{at}}\left(\alpha, \hat{p}_{\text{im}}, p_{\text{ic}}, T_{\text{ic}}\right) - W_{\text{cyl}_{\text{std}}}\left(N, \hat{p}_{\text{im}}, T_{\text{im}}\right)\right) + K_{\text{obs}}\left(p_{\text{im}} - \hat{p}_{\text{im}}\right) \tag{3.9}$$

In Eq. (3.9), the CGEKF design methodology is used to determine the feedback gain K_{obs}.

3.3.1 Tuning

When K_{obs} is determined in Eq. (3.9), the following inputs to the design method are necessary: First, the variance of the state noise $\hat{p}_{\text{im}}$ has to be determined. In Hendricks et al. (1992) the engine pumpings in the intake manifold pressure is considered as state noise. This is here determined by taking the variance of the measured intake manifold pressure in the design points. The second input is the variance of the measurement signal noise in p_{im}. The variance of the measurement noise is determined as in Jensen et al. (1997) by measuring the intake manifold pressure with the engine off but with ignition and dynamometer on. Further no correlation between the measurement and the state noises is assumed. As the system is nonlinear, it is linearized in its stationary points and K_{obs} is determined for each stationary point, where the stationary points (N, p_{im}) are given by a measured engine map. The result is a table of K_{obs} where the current state of the engine (N, p_{im}) are used as lookup keys. The current gain K_{obs} is then determined by taking the nearest neighbor.

3.3.2 Steady-State Properties

As the port air-mass flow is calculated from observed intake manifold pressure it is studied how the feedback gain influences:

1. The observed intake manifold pressure $\hat{p}_{\text{im}}$.

2. The estimated port air-mass flow $\hat{W}_{\text{cyl}}$.

For air/fuel control the latter is most interesting. Two different feedback gains are used to better show how the gain influences the estimated intake manifold pressure and the estimated port air-mass flow. The first gain is referred to as "Design gain" and is determined according to the systematic method described in Section 3.3.1. The design gain $K = 41$. As the intake manifold pressure only changes 2 kPa the feedback gain K is constant for the different wastegate settings in the test case. To illustrate the behavior of a lower feedback gain, a

second gain is used and referred to as "Low gain". The "Low gain" is simply set to 1.

The results of running the observer with "Low" and "Design" gain are presented in Figure 3.5. In the center plot it is clear that the pressure estimation error is inversely proportional to the feedback gain. That is to get a low pressure estimation error a higher feedback gain should be used. However, the primary interest is the port air-mass flow which is estimated using Eq. (3.3) and here the difference

$$W_{\text{at}}\left(\alpha, p_{\text{im}}, p_{\text{ic}}, T_{\text{ic}}\right) - W_{\text{cyl}_{\text{std}}}(N, \hat{p}_{\text{im}}, T_{\text{im}})$$

is shown for the test data set in the bottom of Figure 3.5. For closed wastegate there is no stationary error as the modeled volumetric efficiency is very accurate. When the wastegate is open, there is a stationary error in the estimated port air-mass flow. The port air-mass flow error is higher for the design gain, while the intake manifold pressure error is higher for the low gain.

This can be explained by the fact that when there is an error in the modeled volumetric efficiency, which it is when the wastegate is open, this error propagates to the observed intake manifold pressure. Thus, given a pressure error the corresponding error in port air-mass flow can be determined by setting the left hand side of Eq. (3.9) to zero and solve for the stationary pressure difference $(p_{\text{im}} - \hat{p}_{\text{im}})$:

$$\underbrace{(p_{\text{im}} - \hat{p}_{\text{im}})}_{\neq\, 0} = -\frac{K_{\text{im}}}{K_{\text{obs}}} \underbrace{\left(W_{\text{at}}\left(\alpha, \hat{p}_{\text{im}}, p_{\text{ic}}, T_{\text{ic}}\right) - W_{\text{cyl}_{\text{std}}}\left(N, \hat{p}_{\text{im}}, T_{\text{im}}\right)\right)}_{\neq\, 0} \qquad (3.10)$$

The equation above is nonlinear and to show how the pressure estimation error and port air-mass error depends on observer gain an example where a known error in volumetric efficiency is used. The result, shown in Figure 3.6, is that the error in estimated port air-mass flow increases with the feedback gain. That is if a low error in estimated port air-mass flow is desired then a low gain should be used. As expected, the estimated intake manifold pressure error decreases with increasing feedback gain. When there is an error in the volumetric efficiency, the proportional feedback gain is a compromise between accurate intake manifold pressure estimates (higher gain) or accurate port air-mass flow (lower gain). Hence observers relying on proportional feedback for only the intake manifold pressure state are not suitable for port-air mass estimation in turbocharged engines where the volumetric efficiency changes with wastegate setting.

3.4   Port Air-mass Flow Observer with Additive Offset in η_{vol}

A method capable of dealing with small offsets in volumetric efficiency is developed in Tseng and Cheng (1999). The original method was formulated in discrete time but here a continuous time formulation is used. It estimates a
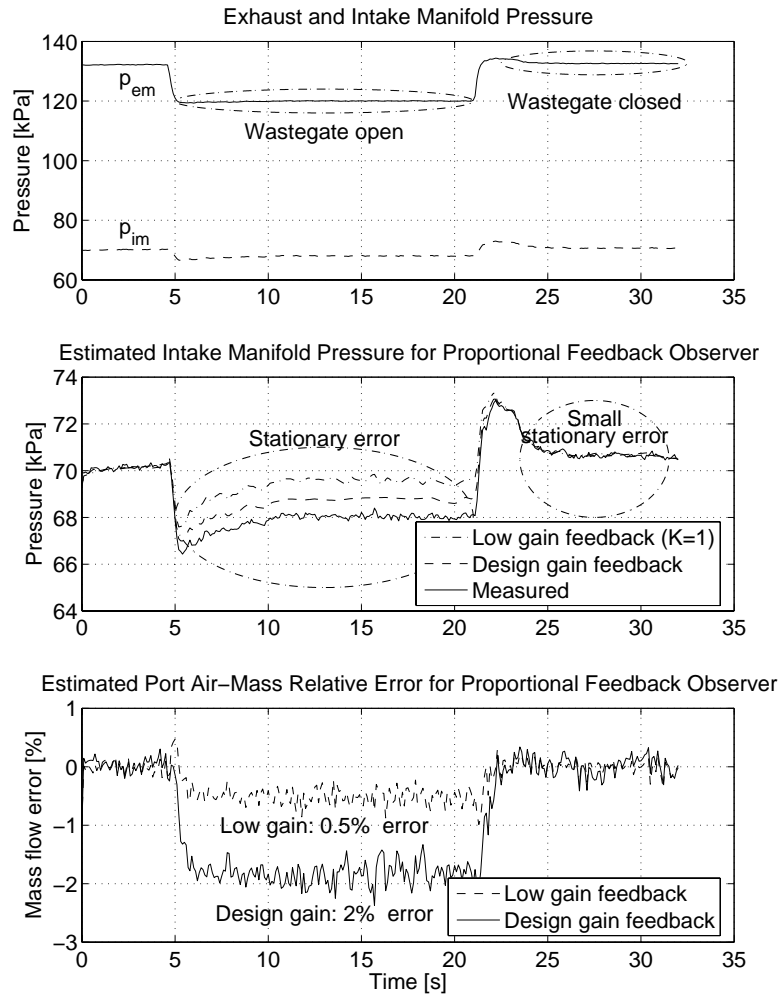
Figure 3.5: Results for observer relying on proportional feedback Eq. (3.9). *Top:* The wastegate is open between time 5 seconds and 21 seconds. *Center:* For closed wastegate, where the description of η_{vol} is correct, the stationary error in the observed intake manifold pressure is independent of the feedback gain. When the wastegate is open the error is inversely proportional to the feedback gain. *Bottom:* In the estimated port air-mass flow there is a stationary error present when the wastegate is open. For the design gain the error is 2%.
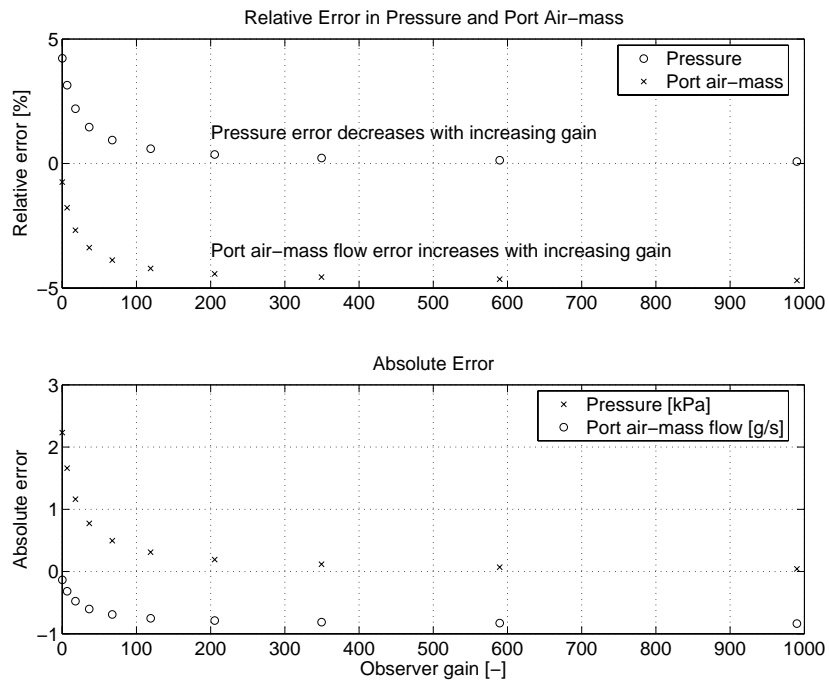
Figure 3.6: Calculated error in observed intake manifold pressure and estimated port-air mass flow using the proportional feedback observer when there is a 5% error in the volumetric efficiency. Engine operating conditions, $N = 2000$ RPM, $\alpha = 14°$, and $p_{\mathrm{im}} \approx 55$ kPa. *Top:* Relative error in pressure and port air-mass flow. It is clear that the port air-mass flow error is lower for small gains and that the intake manifold pressure estimation error decreases with feedback gain. *Bottom:* The absolute pressure estimation error goes to zero for high gains while the port air-mass flow error increases with the gain.

possible bias in η_{vol} by integrating the pressure error. Given this bias the steady-state error in the intake manifold pressure estimate can be removed. In the observer equations the port air-mass flow model is Eq. (3.4) and the air-mass flow into the intake manifold is estimated by Eq. (3.2a). Intake manifold pressure dynamics is given by Eq. (3.1). The port air-mass flow is given by:

$$W_{\text{cyl}} = W_{\text{cyl}_{ts}} \left(N, \hat{p}_{\text{im}}, T_{\text{im}}, \Delta\hat{\eta}_{\text{vol}} \right) = \left(\eta_{\text{vol}} \left(N, \hat{p}_{\text{im}} \right) + \Delta\hat{\eta}_{\text{vol}} \right) \frac{\hat{p}_{\text{im}} V_d}{R_{\text{im}} T_{\text{im}}} \frac{N}{n_r}$$

and the mass flow into the intake manifold is given by Eq. (3.2a). The observer estimates $\Delta\eta_{\text{vol}}$ in a similar manner as in Tseng and Cheng (1999).

$$\frac{\mathrm{d}\hat{p}_{\text{im}}}{\mathrm{d}t} = K_{\text{im}} \left(W_{\text{at}} \left(\alpha, \hat{p}_{\text{im}}, p_{\text{ic}}, T_{\text{ic}}, \Delta\hat{\eta}_{\text{vol}} \right) - W_{\text{cyl}_{ts}} \left(N, \hat{p}_{\text{im}}, T_{\text{im}} \right) \right) \quad \text{(3.11a)}$$

$$\frac{\mathrm{d}\Delta\hat{\eta}_{\text{vol}}}{\mathrm{d}t} = -\frac{1}{L_1} \frac{\left(\eta_{\text{vol}} \left(N, \hat{p}_{\text{im}} \right) + \Delta\hat{\eta}_{\text{vol}} \right)^2 N V_d}{R_{\text{im}} T_{\text{im}} W_{\text{at}} \left(\alpha, \hat{p}_{\text{im}}, p_{\text{ic}}, T_{\text{ic}} \right) n_r} \left(p_{\text{im}} - \hat{p}_{\text{im}} \right) \quad \text{(3.11b)}$$

In Eq. (3.11a) no feedback from the measured intake manifold pressure is used and the feedback gain in Eq. (3.11b) is from Tseng and Cheng (1999) where L_1 is a tuning parameter.

3.4.1 Tuning

The convergence rate of the $\Delta\eta_{\text{vol}}$ estimation in Eq. (3.11b) is controlled by a scaling factor L_1. No systematic tuning method for L_1 is presented in Tseng and Cheng (1999) and here L_1 was simply set to one.

3.4.2 Steady-State Properties

When the observer has converged, Eq. (3.11b) is zero and the estimated intake manifold pressure is equal to the measured. As $\frac{\mathrm{d}\hat{p}_{\text{im}}}{\mathrm{d}t} = 0$ the port air-mass flow $W_{\text{cyl}_{ts}}$ is equal to the estimated air-mass flow into the intake manifold. Therefore, this observer always gives stationary correct port air-mass flow and intake manifold pressure estimates. These properties are shown in Figure 3.7.

A problem is reported in Tseng and Cheng (1999) during intake manifold pressure transients where the observer updates $\Delta\eta_{\text{vol}}$ incorrectly. Therefore, the adaption of $\Delta\eta_{\text{vol}}$ is turned off during large pressure transients. As the pressure transients are small during changes in wastegate position there is no need in this case to turn off the adaption.

3.5 Observer with Air-Mass-Offset Estimation

Of the two previous observers, the first observer using proportional feedback to the estimated intake manifold pressure converges neither to the measured intake
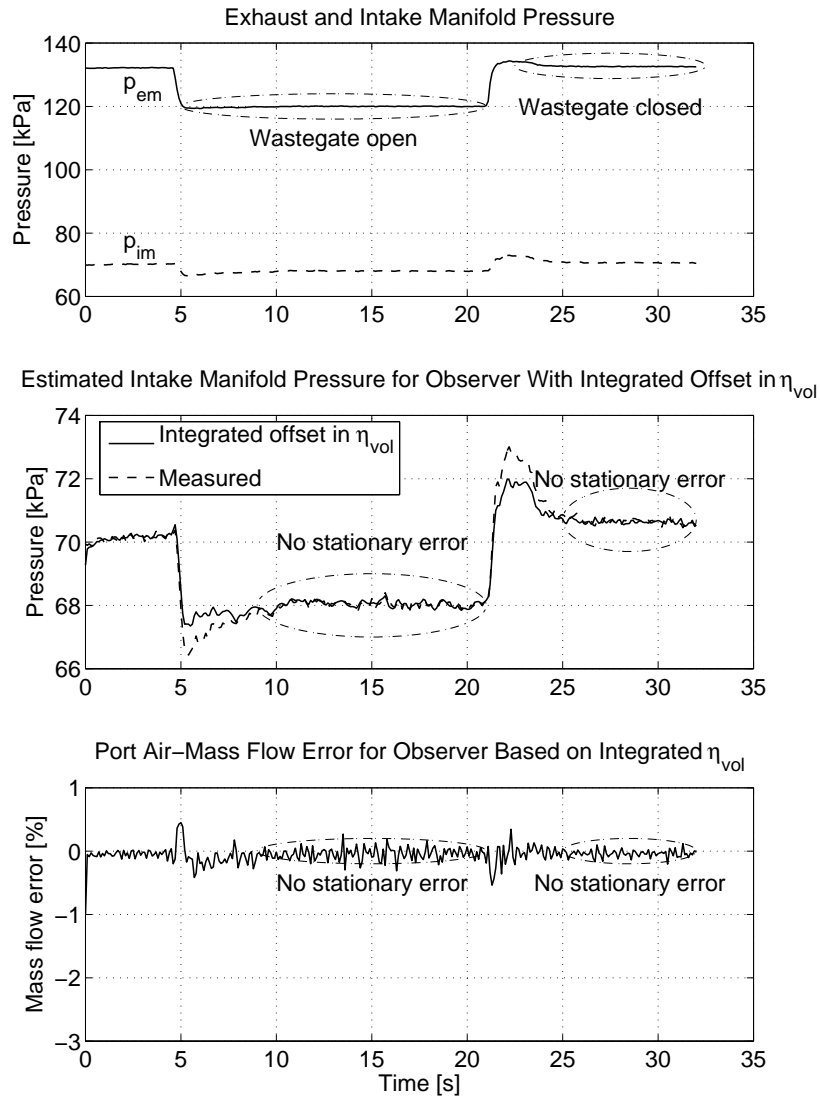
Figure 3.7: Results for the observer that estimates an additive offset in the volumetric efficiency $\Delta\eta_{vol}$. *Top:* The wastegate is open between time 5 and 21 seconds. *Center:* Observed intake manifold pressure tracks the measured intake manifold pressure excellently for stationary conditions. *Bottom:* The estimated port air-mass flow is equal to the estimated air-mass flow through the throttle.

manifold pressure nor to the correct port air-mass flow when the wastegate setting is changed. The second observer, which uses an augmented model, offers stationary correct estimates of the intake manifold pressure and of the port air-mass flow. Here a new observer is suggested that uses feedback of the estimation error to both the pressure state and to an augmented state compared to the previous observers, which only used feedback to one state.

A change in wastegate position results in a changed port air-mass flow. In the port air-mass flow model described by Eq. (3.6) this change is described using the in-cylinder air-mass-offset ΔCAC. Now denote the estimated in-cylinder air-mass-offset $\Delta \widehat{\text{CAC}}$. If $\Delta \widehat{\text{CAC}}$ is assumed to be slowly varying, it can be estimated together with the intake manifold pressure, Eq. (3.1), using integration of the estimation error. $\Delta \widehat{\text{CAC}}$ is then used to determine the port air-mass flow. The observer equations are based on Eq. (3.1) where W_{cyl} is given by Eq. (3.6)

$$W_{\text{cyl}}(\hat{p}_{\text{im}}, \Delta \widehat{\text{CAC}}, N, T_{\text{im}}) = \underbrace{\eta_{\text{vol}}\left(N, p_{\text{im}}\right) \frac{p_{\text{im}} V_d}{R_{\text{im}} T_{\text{im}}} \frac{N}{n_r}}_{W_{\text{cyl}_{std}}} + \Delta \text{CAC} \frac{N}{n_r}$$

and the air-mass flow into the manifold is given by Eq. (3.2a).

$$\frac{\text{d}\hat{p}_{\text{im}}}{\text{d}t} =$$

$$- K_{\text{im}} \left(\underbrace{\overbrace{\eta_{\text{vol}}\left(N, \hat{p}_{\text{man}}\right) \frac{\hat{p}_{\text{im}} V_d N}{R_{\text{im}} T_{\text{im}} n_r}}^{\text{Expected air mass}} + \overbrace{\frac{N}{n_r} \Delta \widehat{\text{CAC}}}^{\text{Offset}}}_{\text{Air mass flow to cylinder}} - W_{\text{at}}\left(\alpha, \hat{p}_{\text{im}}, p_{\text{ic}}, T_{\text{ic}}\right) \right) +$$

$$K_1\left(p_{\text{im}} - \hat{p}_{\text{im}}\right) \quad (3.12\text{a})$$

$$\frac{\text{d}\Delta \widehat{\text{CAC}}}{\text{d}t} = K_2\left(p_{\text{im}} - \hat{p}_{\text{im}}\right) \quad (3.12\text{b})$$

By applying the systematic tuning method given by the CGEKF-theory the feedback gains K_1 and K_2 in Eq. (3.12) are determined.

3.5.1 Tuning

The observer gains, K_1 and K_2, are determined by linearizing Eq. (3.12) in stationary points given by an engine map and applying Constant Gain Extended Kalman filtering technique as in Section 3.3.1. To determine the gains, two noise covariance matrices are required: the state variance and the measurement variance. Using the same method as in Section 3.3 the intake pressure state noise variance and measurement noise variance are determined.

The variance of the in-cylinder air-mass offset state noise is determined by assuming that it is the *change* in cylinder air charge caused by the exhaust

manifold pressure changes. Thus, a model of the cylinder air charge with an explicit exhaust manifold pressure is necessary and therefore the model from Chapter 4 is used:

$$\mathrm{CAC}(p_{\mathrm{im}}, T_{\mathrm{im}}, p_{\mathrm{em}}) = \frac{p_{\mathrm{im}}}{R_{\mathrm{im}} T_{\mathrm{im}}} C_1 \frac{1}{1 + \frac{1}{\lambda\left(\frac{A}{F}\right)_s}} \frac{r_c - \left(\frac{p_{\mathrm{em}}}{p_{\mathrm{im}}}\right)^{\frac{1}{\gamma}}}{r_c - 1} V_{\mathrm{d}}$$

In the model above $\lambda = 1$ is assumed. Now, the variance of $\Delta\mathrm{CAC}$ can be estimated as:

$$\mathrm{var}\ \Delta\mathrm{CAC} = \mathrm{var}\ CAC(p_{\mathrm{im}0}, T_{\mathrm{im}0}, p_{\mathrm{em}}(t))$$

Here $p_{\mathrm{im}0}$ and $T_{\mathrm{im}0}$ means the conditions during closed wastegate and $p_{\mathrm{em}}(t)$ is the *varying* exhaust manifold pressure as the wastegate is opened and closed. To determine the variance of $\Delta\mathrm{CAC}$ for various exhaust manifold pressures it is necessary to have knowledge of the exhaust manifold pressure when the wastegate opens and closes. Here, two methods are considered to determine the exhaust manifold pressure. First, the pressure can be measured during wastegate steps. Second, as the wastegate is controlled by a slow pneumatic actuator, the exhaust manifold pressure is assumed to vary sinusoidally when the wastegate is opened and closed. Its peak-to-peak amplitude is the exhaust pressure difference caused by an opening and closing of the wastegate. Here the second method is chosen.

Further, the intake manifold pressure and air-mass-offset are assumed to be independent. The resulting K_1 and K_2 are stored in a table. In the table $(N, \hat{p}_{\mathrm{im}})$ are used as lookup keys in the same manner as described in Section 3.3.

3.5.2   Properties

The result of applying the test case is shown in Figure 3.8. When the state derivatives are zero, i.e. stationary conditions, two important features of this observer are shown. First, it estimates the same intake manifold pressure as measured. Second, there is no error in the estimated port-air mass flow.

To prove that there is no bias in the pressure nor any port air-mass flow error; start by considering that the following relation holds for stationary conditions:

$$\frac{\mathrm{d}\hat{p}_{\mathrm{im}}}{\mathrm{d}t} = \frac{\mathrm{d}\widehat{\Delta\mathrm{CAC}}}{\mathrm{d}t} = 0$$

Now, as $\frac{\mathrm{d}\widehat{\Delta\mathrm{CAC}}}{\mathrm{d}t} = 0$ this means that the observed intake manifold pressure equals the measured:

$$K_1\left(p_{\mathrm{im}} - \hat{p}_{\mathrm{im}}\right)$$

In turn, this results in that:

$$
\frac{\mathrm{d}\hat{p}_{\mathrm{im}}}{\mathrm{d}t} =
$$

$$
- K_{\mathrm{im}} \left(\overbrace{\underbrace{\eta_{\mathrm{vol}}\left(N,\hat{p}_{\mathrm{man}}\right)\frac{\hat{p}_{\mathrm{im}}V_d N}{R_{\mathrm{im}}T_{\mathrm{im}}n_r}}^{\text{Expected air mass}} + \overbrace{\frac{N}{n_r}\Delta\widehat{\mathrm{CAC}}}^{\text{Offset}}}_{\text{Air mass flow to cylinder}} - W_{\mathrm{at}}\left(\alpha,\hat{p}_{\mathrm{im}},p_{\mathrm{ic}},T_{\mathrm{ic}}\right) \right) +
$$

$$
K_1 \underbrace{\left(p_{\mathrm{im}} - \hat{p}_{\mathrm{im}}\right)}_{=0,\,\text{as }\hat{p}_{\mathrm{im}}=p_{\mathrm{im}}} = 0
$$

The equation above simplifies to:

$$
W_{\mathrm{cyl}_{\mathrm{std}}}(N,\hat{p}_{\mathrm{im}},T_{\mathrm{im}}) + \Delta\widehat{\mathrm{CAC}}\frac{N}{n_r} - W_{\mathrm{at}}\left(\alpha,\hat{p}_{\mathrm{im}},p_{\mathrm{ic}},T_{\mathrm{ic}},\Delta\widehat{\mathrm{CAC}}\right) = 0
$$

This shows that the estimated port air-mass flow now must equal the mass flow into the intake manifold, hence mass balance is fulfilled. Therefore, this observer will estimate stationary correct intake manifold pressure together with the same port air-mass flow as the air-mass flow through the throttle.

3.6 Results

Port air-mass flow estimation using speed-density methods that relies on observed intake manifold pressure has been studied on a turbocharged SI-engine with wastegate. The challenge is that the wastegate influences the *non-measured* exhaust manifold pressure that governs the residual gas mass in the cylinder and thus the volumetric efficiency. Therefore, the volumetric efficiency will change with the wastegate setting and as speed-density methods rely on accurate descriptions of the volumetric efficiency this results in incorrect port-air mass flow estimates. It has been shown using measurements that the *volumetric efficiency can change by 5%* when the wastegate is opened.

Stationary conditions are chosen as it is only possible to validate the port air-mass flow for these conditions. Here, the modeled throttle air-mass flow has been used to validate the estimated port air-mass flow. As the throttle model uses observed intake manifold pressure it is important that the observed intake manifold pressure converges to measured pressure in order to determine the true flow, especially for higher intake manifold pressures which is shown in Figure 3.3.

Three different observers with feedback from measured intake manifold pressure were studied. In the observer evaluation, it was demonstrated that it is not possible to estimate the system state for the observer that relies solely on feedback to the pressure state. There, the feedback gain is a trade-off between pressure convergence or accurate stationary port air-mass flow estimation. A
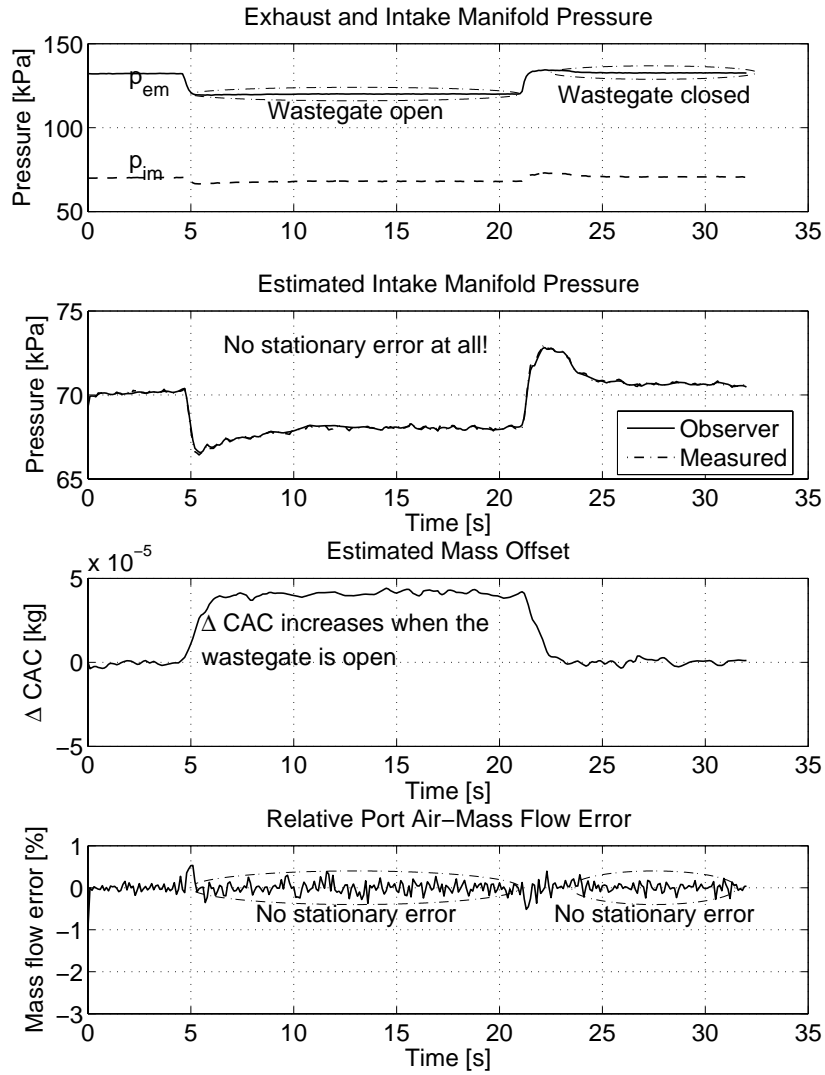
Figure 3.8: Results for the observer with air-mass-offset estimation. *First:* The wastegate is open between time 5 and 21 seconds. *Second:* Observed intake manifold pressure tracks the measured intake manifold pressure excellently for stationary conditions. *Third:* The increase in $\Delta\widehat{\mathrm{CAC}}$ shows that more air is inducted into the cylinder, which is the expected result when the wastegate is opened. *Fourth:* The estimated port air-mass flow is equal to the estimated air-mass flow through the throttle for stationary conditions.

high gain results in fast pressure convergence but a large error in estimated port air-mass flow. Better steady-state port air-mass flow estimates are achieved using observers with an additional state. The additional state represents an offset in the volumetric efficiency or an offset from the expected cylinder air-mass. The estimated offset can be compared to an I-part in a PI-controller and is here able to compensate for model errors caused by for example a change in volumetric efficiency. For the two observers with offset estimation, the intake manifold pressure converges to measured intake manifold pressure and they estimate the same port air-mass flow as the modeled air-mass flow into the intake manifold. Therefore these observers are better suited for port air-mass flow estimation in TC SI-engines.

4

DEVELOPMENT OF A CONTROL ORIENTED CAC MODEL

Today, the demands for lower emissions and improved fuel economy have resulted in an increased popularity of TC SI-engines. An advantage of TC SI engines is their ability to produce high torques as the turbocharger increases the intake manifold pressure and thus increases the cylinder air charge (CAC). A higher CAC allows more fuel to be injected and more torque is produced by the combustion. For high torque output conditions, the engine starts to knock and the ignition is retarded to reduce the knock. Unfortunately, this exhaust temperature increase can destroy the TWC and the turbine. To cool the exhaust gases, fuel enrichment is therefore necessary. Further, at these high torques, it is important to avoid that the maximum torque to the transmission is exceeded. As torque sensors are expensive, models of engine torque based on CAC is used instead. However, at high loads where fuel enrichment is present the traditional CAC-models can give an up to 10% error that propagates to an error in estimated torque. Here the error is reduced down to only 3% by modeling the *additional* charge cooling during fuel enrichment at high loads that also significantly improve the torque estimates.

On SI-engines, it is possible to improve the fuel economy by opening the wastegate at part load. In the previous chapter, it was shown that the exhaust manifold pressure and the cylinder air charge are influenced when the wastegate is operated. As the emissions are reduced using a three way catalyst which is only effective if the ratio of air and fuel is accurately controlled. Precise CAC estimates are therefore *required* at part load. To maintain low emissions at part load it is therefore desirable to find an improved CAC model for air-fuel ratio control that includes exhaust manifold pressure. Further, the model is

used to determine the operating conditions where the CAC is most sensitive
to exhaust manifold pressure changes. It is also used to quantify how large
exhaust manifold pressure changes that can occur in order not to exceed a
pre-determined maximum deviation from stoichiometric.

In this chapter, a speed-density based CAC model for a warmed up TC
SI-engine is developed in two steps. First, a conventional speed density CAC-
model is augmented with a model component that improves CAC estimates
during fuel enrichment. Then, an exhaust manifold pressure dependent model
component is developed. Finally both model components are merged and the
total model, which has only two parameters, is validated using a 2.3 liter tur-
bocharged SAAB 9^5 engine with wastegate. Thus, the model covers a wider
range of the TC SI engines operating region compared to models based on vol-
umetric efficiency. Finally, it is shown how the proposed CAC model improves
torque estimates based on the estimated CAC during fuel enrichment and for
different exhaust manifold pressures.

4.1   CAC and Air-Fuel Ratio

The volumetric efficiency (Heywood, 1988, p. 53) is a parameter that describes
how well the cylinder is filled with air. Using volumetric efficiency η_{vol} and the
ideal gas law the CAC can be estimated as:

$$\mathrm{CAC} = \eta_{\mathrm{vol}} \frac{p_{\mathrm{im}} V_{\mathrm{d}}}{R_{\mathrm{im}} T_{\mathrm{im}}} \tag{4.1}$$

For stationary conditions the volumetric efficiency can be determined from mea-
sured data independently of the air-fuel ratio as:

$$\eta_{\mathrm{vol}_{\mathrm{meas}}} = \frac{\frac{W_{\mathrm{a}} n_r}{N}}{\frac{p_{\mathrm{im}} V_d}{R_{\mathrm{im}} T_{\mathrm{im}}}} = \frac{W_{\mathrm{a}} n_r}{N} \frac{R_{\mathrm{im}} T_{\mathrm{im}}}{p_{\mathrm{im}} V_d} \tag{4.2}$$

Now, how does the volumetric efficiency change when the air-fuel ratio changes?
As the fuel vapor volume changes with the air-fuel ratio, it is natural to start by
considering this effect on the volumetric efficiency. If it is assumed that all fuel
enters the cylinder as vapor, which is reasonable for a warmed up engine, then
the volumetric efficiency for quasi-stationary conditions is inversely proportional
to the volume of fuel vapor (Heywood, 1988, p. 210). Therefore, the volumetric
efficiency should decrease when the air-fuel ratio decreases.

$$\eta_{\mathrm{vol}_{\mathrm{theor}}} \propto \frac{1}{1 + \frac{1}{\left(\frac{A}{F}\right)_s \lambda}} \tag{4.3}$$

In the top of Figure 4.1 this decrease is illustrated. However, when volumetric
efficiency is measured for rich conditions, shown in the bottom of Figure 4.1,
the *opposite* phenomenon occurs. This increase can not be explained by other
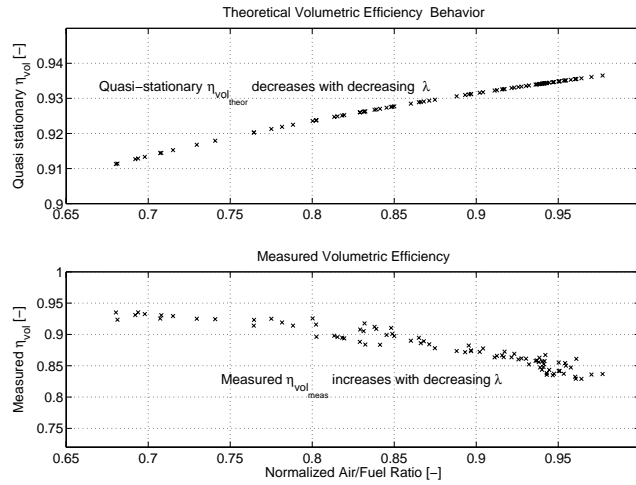
Figure 4.1: Volumetric efficiency for the conditions where the mixture is rich ($\lambda < 1$). *Top:* Theoretically the quasi-stationary volumetric efficiency should decrease with decreasing λ as the fraction of fuel vapor increases. *Bottom:* The estimated volumetric efficiency η_{vol} from measurements with various air-fuel ratios λ. Volumetric efficiency η_{vol} increases significantly for low λ.

volumetric efficiency increasing effects such as intake manifold tuning or RAM-effect. One explanation is the density increase of the charge caused by the charge cooling effect of the *additional* evaporating fuel. When the fuel vaporizes in the air, it causes the charge temperature to drop and thus the charge density to increase more than the fuel vapor volume does (Heywood, 1988, pp. 211). Taylor (1994, pp. 184), gives a similar explanation. Next, this knowledge is included in an augmented temperature model that is inserted into a CAC-model.

4.1.1 Charge Cooling Modeling

In the previous section the effect of charge cooling was pointed out as a strong candidate of the volumetric efficiency increase at rich air-fuel ratios. This means that it is important to study the temperature of the mixture of air and evaporated fuel in the intake manifold when the mixture is about to be inducted into the cylinder. Unfortunately, this temperature is difficult to measure, however the intake manifold temperature T_{im} is easy to obtain. T_{im} is measured upstream of the fuel injectors and therefore the evaporation and charge cooling process have to be described by a physically based model. When the charge cooling model is validated, the modeled CAC is compared to measured CAC for stationary conditions. If the modeled CAC, which includes the charge cooling model, coincide well with measured data the model is assumed to be correct.

In Figure 4.2 the modeling of the temperature into the cylinders start by showing a schematic of the intake manifold where the evaporating fuel and heat
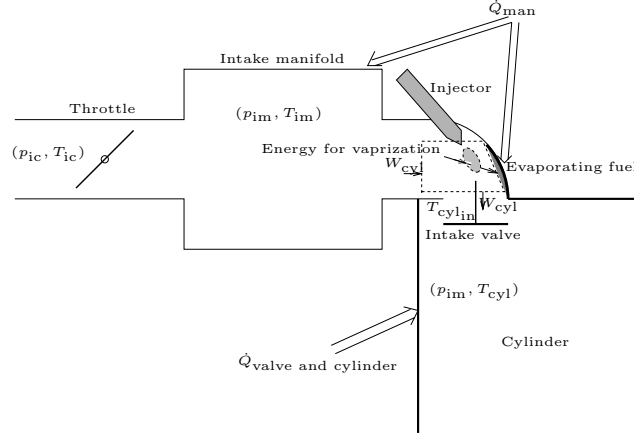
Figure 4.2: A schematic of the intake manifold with throttle and injector located close to the intake valve. To make a thermodynamical model of $T_{\text{cyl}_{\text{in}}}$ only a fraction of the intake manifold is considered. The studied control volume is marked as a dotted box. In the control volume parts of the injected fuel, x_e, evaporates. The remaining fuel evaporates, outside of the control volume, on the intake manifold walls using energy from $\dot{Q}_{\text{man}}$ and do not contribute to the temperature drop.

transfers are shown. It is assumed that parts of the injected fuel vaporize by taking energy from the surrounding air and thus cooling the charge. The rest of the fuel, which hits the wall as liquid, is vaporized as the intake manifold wall heats it. When it is time to induct the air-fuel mixture all fuel has evaporated and the charge temperature is $T_{\text{cyl}_{\text{in}}}$.

The induced mixture temperature $T_{\text{cyl}_{\text{in}}}$ is modeled using the first law of thermodynamics. This law states that the energy is conserved, that is the energy of the entering fluids into the control volume plus heat must equal the energy of the exiting fluid. The dotted box in Figure 4.2 indicates the studied control volume. Its volume is considerably smaller than the volume of the intake manifold and it is therefore assumed that the air-mass flows into and out of the control volume are the same, W_{cyl}. The temperature of the air-mass flow into the control volume is T_{im} and heat transfer to the gas inside of the control volume is not considered during fuel enrichment. The temperature of the flow out of the control volume is $T_{\text{cyl}_{\text{in}}}$. When the liquid fuel with temperature $T_{\text{f}_{\text{inj}}}$ is injected into the control volume a fraction of it, x_e on mass basis, evaporates and in the process consumes energy (heat) from the air-mass flow. The remaining fuel hits the intake manifold wall and is vaporized by heat transfer from the wall to the fuel and after the vaporization it has the same temperature as the surrounding gas, that is $T_{\text{cyl}_{\text{in}}}$. A simplified schematic of the fluid and heat transfer flows of the studied control volume are shown in Figure 4.3. The fuel flow is $W_{\text{f}} = \frac{W_{\text{cyl}}}{\lambda\left(\frac{A}{F}\right)_s}$ and h_{fv} is the heat required to vaporize the liquid. For additional nomenclature, please see Appendix A.
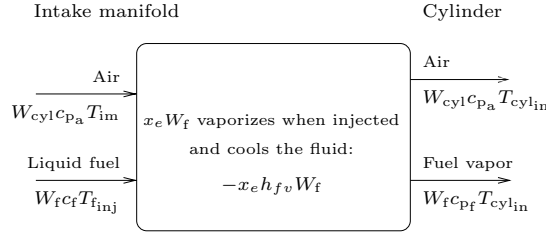
Figure 4.3: A thermodynamical model of the control volume in Figure 4.2. Fluid flows in and out of the volume are shown with their respectively temperature. It is shown that a fraction x_e, on mass basis, of the fuel evaporates in the control volume and consumes energy. All of the fuel enter the cylinder as vapor.

When the energy into the control volume is determined, the air related term is considerably larger than the fuel related term:

$$
\begin{aligned}
c_{\mathrm{f}} W_{\mathrm{f}} T_{\mathrm{f_{inj}}} &= \frac{c_{\mathrm{f}} W_{\mathrm{cyl}}}{\lambda \left(\frac{A}{F} \right)_s} T_{\mathrm{f_{inj}}} \\
c_{\mathrm{f}} &\approx 2 c_{\mathrm{p_a}} \\
c_{\mathrm{f}} W_{\mathrm{f}} T_{\mathrm{f_{inj}}} &\approx \frac{2 c_{\mathrm{p_a}} W_{\mathrm{cyl}}}{\lambda \left(\frac{A}{F} \right)_s} T_{\mathrm{f_{inj}}} = \underbrace{\frac{2}{\lambda \left(\frac{A}{F} \right)_s}}_{0.15\ldots0.26 \ll 1} c_{\mathrm{p_a}} W_{\mathrm{cyl}} T_{\mathrm{f_{inj}}}
\end{aligned}
$$

As the factor in front of $c_{\mathrm{p_a}} W_{\mathrm{cyl}} T_{\mathrm{f_{inj}}}$ is less than 0.3 together with that the fact that the fuel temperature $T_{\mathrm{f_{inj}}}$ is in the same range as the air temperature means that the fuel related term $W_{\mathrm{f}} c_{\mathrm{f}} T_{\mathrm{f_{inj}}}$ can be neglected. The energy flow into the control volume can thus be summarized as:

$$
E_{\mathrm{in}} = \underbrace{W_{\mathrm{cyl}} c_{\mathrm{p_a}} T_{\mathrm{im}}}_{\text{Air}} + \underbrace{W_{\mathrm{f}} c_{\mathrm{f}} T_{\mathrm{f_{inj}}}}_{\text{Fuel}} \approx W_{\mathrm{cyl}} c_{\mathrm{p_a}} T_{\mathrm{im}}
$$

Next, the energy necessary for the fuel vaporization in the control volume is determined. Here, a fraction x_e of the injected fuel vaporizes and consumes energy E_{vap}. This evaporation term is non-negligible as $h_{fv} = (380\ldots500)c_{\mathrm{p_a}}$ (Bauer et al., 1996, p. 238).

$$
E_{\mathrm{vap}} = x_e h_{fv} W_{\mathrm{f}}
$$

When the the energy flow out of the control volume E_{out} is determined, the fuel related term $W_{\mathrm{f}} c_{\mathrm{p_f}} T_{\mathrm{cyl_{in}}}$ is neglected using the same argument as for E_{in}.

$$
E_{\mathrm{out}} = W_{\mathrm{cyl}} c_{\mathrm{p_a}} T_{\mathrm{cyl_{in}}} + W_{\mathrm{f}} c_{\mathrm{p_f}} T_{\mathrm{cyl_{in}}} \approx W_{\mathrm{cyl}} c_{\mathrm{p_a}} T_{\mathrm{cyl_{in}}}
$$

The energy balance becomes:

$$
\begin{aligned}
E_{\mathrm{in}} - E_{\mathrm{vap}} &= E_{\mathrm{out}} \\
W_{\mathrm{cyl}} c_{\mathrm{p_a}} T_{\mathrm{im}} - x_e h_{fv} W_{\mathrm{f}} &= W_{\mathrm{cyl}} c_{\mathrm{p_a}} T_{\mathrm{cyl_{in}}}
\end{aligned}
$$

Now, $T_{\text{cyl}_{\text{in}}}$ can be solved for:

$$T_{\text{cyl}_{\text{in}}} = \frac{W_{\text{cyl}}c_{\text{p}_{\text{a}}}T_{\text{im}} - x_e h_{fv} W_{\text{f}}}{W_{\text{cyl}}c_{\text{p}_{\text{a}}}} = T_{\text{im}} - \frac{x_e h_{fv}}{\lambda\left(\frac{A}{F}\right)_s c_{\text{p}_{\text{a}}}} = T_{\text{cyl}_{\text{in}}}(T_{\text{im}}, x_e, \lambda) \quad (4.4)$$

Eq. (4.4) describes the effect of charge cooling over all the engine's operating regime as a function of T_{im}, x_e, and λ, where all but x_e are known. The fraction of evaporated fuel, x_e, is described by the evaporation curve and for temperatures above 30°C it is almost linear in temperature (Guzzella and Onder, 2004, p. 56). In Figure 4.4 stationary measurements of the intake manifold temperature is shown as a function of $\frac{1}{\lambda}$ and it is clear that $T_{\text{im}} - 310$ can be approximated by a linear function of $\frac{1}{\lambda}$. Further it can be seen that the intake manifold temperature is above 30°C when fuel enrichment is present and thus the fraction of evaporated fuel can be expressed as $x_e = x_{e1}\frac{1}{\lambda} = x_e(\frac{1}{\lambda})$. Now, the temperature of the charge entering the cylinder can be expressed as
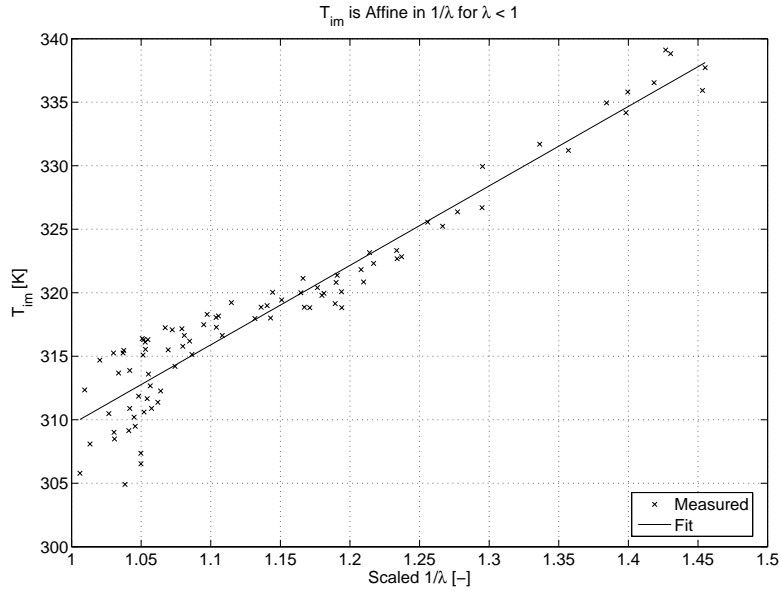
Figure 4.4: For rich mixtures the intake manifold temperature is affine in $\frac{1}{\lambda}$.

a function of T_{im} and $\frac{1}{\lambda}$:

$$T_{\text{cyl}_{\text{in}}}(T_{\text{im}}, \frac{1}{\lambda}) = T_{\text{im}} - \frac{x_e(\frac{1}{\lambda})h_{fv}}{\lambda\left(\frac{A}{F}\right)_s c_{\text{p}_{\text{a}}}} \quad (4.5)$$

As fuel enrichment normally is only present at high loads, that are high intake manifold pressures, only the *additional* cooling compared to stoichiometric is

considered. Now, the additional cooling, for non stoichiometric conditions, can then be expressed as:

$$T_{\text{Additional cooling}} = T_{\text{cyl}_{\text{in}}}\left(T_{\text{im}}\left(\frac{1}{\lambda}\right), \lambda, x_e\left(\frac{1}{\lambda}\right)\right) -$$

$$T_{\text{cyl}_{\text{in}}}\left(T_{\text{im}}\left(\frac{1}{\lambda}\right), \lambda, x_e\left(\frac{1}{\lambda}\right)\right)\bigg|_{\lambda=1} = \underbrace{x_{e_1}\frac{h_{fv}}{c_{\text{p}_a}\left(\frac{A}{F}\right)_s}}_{\text{Constant} = C_1}\left(\frac{1-\lambda^2}{\lambda^2}\right) \quad (4.6)$$

In Eq. (4.6) the factors $x_{e_1}\frac{h_{fv}}{c_{\text{p}_a}}\left(\frac{A}{F}\right)_s$ are lumped together to one parameter C_1. The next step is to include the charge cooling model in a CAC-model, where it describes the *additional* temperature drop in intake manifold temperature for rich mixtures. The total model is then validated using measured CAC-data.

4.1.2 CAC Model with Charge Cooling

In Hendricks et al. (1996) an affine parameterization of the product $\eta_{\text{vol}}p_{\text{im}}$ in Eq. (4.1) is introduced which accurately describes CAC for stoichiometric conditions:

$$\text{CAC} = (a_1 p_{\text{im}} + a_0)\frac{V_{\text{d}}}{R_{\text{im}}T_{\text{im}}} \quad (4.7)$$

To include the density increasing effect of the additional charge cooling, the temperature drop described by Eq. (4.6) is subtracted from the measured T_{im}. The temperature T_{im} in Eq. (4.7) is thus replaced by

$$T_{\text{im,new}} = T_{\text{im}} - T_{\text{Additional cooling}} = T_{\text{im}} - C_1\frac{1-\lambda^2}{\lambda^2} \quad (4.8)$$

By inserting Eq. (4.8) in Eq. (4.7) the augmented CAC-model becomes:

$$\text{CAC} = (a_1 p_{\text{im}} + a_0)\frac{V_{\text{d}}}{R_{\text{im}}\left(T_{\text{im}} - C_1\frac{1-\lambda^2}{\lambda^2}\right)} \quad (4.9)$$

In Eq. (4.9) the parameters C_1, a_0, and a_1 are identified using a nonlinear least-squares technique, the Matlab-function *lsqcurvefit*, for stationary data.

4.1.3 Results Using the Charge Cooling Model

A comparison between measured and estimated CAC using Eq. (4.9) with and without the proposed cooling model Eq. (4.8) is shown in Figure 4.5. By including the charge cooling effect the stationary error when fuel enrichment is present at high loads is successfully reduced from 10% down to 2–3%. The magnitude of the resulting temperature drop is discussed next.

In Figure 4.6 the model is applied to measured engine data and the estimated additional temperature drop is less than 32 K. This value is compared to the
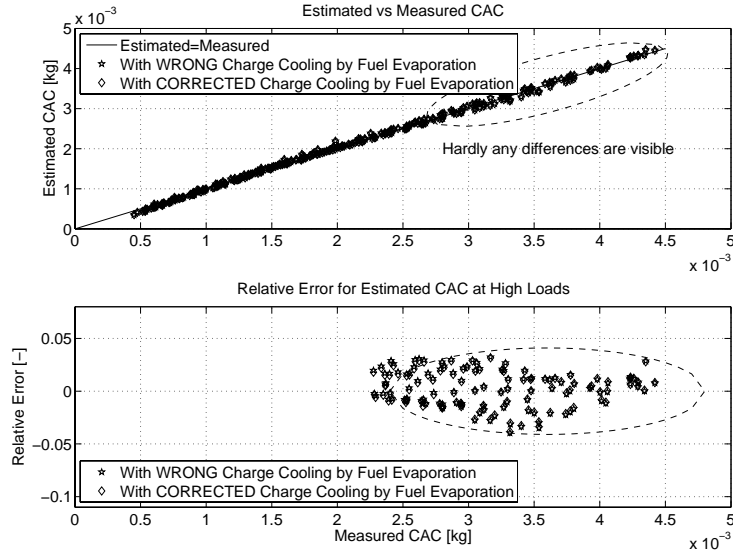
Figure 4.5: *Top:* Measured CAC for stationary engine data is compared to estimated CAC with charge cooling, Eq. (4.9), and estimated CAC without charge cooling, Eq. (4.7). When enrichment is present, the model without charge cooling by fuel evaporation gives up to 10% too low estimates. *Bottom:* With the modeled effect of charge cooling by fuel evaporation the error in CAC is substantially reduced from 10% down to 2–3% for higher CACs.

expected temperature drop at *stoichiometric* conditions for gasoline, with $h_{fv} = (380 \dots 500)c_{\mathrm{P_a}}$ (Bauer et al., 1996, p. 238), which would result in a temperature drop of at least 22 K when all fuel has evaporated. For a theoretical air-fuel ratio of $\lambda = 0.5$ the expected temperature drop would be 53K. As the maximum modeled additional temperature drop is in-between these theoretical values the assumptions of the fraction of evaporated fuel seems correct. The temperature drop depends on the gasoline quality and here winter grade gasoline was used which have a higher volatility (Bauer et al., 1996, p. 233 and p. 238), and may have a higher content of alcohols. These factors contribute to the significant temperature drop when fuel enrichment is present at high loads. With this approach the main advantages are:

- The additional temperature drop for rich mixtures caused by charge cooling at high loads can be compensated using an augmented temperature model.

- Only one additional parameter C_1 is introduced by the augmented model.

It is therefore strongly recommended to include the charge cooling effect in a CAC-model for TC-engines.
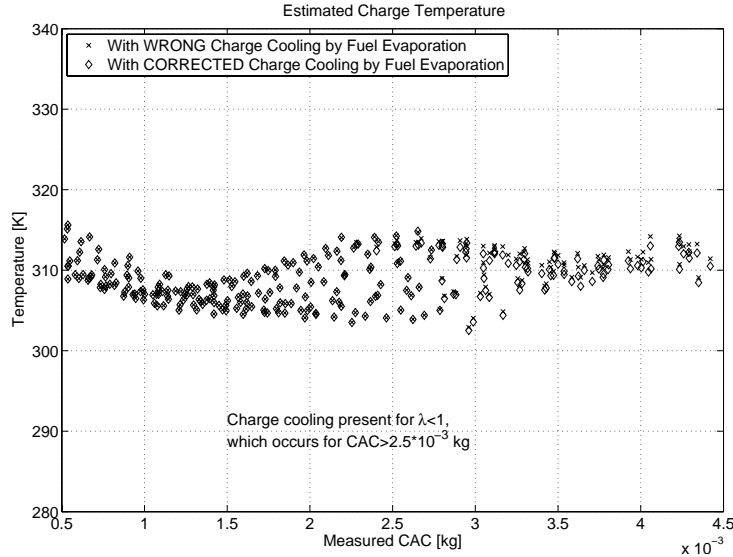
Figure 4.6: Measured intake manifold temperature and modeled temperature with the charge cooling model. The data is measured at stationary conditions. The maximum modeled temperature drop is 32K or 10%.

4.2 CAC and Exhaust Pressure Changes

It has been shown in Eriksson et al. (2002a) that fuel economy can be improved if the wastegate is opened at part load. The fuel economy is improved as the opening of the wastegate reduces the pumping loss and therefore increases the engine efficiency. At part load the engine is running stoichiometricly and with active wastegate control it is important to make precise CAC estimates to maintain a stoichiometric mixture and thus low emissions. The necessary accuracy of the CAC estimate is approximately 2% to 3% (Kiencke and Nielsen, 2000, pp. 69).

In Figure 4.7 an engine experiment at constant engine speed is shown, where the wastegate is opened and closed. From Figure 4.7 it is clear that the CAC estimates made using the mapped volumetric efficiency are incorrect for open wastegate due to the stationary difference between measured and mapped volumetric efficiency. The stationary volumetric efficiency difference is caused by the exhaust manifold pressure change when the wastegate is opened, which has been seen in for example Chapter 3. The reduced exhaust manifold pressure influences the volumetric efficiency as the mass of residual gases in the cylinder depends on the exhaust manifold pressure. This raises the following questions:

1. For what operating condition is CAC most sensitive to exhaust manifold pressure changes?
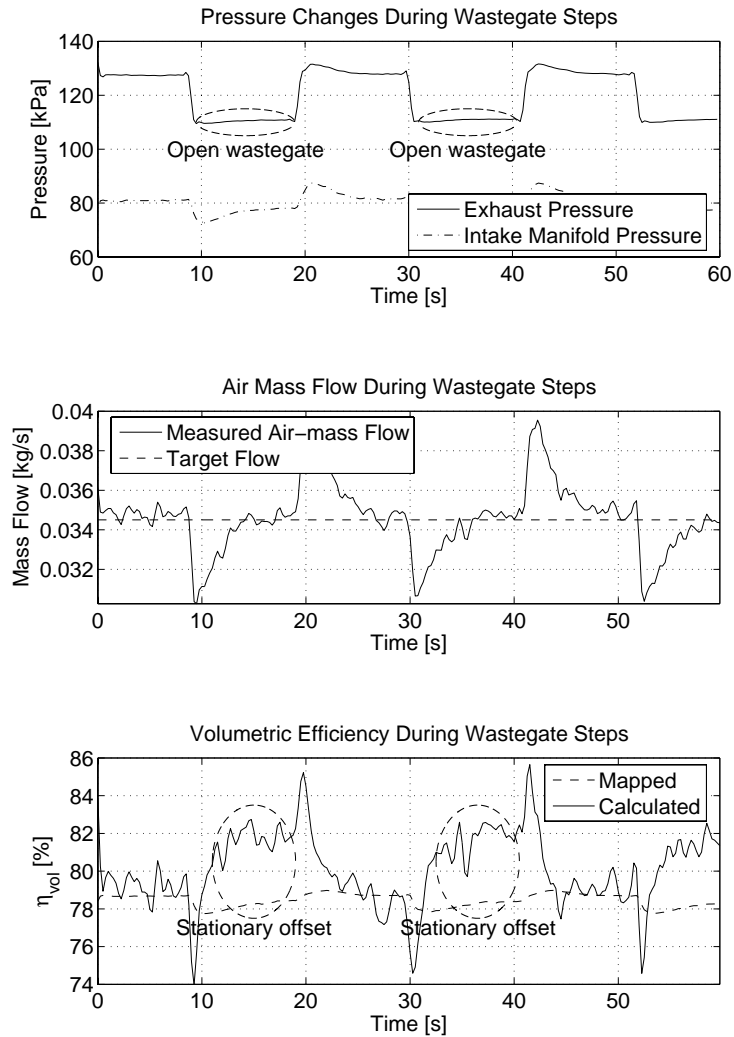
Figure 4.7: An engine experiment performed at constant speed and constant air-mass flow. *Top:* Pressure changes in exhaust system, and intake manifold pressure during manual opening/closing of the wastegate. *Center:* Measured air-mass flow, W_a. As the wastegate is opened the air-mass flow decreases momentarily while the air-mass controller opens the throttle. *Bottom:* Mapped and calculated volumetric efficiency using Eq. (4.2). The calculated volumetric efficiency is only valid at stationary conditions which are marked with ellipses. When the wastegate is *open* the mapped volumetric efficiency is incorrect. The change is $(82 - 78)/78 \approx 5\%$ which would result in a 5% CAC error.

2. Given a desired accuracy of the estimated CAC: How large exhaust manifold pressure changes can be tolerated with an exhaust manifold pressure independent model?

To answer these questions a CAC sensitivity analysis is performed. It is performed using an ideal model of CAC (Eriksson et al., 2002a) that includes exhaust manifold pressure, which is inspired by Fox et al. (1993). The model is then augmented with the charge cooling effect described in the previous sections. The total model is validated in two steps. First, it is validated for stationary data where it is compared to a standard volumetric efficiency based CAC model Eq. (4.7). Then the proposed model and a standard volumetric efficiency based CAC model Eq. (4.7) are compared using varying exhaust manifold pressures. The comparison shows that the exhaust manifold pressure dependent model accurately describes the CAC for both stationary conditions and for varying exhaust manifold pressure. Its ability to describe the magnitude of the CAC change when the exhaust manifold pressure varies makes it very suitable as a base of a sensitivity analysis.

4.2.1 CAC Model with Exhaust Manifold Pressure Dependency

The model's purpose is primarily CAC estimation for air-fuel ratio control where it is possible to include the effects of the exhaust manifold pressure. Here the modeled CAC is based on an estimate of the inducted volume of air V_a. On turbocharged engines with fix valve timing it easy to estimate the volume of inducted air, V_a as the valve overlap is small which enables a simplified gas exchange process to be used. As the valve overlap is small, the backflow is zero. In Figure 4.8 a simplified gas exchange model illustrates how the volume of inducted air V_a is estimated by subtracting the residual gas volume and the volume of evaporated fuel V_f from the total volume at intake valve closing (IVC). In the model IVC occurs at bottom dead center (BDC) and exhaust valve closing (EVC) occurs at top dead center (TDC).

$$\text{CAC} = \frac{p_\text{im}}{R_\text{im} T_\text{im}} V_a = \frac{p_\text{im}}{R_\text{im} T_\text{im}} \overbrace{C_{\eta_\text{vol}} \frac{1}{1 + \frac{1}{\lambda \left(\frac{A}{F} \right)_s}} \left(\frac{r_c - \left(\frac{p_\text{em}}{p_\text{im}} \right)^{\frac{1}{\gamma_e}}}{r_c - 1} \right) V_\text{d}}^{V_\text{a}} \quad (4.10)$$
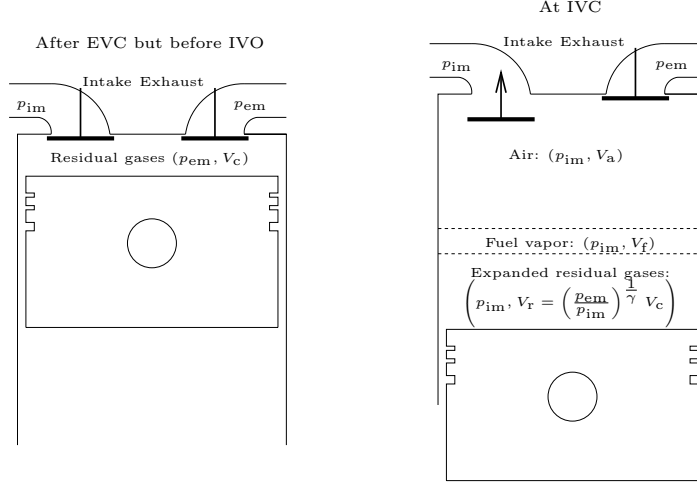
Figure 4.8: An illustration of the idealized induction model to determine the volume of inducted air V_a. *Left:* Prior to the inductions starts, at exhaust valve closing (EVC), the residual gases at pressure p_{em} fill the clearance volume V_c. *Right:* At the end of the intake stroke, when the intake valve is about to close, the volume is $V_d + V_c$ and the residual gases have expanded from p_{em} to p_{im}. At IVC the pressure is p_{im} in all of the volumes. The volume of each component is schematically shown separated by dashed lines and $V_a = V_d + V_c - V_r - V_f$.

A more detailed derivation of the model below is found in Appendix C. Next, the effect of charge cooling by fuel evaporation is included by replacing T_{im} with Eq. (4.8):

$$\text{CAC} = \frac{p_{im}}{R_{im}\left(T_{im} - \underbrace{C_1 \frac{1-\lambda^2}{\lambda^2}}_{\text{Charge cooling}}\right)} C_{\eta_{vol}} \frac{\left(r_c - \left(\frac{p_{em}}{p_{im}}\right)^{\frac{1}{\gamma_e}}\right) V_d}{\left(1 + \frac{1}{\lambda\left(\frac{A}{F}\right)_s}\right)(r_c - 1)} \tag{4.11}$$

The total model given by Eq. (4.11) includes both the exhaust manifold pressure and also the effect of fuel enrichment at high engine loads which was described in the previous section. In the model, there are only two tuning parameters and these are the pumping parameter $C_{\eta_{vol}}$ and the effect of charge cooling by fuel evaporation C_1.

CAC Model Validation

Validation of the CAC model is performed in two steps: First it is validated using stationary measured data and then for data with different exhaust manifold pressures.

Model Validation Using Stationary Data

Validation is performed for stationary conditions by comparing stationary measured CAC to modeled CAC. Two models are used: The exhaust manifold pressure dependent CAC and the CAC based on a parameterization of the volumetric efficiency, Eq. (4.9). The purposes of this validation are to show:

1. That the model including exhaust manifold pressure has the same accuracy, for a nominal wastegate setting, as models based on volumetric efficiency such as Eq. (4.9).

2. That the model including exhaust manifold pressure better describes CAC when the wastegate is opened, or when it is not in its nominal setting, than models based on mapped/parameterized volumetric efficiency such as Eq. (4.9).

In the validation, a *different dataset* has been used compared to the tuning data. The validation data is measured *three years later* than the tuning dataset and with a different gasoline quality. For both datasets, the wastegate is controlled to a nominal opening by the ECU, which means that it is closed for most of the points.

In Figure 4.9 it is shown that the exhaust manifold pressure dependent model shows about the same high accuracy as the model using parameterized volumetric efficiency. In terms of root mean square error, the p_{em} dependent model has an error of $1.8 \cdot 10^{-3}$ compared to $1.9 \cdot 10^{-3}$ for the parameterized volumetric efficiency. As the p_{em} dependent model has one parameter less, the stationary accuracy is very good.

Model Validation Using Different Exhaust Manifold Pressures

Here, measured engine data with different exhaust manifold pressures are used to test how well the models describe the change in CAC. It has not been possible to measure the transient CAC and therefore the estimates are compared to measured air-mass flow after the air filter. This means that the comparison in Figure 4.10 is only valid for stationary conditions due to the filling and emptying of the intake system. The locations of the stationary conditions when the wastegate is open have been marked using ellipses. Both models have been tuned for nominal wastegate settings, which in this case is closed wastegate.

In Figure 4.10 the wastegate is opened and closed several times to vary the exhaust manifold pressure. The p_{em} dependent model Eq. (4.11) better describes the CAC *change* than the parameterized volumetric efficiency, Eq. (4.9). As the exhaust manifold pressure dependent CAC model is able to better describe CAC for conditions where it has not been tuned it is study how sensitive the CAC is to the exhaust manifold pressure changes.
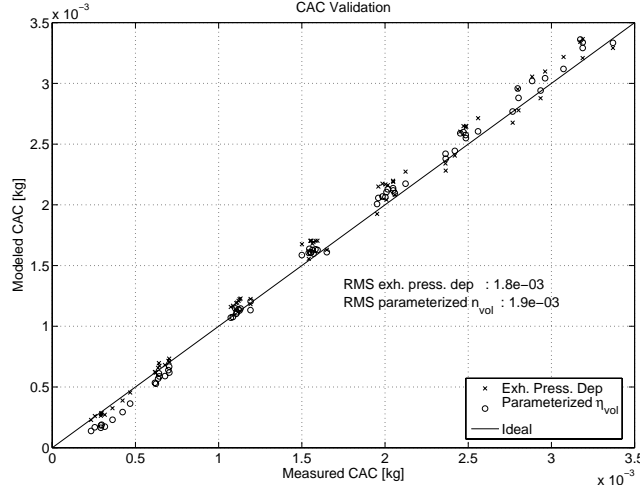
Figure 4.9: Validation of the exhaust manifold pressure dependent CAC model using stationary data. It is compared to a model using parameterized volumetric efficiency and measured data. The accuracy of Eq. (4.11) is in the same magnitude as the model using parameterized volumetric efficiency, Eq. (4.9).

4.2.2   CAC Sensitivity Functions

Now an accurate CAC model exists that considers exhaust manifold pressure. This model can therefore be used to study the CAC sensitivity to changes in exhaust manifold pressure using sensitivity functions. The CAC sensitivity to the parameter x is defined as:

$$\frac{\frac{\partial \text{CAC}}{\partial x}}{\frac{\text{CAC}}{x}}$$

CAC Sensitivity to Exhaust Manifold Pressure Changes

The derivative of Eq. (4.11) with respect to the exhaust manifold pressure is determined and then divided by Eq. (4.11) and p_{em} which yields the sensitivity to exhaust manifold pressure changes:

$$\frac{\frac{\partial \text{CAC}}{\partial p_{\text{em}}}}{\frac{\text{CAC}}{p_{\text{em}}}} = -\left(\frac{p_{\text{em}}}{p_{\text{im}}}\right)^{\frac{1}{\gamma_e}} \frac{1}{\gamma_e \left(r_c - \left(\frac{p_{\text{em}}}{p_{\text{im}}}\right)^{\frac{1}{\gamma_e}}\right)} \tag{4.12}$$

There are two properties of the sensitivity function Eq. (4.12) that makes the results from the analysis general. First, it does not include any specific engine parameters that require tuning to measured data. Second, it only depends on the *pressure ratio* $\frac{p_{\text{em}}}{p_{\text{im}}}$.

   The minus sign in Eq. (4.12) shows that an increase in exhaust manifold pressure decrease CAC. In Figure 4.11 the sensitivity function is evaluated for
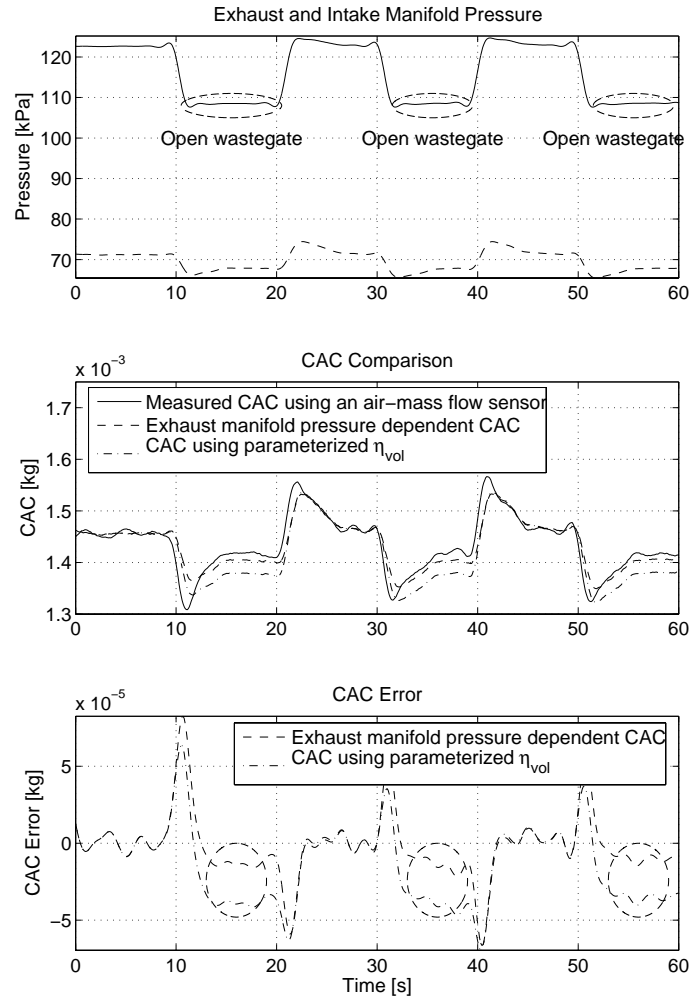
Figure 4.10: Validation using wastegate opening/closing steps. *Top:* Intake manifold pressure and exhaust manifold pressure varies depending on whether the wastegate is open or closed. *Center:* The estimated CAC compared to measured CAC. To better study the estimated *change* in CAC when the wastegate opens the stationary errors for closed wastegate have been removed for both models by adding a constant offset. The model based on parameterized volumetric efficiency underestimates CAC when the wastegate is open. *Bottom:* The CAC error of the exhaust manifold pressure dependent model is smaller.

five fix intake manifold pressures. From the figure it is clear that the CAC is most sensitive to changes in p_{em} for low intake manifold pressures, that is part load conditions. This is a very important observation since at part load, where the engine is run stoichiometricly, it is vital to make precise CAC-estimates. For part load conditions, it is also most beneficial to improve the fuel economy by opening the wastegate that changes the exhaust manifold pressure. Therefore, to estimate the expected CAC change when the wastegate is opened it is necessary to determine the magnitude of the exhaust pressure drop.
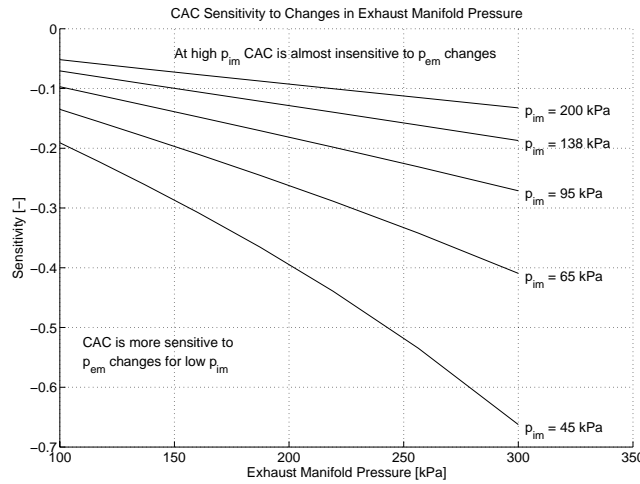
Figure 4.11: The figure shows that CAC decreases with increasing exhaust manifold pressure for a given intake manifold pressure. CAC is almost insensitive to p_{em}-changes at high intake manifold pressures.

4.2.3 Exhaust Manifold Pressure Drop when Wastegate is Opened

The maximum achievable pressure change when the wastegate goes from nominal to open position was estimated by measuring the exhaust manifold pressure when the engine was running in stationary points with open and nominal wastegate. Then third order polynomials in the air-mass flow were fitted to the measured exhaust manifold pressures. By taking the difference between the polynomials the pressure drop at a given air-mass flow can be estimated. In Figure 4.12 the exhaust manifold pressure drop is shown for various air-mass flows. The maximum possible pressure drop is slightly more than 20%.

4.2.4 CAC Change when the Wastegate is Opened

Now a function to determine the magnitude of the CAC change is given by Eq. (4.12) provided that exhaust manifold pressure drop is known. The ex-
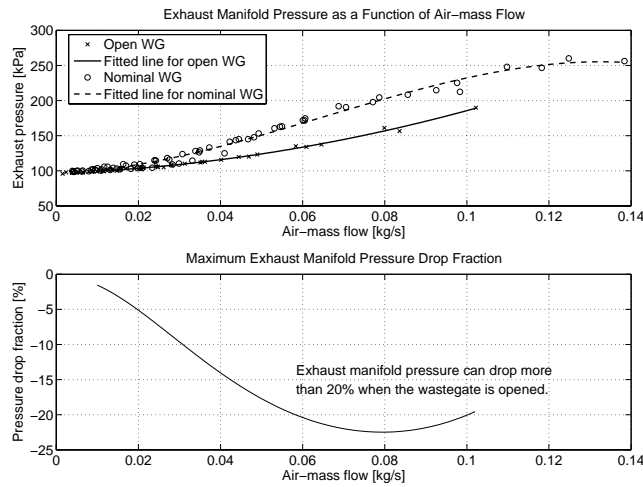
Figure 4.12: Stationary exhaust manifold pressures for different air-mass flows with open and nominal wastegate. *Top:* The exhaust manifold pressures can successfully be described using third order polynomials in air-mass flow. *Bottom:* The exhaust manifold pressure drop when the wastegate is fully opened in percent as a function of air-mass flow. It is calculated using the difference between the fitted lines in the top plot. For this engine the exhaust manifold pressure drops more than 20% when the wastegate is opened.

haust manifold pressure drop is determined by inserting measured data from an engine map with *nominal wastegate setting* into the polynomials for the exhaust manifold pressure for open and closed wastegate. The resulting CAC change is then determined and shown in Figure 4.13. As the boost pressure drops to virtually zero when the wastegate is opened, only points with intake manifold pressure lower than ambient are shown. For the engine map the maximum CAC change would be 5%, which corresponds very well to the measured results in Figure 4.7.

The Necessity of Exhaust Manifold Pressure for CAC Estimation

The base for this investigation is that the necessary accuracy of air-fuel ratio controllers is 2% to 3% (Kiencke and Nielsen, 2000, pp. 69) during stoichiometric conditions. In Figure 4.13 it is shown that during part load, where it is motivated to open the wastegate to improve the fuel economy, the CAC changes up to 5% for the points in the ellipsis. This means that a CAC-estimator without knowledge of exhaust manifold pressure is not sufficiently accurate, that is controllers based on mapped volumetric efficiency.
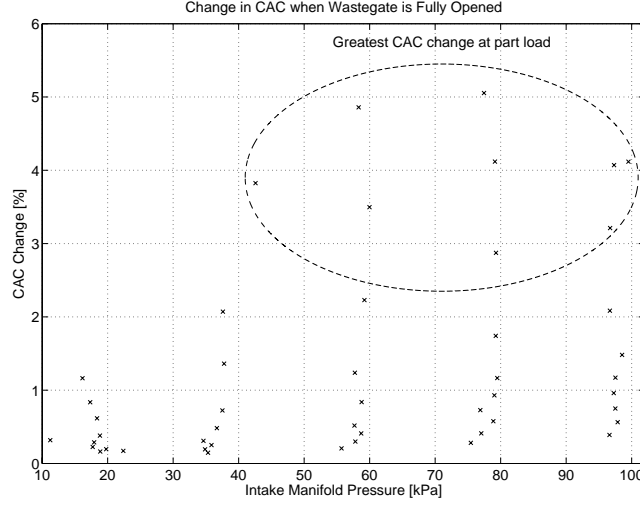
Figure 4.13: Estimated CAC change when the wastegate goes from nominal to fully open for mapped engine data. By applying the pressure drop fraction from Figure 4.12 the change in CAC is estimated using Eq. (4.12). At part load there can be an up to 5% CAC increase.

Maximum Tolerable Pressure Drop For Volumetric Efficiency Based CAC Methods

Since CAC models that relies on mapped or parameterized volumetric efficiency are unaware of the exhaust manifold pressure it is important to estimate how large exhaust manifold pressure drops that can occur in order to keep the CAC error within a certain limit. For a given exhaust manifold pressure drop $\Delta p_{\text{em}_{\text{drop}}}$ the change in CAC is approximated by:

$$\frac{\frac{\partial \text{CAC}}{\partial p_{\text{em}}}}{\text{CAC}} \Delta p_{\text{em}_{\text{drop}}} = \text{CAC change in percent}$$

Thus for a given limit on the CAC change the maximum exhaust manifold pressure drop $\Delta p_{\text{em}_{\text{drop}}}$ can be solved. Here it is calculated for stationary operating points under the assumption that $\frac{\partial \text{CAC}}{\partial p_{\text{em}}}$ is constant when the pressure drop is calculated. Figure 4.14 shows the maximum $\Delta p_{\text{em}_{\text{drop}}}$ which can be occur without changing CAC more than the specified limit.

Example 4.1

The engine is running at part load with $p_{\text{im}} = 60$ kPa and the maximum acceptable CAC error is 3%. The maximum exhaust manifold pressure drop that can be accepted and still keep the CAC change lower than 3% is found by following the 3% "line" in Figure 4.14. The maximum $\Delta p_{\text{em}_{\text{drop}}}$ is estimated to 20 kPa.
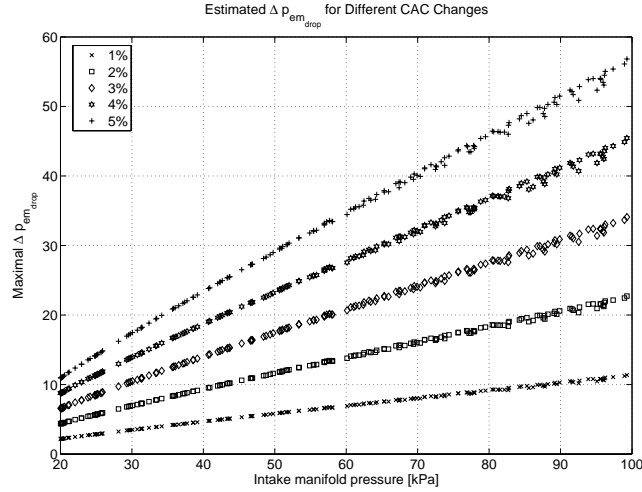
Figure 4.14: Estimated maximal $\Delta p_{\mathrm{em_{drop}}}$ until the CAC changes more than the specified limit.

4.2.5 Results of CAC Exhaust Manifold Pressure Sensitivity Analysis

Using sensitivity analysis it has been investigated how the exhaust manifold pressure influences CAC. From the sensitivity analysis, there are mainly two results:

- Sensitivity to changes in exhaust manifold pressure are most significant at part load conditions.

- With active wastegate control at part load the pressure drop when the wastegate is opened results in a CAC change of up to 5%. This is not properly described by an exhaust manifold pressure independent CAC model. Thus, a CAC model with included exhaust pressure dependency is necessary for accurate CAC estimation on TC engines with wastegate.

These results are general as the sensitivity analysis, Eq. (4.12), does not include any engine specific parameters that require tuning to measured data.

4.3 The Proposed CAC Model Improves Torque Estimates

Engine torque can be well approximated, using an affine function in CAC, for stationary conditions over a wide operating region.

$$T_{q_{cs}} = t_1 \mathrm{CAC} - t_2 \tag{4.13}$$

Figure 4.15 shows the estimated $T_{q_{cs}}$ when t_1 and t_2 has been fitted to measured CAC. This simple model is used to show that the modeled torque from
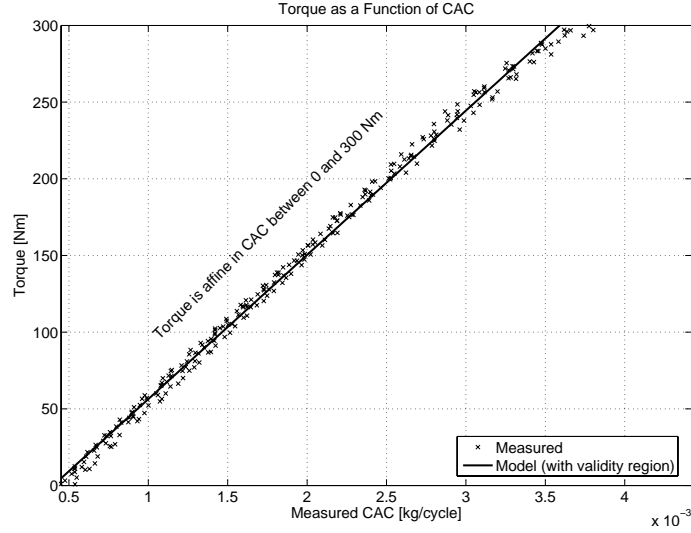
Figure 4.15: *Left:* Measured torque and modeled as a function of measured air-mass/cycle (CAC). The model is valid for a wide range of the engines operating region.

estimated CAC using the proposed CAC model gives better torque estimates when compared to CAC estimates from a conventional speed-density method. The conventional CAC model is represented by Eq. (4.7), which parameters are tuned for stoichiometric conditions and nominal wastegate setting. This model is compared to the proposed model Eq. (4.11) for two conditions: First when fuel enrichment is present and then for part load operation with open wastegate. In the comparison, the parameters t_1 and t_2 are fix, i.e. *not re-tuned* for each model.

4.3.1   Torque Estimates During Fuel Enrichment

Here the torque estimates are validated for stationary conditions when fuel enrichment is present, that is high loads. By inserting the modeled CAC, from Eq. (4.11) and Eq. (4.7) respectively into the torque model Eq. (4.13) the resulting torque estimates are shown in Figure 4.16. The torque model's root mean square errors are 8.5 Nm when the CAC estimates from the proposed model Eq. (4.11) is used and 11.1 Nm when the parameterized volumetric efficiency without charge cooling Eq. (4.7) is used. The root mean square error of the torque estimates is thus 30% higher when the charge cooling is excluded for loads between 180 Nm and 300 Nm. It is therefore essential to include the charge cooling effect to reduce torque estimation errors at high loads.
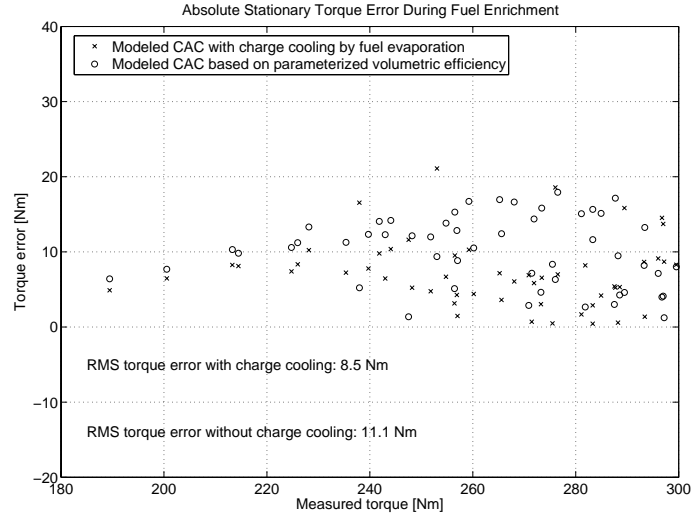
Figure 4.16: Absolute torque model errors using Eq. (4.13) and CAC models with and without charge cooling. Using the proposed CAC model, Eq. (4.11), with charge cooling and exhaust manifold pressure dependency the torque estimates are significantly improved.

4.3.2 Torque Estimates For Different Wastegate Settings

To verify the influence of changing exhaust backpressure on modeled torque from estimated CAC, a dataset with open wastegate was used. For this dataset, the CAC is estimated using the models from Eq. (4.7) and Eq. (4.11) and then the torque is determined using the model in Eq. (4.13). The resulting torque estimates are shown in Figure 4.17. The root mean square errors of the torque estimates are 6.4 Nm using the CAC model Eq. (4.11) and 12.3 Nm using the parameterized volumetric efficiency Eq. (4.7). This means that the root mean square error is more than 90% higher for the model without exhaust pressure dependency. Thus, it is beneficial to include the exhaust manifold pressure in the CAC model when it is to be used for torque estimation.

4.4 Results

Cylinder air charge (CAC) estimation have been studied for turbocharged SI-engines with emphasis on two topics: Fuel enrichment at high loads and varying exhaust manifold pressure. The objective is to investigate whether standard models based on volumetric efficiency can be used or how improvements can be made to find a good model for control and diagnosis.

At high loads where rich air-fuel ratios are used, the additional fuel influences CAC and standard models give an error of up to 10%. The error is caused by the charge cooling effect that the fuel has when it evaporates and thus
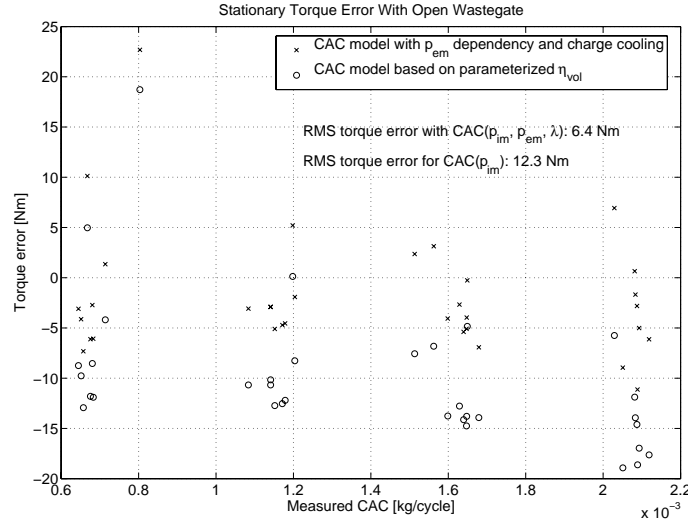
Figure 4.17: Engine torque estimation error for stationary data with open wastegate. It is clear that the torque error for the exhaust pressure dependent CAC model is considerably lower.

increases the charge density. The charge cooling effect is modeled and only one additional parameter is introduced by the model. A standard CAC model is then augmented with the charge cooling model. With the augmented CAC model, the estimation error at rich conditions is reduced from 10% down to 3%.

CAC depends on the exhaust manifold pressure and the exhaust manifold pressure can drop up to 20% when the wastegate is opened. Standard volumetric efficiency based CAC models do not capture this exhaust manifold pressure dependency. A CAC model that includes exhaust manifold pressure is therefore examined and it shows good agreement with measured data even for operating conditions where it has not been tuned. Using the model a CAC sensitivity analysis is performed and it can be concluded that:

- Exhaust manifold pressure influences CAC at most during part load conditions.

- It is necessary to include the exhaust manifold pressure in the CAC model to estimate CAC with an error less than 3% at part load.

When the exhaust manifold pressure dependent CAC model is augmented with the charge cooling model, the total model is able to describe CAC with changing exhaust manifold pressure as well as it describes CAC during fuel enrichment. This was illustrated using a torque model based on estimated CAC. With the suggested CAC model the estimated errors at high loads and with open wastegate were significantly reduced. As the model is able to estimate CAC over a wide range of operating conditions it is therefore highly suitable for CAC estimation for control and diagnosis of turbocharged SI-engines.

Exhaust Manifold Pressure Estimation

Leaks before the first oxygen sensor can result in increased emissions and a defective wastegate can cause expensive damages to the turbine if it exceeds its maximum speed. All of these issues are related to the exhaust manifold pressure. Knowledge of the exhaust manifold pressure is therefore an important tool for diagnosis of the turbine, wastegate, and for leakage detection before the first oxygen sensor (Andersson and Eriksson, 2002). Normally, the exhaust manifold pressure is not measured due to the high temperatures in the exhaust system and the extra cost of an additional sensor. Thus, it is desirable to estimate the exhaust manifold pressure using information from available sensors. A challenge is that all engine sensors, except the oxygen sensor(s), are located on the intake side.

Exhaust manifold pressure and temperature have successfully been estimated on naturally aspirated (NA) engines using mean value models (Maloney and Olin, 1998; Fons et al., 1999). These models rely on the assumption that the exhaust manifold pressure is the result of a mass-flow through a fix restriction. In NA engines the flow restriction on the exhaust side can be can be accurately modeled using this assumption (Eriksson et al., 2001). On TC-engines the wastegate acts as a *variable* restriction, which means that the models successfully used for NA-engines can not be applied directly for exhaust manifold pressure estimation. Further, the position of the wastegate is not fully known which makes exhaust manifold pressure estimation a challenging task.

To estimate the absolute exhaust manifold pressure on a turbocharged engine a two-component model is introduced. The model is based on a separation of the exhaust manifold pressure into two parts, one nominal which is a function

of the air-mass flow and one offset from the nominal pressure. No additional sensors in the exhaust system are needed by the estimator after calibration. Only the following sensors are required: ambient pressure p_a, air-mass flow W_a, intake manifold pressure p_im and temperature T_im, and air-fuel ratio λ. These signals are available on many production engines.

5.1 System Overview

In Figure 5.1 a brief system overview of *relevant* parts of the engine and intake system is shown. For a description of the symbols used, please see the nomenclature in Appendix A.

   In Figure 5.1 the air-mass flow through the air-filter is *measured* by a sensor W_a. The air-mass flow through the engine is normally restricted by the throttle that is controlled by the driver. The port air-mass flow denoted W_cyl is a product of the cylinder air charge, CAC and the engine speed, that is $W_\mathrm{cyl} = \mathrm{CAC}\frac{N}{n_r}$. For stationary conditions W_cyl equals W_a. CAC depends on, among others, the exhaust manifold pressure p_em which in turn depends on the wastegate setting. Normally, the wastegate setting is determined by the ECU and this is referred to as a *nominal* wastegate setting or nominal operating conditions. To make rapid wastegate steps of high amplitude, an additional manual wastegate actuator is installed on the engine.

5.2 Exhaust Pressure Model

The basic idea behind the exhaust manifold pressure model is that p_em can be separated into two components, one nominal exhaust pressure $p_\mathrm{em_{nom}}$ and one offset $p_\mathrm{em_\Delta}$ from the nominal pressure. Nominal exhaust manifold pressure is the exhaust manifold pressure when the wastegate is controlled by the ECU and *not* manually operated.

$$p_\mathrm{em} = p_\mathrm{em_{nom}} + p_\mathrm{em_\Delta} \tag{5.1}$$

At nominal operating conditions $p_\mathrm{em_\Delta}$ is zero. This partition is also illustrated using a resistor analogy in Figure 5.2.

5.2.1 Nominal Exhaust Pressure Model

Exhaust manifold pressure for nominal conditions $p_\mathrm{em_{nom}}$ can be expressed either using a map or a polynomial in air-mass flow (Bergström and Brugård, 1999; Pettersson, 2000; Eriksson et al., 2002b). Here the exhaust manifold pressure drop over the muffler, turbine, and wastegate is modeled as a first order polynomial in air-mass flow with k_1 and k_2 as parameters. To get an absolute exhaust manifold pressure estimate, the ambient pressure p_a is added to the expected pressure drop:

$$p_\mathrm{em_{nom}} = p_\mathrm{a} + k_1 W_\mathrm{at} + k_2 \tag{5.2}$$
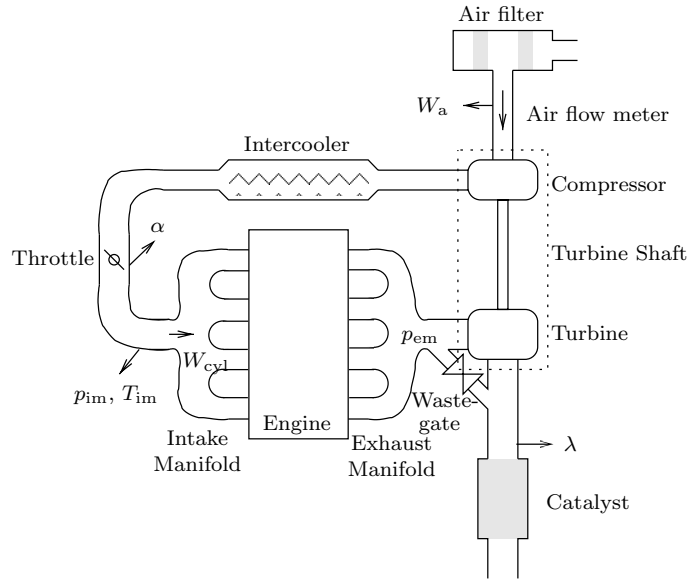
Figure 5.1: Sensors and actuators on the engine. Only the air-mass flow after the air-filter is measured, W_a. For stationary conditions the port air-mass flow W_{cyl} equals W_a. Exhaust manifold pressure p_{em} depends among others on the wastegate setting. On the exhaust side there is only one sensor, the oxygen sensor λ.
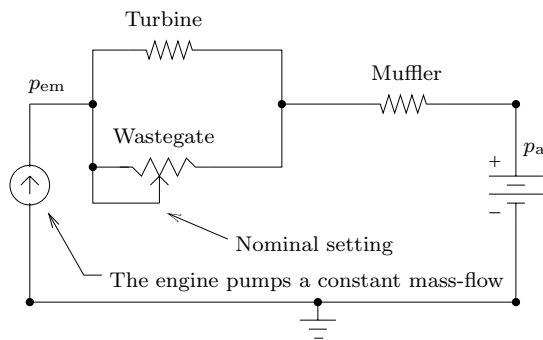
Figure 5.2: Hera a resistor analogy is used to show the partition of the exhaust manifold pressure. The wastegate's effect on the exhaust manifold pressure is like a variable resistor with a "nominal setting". When the wastegate is operated the exhaust manifold pressure changes around its nominal value.

For this polynomial the error is less than 4% and hence it is a good approximation of $p_{\text{em}_{\text{nom}}}$. Figure 5.3 shows the fitted polynomial and measured exhaust manifold pressure as a function of measured air-mass flow.

For low air-mass flows it is possible to improve the accuracy by including a second order term as Bergström and Brugård (1999) did. A second order polynomial describes the exhaust manifold pressure very accurately for closed wastegate. However, the wastegate opens for higher loads, which means that the second order polynomial can not be used to describe the nominal exhaust manifold pressure.

5.2.2   Model of Exhaust Manifold Pressure Offset

At nominal exhaust manifold pressures, the CAC can successfully be described by an affine parameterization in p_{im} of the product $\eta_{\text{vol}} p_{\text{im}}$ according to Eq. (4.9):

$$\text{CAC}(p_{\text{im}}, T_{\text{im}}, \lambda) = \underbrace{(a_1 p_{\text{im}} + a_0)}_{\eta_{\text{vol}} p_{\text{im}}} \frac{V_{\text{d}}}{R_{\text{im}}\left(T_{\text{im}} - C_1 \frac{1-\lambda^2}{\lambda^2}\right)} \qquad (4.9)$$

When the engine is not running with nominal wastegate setting, the exhaust manifold pressure is changed p_{em_Δ} from *nominal* pressure and this changes the residual gas mass. A different mass of residual gases will influence the volumetric efficiency and thus the inducted $\text{CAC}(p_{\text{im}}, T_{\text{im}}, \lambda)$. It will therefore be a difference between measured and modeled CAC when the engine is not running with a nominal wastegate setting. The difference is called ΔCAC and for *stationary* conditions, where W_{at} equals the measured W_{a}, it is calculated by rearranging Eq. (3.12a):

$$\Delta\text{CAC} = W_{\text{a}} \frac{n_r}{N} - \text{CAC}(p_{\text{im}}, T_{\text{im}}, \lambda) \qquad (5.3)$$

An illustration is given in Figure 5.4, where a step in wastegate setting is used to show the change in volumetric efficiency and difference between measured and modeled CAC, ΔCAC. The experiment in Figure 5.4 shows that p_{em_Δ} information is present in the measured signals on the intake side. Next, a method is proposed where ΔCAC is used to estimate p_{em_Δ}.

Exhaust Manifold Pressure Offset as A Function of ΔCAC

A straight forward method to determine the exhaust manifold pressure offset p_{em_Δ} as a function of the air-mass offset ΔCAC is to consider a CAC model with an explicit dependency of the exhaust manifold pressure and then linearize the model around $p_{\text{em}_{\text{nom}}}$. The linearized model then becomes:

$$\text{CAC}(p_{\text{im}}, p_{\text{em}_{\text{nom}}} + p_{\text{em}_\Delta}, T_{\text{im}}, \lambda) = \text{CAC}(p_{\text{im}}, p_{\text{em}_{\text{nom}}}, T_{\text{im}}, \lambda) + \frac{\partial\text{CAC}}{\partial p_{\text{em}}} p_{\text{em}_\Delta}$$

$$(5.4)$$
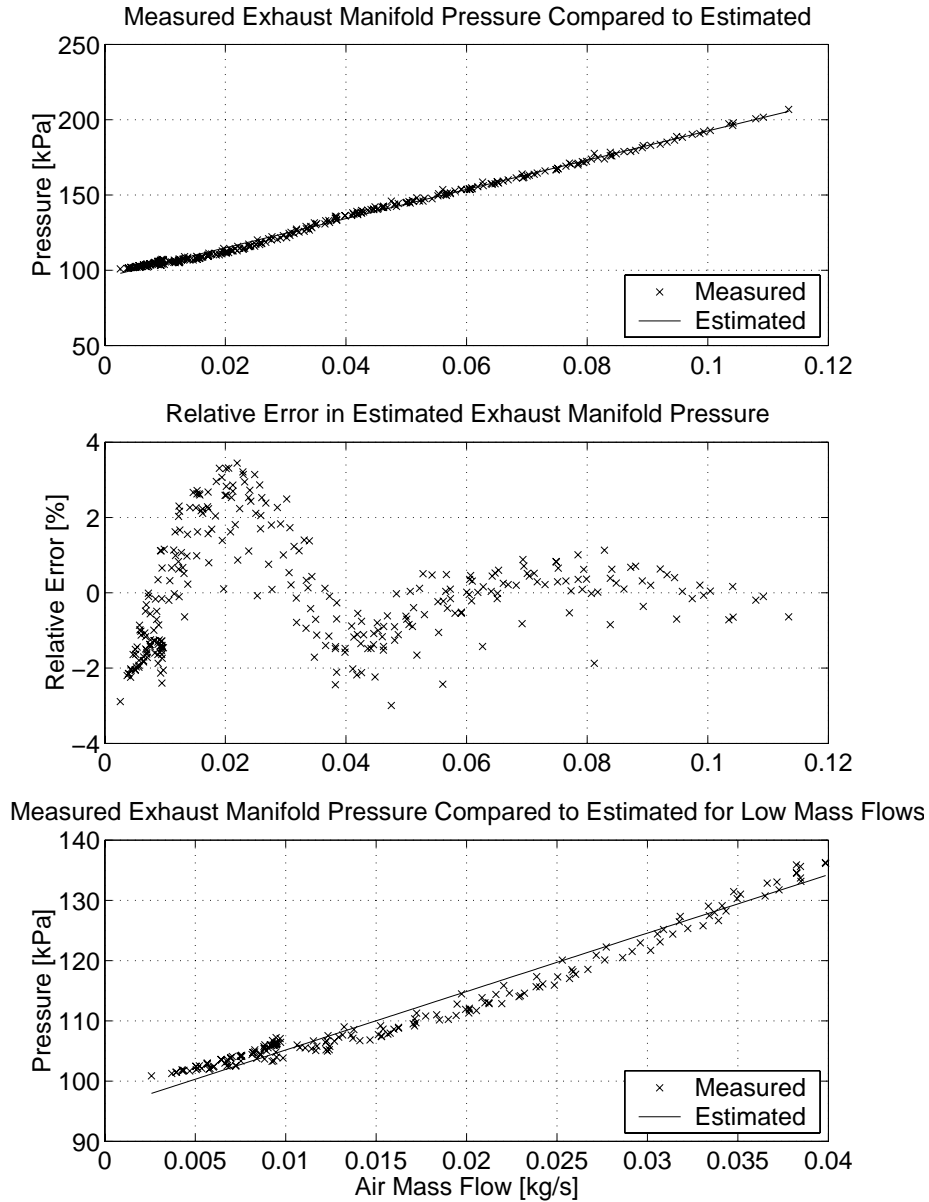
Figure 5.3: *Top:* Exhaust manifold pressure during mapping and fitted first order polynomial in air-mass flow. *Center:* The relative error of the polynomial fitting is less than 4 percent and largest for low mass flows. *Bottom:* For low air-mass flows a second order polynomial would fit better.
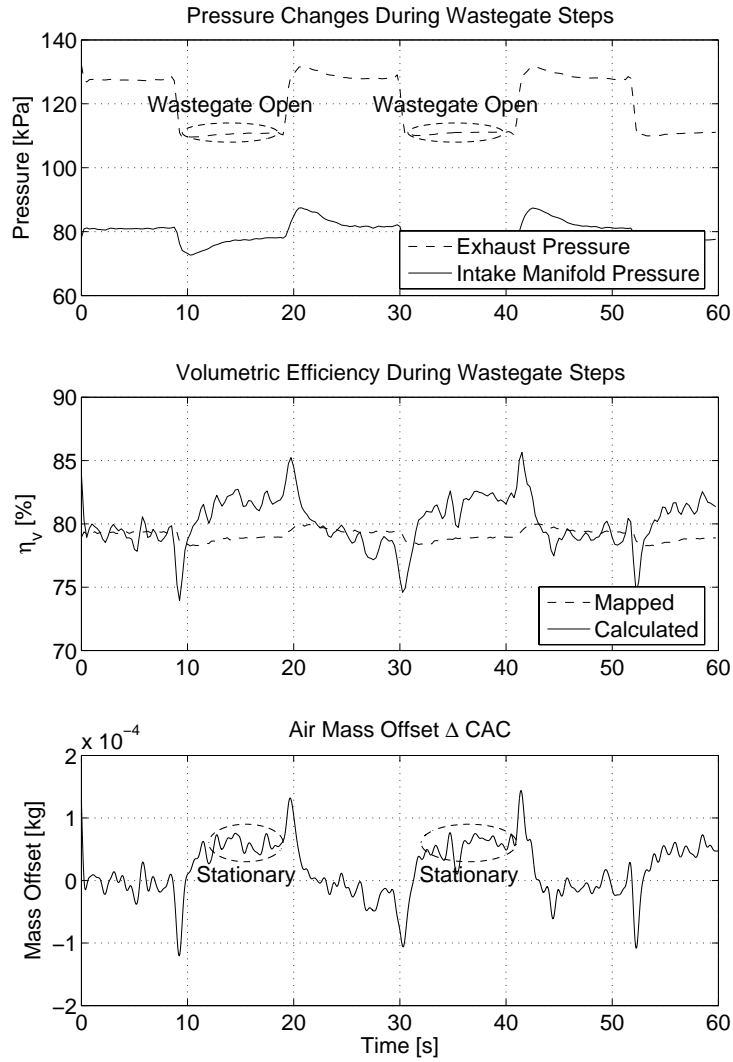
Figure 5.4: Steps from nominal to fully open wastegate at constant engine speed. A controller in the ECU tries to maintain constant air-mass flow. *Top:* When the wastegate has opened, the exhaust manifold pressure drops significantly but the intake manifold pressure drops only slightly. *Center:* Comparison of mapped and calculated volumetric efficiency. Eq. (2.3) was used to determine the calculated volumetric efficiency. Both are equal for nominal wastegate but the volumetric efficiency increases stationary when the wastegate is open. *Bottom:* For open wastegate a there is a stationary offset between the measured and the expected or modeled CAC. The difference between them are called ΔCAC

After some substitutions, it will be shown that the linearized model can be inverted and yield an explicit expression for p_{em_Δ}.

For nominal exhaust manifold pressure, the cylinder air-charge is described well by Eq. (4.9) that is independent of p_{em}:

$$\mathrm{CAC}(p_{\mathrm{im}}, p_{\mathrm{em}_{\mathrm{nom}}}, T_{\mathrm{im}}, \lambda) = \mathrm{CAC}_{p_{\mathrm{em}_{\mathrm{nom}}}}(p_{\mathrm{im}}, T_{\mathrm{im}}, \lambda)$$

Further, the cylinder air charge $\mathrm{CAC}(p_{\mathrm{im}}, p_{\mathrm{em}_{\mathrm{nom}}} + p_{\mathrm{em}_\Delta}, T_{\mathrm{im}}, \lambda)$ in Eq. (5.4) is also measured and this term is therefore replaced by the measurement.

$$\mathrm{CAC}(p_{\mathrm{im}}, p_{\mathrm{em}_{\mathrm{nom}}} + p_{\mathrm{em}_\Delta}, T_{\mathrm{im}}, \lambda) = \underbrace{W_{\mathrm{a}} \frac{n_r}{N}}_{\text{Measured}}$$

By inserting the relation above together with Eq. (4.9) into Eq. (5.4) the result is:

$$\underbrace{W_{\mathrm{a}} \frac{n_r}{N}}_{\text{Measured}} = \mathrm{CAC}_{p_{\mathrm{em}_{\mathrm{nom}}}}(p_{\mathrm{im}}, T_{\mathrm{im}}, \lambda) + \frac{\partial \mathrm{CAC}}{\partial p_{\mathrm{em}}} p_{\mathrm{em}_\Delta}$$

When the terms are rearranged and the relation from Eq. (5.3) is applied, the result is that $\frac{\partial \mathrm{CAC}}{\partial p_{\mathrm{em}}} p_{\mathrm{em}_\Delta}$ must equal $\Delta\mathrm{CAC}$:

$$\underbrace{W_{\mathrm{a}} \frac{n_r}{N} - \mathrm{CAC}_{p_{\mathrm{em}_{\mathrm{nom}}}}(p_{\mathrm{im}}, T_{\mathrm{im}}, \lambda)}_{\Delta\mathrm{CAC}} = \frac{\partial \mathrm{CAC}}{\partial p_{\mathrm{em}}} p_{\mathrm{em}_\Delta} \tag{5.5}$$

Now, if $\frac{\partial \mathrm{CAC}}{\partial p_{\mathrm{em}}}$ is monotone and non-zero it is possible to solve Eq. (5.5) for p_{em_Δ}:

$$p_{\mathrm{em}_\Delta} = \frac{\Delta\mathrm{CAC}}{\frac{\partial \mathrm{CAC}}{\partial p_{\mathrm{em}}}} \tag{5.6}$$

Next, it is necessary to determine the partial derivative $\frac{\partial \mathrm{CAC}}{\partial p_{\mathrm{em}}}$ which requires a CAC model with explicit p_{em} dependency. Fortunately, a p_{em} dependent model of CAC was proposed in Eq. (4.10), Chapter 4:

$$\mathrm{CAC}(p_{\mathrm{im}}, p_{\mathrm{em}}, T_{\mathrm{im}}, \lambda) = \frac{p_{\mathrm{im}}}{R_{\mathrm{im}}\left(T_{\mathrm{im}} - C_1 \frac{1-\lambda^2}{\lambda^2}\right)} C_{\eta_{\mathrm{vol}}} \frac{\left(r_c - \left(\frac{p_{\mathrm{em}}}{p_{\mathrm{im}}}\right)^{\frac{1}{\gamma_e}}\right) V_{\mathrm{d}}}{\left(1 + \frac{1}{\lambda\left(\frac{A}{F}\right)_s}\right)(r_c - 1)} \tag{4.11}$$

To investigate the properties of $\frac{\partial \mathrm{CAC}}{\partial p_{\mathrm{em}}}$, Eq. (4.10) is differentiated with respect to the exhaust manifold pressure p_{em}.

$$\frac{\partial \mathrm{CAC}}{\partial p_{\mathrm{em}}} = -\frac{C_1 \left(\frac{p_{\mathrm{em}}}{p_{\mathrm{im}}}\right)^{\frac{1}{\gamma_{\mathrm{eg}}}} V_{\mathrm{d}}}{\left(1 + \frac{1}{\lambda\left(\frac{A}{F}\right)_s}\right) \gamma_{\mathrm{eg}} (r_c - 1) \left(T_{\mathrm{im}} - \frac{C_2 (1-\lambda^2)}{\lambda^2}\right) R_{\mathrm{a}}} \frac{p_{\mathrm{im}}}{p_{\mathrm{em}}} \tag{5.7}$$
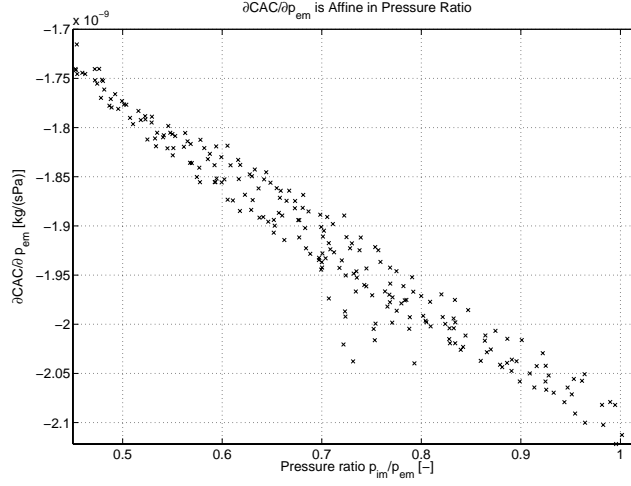
Figure 5.5: $\frac{\partial \text{CAC}}{\partial p_{\text{em}}}$ is affine in the pressure ratio $\frac{p_{\text{im}}}{p_{\text{em}}}$. However, the variations in $\frac{\partial \text{CAC}}{\partial p_{\text{em}}}$ are *small.*

As all factors above are non-zero and do not change sign the partial derivative will always be monotone and negative. Therefore, the inverse given by Eq. (5.6) always exists. Also, note that $\frac{\partial \text{CAC}}{\partial p_{\text{em}}}$, for a given λ, only depends on the ratio $\frac{p_{\text{em}}}{p_{\text{im}}}$. In Figure 5.5 $\frac{\partial \text{CAC}}{\partial p_{\text{em}}}$ has been evaluated for points in an engine map and as the variations around the mean value of $\frac{\partial \text{CAC}}{\partial p_{\text{em}}}$ are small a *constant* $K_e = \frac{\partial \text{CAC}}{\partial p_{\text{em}}}$ will be assumed. The constant K_e had to be slightly increased compared to the theoretical value of $-1.9 \cdot 10^{-9}$. Instead the value $K_e = -4 \cdot 10^{-9}$ was used, which results in the following simple p_{em_Δ} model:

$$p_{\text{em}_\Delta} = K_e \Delta \text{CAC} \qquad (5.8)$$

In Appendix D an alternative derivation of p_{em_Δ} is made that is based on a simplified thermodynamic model, which yields a result that also include T_{im} and λ. As both the intake manifold temperature and λ varies little these can be assumed constant and then the models' structure are equal.

5.2.3   Summary of Exhaust Pressure Calculation Process

First the temperature of the air-fuel mixture is calculated according to Eq. (4.8) and then the air-mass offset ΔCAC, Eq. (5.3), is calculated. The nominal exhaust pressure is determined by Eq. (5.2), the exhaust manifold pressure

offset by Eq. (5.8) and finally inserted into Eq. (5.1) which yields p_{em}.

$$T_{\mathrm{af}}(T_{\mathrm{im}}, \lambda) = T_{\mathrm{im}} - C_1 \left(\frac{\lambda - 1}{\lambda^2} \right)$$

$$\Delta\mathrm{CAC}\left(W_{\mathrm{a}}, N, p_{\mathrm{im}}, T_{\mathrm{im}}, \lambda\right) = W_{\mathrm{at}} \frac{n_r}{N} - \frac{\overbrace{(a_1 p_{\mathrm{im}} + a_0)}^{\eta_{\mathrm{vol}} p_{\mathrm{im}}} V_d}{R T_{\mathrm{af}}(T_{\mathrm{im}}, \lambda)}$$

$$p_{\mathrm{em}_{\mathrm{nom}}}(W_{\mathrm{a}}) = p_{\mathrm{a}} + k_1 W_{\mathrm{a}} + k_2$$

$$p_{\mathrm{em}_{\Delta}}(\Delta\mathrm{CAC}) = K_e \Delta\mathrm{CAC}$$

$$p_{\mathrm{em}}\left(W_{\mathrm{a}}, \Delta\mathrm{CAC}\right) = p_{\mathrm{em}_{\mathrm{nom}}}(W_{\mathrm{a}}) - p_{\mathrm{em}_{\Delta}}(\Delta\mathrm{CAC})$$

Important second order effects, such as heat transfer, and valve overlap etc. are taken into account by $p_{\mathrm{em}_{\mathrm{nom}}}$.

5.3   Exhaust Pressure Estimator Validation

The estimator is validated using measurements of the exhaust pressure when the wastegate valve is manually operated. When the wastegate is opened the power to the turbine drops and hence also the boost pressure. Boost pressure drops cause the air-mass flow controller in the engine management system to open the throttle more to maintain a constant air-mass flow. Now, there are two cases: First, the pressure before the throttle is high enough to supply the engine with the same air-mass flow as before the wastegate was opened. Second, the boost pressure is too low when the wastegate is open to maintain the same air-mass flow. The exhaust manifold pressure estimator is validated for both cases in Section 5.3.1 and Section 5.3.2 respectively.

While the air-mass controller changes the throttle plate angle, there are transients in the air-mass flow and the air dynamics introduce small deviations in the estimated air-mass offset $\Delta\mathrm{CAC}$ until the controller has settled. These deviations are clearly visible in Figure 5.6. Further, in this offline validation all measured signals have been zero phase low pass filtered to reduce the influence of noise.

Measurements have been taken for a number of loads at engine speeds between 1800 and 3100 RPM. In each measurement the engine speed is held constant and the wastegate is initially controlled by the ECU. The wastegate is then manually opened and held constant for approximately 10 seconds and then again closed. This process is repeated a few cycles.

5.3.1   Estimated Exhaust Pressure with Constant Air-mass Flow Before and After the Wastegate Step

Stationary validation is performed with and without the air-mass offset information to show the necessity of the additional information. First, this is shown in

Figure 5.6 where the intake manifold pressure is below ambient and the air-mass flow is controlled to 45 g/s during the experiment.

The controller succeeds in maintaining the desired air-mass flow even when the wastegate is open. The nominal exhaust manifold pressure is expressed as a polynomial in air-mass flow and since the air-mass flow is constant, the estimated exhaust manifold pressure is also constant. When the wastegate is opened, there is an offset from the nominal exhaust manifold pressure. This offset called p_{em_Δ} can be estimated by inverting the linearization of CAC with respect to deviations from nominal exhaust manifold pressure. When the estimated p_{em_Δ} are applied, the drops in exhaust manifold pressure are captured. During transients there are over shoots in the estimated exhaust manifold pressure, which are results of a using a static intake model.

More results of applying the method described by Equations (5.2, 5.8) are shown in Figure 5.7 (low brake mean effective pressures, bmep) and top of Figure 5.8 (high bmep) where different settings of the wastegate are used in four different operating points. The absolute exhaust manifold pressure is described, in most cases, within 5%.

In the bottom of Figure 5.7 it is shown that even when there is a bias in the estimated p_{em_Δ} the exhaust manifold pressure *change* is still correct. The bias in the estimated exhaust manifold pressure change p_{em_Δ} is caused by errors in the modeled volumetric efficiency. This shows that even though there are errors the estimated pressures the estimator still gives useful exhaust manifold pressure information.

5.3.2   Estimated Exhaust Pressure with Different Air-mass Flow Before and After the Wastegate Step

To maintain an intake manifold pressure above ambient it is necessary to provide a certain boost pressure, which can only be achieved when the wastegate is closed or for small openings. If the wastegate is fully opened when a boost pressure is required to maintain a constant air-mass flow, there will be a drop in the air-mass flow as it is not possible to achieve the previous air-mass flow. This is the situation in the bottom of Figure 5.8, where the air-mass-controller is unable to supply the engine with the same air-mass flow when the wastegate is opened as the boost pressure is too low. As the air-mass flow decreases when the wastegate is opened and the nominal exhaust manifold pressure $p_{em_{nom}}$ is a function of the air-mass flow, the polynomial better describes the exhaust manifold pressure change is this case. However, the exhaust manifold pressure estimates are further significantly improved when the p_{em_Δ} component is added.
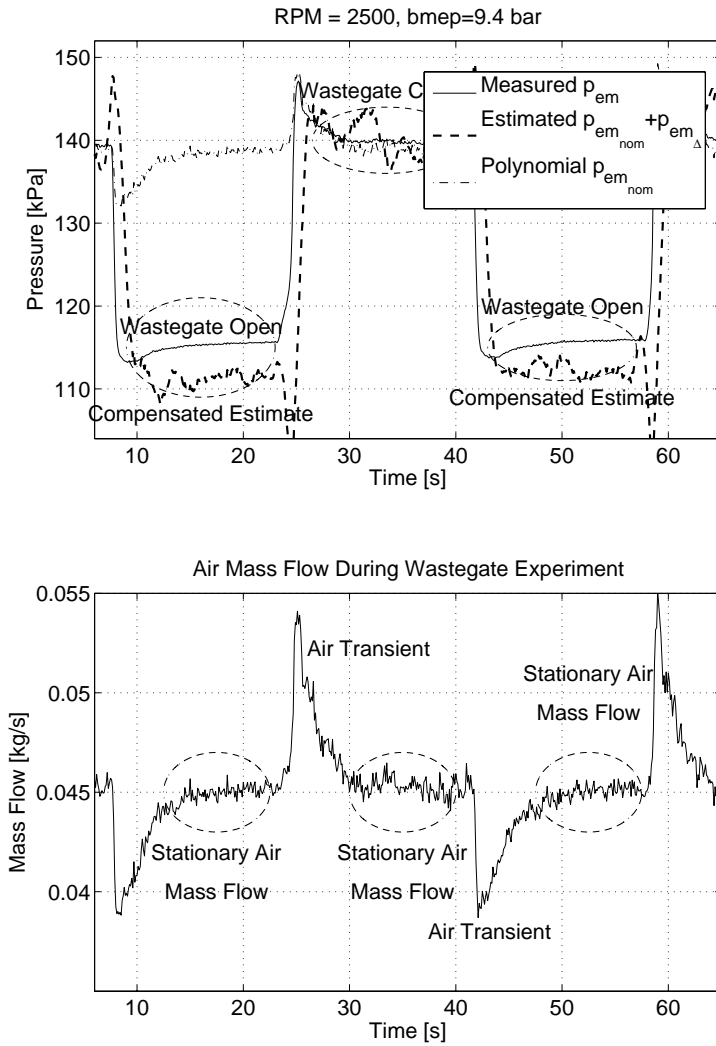
Figure 5.6: *Top:* Measured exhaust manifold pressure data compared to estimated pressure with and without p_{em_Δ} information. The polynomial description gives accurate estimates for nominal wastegate setting, but overestimates the pressure for open wastegate. With the p_{em_Δ} information, Eq. (5.8), it is also possible to describe the pressure for open wastegate. The estimated exhaust manifold pressure follows the measured within 5%. *Bottom:* When the wastegate is operated there is a short transient in the air-mass flow. Between the transients the air-mass flows are constant, which have been marked.
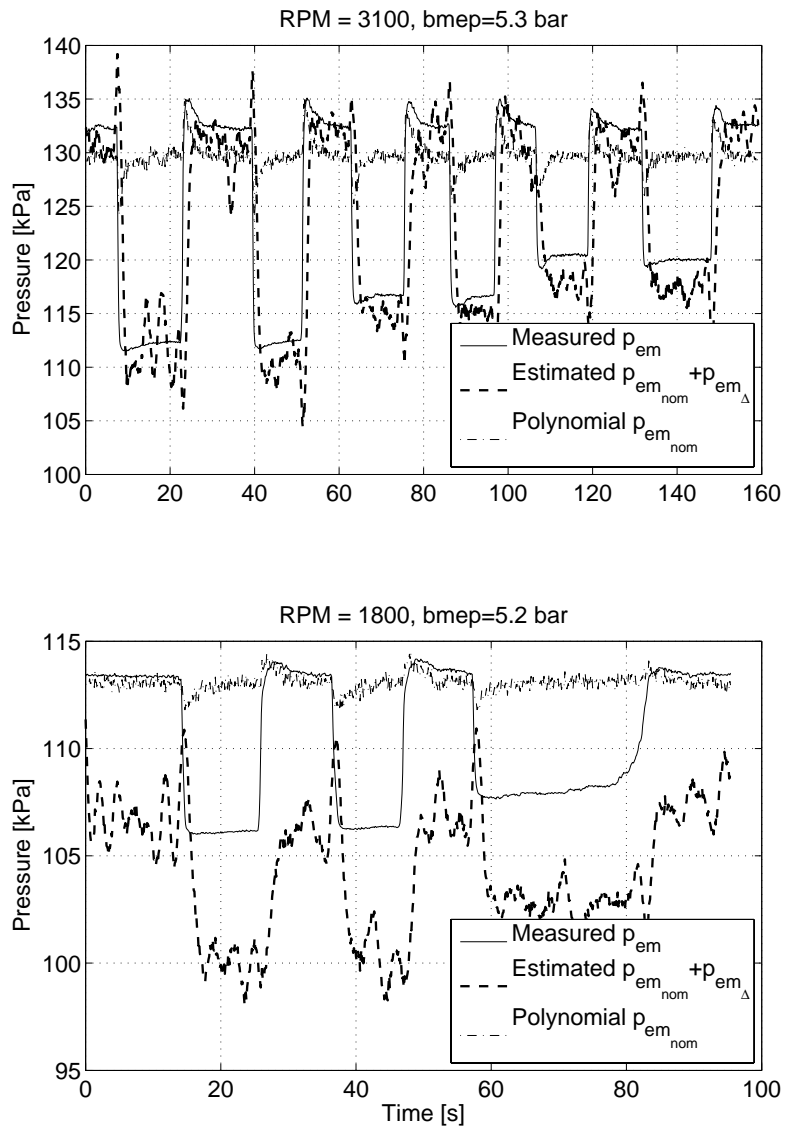
Figure 5.7: Measured exhaust manifold pressure (solid) compared to nominal pressure (dash-dotted), and estimated using the in-cylinder air-mass offset information (dashed). When the additional pressure offset p_{em_Δ} is added, the estimates are improved for open wastegate. In the bottom plot there is a stationary error in p_{em_Δ}, but p_{em_Δ} captures that there is a *change* in exhaust manifold pressure.
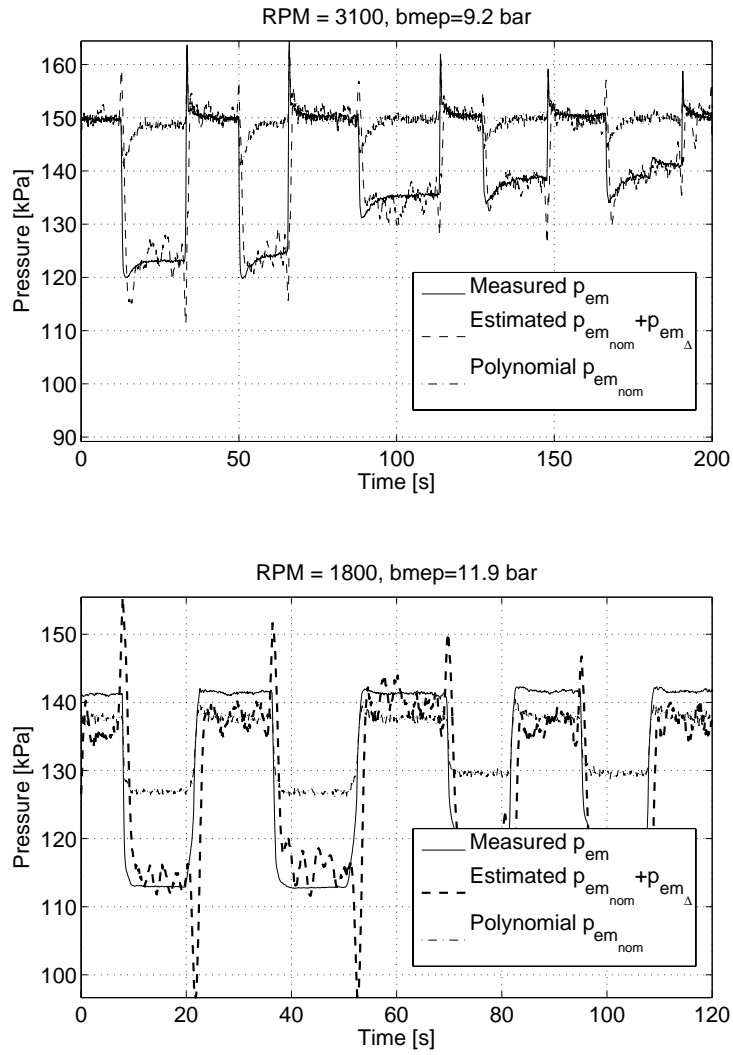
Figure 5.8: Measured exhaust manifold pressure (solid) compared to nominal pressure (dash-dotted), and estimated using the in-cylinder air-mass offset information (dashed). In the bottom plot the air-mass flow through the engine drops when the wastegate is opened and thus also the $p_{\mathrm{em\,nom}}$. However it is still necessary to add the exhaust manifold pressure offset p_{em_Δ} to better describe the exhaust manifold pressure.

5.4 Results

On turbocharged spark-ignition engines with wastegate the absolute exhaust manifold pressure can not be estimated using a simple function of the air mass flow. This as one of the three parts in the exhaust system, the wastegate can not be described as a static restriction while the two other components the muffler and the turbine can be described as a static functions. To resolve this a two-stage exhaust manifold pressure estimator is proposed. It first estimates the nominal exhaust manifold pressure, which is a static function of the ambient pressure and the air-mass flow. Then, changes from nominal exhaust manifold pressures cause the in-cylinder air-mass-offset ΔCAC to be non-zero. Using the estimated ΔCAC the $p_{em_\Delta}(\Delta CAC)$ can then be estimated and added to the nominal exhaust manifold pressure and thus a better estimate of the exhaust manifold pressure is produced when the wastegate is not in its nominal setting.

The estimator is validated using steps in wastegate for various speeds and loads for two cases:

1. When the air-mass flow can be maintained before and after the step in wastegate.

2. When it is not possible to maintain the same air-mass flow since the opening of the wastegate causes the boost pressure to drop too much.

In neither case does the nominal exhaust manifold pressure describe the exhaust manifold pressure sufficiently accurate. It is therefore necessary to consider the varying restriction caused by the wastegate. By adding the estimated pressure offset $p_{em_\Delta}(\Delta CAC)$ caused by the wastegate, the absolute exhaust manifold pressure estimates are improved. Accurate p_{em} estimates are produced, using sensors from the intake side only, provided that there is a precise description of the volumetric efficiency. Here the precision of the estimated absolute exhaust manifold pressure has been within 5% for most cases.

Part II

Dynamics

6

A Mean Value Model of a TC SI Engine

Engine control systems are growing more complex as the demands for low emissions and good fuel economy increase. To facilitate the controller design process, a physically based model of the engine is desirable. Additionally, the model can serve as a virtual engine during the initial tests. For these purposes, a highly suitable model class is mean value engine models (MVEMs) which describe the average behavior of the engine over one to several thousands of engine cycles, see eg. (Aquino, 1981; Hendricks and Sorensen, 1990; Powell et al., 1998a; Müller et al., 1998; Eriksson et al., 2002b).

The objective of this chapter is to present a component based MVEM together with systematic methods to determine its parameters. Here the word component based reflects that the component structure of the engine is preserved. Typical components are air-filter, intercooler, and throttle that are connected by pipes or manifolds. One benefit of this modeling strategy is that every component can be separately identified and then the engine model is built using the separate components. Each component is described in terms of equations, constants, parameters, states, inputs, and outputs.

The intended use of the component based engine model is to form a basis of a pressure, temperature and mass-flow observer along the air-path of a turbocharged engine. The first application is in Chapter 7 where the model is used to determine observability of the model and further which signals that are most suitable for observer feedback. An observer is then designed in Chapter 8 and the resulting observer is used in Chapter 9 to achieve accurate air/fuel control. Other applications of the TC spark ignited (SI) engine model are diagnosis, prediction, estimation of non-measured signals, and turbocharger control.

The presented model is a result of a long term project at Vehicular Systems with the objective to gain knowledge of turbocharged SI-engines for control. More details regarding the selection of the structure of the individual components can be found in Bergström and Brugård (1999), Pettersson (2000), Eriksson et al. (2002b), and Andersson and Eriksson (2004). Most of the following sections therefore only give a short description of each component with focus on how to determine the parameters and the quality of each modeled component. The quality of each modeled component is described by showing the model fit both for a tuning and a validation data set. Here the parameters are tuned to a SAAB B235R engine, which was located in the research laboratory of Vehicular Systems. Using a second engine, a SAAB B207R, the model and parameter tuning methodology was tested with excellent results.

All plots shown in this chapter have been *slightly scaled* in order not to reveal the true engine parameters. As both the modeled and measured values are scaled by the same scaling factor the scaling does not influence the relative error. Therefore, the model quality is best reflected using the relative error.

6.1   Model Structure

The engine consists of components such as air-filter, compressor, intercooler, and so on. Between these components, there are pipes or manifolds. These pipes or manifolds can be considered as *control volumes* where the pressure and temperature of the gas inside depends on the mass-flows into and out of the volume. Mass-flows are determined by *restrictions* that are components that given the pressure and temperature before and after the restriction determine the mass-flow and temperature of the flow.

The modeling principle is thus to place restrictions between control volumes. Therefore, the modeling is reduced to describe the engine components in terms of restrictions and control volumes. Here the design is aided by a Matlab/Simulink toolbox called MVEM-LIBRARY (Frei and Eriksson, 2001), which provides a set of well tested blocks (components). An example where the modeling methodology is applied to an NA-engines air-system is shown in Figure 6.1. It is clear that the modeling methodology preserves the physical structure of the engine, as all of the components exist on a physical engine.

Now, the modeling methodology is applied to a turbocharged engine and the restrictions and control volumes are listed next.
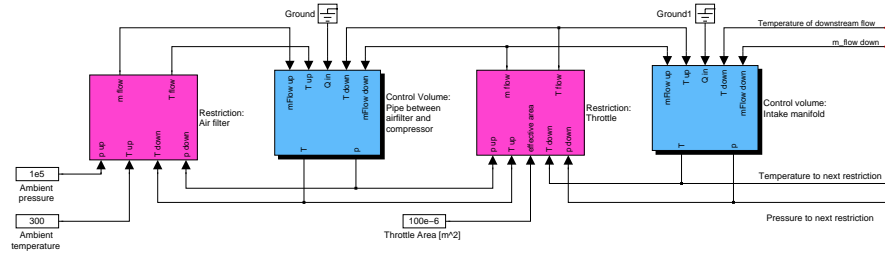
Figure 6.1: Illustration of modeling methodology with control volumes in series with restrictions. From the left there is one restriction (air-filter) which produces a mass-flow into a control volume (the pipe between the air-filter and the throttle). The mass-flow out of the control volume is governed by a restriction (throttle), which in turn is followed by another control volume (intake manifold).

Restriction(R)   Control volume (CV)
Air-filter (R)
    Pipe between air-filter and compressor (CV)
Compressor (R)
    Pipe between and intercooler (CV)
Intercooler (R)
    Pipe between and Intercooler and throttle (CV)
Throttle (R)
    An intake manifold connects the throttle and cylinders (CV)
Engine determines port air-mass flow (R)
    An exhaust manifold connects the cylinders and the turbine/wastegate (CV)
Turbine/wastegate (R)
    Pipe between and turbine/wastegate and the exhaust system (CV)
Exhaust system (R)

To complete the model there only two additional components left. First there is the turbocharger shaft, which is modeled as a rotating inertia, and second the engine torque model. Below the components are divided into groups that will be thoroughly described later:

Restrictions These determine a mass-flow through the restriction with a temperature given pressure and temperature before and after the restriction.

Incompressible flow restrictions: Air-filter, intercooler, and exhaust system are modeled using this MVEM-LIBRARY standard component. See Section 6.2.

Compressible flow restriction: Throttle and wastegate. This component is described in Section 6.3 and it is also a standard MVEM-LIBRARY component.

Custom restrictions These restrictions are application specific:

> **Engine** Determines the port air-mass flow, exhaust mass-flow and temperature of the gases to the exhaust manifold. This block also models the engine torque. See Section 6.4
>
> **Compressor** The compressor is a part of the turbocharger and it is considered as a restriction as it produces a mass-flow through the compressor and models the mass-flow temperature. It also produces a loading torque to the turbine. See Section 6.6.
>
> **Turbine** The turbine part of the turbocharger produces a mass-flow through the turbine, models its temperature, and describes the torque produced by the turbine. See Section 6.7.

Adiabatic mixer This component is used to adiabatically mix flows from two different restrictions, such as when the flows through the turbine and wastegate meet. The outputs are mass-flow and flow temperature. This is a standard MVEM-LIBRARY component and it is described in Section 6.2.3.

Model dynamics Components, which have one or more states. In Section 6.8 the dynamic equations are described.

> **Control volume** A control volume is used to connect two restrictions. It has two states, pressure and temperature. Control volumes are located between the restrictions: air-filter, compressor, intercooler, throttle, engine, turbine, and exhaust system. Inputs: mass-flows in and out of the control volume together with the flow temperatures. It is also possible to specify heat transfer to/from the gas inside the control volume. The control volume is implemented as a standard component in MVEM-LIBRARY.
>
> **Inertia with friction** The axle in the turbocharger is modeled as a rotating inertia, where the inertia is the total inertia of the axle, compressor, and turbine. The angular velocity of the shaft is represented by a state. The inertia is powered by the torque from the turbine and loaded by the compressor and axle friction. The inputs are: Driving torque and loading torque. Output is speed. This is a standard component in MVEM-LIBRARY.

The final component based model is shown in Figure 6.2.

6.1.1   Model Simplifications

As the model will be used for observer design some general simplifications and assumptions are made:

- Flows run only in forward direction. Example: The air always flows from the air-filter to the compressor, never from the compressor to the air-filter.

Figure 6.2: The mean value engine model implemented in Simulink using MVEM-LIBRARY. Note that the modeling methodology with control volumes between restrictions is implemented without exceptions. In the center the turbocharger shaft dynamics block is shown. The blocks with a shadowed backdrop are blocks where dynamics (states) are present.

- No heat transfer to/from the gas inside of the control volumes.

- No compressor by-pass valve as the modeled engine was not initially equipped with such a valve.

- All gases are considered to be ideal and there are two sets of thermodynamic properties:

  1. Air on the intake side has gas constant R_a and the ratio of specific heats is γ_a.

  2. Burned (exhaust) gas has gas constant R_{eg} and the ratio of specific heats is γ_{eg}.

6.1.2 Model Inputs

Inputs to the model are:

Name	Description	Unit
N	Engine speed	RPM
α	Throttle angle	deg
u_{wg}	Wastegate opening. Range 0–1	–
λ	Normalized air/fuel ratio	–
p_a	Ambient pressure	Pa
T_a	Ambient temperature	K

6.1.3 Model States

The model has states for pressures and temperatures in each control volume and one state for the turbocharger speed:

State	Description
p_{af}	Pressure after air-filter
T_{af}	Temperature after air-filter
p_{comp}	Pressure after compressor
T_{comp}	Temperature after compressor
p_{ic}	Pressure after intercooler
T_{ic}	Temperature after intercooler
p_{im}	Intake manifold pressure
T_{im}	Intake manifold temperature
p_{em}	Exhaust manifold pressure
T_{em}	Exhaust manifold temperature
p_t	Pressure after turbine
T_t	Temperature after turbine
ω_{TC}	Turbocharger speed

6.1.4 Data Sets for Parameter Estimation and Validation

Two measured data sets have been used, one for parameter tuning and one for validation. In each data set, all model states and inputs have been measured except for the wastegate position. Additionally the following signals have been measured: air-mass flow after the air-filter, injection time, and engine torque. For more information on how the data sets were acquired, please see Appendix E.

Tuning Data

An engine map with 343 points has been used to determine the engine model parameters. Additional data from the turbocharger manufacturer have been used together with engine specific parameters such as volumes and geometry. In addition, a data set where the engine is run with constant throttle angle is used to determine the throttle model parameters.

Validation Data

This data set has 68 points spread over the entire operating region. It was measured 3 years after the tuning data set. In the meantime, the research laboratory was redesigned and the status of the engine changed. Here is a list of modifications made to the engine compared to its status when the tuning data was measured: a replaced air-mass flow sensor which gave slightly different readings, a modified exhaust system (different back-pressure), modified intercooler installation, different pressure and temperature sensors, and a new dynamometer. The following additions were also made to the engine: crank case ventilation and compressor by-pass valve. The validation data set was measured using a summer grade gasoline while the tuning data was measured using a winter grade gasoline.

6.2 Incompressible Flow Restrictions

The air-filter, intercooler, and the exhaust system all acts like restrictions to the fluid that are assumed to be incompressible and isenthalpic (Frei and Eriksson, 2001; Eriksson et al., 2002b). A restriction determines the mass-flow through it and the temperature of the flow. Lets start by modeling the flow temperature out of the restriction. From the isenthalpic assumption it follows that $T_{\text{after}} = T_{\text{before}}$, that is no temperature change. One exception is the intercooler, which is not isenthalpic, and its flow temperature is therefore modeled in Section 6.2.2.

By assuming a constant Reynolds number, the pressure drop Δp over the restriction can be described as a one parameter function of the mass-flow and the temperature before the restriction (Cengel, 2003, p. 433):

$$\Delta p = p_{\text{before}} - p_{\text{after}} = \mathcal{H} \frac{T_{\text{before}} W^2}{p_{\text{before}}} \qquad (6.1)$$

As the pressure drop Δp is known together with the temperature before the restriction, the mass-flow W is determined by inverting Eq. (6.1):

$$
W = \begin{cases}
\sqrt{p_{\text{before}} \frac{\Delta p}{\mathcal{H} T_{\text{before}}}}, & \Delta p > p_{\text{lin}} \\
\sqrt{\frac{p_{\text{before}}}{\mathcal{H} T_{\text{before}}} \frac{\Delta p}{\sqrt{p_{\text{lin}}}}}, & 0 \leq \Delta p \leq p_{\text{lin}} \\
0, & \Delta p < 0
\end{cases}
\tag{6.2}
$$

For pressure drops $\Delta p \leq p_{\text{lin}}$, the mass-flow is linearized, to reduce the derivative $\frac{\partial W}{\partial \Delta p}$ for small Δp as:

$$
\lim_{\Delta p \to 0} \frac{\partial W}{\partial \Delta p} = \infty
$$

The parameter $\mathcal{H}$ is determined using the method of least squares, given measurements of Δp, p_{before}, and T_{before}. Next tuning and validation of the parameter $\mathcal{H}$ in Eq. (6.1) is shown for the following incompressible restrictions: air-filter, intercooler and exhaust system.

6.2.1 Air Filter Model

The pressure head loss over the air-filter is:

$$
\Delta p_{\text{af}} = p_{\text{a}} - p_{\text{af}} = \mathcal{H}_{\text{af}} \frac{T_{\text{a}} W_{\text{af}}^2}{p_{\text{a}}}
\tag{6.3}
$$

A validation of the modeled pressure drop compared to measured pressure drop is shown in Figure 6.3. In the measurements, it can be noted that the measured pressure drop over the air-filter increases slightly where the laminar mass flow meter LFE3 is connected, as it acts as a small restriction in series with the air-filter. For the operating points where it is not connected, the model shows good agreement with measured data. The air-filter model inputs, parameters, and output are listed in Table 6.1.

Parameters		Inputs		Output		
$\mathcal{H}_{\text{af}}$	$\left[\frac{\text{Pa}^2\text{s}^2}{\text{K}\cdot\text{kg}^2}\right]$	T_{a}	[K]	W_{af}	[kg/s]	Eq. (6.3)
$p_{\text{lin}_{\text{af}}}$	[Pa]	p_{a}	[Pa]			
		p_{af}	[Pa]			

Table 6.1: Air-filter model inputs, parameters, and output.

6.2.2 Intercooler

The intercooler is an incompressible restriction where the pressure drop follows Eq. (6.4). One major difference from the air-filter is that the temperature of the flow out of the intercooler is not equal to the temperature of the gases flowing into the intercooler. The temperature of gases flowing out of the intercooler is instead described by Eq. (6.5a).
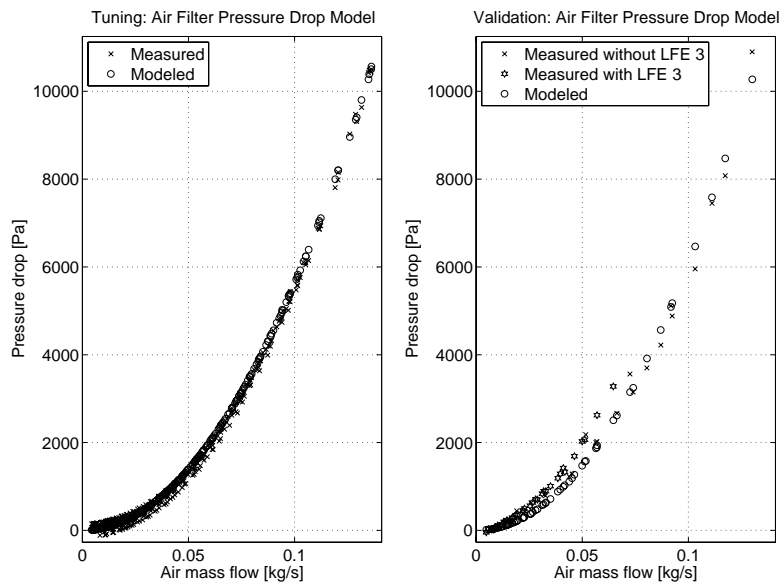
Figure 6.3: Air filter pressure head loss model described by the parameter $\mathcal{H}_{\mathrm{af}}$. *Left:* The model describes the pressure drop very well for all operating points. *Right:* The model describes the pressure drop within 10% for higher mass flows when the laminar mass flow meter LFE 3 is disconnected. When it is connected the model predicts a too low pressure drop which is correct as it is tuned without the LFE3.
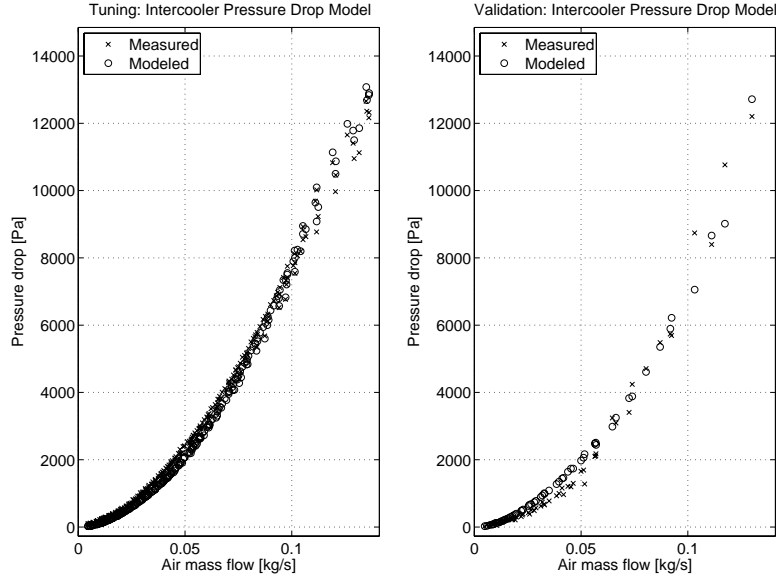
Figure 6.4: Intercooler pressure head loss model described by the parameter $\mathcal{H}_{ic}$. *Left:* Model fit for the tuning data is better than 10% for high air-mass flows. *Right:* For the validation data the fit is better than 20% for high flows.

Pressure Drop

Intercooler pressure head loss is described by

$$\Delta p_{ic} = p_{comp} - p_{ic} = \mathcal{H}_{ic} \frac{T_{comp} W_{ic}^2}{p_{comp}} \tag{6.4}$$

where W_{ic} is the air-mass flow through the intercooler. This kind of intercooler pressure drop model is also suggested in (Watson and Janota, 1982, pp. 321). A validation of modeled data against measured is shown in Figure 6.4.

Temperature Change

The intercooler is a cross-flow heat exchanger with unmixed flows. Here the temperature change is considered and the heat transfer is modeled for stationary conditions by a regression model (Eriksson et al., 2002b):

$$T_{ic_{out}} = \max\left(T_{cool}, T_{comp} + \epsilon\left(T_{comp} - T_{cool}\right)\right) \tag{6.5a}$$

$$\epsilon = a_0 + a_1\left(\frac{T_{comp} + T_{cool}}{2}\right) + a_2 W_{ic} + a_3 \frac{W_{ic}}{W_{cool}} \tag{6.5b}$$

The regressors are inspired by the NTU-model (Holman, 1992) and the parameters are determined using the method of least squares. There is also a saturation
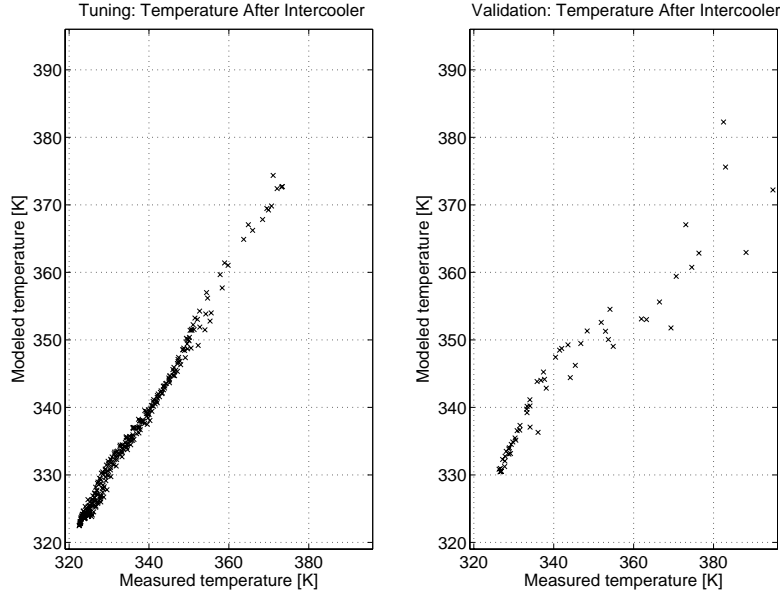
Figure 6.5: Intercooler temperature model. *Left:* For the tuning data the fit is within 1%. *Right:* The model predicts the temperature with an average error of less than 2% for low to medium mass-flows and the maximum error is 8% that occurs for high loads.

that makes sure that the temperature out of the intercooler is not lower than the cooling air.

In Figure 6.5 a validation of the temperature model is shown. For the tuning data, the maximum error is within 1%, but for the validation data the error is larger. The large maximum error in the validation data is probably caused by a lower flow of cooling air though the intercooler. The lower mass-flow of cooling air can be a result of the changed intercooler fan installation.

The intercooler model inputs, parameters, and outputs are listed in Table 6.2.

Parameters		**Inputs**		**Outputs**		
$\mathcal{H}_{ic}$	$\left[\frac{\text{Pa}^2\text{s}^2}{\text{K}\cdot\text{kg}^2}\right]$	T_{comp}	[K]	W_{ic}	[kg/s]	Eq. (6.2)
$p_{lin_{ic}}$	[Pa]	p_{af}	[Pa]	$T_{ic_{out}}$	[K]	Eq. (6.5a)
a_0, a_1, a_2, a_3	[-]	p_{comp}	[Pa]			
T_{cool}	[K]					
W_{cool}	[kg/s]					

Table 6.2: Intercooler model inputs, parameters, and outputs.

6.2.3   Exhaust System

Here the catalyst is considered a part of the exhaust system as it acts as a restriction in series with the muffler. To determine the exhaust system pressure head loss it is necessary to know the temperature of the gases flowing into the exhaust system, $T_{es_{in}}$. The gases flowing into the exhaust system is a mix of the gases from the wastegate and the turbine. Therefore, $T_{es_{in}}$ is modeled using energy conservation during adiabatic mixing of the gases flowing through the turbine and wastegate. Both gases are burned gases and they are assumed to have a constant and equal capacity of specific heats $c_{p_{eg}}$ in Eq. (6.6a).

$$T_{es_{in}} = \frac{c_{p_{eg}} T_{t_{out}} W_t + c_{p_{eg}} T_{em} W_{wg}}{c_{p_{eg}}(W_t + W_{wg})} = \frac{T_{t_{out}} W_t + T_{em} W_{wg}}{W_t + W_{wg}} \qquad (6.6a)$$

$$\Delta p_t = p_t - p_a = \mathcal{H}_{es} \frac{T_{es_{in}} W_{es}^2}{p_t} \qquad (6.6b)$$

As measurements of the temperature into the exhaust system were available, these were used when the pressure head-loss parameter $\mathcal{H}_{es}$ is determined. A validation of modeled data against measured is shown in Figure 6.6. The model fit can be improved by including a linear term, corresponding to d'Arcy's law for head losses (Eriksson et al., 2002b) but this has not been done, as the absolute error is small.

The exhaust system model inputs, parameters, and outputs are listed in Table 6.3.

Parameters		Inputs		Output		
$\mathcal{H}_{es}$	$\left[\frac{Pa^2 s^2}{K \cdot kg^2}\right]$	T_a	[K]	W_{es}	[kg/s]	Eq. (6.6b)
$p_{lin_{es}}$	[Pa]	p_t	[Pa]	$T_{es_{in}}$	[K]	Eq. (6.6a)
		T_{em}	[K]			
		T_t	[K]			
		W_t	[kg/s]			
		W_{wg}	[kg/s]			

Table 6.3: Exhaust system model inputs, parameters, and outputs.

6.3   Compressible Flow Restrictions

Isentropically compressible mass flows (Taylor, 1994, pp. 503–507) are used to describe the flow through the throttle and the wastegate. The flow is modeled by the set of Equations in (6.7).

$$W\left(\alpha, p_{after}, p_{before}, T_{before}\right) = \frac{p_{before}}{\sqrt{R_a T_{before}}} \Psi\left(\Pi\right) C_d A\left(\alpha\right) \qquad (6.7a)$$
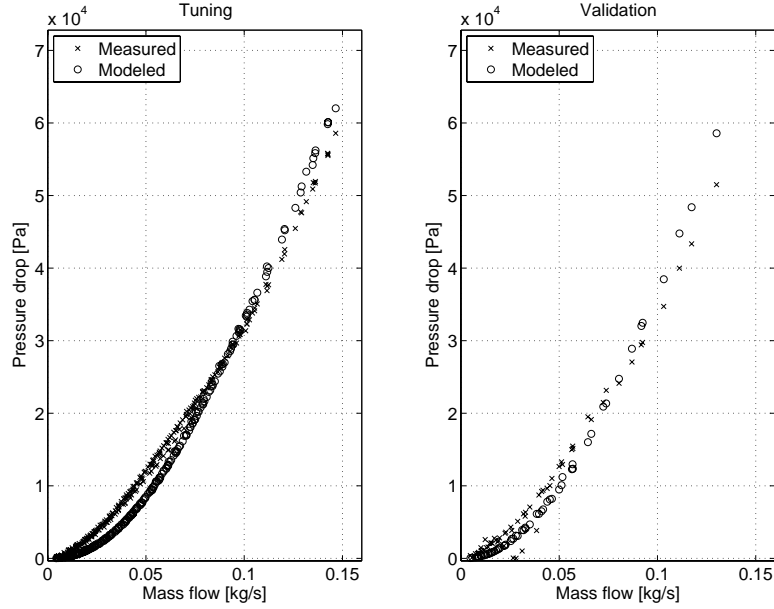
Figure 6.6: Exhaust system pressure head loss. *Left:* For the tuning data there is a systematic error present, which could be reduced by augmenting the model using a linear term. *Right:* The fit for the validation data shows the same trends as the tuning data.

$$\Pi = \begin{cases} \frac{p_{\text{after}}}{p_{\text{before}}}, & p_{\text{after}} < p_{\text{before}} \\ 1, & \text{otherwise} \end{cases} \tag{6.7b}$$

$$\Psi^* (\Pi) = \frac{\sqrt{\frac{2\gamma}{\gamma-1}\left(\Pi^{\frac{2}{\gamma}} - \Pi^{\frac{\gamma+1}{\gamma}}\right)}}{\sqrt{\frac{2\gamma}{\gamma-1}\left(\left(\frac{2}{\gamma+1}\right)^{\frac{2}{\gamma-1}} - \left(\frac{2}{\gamma+1}\right)^{\frac{\gamma+1}{\gamma-1}}\right)}} \tag{6.7c}$$

$$\Psi (\Pi) = \begin{cases} 1 & 0 < \Pi \le \left(\frac{2}{\gamma+1}\right)^{\frac{\gamma}{\gamma+1}} \\ \Psi^*(\Pi) & \left(\frac{2}{\gamma+1}\right)^{\frac{\gamma}{\gamma+1}} < \Pi \le \Pi_{\text{lin}} \\ \frac{\Psi^*(\Pi_{\text{lin}})}{\Pi_{\text{lin}}-1}\left(\Pi - 1\right) & \text{for } \Pi_{\text{lin}} < \Pi \le 1 \end{cases} \tag{6.7d}$$

To prevent $\frac{\mathrm{d}W}{\mathrm{d}\Pi}$ from reaching $-\infty$ for pressure ratios close to 1, Eq. (6.7c) is linearized for pressure ratios above Π_{lin}. In the sections below, the flow through the throttle is described first followed by the flow through the wastegate.

6.3.1 Throttle Flow

When the compressible flow model is applied to a throttle there are a number of challenges that have to be addressed such as:

1. Can the discharge coefficient C_d be regarded as a constant or is a more complex model necessary?

2. Does the compressible flow equation Eq. (6.7d) describe the flow properly?

3. It is necessary to find a parameterization of the geometric area function, $A(\alpha)$.

These topics are discussed in this section.

Discharge Coefficient Model

Starting with the discharge coefficient C_d, there are several references that model it as a varying parameter:

- Blair (1999, pp. 327) models the discharge coefficient as a function of pressure ratio and throttle area.

- Pursifull et al. (2000) studies NA-engines where the pressure before the throttle varies less and there C_d was successfully modeled as area dependent with variations from 0.7 up to 1.

- Arsie et al. (1996) models the discharge coefficient as a function of pressure before and after the throttle, area, and temperature.

- Hendricks et al. (1996) models a pressure ratio dependent C_d by including it in a modified $\Psi(\Pi)$-function which better fits measured data.

Several of the references above model C_d as a function of pressure ratio Π and/or area $A(\alpha)$. As none of the references agree on how to describe C_d an engine experiment has been performed to investigate which parameters that influence the discharge coefficient. Here the purpose is to find a throttle flow model, of the same complexity as the physically based model, which better explains measured data.

The experiment is performed by locking the throttle (fixed geometric area) and use the engine speed to vary the pressure ratio Π. The different sweeps in pressure ratio for a given area are presented in the top of Figure 6.7, where it can be seen that the throttle area varies less than 0.5 degree. By rearranging Eq. (6.7a) an equation is determined for the area and pressure ratio dependent parts of the air-mass flow:

$$A(\alpha)C_d(A(\alpha),\Pi)\Psi(\Pi) = \frac{W_{\text{at}}\sqrt{R_a T_{\text{ic}}}}{p_{\text{ic}}} \tag{6.8}$$

Next the left hand side is normalized by dividing with the mean of the three largest values of the right hand side for each throttle area. The result is called *normalized* $C_d(A(\alpha),\Pi)\Psi(\Pi)$.

$$\text{Normalized } C_d(A(\alpha),\Pi)\Psi(\Pi) = \frac{A(\alpha)C_d(A(\alpha),\Pi)\Psi(\Pi)}{\text{mean}_{\text{of the 3 largest}}(A(\alpha)C_d(A(\alpha),\Pi)\Psi(\Pi))} \tag{6.9}$$

The normalized[1] $C_d(A(\alpha), \Pi)\Psi(\Pi)$, presented in Figure 6.7, follow one curve, as the area dependency is canceled in the normalization, which suggests that C_d can be separated into two functions:

$$C_d(\Pi, A(\alpha)) = C_d(\Pi)C_d\left(A\left(\alpha\right)\right) \qquad (6.10)$$

By inserting Eq. (6.10) into Eq. (6.7a) and rearrange the factors two new functions appear. One function that depends on the pressure ratio Π and one that depends on α:

$$W\left(\alpha, p_{\mathrm{im}}, p_{\mathrm{ic}}, T_{\mathrm{ic}}\right) = \frac{p_{\mathrm{ic}}}{\sqrt{R_{\mathrm{a}}T_{\mathrm{im}}}} \underbrace{\Psi\left(\Pi\right)C_d\left(\Pi\right)}_{\text{Function of }\Pi} \underbrace{C_d\left(A\left(\alpha\right)\right)A\left(\alpha\right)}_{\text{Function of }\alpha} \qquad (6.11)$$

In mean value engine models, functions are commonly parameterized to reduce the need for extensive mapping and in Eq. (6.11) there are two functions to parameterize:

- A pressure ratio dependent product: $\Psi\left(\Pi\right)C_d\left(\Pi\right)$

- A throttle angle dependent product: $C_d\left(\alpha\right)A\left(\alpha\right)$

The pressure ratio dependent product is described in the section *compressible flow model* and the throttle angle dependent factor is described in the section *throttle area model*.

Compressible Flow Model

To check whether the factor $C_d(\Pi)$ in the measured product $C_d(\Pi)\Psi(\Pi)$ can be neglected or not the measurements shown in the bottom of Figure 6.7 are plotted together with the standard $\Psi(\Pi)$ function given by Eq. (6.7d). The result is presented in Figure 6.8 where it is clear that the critical pressure, where the flow reaches sonic condition, does not appear at the same pressure ratio as predicted by the isentropic model, Eq. (6.7d). This has also been observed, in for example Pursifull et al. (2000) and Hendricks et al. (1996). One explanation to why the critical pressure is not reached at the pressure ratio described soley by the compressible flow Eq. (6.7d) is that $C_d(\Pi)$ is non-negligible. This is supported by the fact that the points in Figure 6.8 follow one line which differs from the standard $\Psi(\Pi)$ function. Thus, a model of the product $C_d(\Pi)\Psi(\Pi)$ is desirable. The objective of the model is to describe the critical pressure ratio and also to better capture the shape of measured $C_d(\Pi)\Psi(\Pi)$. Two models are studied which both describe the critical pressure better than the original model. First the models are presented and compared, then it is decided which one of the models that will be used.

---

[1]The normalized flow was compensated for the small changes in throttle area are during the experiment.
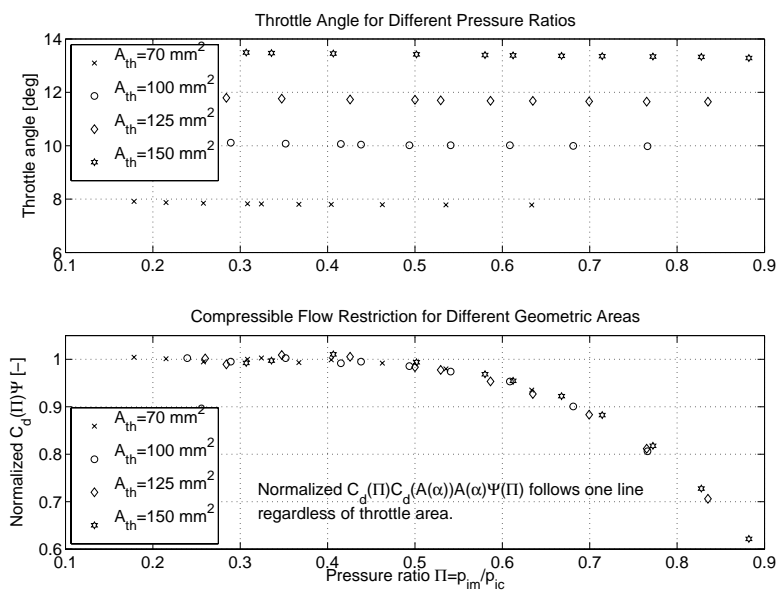
Figure 6.7: Measurements with different pressure ratios Π over the throttle for four fix throttle areas. *Top*: The maximum deviation in throttle angle is less than 0.5 degree and the median deviation is 0.2 degree for each sweep in pressure ratio Π. *Bottom*: The normalized $C_d(A(\alpha), \Pi)\Psi(\Pi)$ follow one curve which shows that the area dependency of $C_d(A(\alpha), \Pi)\Psi(\Pi)$ is canceled and thus it can be factorized into $C_d(A(\alpha))C_d(\Pi)\Psi(\Pi)$.
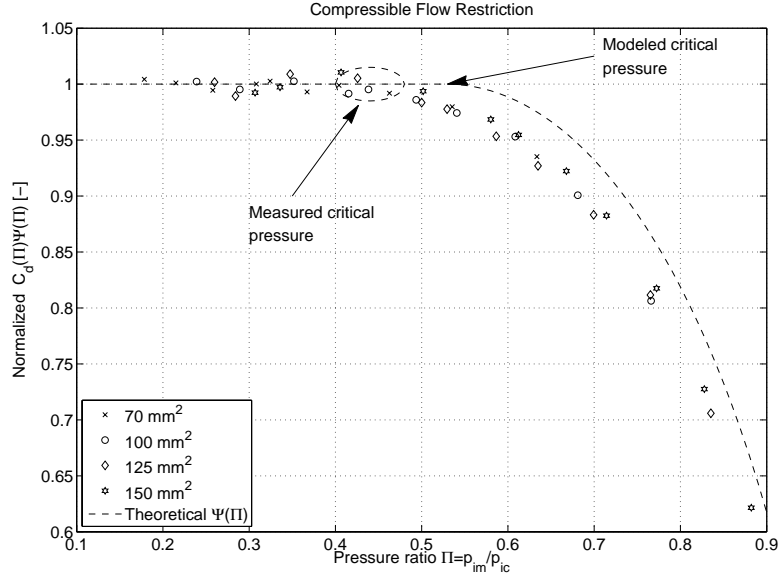
Figure 6.8: Normalized $\Psi(\Pi)C_d(\Pi)$ and modeled compressible flow function $\Psi(\Pi)$, Eq. (3.2d). The modeled $\Psi(\Pi)$ is shown as a dashed line. It has the same shape but the modeled critical pressure (the "knee") appears at a too high pressure ratio.

In the first model, presented in Hendricks et al. (1996), the ordinary $\Psi(\Pi)$-function is replaced by:

$$\Psi_\beta(\Pi) = \begin{cases} \frac{1}{p_n}\sqrt{\Pi^{p_1} - \Pi^{p_2}}, & \Pi \geq p_{\mathrm{crit}} \\ 1, & \Pi < p_{\mathrm{crit}} \end{cases} \tag{6.12}$$

$$p_{\mathrm{crit}} = \left(\frac{p_1}{p_2}\right)^{\frac{1}{p_2 - p_1}} \tag{6.13}$$

$$p_n = \sqrt{p_{\mathrm{crit}}^{p_1} - p_{\mathrm{crit}}^{p_2}} \tag{6.14}$$

There are two tunable parameters p_1 and p_2 in Eq. (6.12), which were determined using the MATLAB function *lsqcurvefit.*

The second model is based on the fact that the critical pressure is a function of γ. By replacing the physical value of γ in Eq. (6.7d) with a value determined using optimization to better describe the measured $\Psi(\Pi)C_d(\Pi)$. The optimization was carried out using the MATLAB function *lsqcurvefit* and the new γ was chosen in a way such that the difference between the measured product and the modeled product of $\Psi_\gamma(\Pi) = C_d(\Pi)\Psi(\Pi)$ was minimized on the experimental data in Figure 6.8.

In Figure 6.9 a comparison is shown between $\Psi(\Pi)$, $\Psi_\beta(\Pi)$, and $\Psi_\gamma(\Pi)$. For pressure ratios between 0.4 and 0.7, $\Psi_\beta(\Pi)$ shows a slightly better behavior over $\Psi_\gamma(\Pi)$. However as the differences between them are small, approximately 1%,
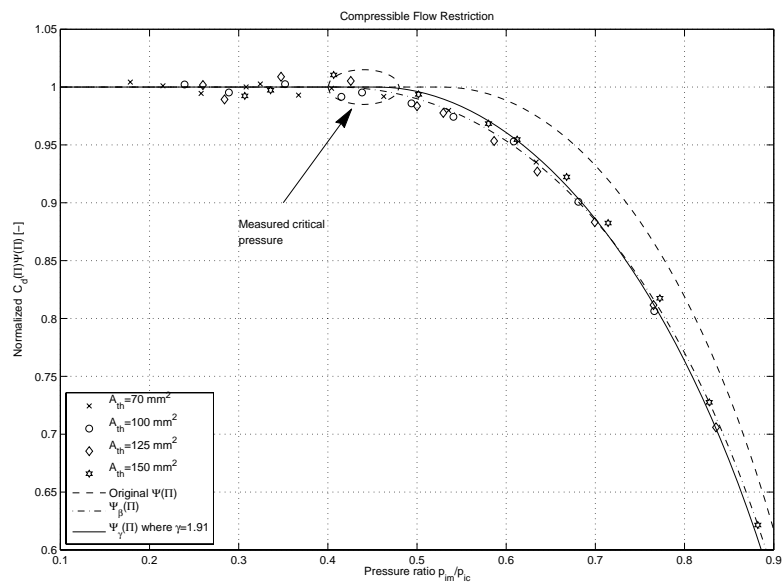
Figure 6.9: Improved versions of the compressible flow restriction function $\Psi(\Pi)$. Two models are shown together with measured data and the original function Eq. (6.7d). Both new models show a considerable improvement compared to the original function (dashed). All fitted functions have been normalized to one at sonic flows. The $\Psi_\gamma(\Pi)$ with $\gamma = 1.91$ reduces the error from 10% down to less than 3%.

for pressure ratios between 0.4 and 0.7, $\Psi_\gamma(\Pi)$ is chosen as it has only one parameter and its structure is well known.

Throttle Area Parameterization

The product of $C_d(\alpha)A(\alpha)$ can now be calculated from mapped engine data by inverting Eq. (6.11):

$$C_d(\alpha)A(\alpha) = \frac{W_{\mathrm{at}}\left(\alpha, p_{\mathrm{im}}, p_{\mathrm{ic}}, T_{\mathrm{ic}}\right)}{\underbrace{\Psi\left(\frac{p_{\mathrm{im}}}{p_{\mathrm{ic}}}\right) C_d\left(\frac{p_{\mathrm{im}}}{p_{\mathrm{ic}}}\right)}_{\text{Modeled by Eq. (6.7d) with a tuned } \gamma}} \frac{\sqrt{R_{\mathrm{a}} T_{\mathrm{ic}}}}{p_{\mathrm{ic}}} \tag{6.15}$$

For this engine a throttle area model has been developed with the following appearance (Nyberg and Nielsen, 1997):

$$C_d(\alpha)A(\alpha) = A_1\left(1 - \cos(a_2\alpha^2 + a_1\alpha + a_0)\right) + A_0 \tag{6.16}$$

The MATLAB function *lsqcurvefit* was used to determine the model parameters and the resulting area estimates are shown in Figure 6.10. Points with pressure ratios close to one have been omitted during the tuning as the $\Psi(\Pi)$ function is very sensitive to small changes in Π, caused by for example pressure sensor errors.

There is a large discrepancy between the model error for the tuning data and the model errors for the validation data. Therefore the cause of the increased error was investigated and was traced to a slight change in the parameters A_0 and A_1. This was verified by re-tuning the throttle area parameters using the validation data and there was only a significant change in two parameters A_0 (30% increase) and A_1 (7% decrease). The cause of the parameter change is most likely the exchange of air-mass flow sensor and the pressure sensor before the throttle. These sensors were replaced in the time between the measurements of the tuning and the validation data.

Resulting Throttle Model Validation

As $C_d(\Pi)\Psi(\Pi)$ and $C_d(\alpha)A(\alpha)$ have been separately validated, the next step is to validate the estimated throttle air-mass flow. In Figure 6.11 comparisons of modeled air-mass flow and measured air-mass flow are shown. For small flows the large relative error are explained by the fact that a small absolute error results in a large relative error for small flows. Most of the points have a precision within 5% and if the throttle area parameters A_0 and A_1 are tuned using the validation data then the error for the validation data takes the same shape as for the tuning data. Thus the larger error for the validation data is explained by a change in throttle area parameters.

Throttle model inputs, parameters, and outputs are listed in Table 6.4.
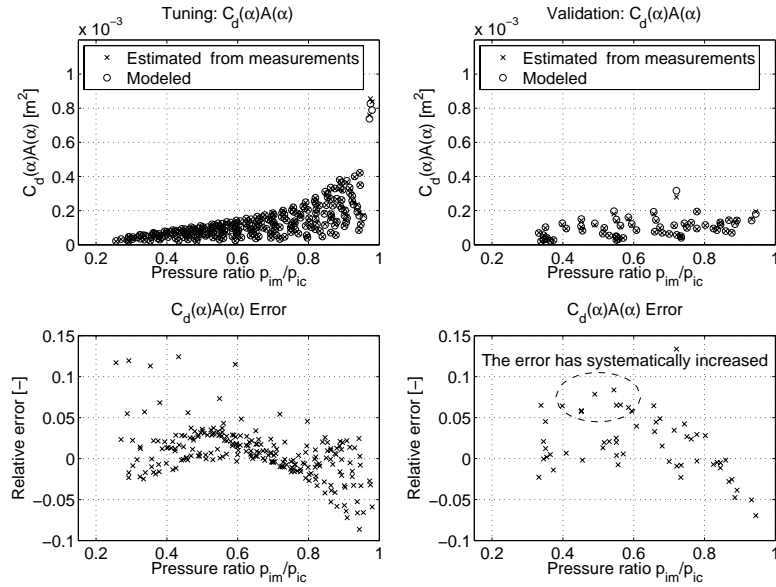
Figure 6.10: Validation of throttle area model. In the left column, the tuning data is shown and to the right is the validation data shown. *Top:* Modeled and estimated area from measurements using Eq. (6.15). *Bottom:* Relative error in the throttle area model. For the tuning data the model error is less than 5% for most of the points. In the validation the errors are larger but this is explained by a change in the throttle area parameters A_0 and A_1 due to different sensors.

Parameters		Inputs		Output		
γ	[-]	T_{ic}	[K]	W_{at}	[kg/s]	Eq. (3.2a)
A_0, A_1, a_0, a_1, a_2		p_{ic}	[Pa]	T_{th}	[T]	Equal to T_{ic}
		p_{im}	[Pa]			
		α	[deg]			

Table 6.4: Throttle model inputs, parameters, and outputs.
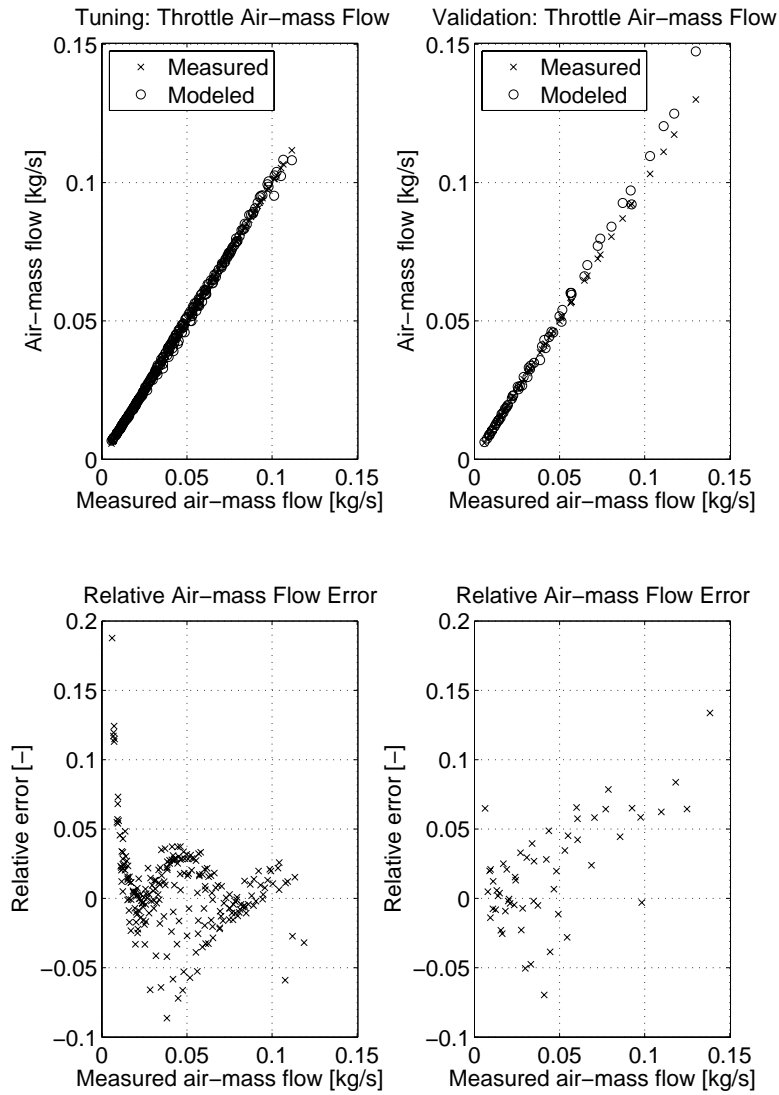
Figure 6.11: Measured and modeled air-mass flow past the throttle. *Left:* Tuning data. *Right:* Validation data. *Bottom:* Relative error in air-mass estimations as a function of measured air-mass flow. There is a systematic relative error in the validation data that is caused by offsets in the throttle area parameters A_0 and A_1. By re-fitting A_0 and A_1 the error has the same shape as for the tuning data, which show that these parameters have changed slightly due to changed sensors.

6.3.2   Wastegate Flow

For the wastegate, the standard flow equations (6.7a, 6.7b, 6.7d) are used. As it is not possible to measure the wastegate flow, a validation has not been performed for this component. The value of γ is set to γ_{eg} for the flow through the wastegate.

$$A_{\mathrm{eff}_{\mathrm{wg}}} = C_d A_{\mathrm{wg}_{\mathrm{max}}} u_{\mathrm{wg}} \qquad u_{\mathrm{wg}} \in [0,1]$$

Measurements of the wastegate valve diameter approximates the maximum open wastegate area parameter $A_{\mathrm{wg}_{\mathrm{max}}}$. In Table 6.5 a summary of the wastegate flow model inputs, parameters, and outputs are listed.

Parameters		Inputs		Output		
$\gamma = \gamma_{\mathrm{eg}}$	[-]	u_{wg}	[-]	W_{wg}	[kg/s]	Eq. (6.7a)
$A_{\mathrm{wg}_{\mathrm{max}}}$	[m^2]	T_{em}	[K]	$T_{\mathrm{wg}} = T_{\mathrm{em}}$	[K]	
$C_d = 0.9$	[-]	p_{em}	[Pa]			
		p_{t}	[Pa]			

Table 6.5: Wastegate flow model inputs, parameters, and outputs.

6.4   Engine

The engine produces a port air-mass flow, exhaust-mass flow, temperature of the latter, and also torque to the crank shaft:

Port air-mass flow Mass-flow from the intake manifold into the cylinder.

Exhaust-mass flow Mass-flow from the combustion, that is cylinder air-mass flow and fuel mass-flow into the exhaust manifold. The temperature of the exhaust-mass flow is determined in two steps including heat transfer from the exhaust manifold.

Torque The engine torque model includes pumping and friction effects.

Both the exhaust manifold mass-flow and the engine torque are modeled as instantaneous, that is the delay caused by the cycles in the four stroke engine is neglected.

6.4.1   Port Air-mass Flow Model

Several effects govern the amount of air entering the cylinder, such as pressure ratio between intake and exhaust ports, air-fuel ratio, heat transfer, engine speed, engine geometry and design (Heywood, 1988, p. 209).
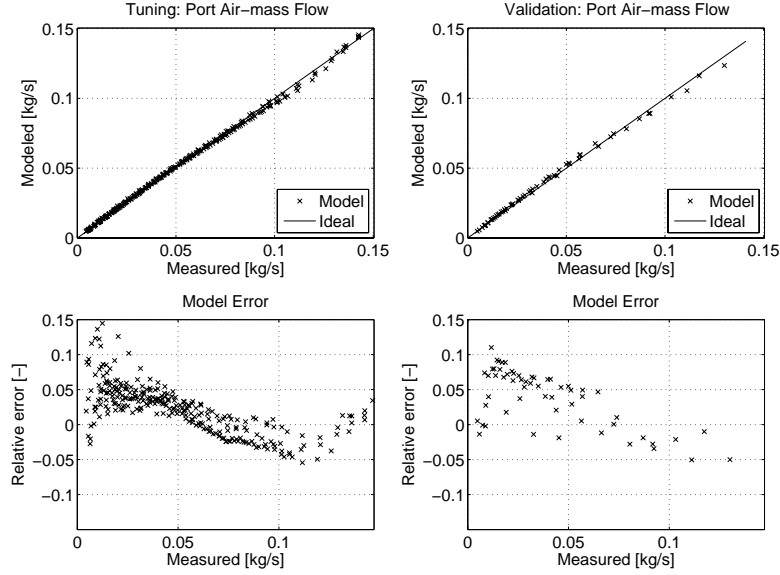
Figure 6.12: Modeled and measured port air-mass flow where the wastegate is controlled by the ECU. In the left column, the tuning data is shown and to the right the validation data is shown. *Top:* The ideal air-mass flow refers to when the modeled flow and the measured flow are equal. *Bottom:* The accuracy of Eq. (6.17) is better than 10% for most points. The model has largest relative errors for low flows where small absolute errors result in large relative errors.

Here the port air-mass flow model with included exhaust manifold pressure dependency and fuel charge cooling effect is used from Chapter 4:

$$
W_{\mathrm{cyl}} = p_{\mathrm{im}} C_1 \frac{1}{1 + \frac{1}{\lambda\left(\frac{A}{F}\right)_s}} \frac{r_c - \left(\frac{p_{\mathrm{em}}}{p_{\mathrm{im}}}\right)^{\frac{1}{\gamma}}}{r_c - 1} V_{\mathrm{d}} \cdot \frac{N}{R_{\mathrm{im}}\left(T_{\mathrm{im}} - \underbrace{C_2 \frac{1 - \lambda^2}{\lambda^2}}_{\text{Charge cooling}}\right) 120}
$$

(6.17)

The model has only two engine specific parameters, and those are the gain parameter C_1, which describes the engine pumping capabilities, and the effect of charge cooling by fuel evaporation C_2. The parameters are determined using the MATLAB-function *lsqnonlin*.

The high accuracy of Eq. (6.17) is shown in the top of Figure 6.12 for stationary data where the engine is running with the wastegate controlled by the ECU. For most points the error is less than 10% even though a different gasoline quality has been used in this validation compared to the tuning data set.

A validation using different exhaust manifold pressures are shown in Chap-

ter 4, Figure 4.10. The port-air mass flow model inputs, parameters, and outputs are listed in Table 6.6.

Parameters		Inputs		Output		
γ_{a}	[-]	p_{im}	[Pa]	W_{cyl}	[kg/s]	Eq. (6.17)
$\left(\frac{A}{F}\right)_s$	[-]	T_{im}	[K]	$T_{c_{\mathrm{flow}}} = T_{\mathrm{im}}$	[K]	
R_{a}	[J/kg/K]	p_{em}	[Pa]			
r_c	[-]	λ	[-]			
V_{d}	[m^3]	N	[RPM]			
C_1, C_2	[-]					

Table 6.6: Throttle model inputs, parameters, and outputs.

6.4.2   Exhaust Mass-flow Model

When the air-fuel mixture has been combusted it enters the exhaust manifold and the mass-flow W_{e} is modeled as instantaneous, that is without taking the rotational delay of the engine into account:

$$W_{\mathrm{e}} = W_{\mathrm{cyl}} + W_{\mathrm{f}} = W_{\mathrm{cyl}} \left(1 + \frac{1}{\lambda \left(\frac{A}{F}\right)_s} \right) \tag{6.18}$$

The temperature of the flow is crucial as it determines the flow of energy to the turbine. Therefore, the next section is devoted to the exhaust mass-flow temperature. The exhaust mass-flow model inputs, parameter, and output are listed in Table 6.7.

Parameter		Inputs		Output		
$\left(\frac{A}{F}\right)_s$	[-]	W_{cyl}	[kg/s]	W_{e}	[kg/s]	Eq. (6.18)
		λ	[-]			

Table 6.7: Exhaust mass-flow model inputs, parameter, and output.

Exhaust Mass-flow Temperature

There is considerable heat transfer in the exhaust manifold and therefore it is hard to measure the exhaust mass-flow temperature. Further, there is a non-negligible thermal mass on the exhaust side, which has to reach thermal equilibrium, and this means that the settling time for exhaust temperatures is long. Only the stationary temperature close to the turbine inlet has been measured. At this point, it is important to know the temperature as it determines the energy into the turbine. As only stationary measurements are present, only the stationary temperature has been modeled.

Using the first law of thermodynamics, for stationary conditions, the heat transfer from the gas inside the exhaust manifold can be superpositioned as a temperature drop on the gas entering the exhaust manifold. This technicality simplifies the modeling and is easy to implement in the model. The temperature model is based on the stationary model presented in Eriksson (2002), where the modeling starts by describing the temperature out of the engine. By assuming a nominal λ and spark-timing, the temperature is modeled as an affine function of mass flow:

$$T_{\mathrm{e}} = T_{\mathrm{e}_0} + \Delta T_{\mathrm{e}_{\max}} \frac{W_{\mathrm{e}}}{W_{\mathrm{e}_{\max}}} \tag{6.19}$$

The heat transfer from the gas is then superpositioned on this temperature:

$$
\begin{aligned}
T_{\mathrm{em}_{\mathrm{in}}} &= T_{\mathrm{a}} + (T_{\mathrm{e}} - T_{\mathrm{a}})e^{-\frac{h_{\mathrm{tot}}\pi D_{\mathrm{em}} l_{\mathrm{em}}}{W_{\mathrm{airfuel}} c_{\mathrm{P_{eg}}}}} \tag{6.20}\\
h_{\mathrm{exh}_{\mathrm{int}}} &= \mathrm{HT}_{\mathrm{exh}_0} \lambda_{\mathrm{exh}} \left(\frac{4}{\pi} \frac{W_{\mathrm{e}}}{\mu_{\mathrm{exh}} n_{\mathrm{cyl}} D_{\mathrm{em}}} \right)^{\mathrm{HT}_{\mathrm{exh}_1}} \left(\frac{7}{10} \right)^{\mathrm{HT}_{\mathrm{exh}_2}} \frac{1}{D_{\mathrm{em}}} \tag{6.21}\\
h_{\mathrm{tot}} &= \pi D_{\mathrm{em}} l_{\mathrm{em}} n_{\mathrm{cyl}} \left(\gamma_{eg} - 1 \right) \frac{1}{\frac{1}{h_{\mathrm{exh}_{\mathrm{int}}}} + \frac{1}{h_{\mathrm{exh}_{\mathrm{ext}}}}} \frac{1}{W_{\mathrm{e}} R_{\mathrm{e}} \gamma_{eg}} \tag{6.22}
\end{aligned}
$$

A validation of the total model, Equations (6.19, 6.20), is shown in Figure 6.13, where the fit for stoichiometric conditions is within 20% for all of the tuning data points and within 25% for the validation data points. The error decreases rapidly with increasing load and for part load conditions, the error is less than 5% which is about the same accuracy as the other models. Therefore this model is sufficiently accurate.

The parameters are determined using the MATLAB-function *lsqcurvefit*. To determine the thermal conductivity and dynamic viscosity, the polynomials from Cho et al. (1997) were evaluated at 1100K. The exhaust mass flow temperature model input, parameters, and output are listed in Table 6.8.

6.4.3 Engine Torque

The engine torque model is based on a model of the brake mean effective pressure (BMEP). BMEP is estimated by subtracting pumping (PMEP) and friction work (FMEP) from the supplied work from the fuel (IMEP).

$$
\begin{aligned}
\mathrm{Tq}_{\mathrm{cs}} &= \frac{\mathrm{BMEP} \cdot V_{\mathrm{d}}}{4\pi} \tag{6.23}\\
\mathrm{BMEP} &= \mathrm{IMEP} - \mathrm{PMEP} - \mathrm{FMEP} \tag{6.24}\\
\mathrm{IMEP} &= W_{\mathrm{cyl}} \frac{60 \cdot 2}{N} \frac{q_{\mathrm{HV}}}{\lambda \left(\frac{A}{F} \right)_s} \frac{\min(\lambda, 1)}{V_{\mathrm{d}}} \eta_{\mathrm{e}} \tag{6.25}\\
\mathrm{PMEP} &= p_{\mathrm{em}} - p_{\mathrm{im}} \tag{6.26}\\
\mathrm{mps} &= 2 \frac{N}{60} \cdot \mathrm{Stroke} \tag{6.27}
\end{aligned}
$$

Parameters		Input		Output		
$W_{\mathrm{e_{max}}}$	[kg/s]	W_{e}	[kg/s]	$T_{\mathrm{em_{in}}}$	[K]	Eq. (6.20)
$\mathrm{HT}_{\mathrm{exh_0}} = 0.26$	[-]					
$\mathrm{HT}_{\mathrm{exh_1}} = 0.6$	[-]					
$\mathrm{HT}_{\mathrm{exh_2}} = 0$	[-]					
$c_{\mathrm{p_{eg}}}$	[J/kg/K]					
γ_{eg}	[-]					
$\lambda_{\mathrm{exh}} = 6.85 \cdot 10^{-2}$	[W/mK]					
$\mu_{\mathrm{exh}} = 4.23 \cdot 10^{-5}$	[kg/(ms)]					
n_{cyl}	[-]					
D_{em}	[m]					
l_{em}	[m]					
$T_{\mathrm{e_0}}$	[K]					
$\Delta T_{\mathrm{e_{max}}}$	[Ks/kg]					

Table 6.8: Exhaust mass flow temperature model input, parameters, and output. W_{e} is determined using Eq. (6.18). λ_{exh} and μ_{exh} were determined at 1100 K.
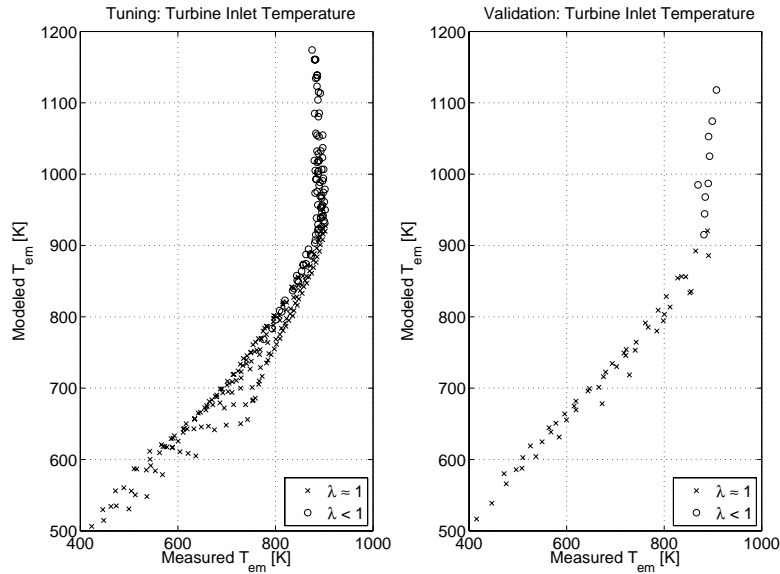
Figure 6.13: Measured and modeled turbine inlet temperature. The model has been tuned for *stoichiometric* conditions ($\lambda = 1$) and the non stoichiometric conditions are only shown for the sake of completeness. *Left:* For the tuning data the maximum error is 20% that occurs for low loads. *Right:* The model predicts up to 25% too high temperatures for low exhaust temperatures but the error decreases to a 5% error for part load conditions.

$$\text{FMEP} = \zeta \sqrt{\frac{75}{1000 \cdot \text{Bore}}} \cdot$$

$$\left(\left(0.464 + 0.0072 \text{mps}^{1.8} \right) \Pi_{\text{bl}} \cdot 10^5 + \underbrace{0.0215 \text{BMEP}}_{\text{BMEP} \approx W_{\text{cyl}} \frac{60 n_r}{N V_{\text{d}}} C_{\text{Tq}_1} + C_{\text{Tq}_2}} \right) \quad (6.28)$$

The friction model originates from ETH, see e.g. Soltic (2000). In the torque model above all parameters are fitted using the method of least squares in two steps. First the parameters C_{Tq_1} and C_{Tq_2} are determined, followed by the two remaining parameters ζ and η_{e}. During the parameter tuning only air-fuel ratios close to stoichiometric have been used. The resulting model is compared to measured data in Figure 6.14, where it is shown that the model describes the torque to within 20% for all but very low loads. By including the effects of fuel enrichment and retarded spark advance it is possible to further improve the torque model.

In Table 6.9 a summary of the torque model inputs, parameters, and output are listed.

Parameters		Inputs		Output		
$q_{\text{HV}} = 44 \cdot 10^6$	[J/kg]	p_{im}	[Pa]	Tq_{cs}	[Nm]	Eq. (6.23)
$\left(\frac{A}{F} \right)_s$	[-]	p_{em}	[Pa]			
V_{d}	[m^3]	λ	[-]			
Stroke	[m]	W_{cyl}	[kg/s]			
Bore	[m]	N	[RPM]			
$\Pi_{\text{bl}} = \max \left(\frac{p_{\text{im}}}{p_{\text{a}}} \right)$	[-]					
η_e	[-]					
ζ	[-]					
$C_{\text{Tq}_1}, C_{\text{Tq}_2}$	[-]					

Table 6.9: Torque model inputs, parameters, and output. The port-air mass-flow input W_{cyl} is given by Eq. (6.17).

6.5 Turbocharger

The turbocharger consists of three components:

Compressor It produces the mass-flow through the compressor and its temperature. To produce the air-mass flow a driving torque is required that also is modeled. See Section 6.6.

Turbine It generates the turbine mass-flow, its temperature, and torque delivered to the turbine shaft. See Section 6.7.
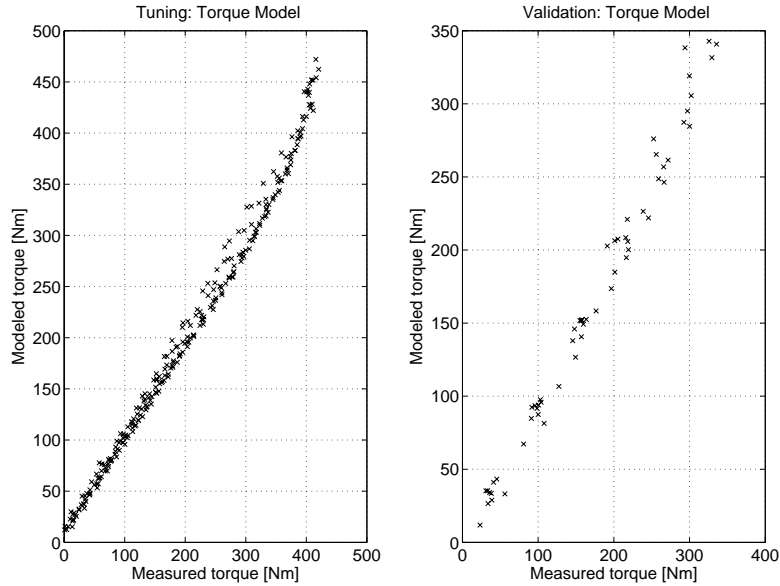
Figure 6.14: Validation of measured and modeled crank shaft torque. *Left:* Modeled and measured torque for the tuning data. Here the model overestimates low torques. *Right:* The torque is described within 20% for the validation data.

Connecting axle Connects the turbine and compressor. This part models the dynamic behavior of the turbocharger speed. See Section 6.8.2.

6.6   Compressor Model

The compressor model is divided into following sub-models:

- Air-mass flow through the compressor

- Efficiency, needed by the temperature and torque model

- Temperature of the mass flow out of the compressor

- Loading torque, needed by the turbocharger speed dynamics model

The models are tuned using mapped data from the manufacturer.

6.6.1   Compressor Air-mass Flow Models

In Moraal and Kolmanovsky (1999) the model by Jensen et al. (1991) is suggested as a suitable compressor air-mass flow model. It is based on a parameterization of the normalized air-mass flow using six parameters. By making a different parameterization, a simpler model is developed and it is shown that

this simple model gives similar precision as the model by Jensen et al. (1991) over the most interesting region of the compressor map. Advantages of the simpler model are:

- Good description of the air-mass flow in the low load region where the engine operates most of the time.

- Simple tuning.

Both models are based on a parameterization of the dimensionless normalized air-mass flow Φ_{comp}:

$$\Phi_{\text{comp}} = \frac{W_{\text{comp}}}{\underbrace{\frac{p_{\text{af}}}{R_{\text{a}}T_{\text{af}}}}_{\text{Density}} \underbrace{\frac{\pi}{4}D_{\text{c}}^2}_{\text{Area}} U_{\text{comp}}} \tag{6.29}$$

In Eq. (6.29) the blade tip speed is required:

$$U_{\text{comp}} = \omega_{\text{TC}}\frac{D_{\text{c}}}{2} \tag{6.30}$$

Assuming that the normalized air-mass flow can be parameterized as $\Phi_{\text{comp}_{\text{par}}}$, then it is possible to invert Eq. (6.29) and express the air-mass flow as a function of $\Phi_{\text{comp}_{\text{par}}}$:

$$W_{\text{comp}} = \left(\frac{p_{\text{af}}}{R_{\text{a}}T_{\text{af}}}\frac{\pi}{4}D_{\text{c}}^2 U_{\text{comp}}\right)\Phi_{\text{comp}_{\text{par}}} \tag{6.31}$$

Now it remains to find a model (parameterization) of the normalized air-mass flow. Here, two models of the normalized air-mass flow are studied. First the model proposed by Jensen and Kristensen where the head parameter Ψ_{comp} and the Mach-number M are used.

$$\Psi_{\text{comp}} = c_{\text{p}_{\text{a}}}T_{\text{af}}\frac{\Pi_{\text{comp}}^{\frac{\gamma_{\text{a}}-1}{\gamma_{\text{a}}}} - 1}{\frac{1}{2}U_{\text{comp}}^2} \tag{6.32}$$

$$M = \frac{U_{\text{comp}}}{\sqrt{\gamma_{\text{a}}RT}} \tag{6.33}$$

In the second model only the head-parameter Ψ_{comp} is used.

Jensen and Kristensen

The compressor air-mass flow model by Jensen, A.F, Sorenson, Houbak, and Hendricks (1991) is based on a parameterization of Φ_{comp_1} using Ψ_{comp}, the

Mach number M, and six parameters k_1 to k_6.

$$\Pi_{\text{comp}} = \frac{p_{\text{comp}}}{p_{\text{af}}} \tag{6.34}$$

$$K3 = k_5 + k_6 M \tag{6.35}$$

$$K2 = k_3 + k_4 M \tag{6.36}$$

$$K1 = k_1 + k_2 M \tag{6.37}$$

$$\Phi_{\text{comp}_1} = \frac{K3\Psi_{\text{comp}} - K1}{K2 + \Psi_{\text{comp}}} \tag{6.38}$$

To determine the air-mass flow parameters the MATLAB-function *lsqcurvefit* is applied to Eq. (6.31) with $\Phi_{\text{comp}_{\text{par}}} = \Phi_{\text{comp}_1}$. In Eq. (6.38) Ψ_{comp} is calculated using Eq. (6.32). When the parameters are fitted to the measured data it is important that $K3$ is positive to avoid negative flows (Moraal and Kolmanovsky, 1999). Even with this constraint, it is hard to get a good fit as there are several local minima which requires manual adjustment of the initial conditions.

By rewriting the optimization problem as

$$K3\Psi_{\text{comp}} - K1 - \Phi_{\text{comp}}K2 = \Psi_{\text{comp}}\Phi_{\text{comp}}$$

the method of least squares can be used to find the parameters k_1 to k_6. However, this method gave a poor result as it optimizes the parameters to minimize the distance to $\Psi_{\text{comp}}\Phi_{\text{comp}}$ instead of the desired Φ_{comp}! Therefore, *lsqcurvefit* was used instead.

Table 6.10 lists a summary of the Jensen and Kristensen compressor air-mass flow model inputs, parameters, and output.

Parameters		Inputs		Output		
γ_{a}	[-]	T_{af}	[K]	W_{comp}	[kg/s] Eq. (6.31)	
D_{c}	[m]	p_{af}	[Pa]			
$k_i, 1 \le i \le 6$	[-]	U_{comp}	[m/s]			

Table 6.10: Jensen and Kristensen compressor air-mass flow model inputs, parameters, and output. The blade speed U_{comp} is determined using Eq. (6.30).

Fitting of Dimensionless Numbers

In Figure 6.15 it is shown that Φ_{comp} and Ψ_{comp} form a quarter of an ellipsis, which results in that the normalized flow Φ_{comp} can be described using only the head parameter Ψ_{comp}, Eq. (6.32):

$$\Phi_{\text{comp}_2} = \sqrt{\frac{1 - K_1\Psi_{\text{comp}}^2}{K_2}}, \qquad \text{where} \quad 1 - K_1\Psi_{\text{comp}}^2 \ge 0 \tag{6.39}$$

In Eq. (6.39) the parameters K_1 and K_2 are determined using the method of least squares after rewriting the problem as $\Psi_{\text{comp}}^2 K_1 + \Phi_{\text{comp}_2}^2 K_2 = 1$. Here this method gave sufficiently accurate results.
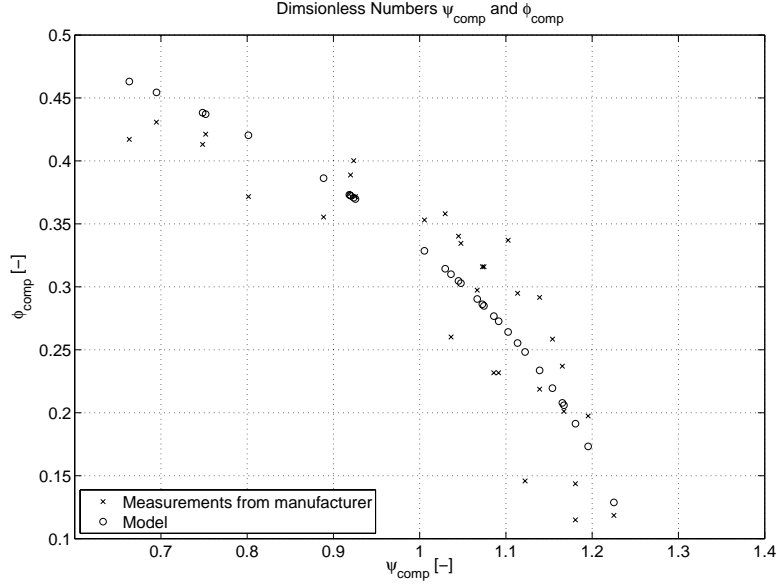
Figure 6.15: Ψ_{comp} and Φ_{comp} follows a quarter of an ellipsis. Here measured and modeled Φ_{comp} are shown as a function of Ψ_{comp}.

Using Eq. (6.31) with $\Phi_{\mathrm{comp}_{\mathrm{par}}} = \Phi_{\mathrm{comp}_2}$ from Eq. (6.39), the air-mass flow through the compressor is determined. In Eq. (6.39) the head parameter Ψ_{comp} is calculated using Eq. (6.32). To ensure that Eq. (6.39) is not complex Π_{comp} must fulfill:

$$\left(\frac{1}{16} \frac{16\,K_1\,c_{\mathrm{p_a}}\,T_{\mathrm{af}} - 2\,D_{\mathrm{c}}{}^2\,\omega_{\mathrm{TC}}{}^2\sqrt{K_1}}{K_1\,c_{\mathrm{p_a}}\,T_{\mathrm{af}}}\right)^{\frac{\gamma_{\mathrm{a}}}{\gamma_{\mathrm{a}}-1}} \leq \Pi_{\mathrm{comp}} \leq$$

$$\left(\frac{1}{16} \frac{16\,K_1\,c_{\mathrm{p_a}}\,T_{\mathrm{af}} + 2\,D_{\mathrm{c}}^2\,\omega_{\mathrm{TC}}^2\sqrt{K_1}}{K_1\,c_{\mathrm{p_a}}\,T_{\mathrm{af}}}\right)^{\frac{\gamma_{\mathrm{a}}}{\gamma_{\mathrm{a}}-1}} \quad (6.40)$$

In Table 6.11 a summary of the compressor air-mass flow model inputs, parameters, and output are listed.

Parameters		Inputs		Output		
γ_{a}	[-]	T_{af}	[K]	W_{comp}	[kg/s]	Eq. (6.31)
D_{c}	[m]	p_{af}	[Pa]			
$K1, K2$	[-]	U_{comp}	[m/s]			

Table 6.11: Compressor mass-flow model based on parameterized dimensionless numbers inputs, parameters, and output. The blade speed U_{comp} is determined using Eq. (6.30).

Mapped and Modeled Compressor Air–mass Flow
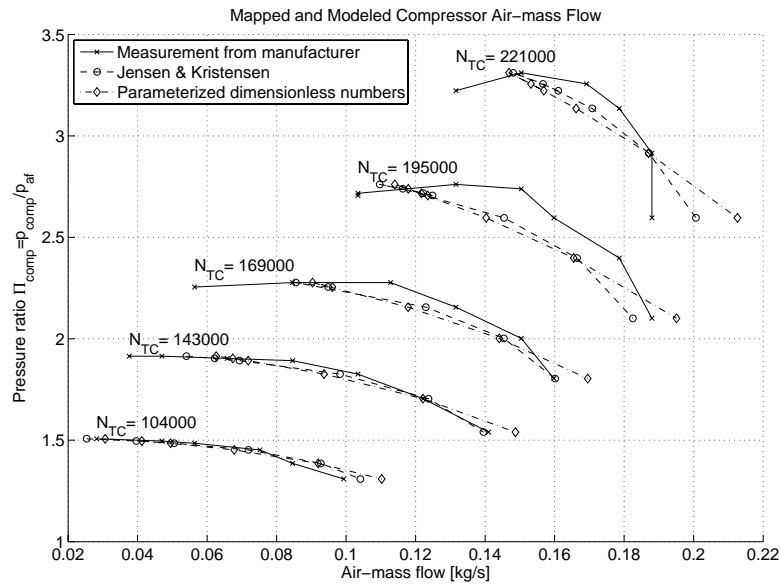
Figure 6.16: Two different compressor air-mass flow models are compared to measured data from the manufacturer. For low to medium compressor speeds both models give accurate estimates of air-mass flow through the compressor. At higher compressor speeds and high mass-flows, none of the models give good agreements with measured data as the models do not include choke. The speed lines show corrected compressor speed. Due to lack of data the same data has been used for tuning and validation.

Selection of Compressor Air-mass Flow Model

In Figure 6.16 the two models are compared to measured data from the turbocharger manufacturer. Both models show similar accuracy for low to medium turbocharger speeds but the Jensen and Kristensen model gives slightly better agreement at higher compressor speeds. However it is considerably harder to tune the Jensen and Kristensen model as it has six parameters and the objective function has several local minima. The parameterized dimensionless numbers method does not require any manual input to determine the correct parameters and the model gives the same accuracy for lower compressor speeds. As the engine operates most of the time in the part load region where both models give the same accuracy, the model using parameterized dimensionless numbers is chosen to model compressor air-mass flow.

6.6.2 Compressor Efficiency Model

The efficiency is modeled based on the proposed model by (Guzzella and Amstutz, 1998). Here it has been improved by substituting Π_{comp} to $1+\sqrt{\Pi_{\text{comp}} - 1}$ as this gives a better agreement with measured data. The model requires the
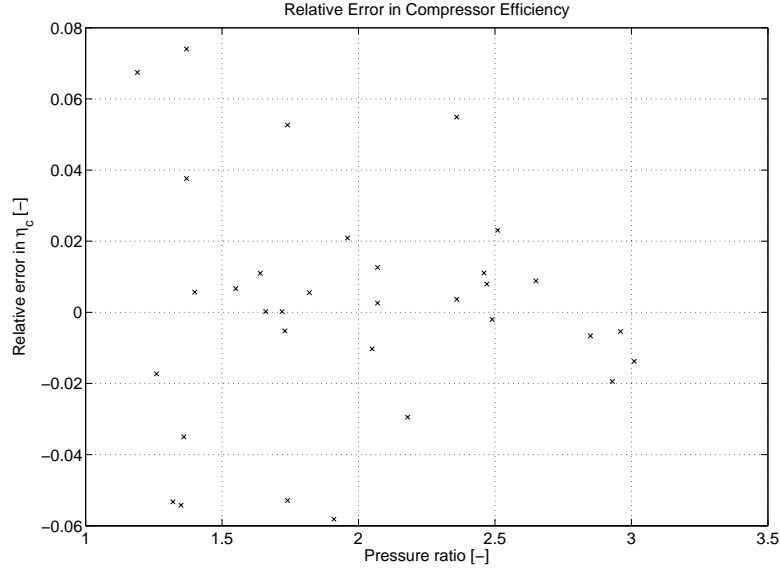
Figure 6.17: The modeled and measured compressor efficiency for the data supplied by the manufacturer (the same data have been used for tuning and validation). The accuracy is within 8% and the error is largest for low pressure ratios. For high pressure ratios the error is less than 2%.

location of the maximum efficiency, $\eta_{\max}$, pressure ratio, corrected air-mass flow (Heywood, 1988, p. 262), and three tunable parameters, a_{11}, a_{12}, and a_{22}:

$$W_{\mathrm{comp_{corr}}} = W_{\mathrm{comp}} \frac{\sqrt{T_0/T_{\mathrm{std}}}}{p_0/p_{\mathrm{std}}} \tag{6.41a}$$

$$Q = \begin{bmatrix} a_{11} & a_{12} \\ a_{12} & a_{22} \end{bmatrix} \tag{6.41b}$$

$$\chi = \begin{bmatrix} W_{\mathrm{comp_{corr}}} - W_{\mathrm{comp}_{\eta_{\max}}} \\ 1 + \sqrt{\Pi_{\mathrm{comp}} - 1} - \Pi_{\mathrm{comp}_{\eta_{\max}}} \end{bmatrix} \tag{6.41c}$$

$$\eta_{\mathrm{comp}} = \eta_{\max} - \chi^T Q \chi \tag{6.41d}$$

Equations 6.41c and 6.41d require the maximum efficiency $\eta_{\max}$ and its location in terms of corrected mass-flow $W_{\mathrm{comp}_{\eta_{\max}}}$ and pressure ratio $\Pi_{\mathrm{comp}_{\eta_{\max}}}$. It is not probable that this point is included in the measured data supplied by the manufacturer and therefore $\eta_{\max}$, $W_{\mathrm{comp}_{\eta_{\max}}}$, and $\Pi_{\mathrm{comp}_{\eta_{\max}}}$ are considered as parameters which are determined using the MATLAB-function *lsqcurvefit*. Given the maximum efficiency and its location the parameters a_{11}, a_{12}, a_{22} are given by the method of least squares. To make sure that the efficiency is not complex, the pressure ratio must fulfill $\Pi_{\mathrm{comp}} \geq 1$. The resulting model validation is shown in Figure 6.17.

In Table 6.12 a summary of the compressor efficiency model inputs, parameters, and output are listed.

Parameters		Inputs		Output		
$W_{\mathrm{comp}_{\eta_{\max}}}$	[kg/s]	Π_{comp}	[-]	η_{comp}	[-]	Eq. (6.41d)
$\Pi_{\mathrm{comp}_{\eta_{\max}}}$	[-]	ω_{TC}	[rad/s]			
$\eta_{\max}$	[-]					
a_{11}, a_{21}, a_{22}	[-]					

Table 6.12: Compressor efficiency model inputs, parameters, and output.

6.6.3   Compressor Temperature Out

The temperature out of the compressor is modeled by inverting the efficiency definition (Heywood, 1988, pp. 252):

$$T_{\mathrm{comp}_{\mathrm{out}}} = T_{\mathrm{af}} \left(1 + \frac{\Pi_{\mathrm{comp}}^{\frac{\gamma_{\mathrm{a}}-1}{\gamma_{\mathrm{a}}}} - 1}{\eta_{\mathrm{comp}}} \right) \tag{6.42}$$

In Figure 6.18 a validation plot is shown. In Table 6.13 a summary of the compressor outlet temperature model inputs, parameter, and output are listed.

Parameter		Inputs		Output		
γ_{a}	[-]	T_{af}	[K]	$T_{\mathrm{comp}_{\mathrm{out}}}$	[K]	Eq. (6.42)
		η_{comp}	[-]			
		Π_{comp}	[-]			

Table 6.13: Summary of inputs, parameter, and output of the temperature model of the air leaving the compressor. The compressor efficiency η_{comp} is determined using Eq. (6.41d).

6.6.4   Compressor Torque

This model is based on power balance of the power to the compressor $P = T_{\mathrm{q}_{\mathrm{comp}}} \omega_{\mathrm{TC}}$ which equals the necessary work transfer rate performed by the compressor (Heywood, 1988, p. 252).

$$T_{\mathrm{q}_{\mathrm{comp}}} = \frac{c_{\mathrm{p_a}} W_{\mathrm{comp}} (T_{\mathrm{comp}_{\mathrm{out}}} - T_{\mathrm{af}})}{\omega_{\mathrm{TC}}} \tag{6.43}$$

In Table 6.14 a summary of the compressor torque model inputs, parameters, and output are listed.

As no measured compressor torque exists, this model component can not be separately validated.
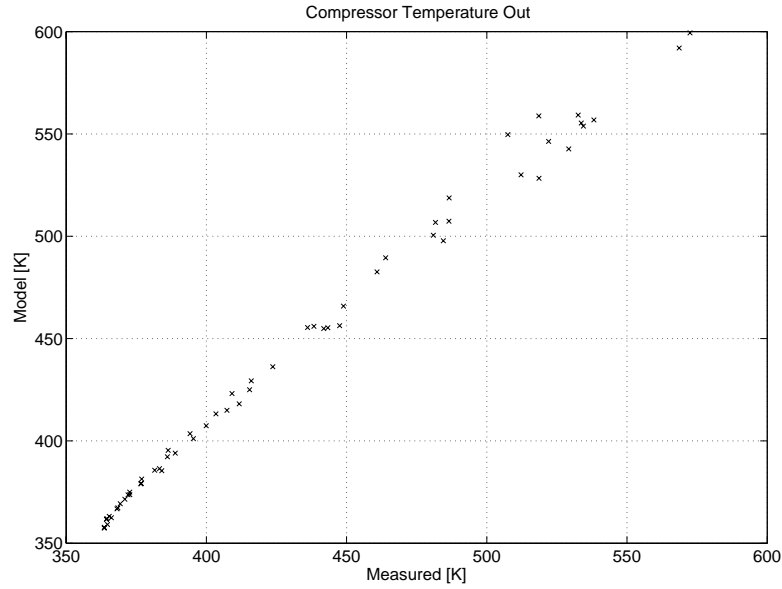
Figure 6.18: Validation of compressor temperature out model using the validation data set instead of the compressor map. The average error is less than 3% and the maximum error is 8%.

Parameters		Inputs		Output		
γ_a	[-]	T_{af}	[K]	$T_{q_{comp}}$	[Nm]	Eq. (6.43)
c_{p_a}	[J/kg/K]	W_{comp}	[kg/s]			
		ω_{TC}	[rad/s]			

Table 6.14: Compressor torque model inputs, parameter, and output.

6.7 Turbine

Four sub-models describe the turbine:

- Mass flow model

- Efficiency model, needed by the temperature and torque models

- Temperature of gas flowing out of the turbine

- Torque model, which is needed by the turbocharger speed dynamics

6.7.1 Turbine Mass-flow

It has been noted that the turbine mass flow is almost independent of the turbine speed and can therefore be effectively described by the pressure ratio over the turbine. Here the corrected turbine mass flow is modeled as a restriction like in Eriksson et al. (2002b):

$$\Pi_t = \frac{p_t}{p_{em}} \tag{6.44}$$

$$W_{t_{corr}} = \begin{cases} k_1 \sqrt{1 - \Pi_t^{k_2}}, & \Pi_t^{k_2} \leq 1 \\ 0, & \text{otherwise} \end{cases} \tag{6.45}$$

The corrected mass flow $W_{t_{corr}}$ is defined as (Heywood, 1988, p. 255):

$$W_{t_{corr}} = W_t \frac{\sqrt{T_{em}}}{p_{em}} \tag{6.46}$$

The parameters k_1 and k_2 in Eq. (6.45) are determined using the MATLAB-function *lsqcurvefit* and the validation is shown in Figure 6.19. The relative error is less than 5% for the data supplied by the manufacturer and for the measured validation data, the fit is good considering the uncertainties regarding the temperature before the turbine.

In Table 6.15 a summary of the turbine mass-flow model inputs, parameters, and output are listed.

Parameters	Inputs	Output		
k_1, k_2 [-]	p_t [Pa]	W_t	[kg/s]	Eq. (6.46)
	p_{em} [Pa]			
	T_{em} [K]			

Table 6.15: Turbine mass-flow model inputs, parameters, and output.
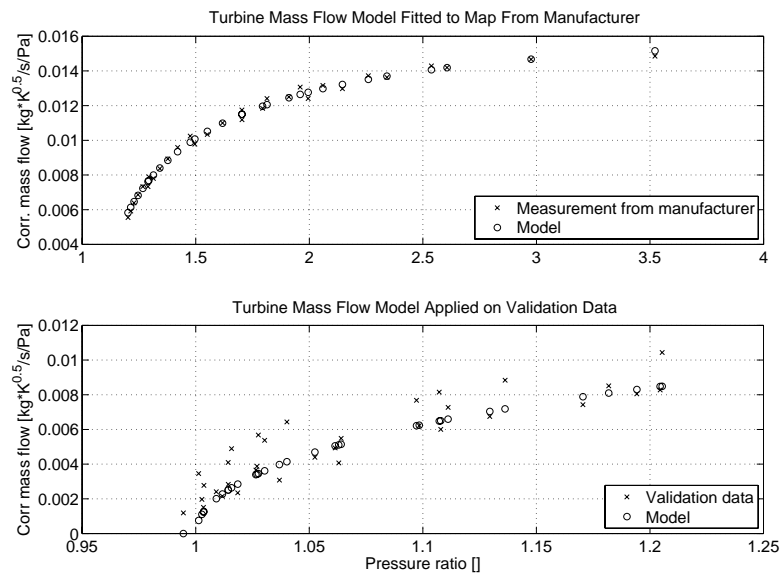
Figure 6.19: Validation of corrected turbine mass flow. *Top:* Modeled data is compared to measured data from the manufacturer and the error is less than 5% for all points. *Bottom:* Measured data in the engine lab is compared to modeled data for operating points where the wastegate is closed. The measured corrected mass-flow is higher than the modeled data as the measured temperature did not reach stationary conditions at low loads and at higher loads the engine knocks and retard the ignition timing which increases the temperature and thus the corrected mass flow.

6.7.2 Turbine Efficiency

Turbine efficiency depends on the blade speed ratio, BSR, as seen in Watson and Janota (1982, pp. 164) and Dixion (1998, p. 284). BSR is defined as:

$$
\text{BSR} \quad = \quad \frac{D_t}{2} \frac{\omega_{\text{TC}}}{\sqrt{2 c_{\text{P}_{\text{eg}}} T_{\text{em}} \left(1 - \left(\frac{1}{\Pi_t}\right)^{\frac{1 - \gamma_{\text{eg}}}{\gamma_{\text{eg}}}}\right)}}
\tag{6.47}
$$

To make sure that the BSR is not complex the following inequality must hold:

$$
\left(\frac{1}{\Pi_t}\right)^{\frac{1 - \gamma_{\text{eg}}}{\gamma_{\text{eg}}}} < 1
$$

Given the BSR the turbine efficiency is modeled using two parameters. The first parameter is the maximum efficiency $\eta_{t_{\max}}$ and the second is its corresponding blade speed ratio $\text{BSR}_{\eta_{t_{\max}}}$.

$$
\eta_t \quad = \quad \eta_{t_{\max}} \left(1 - \left(\frac{\text{BSR} - \text{BSR}_{\eta_{t_{\max}}}}{\text{BSR}_{\eta_{t_{\max}}}}\right)^2\right)
\tag{6.48}
$$

The turbine efficiency model parameters are determined using the MATLAB-function *lsqcurvefit*. In Figure 6.20 the efficiency model is validated using data supplied by the manufacturer and it shows a very good fit. A summary of the turbine efficiency model inputs, parameters, and output are listed in Table 6.16.

Parameters		Inputs		Output		
D_t	[m]	T_{em}	[K]	η_t	[-]	Eq. (6.48)
$c_{\text{P}_{\text{eg}}}$	[J/K/kg]	W_t	[kg/s]			
γ_{eg}	[-]	T_{em}	[K]			
$\eta_{t_{\max}}$	[-]					
$\text{BSR}_{\eta_{t_{\max}}}$	[-]					

Table 6.16: Turbine efficiency model inputs, parameters, and output.

6.7.3 Turbine Temperature Out

This is calculated from the definition of turbine efficiency, see (Heywood, 1988, pp. 254):

$$
T_{t_{\text{out}}} = T_{\text{em}} - T_{\text{em}} \left(1 - \Pi_t^{\frac{\gamma_{\text{eg}} - 1}{\gamma_{\text{eg}}}}\right) \eta_t
\tag{6.49}
$$

In Figure 6.21 the model is validated to measured temperature after the turbine. The model underestimates the temperature with at most 10%.

A summary of the turbine temperature out model inputs, parameters and output are listed in Table 6.17.
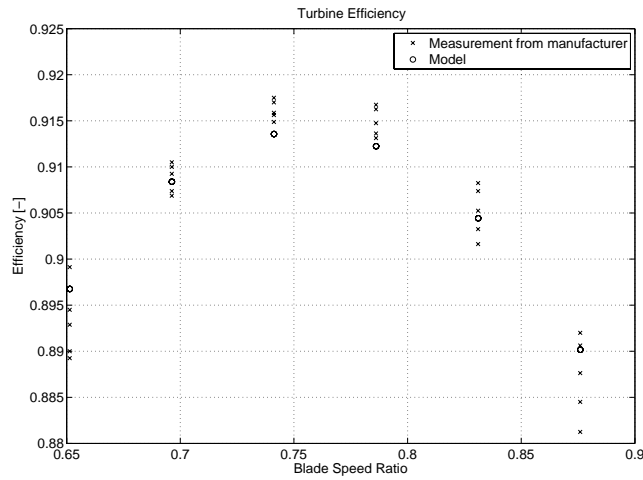
Figure 6.20: *Top*: Validation of efficiency as a function of blade speed ratio using the tuning data supplied by the manufacturer. Here the fit is within 1%.

Parameters		Inputs		Output		
γ_{eg}	[-]	T_{em}	[K]	$T_{\mathrm{t_{out}}}$	[K]	Eq. (6.49)
$c_{\mathrm{p_{eg}}}$	[J/kg/K]	W_{t}	[kg/s]			
		W_{t}	[kg/s]			
		η_{t}	[-]			

Table 6.17: Inputs, parameters of the turbine exit mass-flow temperature.
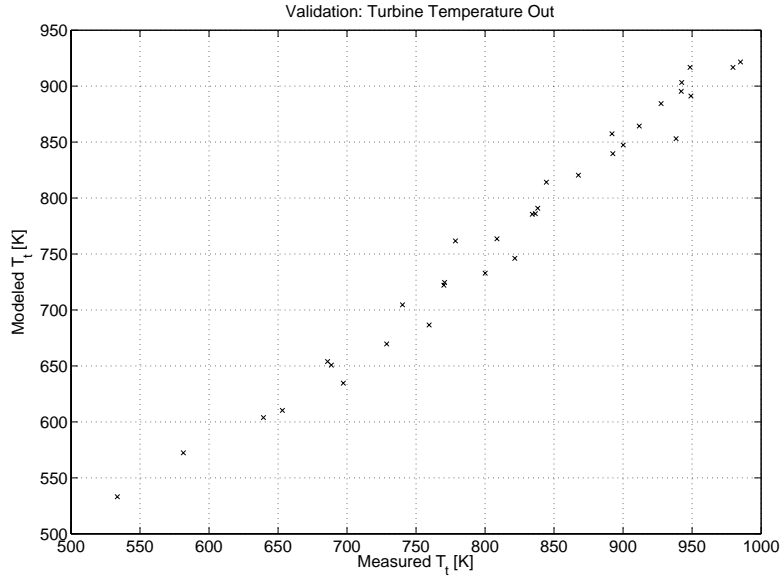
Figure 6.21: The temperature is described within 10%. This model can only be validated in operating points where the wastegate is closed as the mass-flow through the wastegate is unknown.

6.7.4   Turbine Torque

Produced torque from the turbine is estimated from the change in gas temperature times the efficiency:

$$T_{q_t} = \frac{\eta_t W_t c_{p_{eg}} T_{em} \left(1 - \Pi_t^{\frac{\gamma_{eg}-1}{\gamma_{eg}}}\right)}{\omega_{TC}} \tag{6.50}$$

In Table 6.18 a summary of the model inputs, parameters, and output are listed.

Parameters		Inputs		Output		
γ_{eg}	[-]	W_t	[kg/s]	T_{q_t}	[Nm]	Eq. (6.50)
$c_{p_{eg}}$	[J/kg/K]	T_{em}				
		η_t	[-]			

Table 6.18: Turbine torque model inputs, parameters, and output.

6.8   Model Dynamics

In the engine model, there are two kinds of dynamics:

Receiver filling and emptying All control volumes are modeled with filling and emptying dynamics using two states: pressure and temperature.

Turbocharger speed The connecting axle between the turbine and compressor has dynamics as it is driven by the turbine torque and loaded by the compressor and friction.

6.8.1 Control Volumes with Filling and Emptying Dynamics

Using the ideal gas law together with mass and energy conservation, the pressure and temperature dynamics in a control volume is modeled. The pressure derivative originates from differentiation of the ideal gas law and the temperature derivative is given by differentiating the energy conservation law.

$$m = \frac{pV}{RT} \tag{6.51a}$$

$$\frac{\mathrm{d}T}{\mathrm{d}t} = \frac{1}{mc_v}\left(W_{\text{in}}c_v\left(T_{\text{in}} - T\right)\right) + \frac{1}{mc_v}\left(R\left(T_{\text{in}}W_{\text{in}} - TW_{\text{out}}\right) + \dot{Q}\right) = \\ f_{\frac{\mathrm{d}T}{\mathrm{d}t}}\left(p, T, T_{\text{in}}, W_{\text{in}}, W_{\text{out}}, m, R, V, c_v, \dot{Q}\right) \tag{6.51b}$$

$$\frac{\mathrm{d}p}{\mathrm{d}t} = \frac{RT}{V}\left(W_{\text{in}} - W_{\text{out}}\right) + \frac{mR}{V}\frac{\mathrm{d}T}{\mathrm{d}t} = f_{\frac{\mathrm{d}p}{\mathrm{d}t}}\left(p, T, W_{\text{in}}, W_{\text{out}}, m, R, V, f_{\frac{\mathrm{d}T}{\mathrm{d}t}}\right) \tag{6.51c}$$

The locations of the control volumes are described in Table 6.19.

	Control volume between restrictions	
Name	Restriction 1	Restriction 2
af	air-filter	compressor
comp	compressor	intercooler
ic	intercooler	throttle
im	throttle	cylinder (intake valve)
em	cylinder (exhaust valve)	turbine
t	turbine	exhaust system

Table 6.19: Control volume locations.

In Table 6.20 the inputs, parameters, and states/outputs are listed for each control volume.

Here the volume parameter is determined using known engine geometry, and measurements of the pipe volumes etc. To validate the control volume it is necessary to know the flows into and out of the volume. Since there is only one mass-flow sensor, this is not possible. Therefore, the control volume dynamics are validated during the total model validation.

Parameters		Inputs		States, Outputs		
V	[m^3]	T_{in}	[K]	T	[K]	Eq. (6.51b)
R	[J/kg/K]	W_{in}	[kg/s]	p	[Pa]	Eq. (6.51c)
c_{v}	[J/kg/K]	W_{out}	[kg/s]			
		$\dot{Q}$	[J/s]			

Table 6.20: Adiabatic control volume inputs, parameters, and states/outputs.

6.8.2 Turbocharger Speed Dynamics

The turbocharger speed dynamics is modeled using Newton's second law for rotating systems. Inputs are the difference between the driving torque from the turbine and the loading torque from the compressor. A friction term is included as it improves stability (Eriksson et al., 2002b). The identified friction$_{\text{TC}}$ should be small as this term also is included in the efficiency of the turbine.

$$I_{\text{TC}} \frac{\mathrm{d}\omega_{\text{TC}}}{\mathrm{d}t} = \left(T_{\text{q}_\text{t}} - T_{\text{q}_{\text{comp}}} - \omega_{\text{TC}} \cdot \text{friction}_{\text{TC}} \right) \tag{6.52}$$

There are two parameters I_{TC} and friction$_{\text{TC}}$ which are tuned manually. The inertia is tuned by step response experiments and friction$_{\text{TC}}$ is estimated using the following relation: friction$_{\text{TC}} = \frac{T_{\text{q}_\text{t}} - T_{\text{q}_\text{c}}}{\omega_{\text{TC}}}$ applied on the validation data. When friction$_{\text{TC}}$ is determined, only points with closed wastegate and where the engine delivers a positive torque is used.

In Table 6.21 a summary of the turbocharger speed model inputs, parameters, and state/output are listed.

Parameters		Inputs		State, Output		
I_{TC}	[Js^2/rad]	T_{q_t}	[Nm]	ω_{TC}	[rad/s]	Eq. (6.52)
friction$_{\text{TC}}$	[Js/rad]	$T_{\text{q}_{\text{comp}}}$	[Nm]			

Table 6.21: Turbocharger speed dynamics inputs, parameters, and state/output.

6.9 Summary of Model Equations

Next follows a summary of the equations that have been developed for this family of turbocharged SI-engines.

6.9.1 Air-filter Control Volume Dynamics

$$\frac{\mathrm{d}T_{\text{af}}}{\mathrm{d}t} = \frac{1}{m_{\text{af}}c_{\text{v}_\text{a}}} \left(W_{\text{af}}c_{\text{v}_\text{a}} \left(T_\text{a} - T_{\text{af}} \right) \right) +$$
$$\frac{1}{m_{\text{af}}c_{\text{v}_\text{a}}} \left(R_\text{a} \left(T_\text{a} W_{\text{af}} - T_{\text{af}} W_{\text{comp}} \right) + \dot{Q} \right) \tag{6.53a}$$

$$\frac{\mathrm{d}p_{\mathrm{af}}}{\mathrm{d}t} \quad = \quad \frac{R_{\mathrm{a}}T_{\mathrm{af}}}{V_{\mathrm{af}}}\left(W_{\mathrm{af}} - W_{\mathrm{comp}}\right) \quad + \quad \frac{m_{\mathrm{af}}R_{\mathrm{a}}}{V_{\mathrm{af}}}\frac{\mathrm{d}T_{\mathrm{af}}}{\mathrm{d}t} \quad \text{(6.53b)}$$

$$m_{\mathrm{af}} = \frac{p_{\mathrm{af}}V_{\mathrm{af}}}{R_{\mathrm{a}}T_{\mathrm{af}}} \quad \text{(6.53c)}$$

$$W_{\mathrm{af}} = \begin{cases} \sqrt{p_{\mathrm{a}}\frac{p_{\mathrm{a}}-p_{\mathrm{af}}}{\mathcal{H}_{\mathrm{af}}T_{\mathrm{af}}}}, & p_{\mathrm{a}} - p_{\mathrm{af}} > p_{\mathrm{lin}} \\ \sqrt{\frac{p_{\mathrm{a}}}{\mathcal{H}_{\mathrm{af}}T_{\mathrm{a}}}}\frac{p_{\mathrm{a}}-p_{\mathrm{af}}}{\sqrt{p_{\mathrm{lin}}}}, & 0 \le p_{\mathrm{a}} - p_{\mathrm{af}} \le p_{\mathrm{lin}} \\ 0, & p_{\mathrm{a}} - p_{\mathrm{af}} < 0 \end{cases} \quad \text{(6.53d)}$$

$$W_{\mathrm{comp}} = \left(\frac{p_{\mathrm{af}}}{R_{\mathrm{a}}T_{\mathrm{af}}}\frac{\pi}{4}D_{\mathrm{c}}^2 U_{\mathrm{comp}}\right)\sqrt{\frac{1 - \min\left(K_1\left(c_{\mathrm{p_a}}T_{\mathrm{af}}\frac{\Pi_{\mathrm{comp}}^{\frac{\gamma_{\mathrm{a}}-1}{\gamma_{\mathrm{a}}}}-1}{\frac{1}{2}U_{\mathrm{comp}}^2}\right)^2, 1\right)}{K_2}}$$
$$\text{(6.53e)}$$

$$U_{\mathrm{comp}} = \omega_{\mathrm{TC}}\frac{D_{\mathrm{c}}}{2} \quad \text{(6.53f)}$$

6.9.2 Compressor Control Volume Dynamics

$$\frac{\mathrm{d}T_{\mathrm{comp}}}{\mathrm{d}t} = \frac{1}{m_{\mathrm{comp}}c_{\mathrm{v_a}}}\left(W_{\mathrm{comp}}c_{\mathrm{v_a}}\left(T_{\mathrm{comp_{out}}} - T_{\mathrm{comp}}\right)\right) +$$
$$\frac{1}{m_{\mathrm{comp}}c_{\mathrm{v_a}}}\left(R_{\mathrm{a}}\left(T_{\mathrm{comp_{out}}}W_{\mathrm{comp}} - T_{\mathrm{comp}}W_{\mathrm{ic}}\right) + \dot{Q}\right) \quad \text{(6.54a)}$$

$$\frac{\mathrm{d}p_{\mathrm{comp}}}{\mathrm{d}t} \quad = \quad \frac{R_{\mathrm{a}}T_{\mathrm{comp}}}{V_{\mathrm{comp}}}\left(W_{\mathrm{comp}} - W_{\mathrm{ic}}\right) \quad + \quad \frac{m_{\mathrm{comp}}R_{\mathrm{a}}}{V_{\mathrm{comp}}}\frac{\mathrm{d}T_{\mathrm{comp}}}{\mathrm{d}t} \quad \text{(6.54b)}$$

$$m_{\mathrm{comp}} \quad = \quad \frac{p_{\mathrm{comp}}V_{\mathrm{comp}}}{R_{\mathrm{a}}T_{\mathrm{comp}}} \quad \text{(6.54c)}$$

$$T_{\mathrm{comp_{out}}} = T_{\mathrm{af}} +$$
$$\frac{T_{\mathrm{af}}\left(\Pi_{\mathrm{comp}}^{\frac{\gamma_{\mathrm{a}}-1}{\gamma_{\mathrm{a}}}} - 1\right)}{\eta_{\max} - \left[\begin{array}{c}W_{\mathrm{comp}}\frac{\sqrt{T_0/T_{\mathrm{std}}}}{p_0/p_{\mathrm{std}}} - W_{\mathrm{comp}\eta_{\max}} \\ \frac{1 + \sqrt{\Pi_{\mathrm{comp}} - 1} - \Pi_{\mathrm{comp}\eta_{\max}}}{}\end{array}\right]^T\left[\begin{array}{cc}a_{11} & a_{12} \\ a_{12} & a_{22}\end{array}\right]\left[\begin{array}{c}W_{\mathrm{comp}}\frac{\sqrt{T_0/T_{\mathrm{std}}}}{p_0/p_{\mathrm{std}}} - W_{\mathrm{comp}\eta_{\max}} \\ \frac{1 + \sqrt{\Pi_{\mathrm{comp}} - 1} - \Pi_{\mathrm{comp}\eta_{\max}}}{}\end{array}\right]}$$
$$\text{(6.54d)}$$

$$W_{\mathrm{ic}} = \begin{cases} \sqrt{p_{\mathrm{comp}}\frac{p_{\mathrm{comp}}-p_{\mathrm{ic}}}{\mathcal{H}_{\mathrm{ic}}T_{\mathrm{comp}}}}, & p_{\mathrm{comp}} - p_{\mathrm{ic}} > p_{\mathrm{lin}} \\ \sqrt{\frac{p_{\mathrm{comp}}}{\mathcal{H}_{\mathrm{ic}}T_{\mathrm{comp}}}}\frac{p_{\mathrm{comp}}-p_{\mathrm{ic}}}{\sqrt{p_{\mathrm{lin}}}}, & 0 \le p_{\mathrm{comp}} - p_{\mathrm{ic}} \le p_{\mathrm{lin}} \\ 0, & p_{\mathrm{comp}} - p_{\mathrm{ic}} < 0 \end{cases} \quad \text{(6.54e)}$$

6.9.3   Intercooler Control Volume Dynamics

$$\frac{\mathrm{d}T_{\mathrm{ic}}}{\mathrm{d}t} = \frac{1}{m_{\mathrm{ic}}c_{\mathrm{v_a}}} \left(W_{\mathrm{ic}}c_{\mathrm{v_a}} \left(T_{\mathrm{ic_{out}}} - T_{\mathrm{ic}} \right) \right) +$$
$$\frac{1}{m_{\mathrm{ic}}c_{\mathrm{v_a}}} \left(R_{\mathrm{a}} \left(T_{\mathrm{ic_{out}}} W_{\mathrm{ic}} - T_{\mathrm{ic}} W_{\mathrm{at}} \right) + \dot{Q} \right) \quad (6.55\mathrm{a})$$

$$\frac{\mathrm{d}p_{\mathrm{ic}}}{\mathrm{d}t} = \frac{R_{\mathrm{a}} T_{\mathrm{ic}}}{V_{\mathrm{ic}}} \left(W_{\mathrm{ic}} - W_{\mathrm{at}} \right) + \frac{m_{\mathrm{ic}} R_{\mathrm{a}}}{V_{\mathrm{ic}}} \frac{\mathrm{d}T_{\mathrm{ic}}}{\mathrm{d}t} \quad (6.55\mathrm{b})$$

$$m_{\mathrm{ic}} = \frac{p_{\mathrm{ic}} V_{\mathrm{ic}}}{R_{\mathrm{a}} T_{\mathrm{ic}}} \quad (6.55\mathrm{c})$$

$$W_{\mathrm{at}} = \frac{p_{\mathrm{ic}}}{\sqrt{R_{\mathrm{a}} T_{\mathrm{ic}}}} \Psi \left(\Pi \right) A_{\mathrm{eff}} \left(\alpha \right) \quad (6.55\mathrm{d})$$

$$\Pi = \frac{p_{\mathrm{im}}}{p_{\mathrm{ic}}} \quad (6.55\mathrm{e})$$

$$\Psi^* \left(\Pi \right) = \frac{\sqrt{\frac{2\gamma}{\gamma-1} \left(\Pi^{\frac{2}{\gamma}} - \Pi^{\frac{\gamma+1}{\gamma}} \right)}}{\sqrt{\frac{2\gamma}{\gamma-1} \left(\left(\frac{2}{\gamma+1} \right)^{\frac{2}{\gamma-1}} - \left(\frac{2}{\gamma+1} \right)^{\frac{\gamma+1}{\gamma-1}} \right)}} \quad (6.55\mathrm{f})$$

$$\Psi \left(\Pi \right) = \begin{cases} 1 & 0 < \Pi \leq \left(\frac{2}{\gamma+1} \right)^{\frac{\gamma}{\gamma+1}} \\ \Psi^*(\Pi) & \left(\frac{2}{\gamma+1} \right)^{\frac{\gamma}{\gamma+1}} < \Pi \leq \Pi_{\mathrm{lin}} \\ \frac{\Psi^*(\Pi_{\mathrm{lin}})}{\Pi_{\mathrm{lin}}-1} \left(\Pi - 1 \right) & \text{for } \Pi_{\mathrm{lin}} < \Pi \leq 1 \end{cases} \quad (6.55\mathrm{g})$$

$$A_{\mathrm{eff}}(\alpha) = A_1 \left(1 - \cos(a_2 \alpha^2 + a_1 \alpha + a_0) \right) + A_0 \quad (6.55\mathrm{h})$$

$$T_{\mathrm{ic_{out}}} = \max \left(T_{\mathrm{cool}}, T_{\mathrm{comp}} + \left(a_0 + a_1 \left(\frac{T_{\mathrm{comp}} + T_{\mathrm{cool}}}{2} \right) + a_2 W_{\mathrm{ic}} + a_3 \frac{W_{\mathrm{ic}}}{W_{\mathrm{cool}}} \right) \left(T_{\mathrm{comp}} - T_{\mathrm{cool}} \right) \right) \quad (6.55\mathrm{i})$$

6.9.4   Intake Manifold Control Volume Dynamics

$$\frac{\mathrm{d}T_{\mathrm{im}}}{\mathrm{d}t} = \frac{1}{m_{\mathrm{im}}c_{\mathrm{v_a}}} \left(W_{\mathrm{at}}c_{\mathrm{v_a}} \left(T_{\mathrm{ic}} - T_{\mathrm{im}} \right) \right) +$$
$$\frac{1}{m_{\mathrm{im}}c_{\mathrm{v_a}}} \left(R_{\mathrm{a}} \left(T_{\mathrm{ic}} W_{\mathrm{at}} - T_{\mathrm{im}} W_{\mathrm{cyl}} \right) + \dot{Q} \right) \quad (6.56\mathrm{a})$$

$$\frac{\mathrm{d}p_{\mathrm{im}}}{\mathrm{d}t} = \frac{R_{\mathrm{a}} T_{\mathrm{im}}}{V_{\mathrm{im}}} \left(W_{\mathrm{at}} - W_{\mathrm{cyl}} \right) + \frac{m_{\mathrm{im}} R_{\mathrm{a}}}{V_{\mathrm{im}}} \frac{\mathrm{d}T_{\mathrm{im}}}{\mathrm{d}t} \quad (6.56\mathrm{b})$$

$$m_{\text{im}} = \frac{p_{\text{im}} V_{\text{im}}}{R_{\text{a}} T_{\text{im}}} \tag{6.56c}$$

$$W_{\text{cyl}} = p_{\text{im}} C_1 \frac{1}{1 + \frac{1}{\lambda \left(\frac{A}{F}\right)_s}} \frac{r_c - \left(\frac{p_{\text{em}}}{p_{\text{im}}}\right)^{\frac{1}{\gamma}}}{r_c - 1} V_{\text{d}} \frac{N}{R_{\text{im}} \left(T_{\text{im}} - C_2 \frac{1 - \lambda^2}{\lambda^2}\right) 120} \tag{6.56d}$$

6.9.5   Exhaust Manifold Control Volume Dynamics

$$\frac{\mathrm{d}T_{\text{em}}}{\mathrm{d}t} = \frac{1}{m_{\text{em}} c_{\text{v}_{\text{eg}}}} \left(W_{\text{e}} c_{\text{v}_{\text{eg}}} \left(T_{\text{em}_{\text{in}}} - T_{\text{em}}\right)\right) +$$
$$\frac{1}{m_{\text{em}} c_{\text{v}_{\text{eg}}}} \left(R_{\text{eg}} \left(T_{\text{em}_{\text{in}}} W_{\text{e}} - T_{\text{em}} (W_{\text{t}} + W_{\text{wg}})\right) + \dot{Q}\right) \tag{6.57a}$$

$$\frac{\mathrm{d}p_{\text{em}}}{\mathrm{d}t} = \frac{R_{\text{eg}} T_{\text{em}}}{V_{\text{em}}} \left(W_{\text{e}} - (W_{\text{t}} + W_{\text{wg}})\right) + \frac{m_{\text{em}} R_{\text{eg}}}{V_{\text{em}}} \frac{\mathrm{d}T_{\text{em}}}{\mathrm{d}t} \tag{6.57b}$$

$$m_{\text{em}} = \frac{p_{\text{em}} V_{\text{em}}}{R_{\text{eg}} T_{\text{em}}} \tag{6.57c}$$

$$W_{\text{e}} = W_{\text{cyl}} \left(1 + \frac{1}{\lambda \left(\frac{A}{F}\right)_s}\right) \tag{6.57d}$$

$$T_{\text{em}_{\text{in}}} = T_{\text{a}} + (T_{\text{e}_0} + \Delta T_{\text{e}_{\text{max}}} \frac{W_{\text{e}}}{W_{\text{e}_{\text{max}}}} - T_{\text{a}}) e^{-\frac{h_{\text{tot}} \pi D_{\text{em}} l_{\text{em}}}{W_{\text{airfuel}} c_{\text{Peg}}}} \tag{6.57e}$$

$$h_{\text{exh}_{\text{int}}} = \text{HT}_{\text{exh}_0} \lambda_{\text{exh}} \left(\frac{4}{\pi} \frac{W_{\text{e}}}{\mu_{\text{exh}} n_{\text{cyl}} D_{\text{em}}}\right)^{\text{HT}_{\text{exh}_1}} \left(\frac{7}{10}\right)^{\text{HT}_{\text{exh}_2}} \frac{1}{D_{\text{em}}} \tag{6.57f}$$

$$h_{\text{tot}} = \pi D_{\text{em}} l_{\text{em}} n_{\text{cyl}} \left(\gamma_{eg} - 1\right) \frac{1}{\frac{1}{h_{\text{exh}_{\text{int}}}} + \frac{1}{h_{\text{exh}_{\text{ext}}}}} \frac{1}{W_{\text{e}} R_{\text{e}} \gamma_{eg}} \tag{6.57g}$$

$$W_{\text{t}} = \begin{cases} \frac{p_{\text{em}}}{\sqrt{T_{\text{em}}}} k_1 \sqrt{1 - \Pi_t^{k_2}}, & \Pi_t^{k_2} \leq 1 \\ 0, & \text{otherwise} \end{cases} \tag{6.57h}$$

$$W_{\text{wg}} = \frac{p_{\text{em}}}{\sqrt{R_{\text{eg}}T_{\text{em}}}}\Psi_{\text{em}}\left(\Pi_{\text{em}}\right)A_{\text{eff}_{\text{wg}}}\left(u_{\text{wg}}\right) \tag{6.57i}$$

$$\Pi_{\text{em}} = \frac{p_{\text{t}}}{p_{\text{em}}} \tag{6.57j}$$

$$\Psi_{\text{em}}^{*}\left(\Pi_{\text{em}}\right) = \frac{\sqrt{\frac{2\gamma_{\text{eg}}}{\gamma_{\text{eg}}-1}\left(\Pi^{\frac{2}{\gamma_{\text{eg}}}} - \Pi^{\frac{\gamma_{\text{eg}}+1}{\gamma_{\text{eg}}}}\right)}}{\sqrt{\frac{2\gamma_{\text{eg}}}{\gamma_{\text{eg}}-1}\left(\left(\frac{2}{\gamma_{\text{eg}}+1}\right)^{\frac{2}{\gamma_{\text{eg}}-1}} - \left(\frac{2}{\gamma_{\text{eg}}+1}\right)^{\frac{\gamma_{\text{eg}}+1}{\gamma_{\text{eg}}-1}}\right)}} \tag{6.57k}$$

$$\Psi_{\text{em}}\left(\Pi_{\text{em}}\right) = \begin{cases} 1 & 0 < \Pi_{\text{em}} \leq \left(\frac{2}{\gamma_{\text{eg}}+1}\right)^{\frac{\gamma_{\text{eg}}}{\gamma_{\text{eg}}+1}} \\ \Psi_{\text{em}}^{*}(\Pi_{\text{em}}) & \left(\frac{2}{\gamma_{\text{eg}}+1}\right)^{\frac{\gamma_{\text{eg}}}{\gamma_{\text{eg}}+1}} < \Pi_{\text{em}} \leq \Pi_{\text{lin}} \\ \frac{\Psi_{\text{em}}^{*}(\Pi_{\text{lin}})}{\Pi_{\text{lin}}-1}\left(\Pi_{\text{em}} - 1\right) & \text{for } \Pi_{\text{lin}} < \Pi \leq 1 \end{cases} \tag{6.57l}$$

$$A_{\text{eff}_{\text{wg}}}(u_{\text{wg}}) = C_d A_{\text{wg}_{\text{max}}} u_{\text{wg}} \qquad u_{\text{wg}} \in [0,1] \tag{6.57m}$$

6.9.6 Exhaust System Control Volume Dynamics

$$\frac{\mathrm{d}T_{\text{t}}}{\mathrm{d}t} = \frac{1}{m_{\text{t}}c_{\text{v}_{\text{eg}}}}\left((W_{\text{t}} + W_{\text{wg}})c_{\text{v}_{\text{eg}}}\left(T_{\text{es}_{\text{in}}} - T_{\text{t}}\right)\right) +$$
$$\frac{1}{m_{\text{t}}c_{\text{v}_{\text{eg}}}}\left(R_{\text{eg}}\left(T_{\text{es}_{\text{in}}}(W_{\text{t}} + W_{\text{wg}}) - T_{\text{t}}W_{\text{es}}\right) + \dot{Q}\right) \tag{6.58a}$$

$$\frac{\mathrm{d}p_{\text{t}}}{\mathrm{d}t} = \frac{R_{\text{eg}}T_{\text{t}}}{V_{\text{t}}}\left((W_{\text{t}} + W_{\text{wg}}) - W_{\text{es}}\right) + \frac{m_{\text{t}}R_{\text{eg}}}{V_{\text{t}}}\frac{\mathrm{d}T_{\text{t}}}{\mathrm{d}t} \tag{6.58b}$$

$$m_{\text{t}} = \frac{p_{\text{t}}V_{\text{t}}}{R_{\text{eg}}T_{\text{t}}} \tag{6.58c}$$

$$W_{\text{es}} = \begin{cases} \sqrt{p_{\text{t}}\frac{p_{\text{t}}-p_{\text{a}}}{\mathcal{H}_{\text{es}}T_{\text{t}}}}, & p_{\text{t}} - p_{\text{a}} > p_{\text{lin}} \\ \sqrt{\frac{p_{\text{t}}}{\mathcal{H}_{\text{es}}T_{\text{t}}}}\frac{p_{\text{t}}-p_{\text{a}}}{\sqrt{p_{\text{lin}}}}, & 0 \leq p_{\text{t}} - p_{\text{a}} \leq p_{\text{lin}} \\ 0, & p_{\text{comp}} - p_{\text{ic}} < 0 \end{cases} \tag{6.58d}$$

$$T_{\text{es}_{\text{in}}} = \frac{c_{\text{p}_{\text{eg}}}T_{\text{t}_{\text{out}}}W_{\text{t}} + c_{\text{p}_{\text{eg}}}T_{\text{em}}W_{\text{wg}}}{c_{\text{p}_{\text{eg}}}(W_{\text{t}} + W_{\text{wg}})} = \frac{T_{\text{t}_{\text{out}}}W_{\text{t}} + T_{\text{em}}W_{\text{wg}}}{W_{\text{t}} + W_{\text{wg}}} \tag{6.58e}$$

$$T_{t_{\text{out}}} = T_{\text{em}} - T_{\text{em}} \left(1 - \Pi_t^{\frac{\gamma_{\text{eg}}-1}{\gamma_{\text{eg}}}} \right) \cdot$$

$$\eta_{t_{\text{max}}} \left(1 - \left(\frac{\frac{D_t}{2} \frac{\omega_{\text{TC}}}{\sqrt{2 c_{\text{P}_{\text{eg}}} T_{\text{em}} \left(1 - \left(\frac{1}{\Pi_t} \right)^{\frac{1-\gamma_{\text{eg}}}{\gamma_{\text{eg}}}} \right)}} - \text{BSR}_{\eta_{t_{\text{max}}}}}{\text{BSR}_{\eta_{t_{\text{max}}}}} \right)^2 \right) \quad (6.58\text{f})$$

6.9.7 Turboshaft Dynamics

$$I_{\text{TC}} \frac{\mathrm{d}\omega_{\text{TC}}}{\mathrm{d}t} = \left(T_{q_t} - T_{q_{\text{comp}}} - \omega_{\text{TC}} \cdot \text{friction}_{\text{TC}} \right) \quad (6.59\text{a})$$

$$T_{q_{\text{comp}}} = \frac{c_{\text{p}_a} W_{\text{comp}} (T_{\text{comp}_{\text{out}}} - T_{\text{af}})}{\omega_{\text{TC}}} \quad (6.59\text{b})$$

$$T_{q_t} = \frac{\eta_t W_t c_{\text{P}_{\text{eg}}} T_{\text{em}} \left(1 - \Pi_t^{\frac{\gamma_{eg}-1}{\gamma_{eg}}} \right)}{\omega_{\text{TC}}} \quad (6.59\text{c})$$

6.10 Total Model Validation

Now all components have been separately validated and it is time to validate the total model. First, the model is validated for stationary conditions and then step response experiments are used for the dynamics.

All engine experiments have been performed at room temperature and the ambient conditions are given as inputs to the model. As the ambient conditions change more than in the laboratory, a sensitivity analysis has been performed to check how sensitive the models stationary points are to changes in ambient conditions. The results of this analysis are presented after the stationary validation.

6.10.1 Stationary Validation

To validate the entire model for stationary conditions, the same stationary operating points are used as for the component validation. The inputs to the model are $(N, \alpha, \lambda, u_{\text{wg}}, p_a, T_a)$ and most of them (N, λ, p_a, T_a) have been measured in the validation data set. As there are uncertainties in throttle position and wastegate position, these pose two challenges. The uncertainty in the throttle plate angle relates to the fact that the throttle parameters have changed somewhat as described on p. 99. As the wastegate position u_{wg} is not measurable on the engine, it is necessary to determine this input during the validation. On the engine u_{wg} is determined by a controller, but the exact implementation of the controller is not known.

Two PI-controllers are introduced to handle the throttle and wastegate. One fast that controls the throttle angle α to achieve a desired (measured) air-mass flow and a second slower controller that controls the wastegate u_{wg} in order to get the same pressure after the intercooler as in the measured data set. The latter controller is disabled for low boost pressures as on the modeled engine. These controllers are used when the stationary model validation is performed by simulating the system in Figure 6.2.

Results of the stationary validation are shown in the following figures with measured values on the x-axis and simulated values on the y-axis with one exception for the wastegate opening that is shown as a function of air-mass flow.

Validation of Model Inputs

The inputs to the model are shown in Figure 6.22. As the throttle angle was determined using a controller it is encouraging to see that the relative error is less than 5% for all but very low and high pressure ratios over the throttle.

Validation of Pressure States

The modeled and measured pressures are shown in Figure 6.23 and the relative errors are shown in Figure 6.24. The pressure errors are generally small, only a few percent, except for the intake manifold pressure where there is a mean error of -5%. To investigate the causes remember that, the throttle plate is controlled to achieve the measured flow as measured in the validation data. Further, there is a new air-mass flow sensor compared to when the tuning data was measured. Now, since the intake manifold pressure is the most important input to the port air-mass flow model, model errors in the port air-mass flow will propagate to mostly the intake manifold pressure. Additionally the pressures are controlled on the intake side to measured pressure, at least after the intercooler, which reduce their errors when the wastegate is open.

Small, but systematic, underestimations of the pressures on the intake side are present when the wastegate is closed. On the exhaust side, these errors are present as a small negative trend in especially p_{t}.

Temperature State Validation

Figure 6.25 shows the modeled temperatures and the relative errors are shown in Figure 6.26. Here all temperatures on the intake side are modeled within 6% even though no heat transfer is modeled in the control volumes. On the exhaust side the temperatures are described within 22%. The temperature after the turbine is overestimated partly due to the large error in the exhaust manifold temperature.
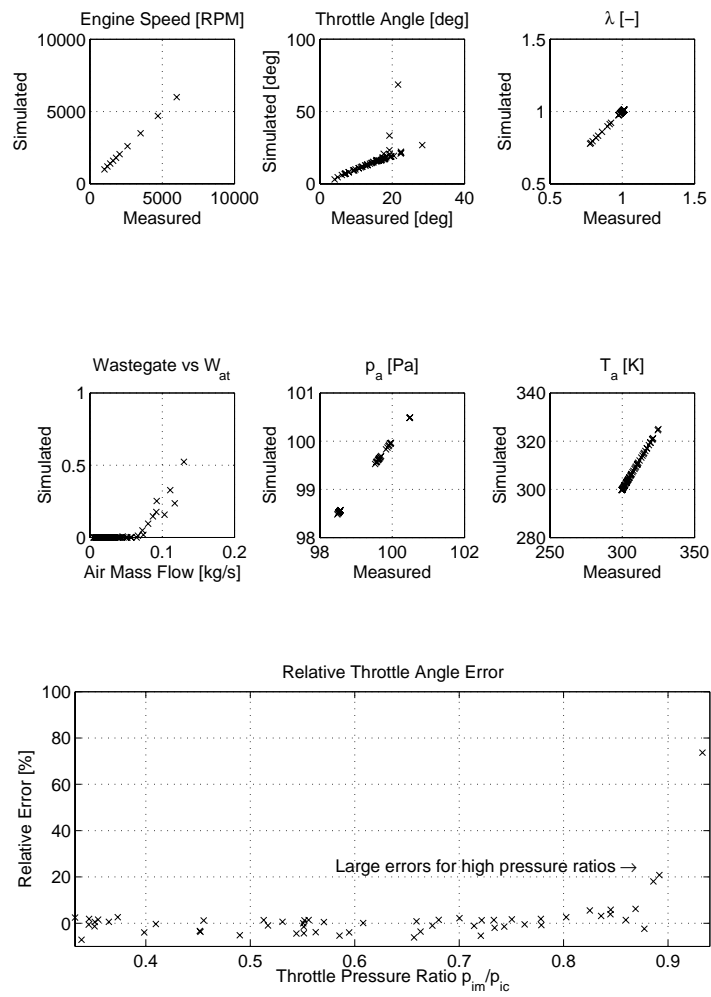
Figure 6.22: Stationary model validation. Here the inputs are shown for each operating point. *Bottom:* The relative error in modeled throttle angle compared to measured. Except for high pressure ratios, the errors are only a few percent.
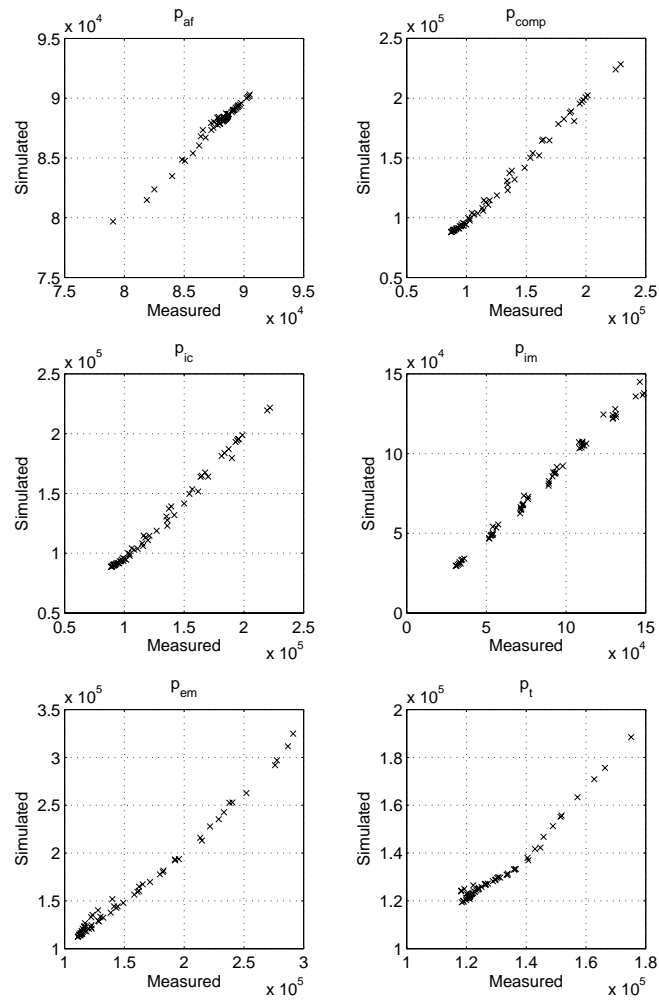
Figure 6.23: Stationary model validation of the pressure states. The maximum error on the intake side is 12% and 10% on the exhaust side.
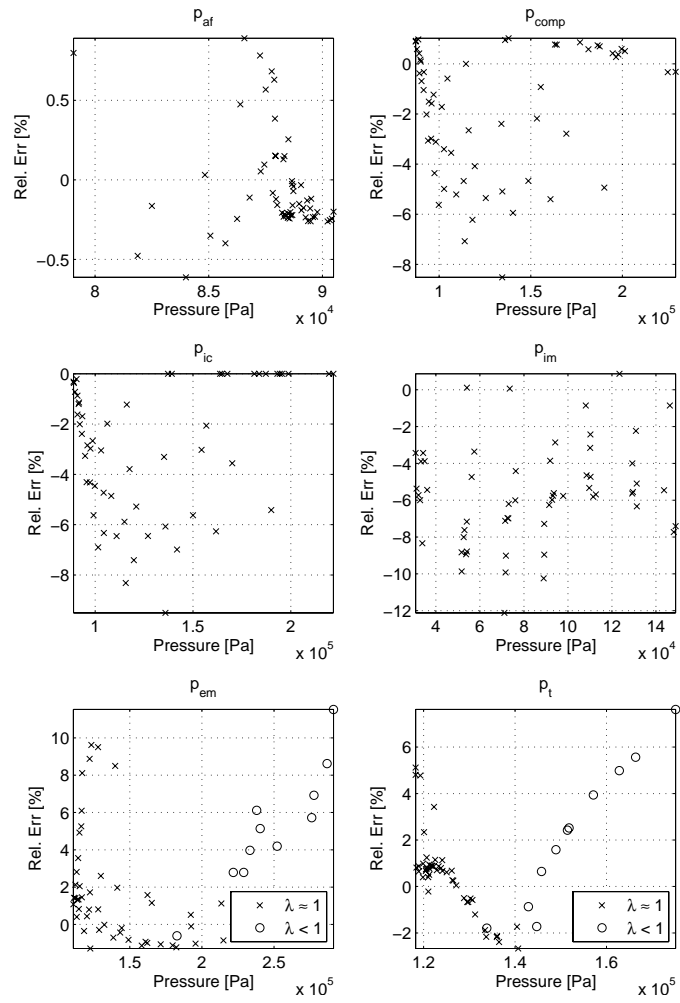
Figure 6.24: Relative errors for modeled pressures.
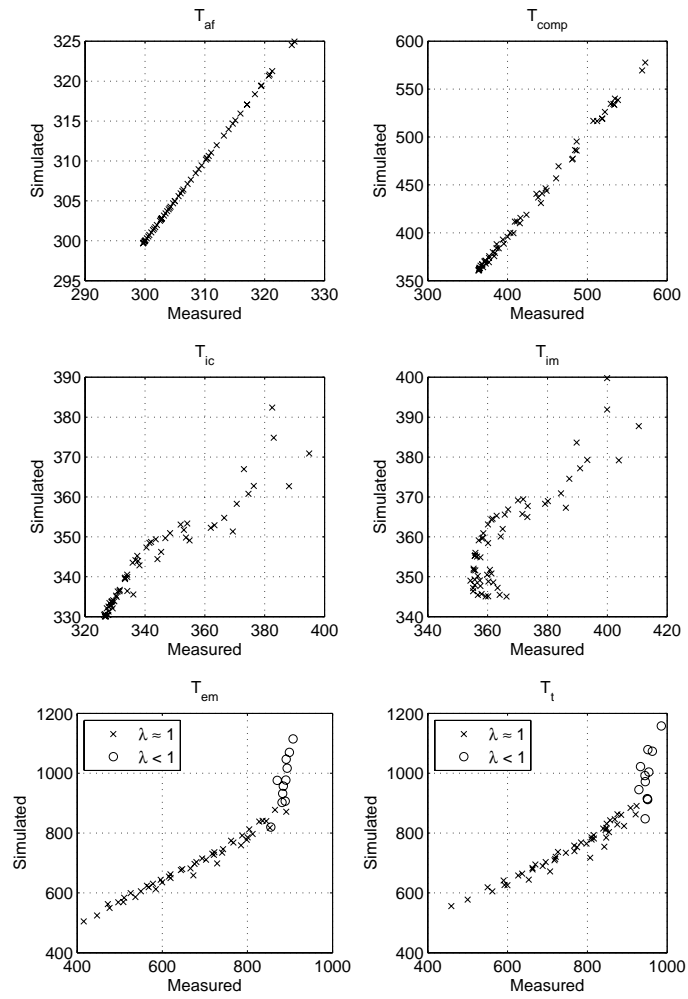
Figure 6.25: Stationary temperature model validation.
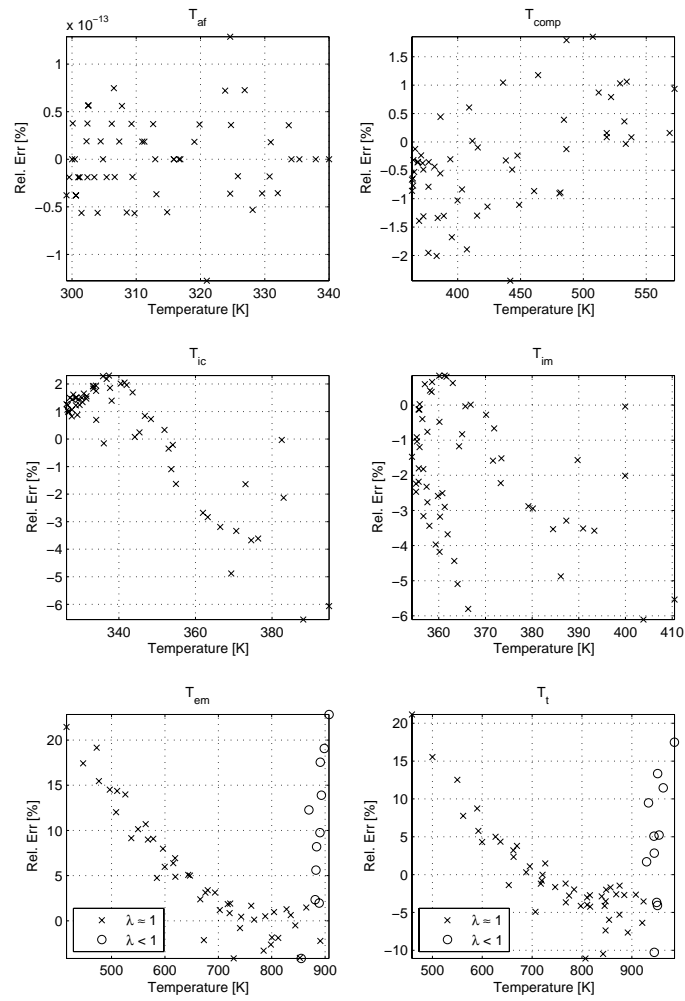
Figure 6.26: Relative errors for the modeled temperatures. On the exhaust side the temperatures are overestimated for high temperatures as the temperature model lacks the cooling effect when fuel enrichment is present.

Turbine Speed Validation

Figure 6.27 shows the resulting turbine speed and relative error in turbine speed. The turbocharger speed is shown separately as this is a key component that connects the intake side to the exhaust side. Turbocharger speed is described within 10% for most points at medium to high turbocharger speeds. At lower speeds, the model underestimates the turbine speed.
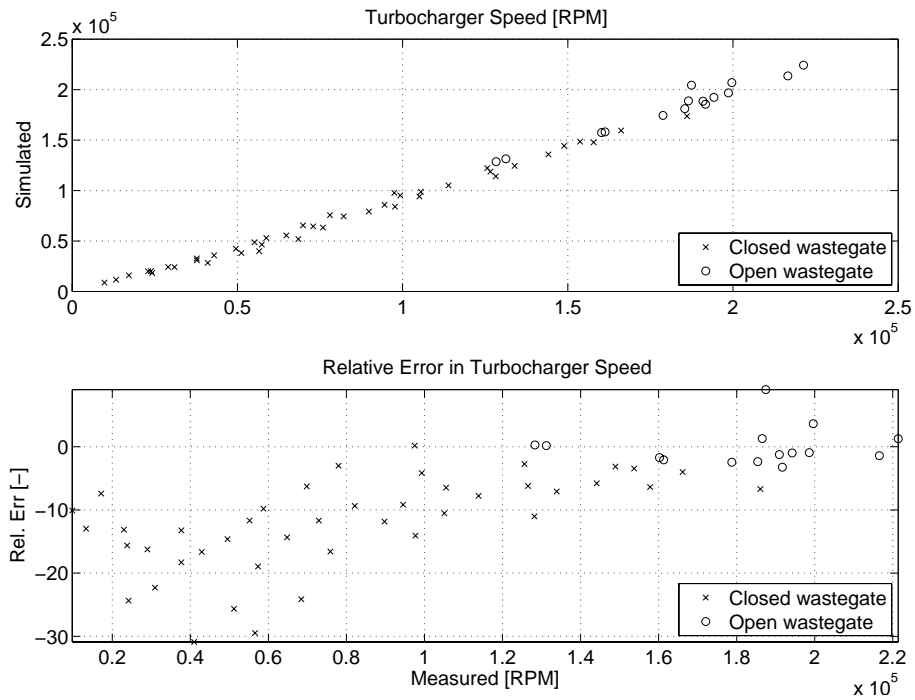
Figure 6.27: Validation of turbocharger speed. In the plots it is shown where the controller has opened the wastegate as these point are marked using circles.

Sensitivity to Changes in Ambient Conditions

As the ambient conditions p_a and T_a are inputs to the model it is important to study how sensitive the estimated states are to changes in ambient conditions. These studies were conducted by simulating the model with different ambient conditions and then calculate the sensitivity in each state. The sensitivity function of the state x_i to the ambient pressure p_a is for example:

$$\frac{\frac{\partial x_i}{\partial p_a}}{\frac{x_i}{p_a}}$$

The result of the sensitivity analysis is that no state is particularly sensitive to changes in ambient conditions for a given operating condition. A typical example is the turbocharger speed that has the following sensitivity to changes in ambient pressure and temperature:

- It decreases linearly with an increase in ambient pressure.

- It increases only 60% of the increase in ambient temperature.

The model does not amplify changes in ambient conditions and therefore it is sufficient to validate the model using the measurements at room temperature.

6.10.2   Transient Validation

Step response experiments have been performed to validate the dynamic properties of the model where the model is compared to measured data. The measured engine data depends on controllers in the ECU, such as the wastegate controller and the by-pass valve controller. These controllers are not known and therefore they can not be properly modeled. Thus can only data measured with closed wastegate and closed by-pass valve be used for validation. In the test cell, it would be possible to disable both the wastegate and the by-pass valve but this increases the risk of damaging the engine or turbocharger.

Consequently, the model is not fully able to describe rapid throttle closings where the by-pass valve is open and it will overestimate the states when the engine's wastegate is open. Further, the measured throttle angle is fed directly to the model instead of being determined using a controller as during the stationary validation. As the throttle parameters have changed, see p. 99, there will be small offsets in all states as they depend on the air-mass flow.

The operating points that have been selected for the validation reflects the operating region of normal driving, that is part load transients, a full load transient at approximately 2000 RPM, and an engine speed transient to simulate a rapid gear-shift. In Figure 6.28, Figure 6.29, and Figure 6.30 the model is compared to measured transient data and the result can be summarized as:

- Pressure dynamics and the speed dynamics of the turbocharger are accurately described by the model. These are good indicators of that the control volume parameters are correct. The turbocharger inertia is correct as the turbocharger speed tracks the measured in terms of time constants.

- Fast temperature changes are captured by the model, which the sensors miss as they are too slow.

- The model has a good attenuation of noise in the measured pressure signals.

Additional tests have been performed using steps in throttle, wastegate and engine speed. For all cases, the model converged and the rise time of turbocharger speed and pressures are close to the measured data.
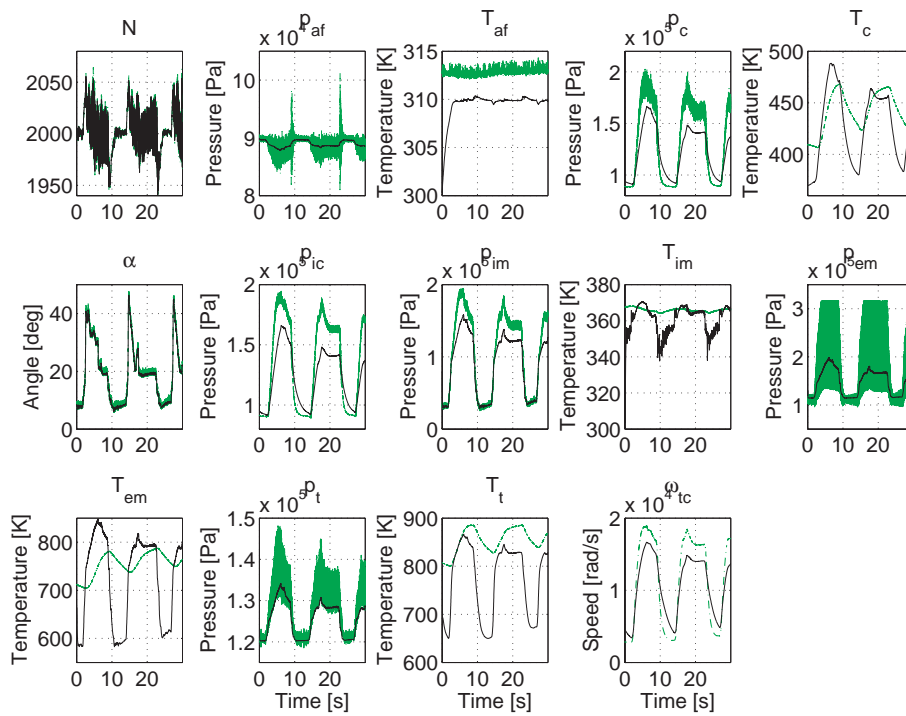
Figure 6.28: Dynamic model validation using large throttle steps at 2000 RPM. Solid lines are the models and the dash-dotted (gray) are measured data. Initially a few seconds are necessary for the model to converge as it starts from a fix initial state. During the experiment, the wastegate did not open or just opened slightly as the model accurately describes pressures on the intake side just before the tip-outs. Also, the model captures the fast temperature dynamics in the intake manifold, which is important for air/fuel ratio control. Further, it also suppresses noise in the measured pressure signals.
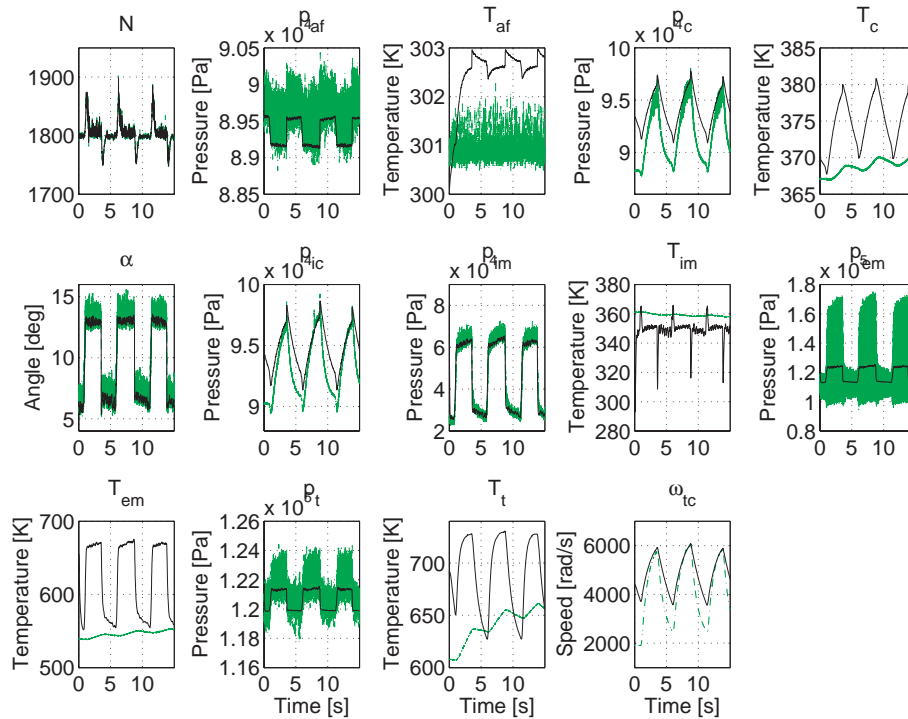
Figure 6.29: Dynamic model validation at low load using medium throttle steps at 1800 RPM. Solid lines are the model and the dash-dotted (gray) are measured data. Initially a few seconds are necessary for the model to converge as it starts from a fixed initial state. Here it is shown that even for small steps, the model captures the mean value of the pressure. Further, the time constant of the turbocharger speed is correct even though the speed is underestimated.

6.11 Modeling Methodology Applied to a Different Engine

The methodology has been developed and applied first on the B235R-engine and to verify the generality of the model and methodology it was applied to a different engine (SAAB B207R). The new engine has the same structure but different sizes. This model with re-fitted parameters is used in Chapter 9. A map consisting of 45 points was used together with maps from the turbocharger manufacturer.

The parameter tuning was applied in the same manner with only two minor modifications. Firstly the throttle angle was not available on the new engine and was instead taken from the ECU. Secondly, when the tuning data set was used the resulting parameter values of the intercooler temperature model Eq. (6.5a) were not physically reasonable. The problem was caused by the new engine map where a shorter settling time was used in order to save time. This resulted
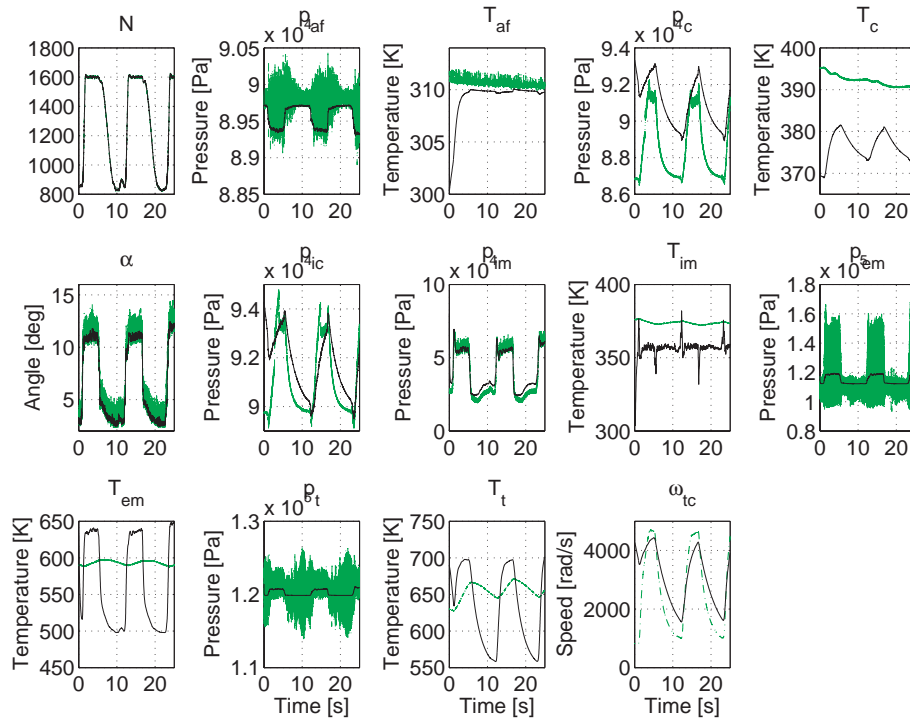
Figure 6.30: Dynamic model validation using engine speed steps between 900 and 1600 RPM. Solid lines are the model and the dash-dotted (gray) are measured data.

in that the temperature out of the intercooler had not settled properly for low mass-flows. Therefore, the parameter values from the B235R intercooler temperature model was reused as the intercoolers are similar.

To compare the quality of the models, the root mean square of the stationary model error in percent is used. The results are summarized in Table 6.22. On the B207R, the errors on the exhaust side are slightly larger except for p_t. This is partly caused by the turbine efficiency where the maximum efficiency is speed dependent and this is not captured by the model. Also, the turbocharger speed error is lower for the B207R which is result of that the wastegate opens earlier on this engine and thus enables the modeled wastegate controller. During the stationary validation the same type of wastegate controller was used as for the B235R but with a lower activation pressure. It is therefore concluded that the model and tuning methodology works for engines of the same physical structure.

	RMS Error	
State	**B235R**	**B207R**
p_{af}	0.3	0.2
T_{af}	0	0
p_{comp}	3.1	2.1
T_{comp}	1.2	2.1
p_{ic}	3.8	2
T_{ic}	2.1	3.1
p_{im}	5.9	3.9
T_{im}	3.3	2.5
p_{em}	3.8	7.5
T_{em}	9.4	10.6
p_{t}	2.1	0.6
T_{t}	8.2	16.3
ω_{TC}	21.5	13.7

Table 6.22: Root mean square of the relative errors for the B235R and B207R engine models.

6.12 Results

A component based mean value engine model of a turbocharged SI engine is presented. The model is suitable for observer design, diagnosis, and control. For each component, it is described how to determine its parameter(s). To determine the parameters measured engine data, engine geometry, and data from the turbocharger manufacturer are required. During the modeling work, it was observed that the throttle model needs improvement which was realized by introducing a non-physical value of the ratio of specific heats in the incompressible flow model. Further it is shown that the discharge coefficient in the compressible flow model can be separated into two factors, one that depends on the throttle area and one that depends on the pressure ratio.

The model has been validated in several steps. First, each component is validated and then the total model is validated both for stationary conditions and for different transients. The stationary validation of the total model shows that the accuracy on pressures and temperatures on the intake side is better than 5% for most of the points. In addition, the model is able to predict turbocharger speed within 5% for medium to high turbocharger speeds. Further, the model attenuates pumping fluctuations in the measured pressure signals. In step response experiments the model has the same time constants as the physical engine. In addition, a sensitivity analysis to changes in ambient conditions was performed and none of the modeled states are particularly sensitive to changes in ambient pressure or temperature.

Finally it can be concluded that the component based modeling methodology is successful in describing the air-system dynamics of a turbocharged SI-engine and the parameter tuning method makes it easy to tune the model to different engines.

7

Sensor Selection for Observer Feedback

In the previous chapter, a mean value engine model was presented which includes descriptions of the intake and exhaust side. Using this model it is possible to estimate pressures, temperatures, mass-flows, and turbocharger speed. However, the estimates can be improved if some signals can be measured on the real process. On TC SI-engines, several signals are normally measured such as pressures before and after the throttle, temperatures in various locations and the air-mass flow. When a model's estimates of states are improved by feedback from measured signals, it is called an observer. Using an observer it is possible to estimate signals that otherwise would have been necessary to measure. This enables the number of sensors to be reduced which means that the cost of sensors is lower. Further, the observer can be used to create redundant information to provide sensor diagnosis opportunities etc. All of this requires that the sensor(s) used for observer feedback are carefully chosen.

Observers require feedback from one or more sensors and an important question that arises during the design phase is: – Given a limited number of sensors, what sensors or sensor configurations are the best choices? This question is addressed in this chapter. A challenge is that the number of possible sensor combinations virtually explode when more than one sensor is used, which is illustrated in the following example. Here there are 17 possible sensor sources. When two sensors are used there are $\binom{17}{2} = 136$ combinations and if three sensors are used then there are $\binom{17}{3} = 680$ combinations. Therefore, a systematic method is proposed to reduce the number of possible candidates and aid the selection of sensors.

A necessary condition in observer design is that the system is observable from

the selected feedback signal(s). It is shown that the system is locally structurally observable from any measured state or function of measured states such as air-mass flows. Thus, there are a vast number of possible sensor configurations.

The observed system has 13 states and the primary objective of the model is air-fuel control that relies on proper cylinder air charge estimates. When a systematic method to select sensors for observer feedback is proposed, the fact that only a subset of the states are required for cylinder air charge estimation is taken into account.

7.1   Engine Model

Turbocharged engines are similar in their structure: They have air-filter, compressor, intercooler, throttle, intake manifold, exhaust manifold, turbine, and an exhaust system. At most of these components, it is possible to measure pressure and temperature and air-mass flow.

The observer design relies on a nonlinear mean value engine model of a turbocharged SI-engine. To model the engine, the methodology of placing control volumes between restrictions (Eriksson et al., 2002b) is applied. This preserves the physical structure of the turbocharged engine in the model. The structure of the physical system used is shown in Figure 7.1 where also some possible sensor locations are shown. In the model, described in detail in Chapter 6, there are 13 states and 5 inputs.
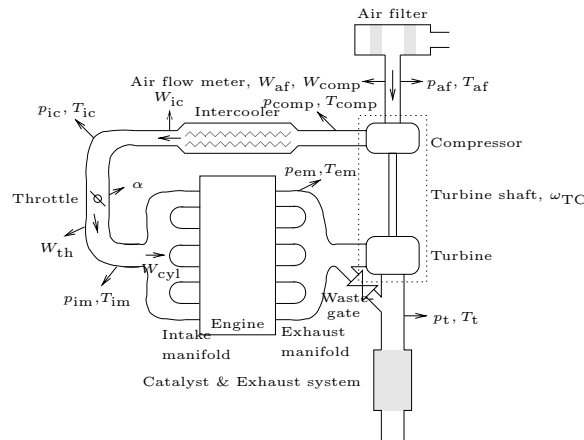
Figure 7.1: A schematic of a turbocharged SI-engine. Arrows pointing out of the engine indicate possible sensor placements. Arrows inside the engine indicate air-mass flows, of which the air-mass flow into the cylinders W_{cyl} is of particular interest for air/fuel ratio control.

The nomenclature is that pressures are denoted p, temperatures T, air-mass flows W, and the index shows the location. The locations are: air-filter (af),

compressor (comp), intercooler (ic), intake manifold (im), exhaust manifold (em), and turbine (t). The turbocharger speed is indicated by ω_{TC}. For more details please consult the nomenclature in Appendix A. Next model inputs, states, and outputs are explained.

7.1.1 Inputs

Inputs to this model are engine speed N, throttle plate angle α, the air/fuel ratio λ, opening of the wastegate u_{wg}, together with ambient conditions such as pressure p_a and temperature T_a.

7.1.2 States and State Equations

The states in the model are six pairs of pressure and temperature states and the turbocharger speed, ω_{TC}. In Chapter 6 the model is described in detail and all of the differential equations are listed in Section 6.9 and below only the structure of the equations are shown.

$$
\begin{align}
\dot{p}_{af} &= f_{p_{af}}\left(p_{af}, T_{af}, p_{comp}, \omega_{TC}, p_a, T_a\right) \tag{7.1a}\\
\dot{T}_{af} &= f_{T_{af}}\left(p_{af}, T_{af}, p_{comp}, \omega_{TC}, p_a, T_a\right) \tag{7.1b}\\
\dot{p}_{comp} &= f_{p_{comp}}\left(p_{af}, T_{af}, p_{comp}, T_{comp}, p_{ic}, \omega_{TC}\right) \tag{7.1c}\\
\dot{T}_{comp} &= f_{T_{comp}}\left(p_{af}, T_{af}, p_{comp}, T_{comp}, p_{ic}, \omega_{TC}\right) \tag{7.1d}\\
\dot{p}_{ic} &= f_{p_{ic}}\left(p_{comp}, T_{comp}, p_{ic}, T_{ic}, p_{im}, \alpha\right) \tag{7.1e}\\
\dot{T}_{ic} &= f_{T_{ic}}\left(p_{comp}, T_{comp}, p_{ic}, T_{ic}, p_{im}, \alpha\right) \tag{7.1f}\\
\dot{p}_{im} &= f_{p_{im}}\left(p_{ic}, T_{ic}, T_{im}, p_{im}, p_{em}, N, \alpha, \lambda\right) \tag{7.1g}\\
\dot{T}_{im} &= f_{T_{im}}\left(p_{ic}, T_{ic}, T_{im}, p_{im}, p_{em}, N, \alpha, \lambda\right) \tag{7.1h}\\
\dot{p}_{em} &= f_{p_{em}}\left(p_{im}, T_{im}, p_{em}, T_{em}, p_t, N, \lambda, u_{wg}, T_a\right) \tag{7.1i}\\
\dot{T}_{em} &= f_{T_{em}}\left(p_{im}, T_{im}, p_{em}, T_{em}, p_t, N, \lambda, u_{wg}, T_a\right) \tag{7.1j}\\
\dot{p}_t &= f_{p_t}\left(p_{em}, T_{em}, p_t, T_t, \omega_{TC}, u_{wg}, p_a\right) \tag{7.1k}\\
\dot{T}_t &= f_{T_t}\left(p_{em}, T_{em}, p_t, T_t, \omega_{TC}, u_{wg}, p_a\right) \tag{7.1l}\\
\dot{\omega}_{tc} &= f_{\omega_{TC}}\left(p_{af}, T_{af}, p_{comp}, p_{em}, T_{em}, p_t, \omega_{TC}\right) \tag{7.1m}
\end{align}
$$

7.1.3 Measured Signals

Measured signals are outputs of the system which are states and/or functions of states and inputs:

$$y = g(x, u) \tag{7.2}$$

An example of a function of states and inputs is the measured air-mass flow after the air-filter which can be expressed as a function of the pressure after the

air-filter, a constant parameter $\mathcal{H}_{\text{af}}$, and the inputs p_{a} and T_{a}:

$$W_{\text{af}} = g(\underbrace{p_{\text{af}}}_{x}, \underbrace{p_{\text{a}}, T_{\text{a}}}_{u}) = \sqrt{\frac{p_{\text{a}}(p_{\text{a}} - p_{\text{af}})}{\mathcal{H}_{\text{af}}T_{\text{a}}}}$$

Thus it depends only on one state, the pressure after the air-filter. For the other possible air-mass flows in the intake side the state dependencies are as follows:

Compressor air-mass flow: $W_{\text{comp}} = g(p_{\text{af}}, T_{\text{af}}, p_{\text{comp}}, \omega_{\text{TC}})$
Intercooler air-mass flow: $W_{\text{ic}} = g(p_{\text{comp}}, T_{\text{comp}}, p_{\text{ic}})$
Throttle air-mass flow: $W_{\text{th}} = g(p_{\text{im}}, p_{\text{ic}}, T_{\text{ic}})$

Available Sensor Signals and Sensor Dynamics

All states are considered to be measurable and functions of states and inputs such as air-mass flows are only measurable on the intake side. One practical consideration is necessary for temperature sensors as their time constant is in the order of several seconds compared to the considerably faster pressure sensors and air-mass flow sensors. Therefore, the system is augmented with temperature sensor dynamics for each temperature sensor (Chevalier et al., 2000):

$$\dot{T}_{\text{sensor}} = \frac{1}{\tau}(T - T_{\text{sensor}})$$

The set of sensors considered here are thus:

$$\mathcal{Y} = \{p_{\text{af}}, T_{\text{af}}, p_{\text{comp}}, T_{\text{comp}}, p_{\text{ic}}, T_{\text{ic}}, p_{\text{im}}, T_{\text{im}},$$
$$p_{\text{em}}, T_{\text{em}}, p_{\text{t}}, T_{\text{t}}, \omega_{\text{TC}}, W_{\text{af}}, W_{\text{comp}}, W_{\text{ic}}, W_{\text{th}}\}$$

Note that all states are considered measurable, but for each temperature sensor the system has to be augmented with one state.

7.2 Observability

Before an observer is designed, it must be determined whether the system is observable and as the system is nonlinear, this is not an easy task. One method to show that the system is at least locally observable is to linearize the equation system in Section 7.1.2 in stationary points and then use linear theory to determine observability. Given that $f_x(x, u)$ is the partial derivative of $f(x, u)$ w.r.t. x, (x_0, u_0) is a stationary point, then the linearized system matrices A, B, C and D are defined as follows:

$$\begin{aligned} A &= f_x(x_0, u_0) & B &= f_u(x_0, u_0) \\ C &= g_x(x_0, u_0) & D &= g_u(x_0, u_0) \end{aligned}$$

The linearized system can now be written as

$$\dot{x} = Ax + Bu$$

and the measured signal(s)

$$y = Cx + Du$$

Measured signals y are selected from the set $\mathcal{Y}$. Introduce the standard notation

$$\mathcal{O}_\rho = \begin{bmatrix} C \\ CA \\ \vdots \\ CA^{\rho-1} \end{bmatrix} \tag{7.3}$$

where the matrix $\mathcal{O}$ without index means $\rho = n$, i.e. $\mathcal{O} = \mathcal{O}_n$. Then the system is observable if and only if $\mathcal{O}$ has full column rank (Kailath, 1980, p. 81). The smallest ρ that makes the system observable is called the observability index. Unfortunately, the linearized system matrix A is ill-conditioned due to large differences in time-constants in the engine dynamics. This makes it hard to numerically determine the observability index using Eq. (7.3) as it, for example when one feedback is used, involves taking A to the power of 12.

Definition 7.1 (Observability index). *The observability index is defined as the smallest positive integer ρ such that $\mathcal{O}_\rho$ has full column rank.*

The numerical challenge is a result of considering the observability of the entire system. In several applications, there is only a fraction of the state space that is more interesting than others. This is especially true for cylinder air charge estimation. The following states are included in the cylinder air charge model: p_{im}, T_{im}, and p_{em} (Andersson and Eriksson, 2004), which are only 3 out of 13 states and thus the question is asked whether there are combinations of measured signals that better observe these variables. We therefore use observability index of only a part of the state vector as a metric to evaluate sensor configurations. The metric is further discussed in Section 7.4.

7.2.1 Observability Index of A Subset of States

Start by partitioning the state vector x into $x = (x_1, x_2)$, where x_1 are the states we want to observe. The vector x_1 has n_1 states, x_2 has n_2 states, and $n_1 + n_2 = n$. Now the columns of the observability matrix $\mathcal{O} \in \mathbb{R}^{m \times n}$ are rearranged into $\mathcal{O}_n = [\mathcal{O}_n^1 \; \mathcal{O}_n^2]$, where $\mathcal{O}_n^1 \in \mathbb{R}^{m \times n_1}$ and $\mathcal{O}_n^2 \in \mathbb{R}^{m \times n_2}$. After the rearrangement the first n_1 columns in $\mathcal{O}$ correspond to the states in x_1. Next observability of a subset of states and its associated observability index are defined.

Definition 7.2 (Observability of a set of states x_1). *The state vector x_1 is observable if and only if $\mathcal{O}_n = [\mathcal{O}_n^1 \; \mathcal{O}_n^2]$ is 1-full rank (Terrell, 2001) w.r.t. the n_1 first columns, i.e.*

$$rank \; \mathcal{O}_n = n_1 \; + \; rank \; \mathcal{O}_n^2$$

Using this definition, the observability index for a subset of the states can be defined.

Definition 7.3. *(Observability index of a set of states x_1) Let (C, A) be an observable pair, then the observability index w.r.t. x_1 is the smallest positive integer ρ such that $\mathcal{O}_\rho = [\mathcal{O}_\rho^1 \ \mathcal{O}_\rho^2]$ is 1-full rank w.r.t. the n_1 first columns, i.e.*

$$rank \ \mathcal{O}_\rho = n_1 \ + \ rank \ \mathcal{O}_\rho^2$$

As can be seen in Definition 7.3 it is possible that fewer differentiations, and hence lower powers of the ill-conditioned A will be required, as it is now only required that the rank of $\mathcal{O}_\rho$ is at least n_1. Since fewer differentiations are needed than before, the numerical problems are not as severe for the partial observability problem.

7.2.2   Structural Observability

Structural observability makes it possible to avoid the numerical problems with high powers of A in $\mathcal{O}_n$. Structural observability only considers the structure of the model and thus only provides a *necessary* condition for observability. However, for physically based models it is reasonable to assume that structural observability also implies analytical observability (Lin, 1974).

Lin (1974) introduced the concept of structure to analyze controllability of linear systems. The approach is based on the assumption that a qualitative property such as controllability is determined by the structure of the model, rather than the values of the actual system parameters. Structure here means the zero/non-zero structure of the model matrices (A, B, C, D).

A dual formulation of the controllability definition in (Lin, 1974) gives the following definition of structural observability.

Definition 7.4 (Structural observability)**.** *The pair (C, A) is structural observable if there exists an observable pair (C_0, A_0) with the same structure.*

Structural rank, sometimes referred to as generic rank or normal rank, of a matrix A is here defined as the maximum rank possible for any matrix with the same structure as A. Then it is tempting to think that a pair (C, A) is structurally observable if and only if the observability matrix has full structural rank. However, this is not true (Shields and Pearson, 1976; Lin, 1974) and therefore the following result from (Shields and Pearson, 1976) is used:

Theorem 7.1 (Structural observability)**.** *Let $A \in \mathbb{R}^{n \times n}$ and $C \in \mathbb{R}^{m \times n}$. Then the pair (C, A) is structurally observable if and only if the following $[n^2 + n(m-$*

1)] $\times n^2$ *matrix has structural rank* n^2.

$$\begin{bmatrix} I & -A & 0 & \cdots & 0 & 0 \\ 0 & I & -A & \cdots & 0 & 0 \\ \vdots & \vdots & \vdots & & \vdots & \vdots \\ 0 & 0 & 0 & \cdots & I & -A \\ 0 & 0 & 0 & \cdots & 0 & C \\ 0 & 0 & 0 & \cdots & C & 0 \\ \vdots & \vdots & \vdots & & \vdots & \vdots \\ 0 & 0 & C & \cdots & 0 & 0 \\ 0 & C & 0 & \cdots & 0 & 0 \\ C & 0 & 0 & \cdots & 0 & 0 \end{bmatrix}$$

The structural rank of a matrix can be efficiently computed using graph theoretical algorithms for matchings in bipartite graphs. In Matlab, the structural rank is computed using the `dmperm` command.

7.3 Observability of the Engine Model

The first question to answer is whether the engine model in Eq. (7.1) is observable using feedback from $\mathcal{Y}$. As there are numerical difficulties when the analytic observability matrix is computed the structural approach is taken instead.

Looking at the structure of the engine model one can verify that the linearized system only has two structures over the engines entire operating region. The cause of the structural change is that for low pressure ratios over the throttle the pressure and temperature states before the throttle do not depend on the intake manifold pressure.

Below all nonzero elements of the A-matrix are shown using an X, and the elements that can be zero in one of the two structures are marked using parentheses.

Eqn.	p_{af}	T_{af}	p_{comp}	T_{comp}	p_{ic}	T_{ic}	p_{im}	T_{im}	p_{em}	T_{em}	p_t	T_t	ω_{TC}
Eq. (7.1a)	X	X	X	0	0	0	0	0	0	0	0	0	X
Eq. (7.1b)	X	X	X	0	0	0	0	0	0	0	0	0	X
Eq. (7.1c)	X	X	X	X	X	0	0	0	0	0	0	0	X
Eq. (7.1d)	X	X	X	X	X	0	0	0	0	0	0	0	X
Eq. (7.1e)	0	0	X	X	X	X	(X)	0	0	0	0	0	0
Eq. (7.1f)	0	0	X	X	X	X	(X)	0	0	0	0	0	0
Eq. (7.1g)	0	0	0	0	X	X	X	X	X	0	0	0	0
Eq. (7.1h)	0	0	0	0	X	X	X	X	X	0	0	0	0
Eq. (7.1i)	0	0	0	0	0	0	X	X	X	X	X	0	0
Eq. (7.1j)	0	0	0	0	0	0	X	X	X	X	X	0	0
Eq. (7.1k)	0	0	0	0	0	0	0	0	X	X	X	X	X
Eq. (7.1l)	0	0	0	0	0	0	0	0	X	X	X	X	X
Eq. (7.1m)	X	X	X	0	0	0	0	0	X	X	X	0	X

Using Theorem 7.1 it can be verified that the linearized engine model is structurally observable from *any* single sensor signal. Thus the system is locally structurally observable using one feedback from $\mathcal{Y}$ and as $\mathcal{Y}$ includes all states the system is locally structurally observable with feedback from any measured state. This result is valid for all TC SI-engines with the same structure.

7.4   Signal Selection

A selection metric is necessary in order to systematically determine what feedback signal(s) or combination(s) of feedback signals to use. Here the selected metrics are based on observability index and two scenarios are studied: Signal selection for best observability of the total system and signal selection for best CAC observability.

7.4.1   Signal Selection for Best System Observability

When an arbitrary signal in $\mathcal{Y}$ is used for observer feedback the system is locally structurally observable, as shown in Section 7.2.2. Given that more than one signal from $\mathcal{Y}$ is selected, is it then possible to find a combination of measured signals that is most suitable, i.e. results in a minimized observability index? Consider $m > 1$ feedback signals which result in a C matrix with m-rows. The total number of rows in $\mathcal{O}$ still has to be at least n, in order for the rank to be n. The introduction of more than one measured signal does not reduce the number of necessary rows in $\mathcal{O}$. However the lower bound of the observability index is inversely proportional to the number of feedback signals m:

$$\rho \geq \left\lceil \frac{n}{m} \right\rceil \tag{7.4}$$

Consequently, for the total system the lower bound[1] of the observability index depends on the number of system states. As slow sensors introduce additional states, it is better to use fast sensors. Further, a specific combination of feedbacks that would give a minimized observability index can not be found using the test given by Theorem 7.1 as it only gives a true or false result. To determine the best combination it is necessary to know if more than the minimum number of differentiations is required. Therefore, it is only possible to give a lower bound of the observability index through Eq. (7.4).

7.4.2   Signal Selection for Best CAC Observability

The primary objective in engine air/fuel control is to observe the states necessary for CAC estimation and the states involved in the CAC calculation are p_{im}, T_{im}, and p_{em}. The criterion for sensor selection is thus to minimize the observability index, according to Definition 7.3, for the subset of states $x_1 = \{p_{\mathrm{im}}, T_{\mathrm{im}}, p_{\mathrm{em}}\}$. Here this method is illustrated for three feedback signals, which is a case where there are $\binom{17}{3} = 680$ combinations.

When three signals are selected from $\mathcal{Y}$ for observer feedback and the observability index for the subset of states x_1 is evaluated the result are three interesting groups of feedback signals which all have observability index less or equal to 4. These are summarized in Table 7.1.

---

[1]Notation: $\lceil n \rceil$ means n rounded towards the closest upper integer.

Table 7.1: Observability index for the subset $x_1 = \{p_{\text{im}}, T_{\text{im}}, p_{\text{em}}\}$ using three feedback signals.

Index	Signal 1	Signal 2	Signal 3
2	p_{im}	T_{im}	p_{em}
3	p_{ic}	p_{im}	T_{im}
3	p_{im}	T_{im}	W_{th}
3	p_{im}	p_{em}	T_{em}
4	p_{im}	p_{em}	p_{t}
4	T_{im}	p_{em}	T_{em}

The results from Table 7.1 are:

- Only one combination with index 2. The obvious selection to measure the signals in x_1 is the best choice, even though it involves augmenting the system by one additional state for the temperature sensor dynamics. A practical aspect is that the exhaust manifold pressure is hard to measure.

- Three combinations with index 3. One of them is the combination p_{ic}, p_{im}, and T_{im} that are normally measured signals on TC SI-engines.

- Two combinations with index 4, which both include temperatures.

In the cases above, the highest power of A is three, and therefore the numerical problems are avoided. Thus, the analytical method is able to produce a very short list of good candidates. As the underlying engine model has physically based parameters, it is reasonable to assume that this result is valid for all TC SI-engines with the same structure.

7.5 Results

The problem of selecting signals for observer feedback has been studied. Using a structural method, it is possible to show that the studied system is locally structurally observable from any measured state or combination of states. A metric, observability index, is used to aid the selection of what signals that are most suitable for observer feedback. Two scenarios are considered: The entire system and a subset of the system. In the latter case the selected subset of states are those involved in the CAC estimation but the methodology is generally applicable.

In the first scenario, observability of the entire system, it is best to use sensors that do not require the system to be augmented with sensor dynamics. When the system is augmented with sensor dynamics the minimum number of required differentiations increase and hence the observability index.

In the second scenario, when the application cylinder air charge estimation is considered, only a fraction of the state space is required to determine the

cylinder air charge. Therefore, the observability index of this subset of states
is used to evaluate which feedback signal and/or combination of signals that
observes this subset best. When three sensors are used only 6 configurations
of 680 possible reach an observability index less or equal to 4. One unique
combination is best and reaches the observability index 2. It is the obvious
combination of measuring p_{im}, T_{im}, and p_{em}. Even though it requires that
the system is augmented with one additional state to describe the temperature
sensor dynamics it is the best choice. In addition, the normally measured p_{ic},
p_{im}, and T_{im} is a very good combination with observability index 3.

   Thus, the proposed method provides the observer designer with valuable
information during the sensor selection. An advantage is that only the model
equations are necessary inputs to the method. To test the observability of the
entire system it is sufficient to know only the structure. As most TC SI engines
are similar in structure, the observability results are valid for all engines of the
same structure.

8

Air-System Observer Design

A key element to precise air/fuel ratio control is accurate estimates of cylinder air charge (CAC). Since the CAC is not measurable, it has to be estimated. Here CAC estimates are based on the CAC-model for TC engines proposed in Chapter 4. This CAC model relies on the following signals: intake manifold pressure p_{im}, intake manifold temperature T_{im}, and exhaust manifold pressure p_{em}. Now, three challenges become evident: the measured p_{im} is very noisy, the T_{im} sensor is considerably slower than the temperature dynamics, and p_{em} is not normally measured. Again, a model such as the one proposed in Chapter 6 can estimate these signals. Unfortunately, there are model errors that cause estimation biases and a remedy is to improve the estimates using feedback from measured signal(s). A model of a process that takes, in addition to the process inputs, measured signals from the process as feedback to improve state estimates is called an observer.

In addition to CAC estimation, there are other observer applications such as diagnosis of sensors and actuators. By observing a signal that is measured and *not* used by the observer, the measured and observed signal can be compared. If the difference is large then it can be concluded that, with some degree of certainty, an error is present. Thus, there are several applications of observers and a systematic observer design method is desirable.

The focus of this chapter is to present a systematic and automatized design method for a basic TC SI-engine observer. The resulting observer can be used for noise reduction, estimate non-measured signals, decrease the effects of sensor dynamics, diagnosis and also for prediction. The observer relies on the mean value engine model developed in Chapter 6 that is briefly summarized in the

next section. Then the chapter continues with a more detailed description of the observer design.

8.1   Mean Value Air-System Model

A component based mean value model of the air system, exhaust system, and turbocharger forms the base of the observer design. The model is described in Chapter 6 and it is suitable for air-fuel control and diagnosis. Model inputs are N, α, λ, u_{wg}, p_{a}, and T_{a}. The nomenclature is described in Appendix A. Below, in Eq. (8.1), a summary of the model equations are shown. An important observation is that several state equations have dependencies on both intake and exhaust conditions. Such couplings are present in e.g. the intake manifold pressure and temperature states. A consequence of the couplings is that it is not sufficient to only model the intake side on TC SI-engines, hence the model includes the exhaust side and turbocharger speed dynamics.

$$
\begin{bmatrix}
\dot{p}_{\text{af}} \\
\dot{T}_{\text{af}} \\
\dot{p}_{\text{comp}} \\
\dot{T}_{\text{comp}} \\
\dot{p}_{\text{ic}} \\
\dot{T}_{\text{ic}} \\
\dot{p}_{\text{im}} \\
\dot{T}_{\text{im}} \\
\dot{p}_{\text{em}} \\
\dot{T}_{\text{em}} \\
\dot{p}_{\text{t}} \\
\dot{T}_{\text{t}} \\
\dot{\omega}_{\text{tc}}
\end{bmatrix}
=
\begin{bmatrix}
f_{p_{\text{af}}}\left(p_{\text{af}}, T_{\text{af}}, p_{\text{comp}}, \omega_{\text{TC}}, p_{\text{a}}, T_{\text{a}}\right) \\
f_{T_{\text{af}}}\left(p_{\text{af}}, T_{\text{af}}, p_{\text{comp}}, \omega_{\text{TC}}, p_{\text{a}}, T_{\text{a}}\right) \\
f_{p_{\text{comp}}}\left(p_{\text{af}}, T_{\text{af}}, p_{\text{comp}}, T_{\text{comp}}, p_{\text{ic}}, \omega_{\text{TC}}\right) \\
f_{T_{\text{comp}}}\left(p_{\text{af}}, T_{\text{af}}, p_{\text{comp}}, T_{\text{comp}}, p_{\text{ic}}, \omega_{\text{TC}}\right) \\
f_{p_{\text{ic}}}\left(p_{\text{comp}}, T_{\text{comp}}, p_{\text{ic}}, T_{\text{ic}}, p_{\text{im}}, \alpha\right) \\
f_{T_{\text{ic}}}\left(p_{\text{comp}}, T_{\text{comp}}, p_{\text{ic}}, T_{\text{ic}}, p_{\text{im}}, \alpha\right) \\
f_{p_{\text{im}}}\left(p_{\text{ic}}, T_{\text{ic}}, T_{\text{im}}, p_{\text{im}}, p_{\text{em}}, N, \alpha, \lambda\right) \\
f_{T_{\text{im}}}\left(p_{\text{ic}}, T_{\text{ic}}, T_{\text{im}}, p_{\text{im}}, p_{\text{em}}, N, \alpha, \lambda\right) \\
f_{p_{\text{em}}}\left(p_{\text{im}}, T_{\text{im}}, p_{\text{em}}, T_{\text{em}}, p_{\text{t}}, N, \lambda, u_{\text{wg}}, T_{\text{a}}\right) \\
f_{T_{\text{em}}}\left(p_{\text{im}}, T_{\text{im}}, p_{\text{em}}, T_{\text{em}}, p_{\text{t}}, N, \lambda, u_{\text{wg}}, T_{\text{a}}\right) \\
f_{p_{\text{t}}}\left(p_{\text{em}}, T_{\text{em}}, p_{\text{t}}, T_{\text{t}}, \omega_{\text{TC}}, u_{\text{wg}}, p_{\text{a}}\right) \\
f_{T_{\text{t}}}\left(p_{\text{em}}, T_{\text{em}}, p_{\text{t}}, T_{\text{t}}, \omega_{\text{TC}}, u_{\text{wg}}, p_{\text{a}}\right) \\
f_{\omega_{\text{TC}}}\left(p_{\text{af}}, T_{\text{af}}, p_{\text{comp}}, p_{\text{em}}, T_{\text{em}}, p_{\text{t}}, \omega_{\text{TC}}\right)
\end{bmatrix}
\tag{8.1}
$$

8.1.1   Feedback is Necessary

Figure 8.1 shows the results of an open loop simulation of a throttle step at constant engine speed, where the model is compared to measured engine data. Initial values for the simulation was set to ambient conditions and the results shown here are after the initial transient. The selected signals for the comparison are those involved in the CAC estimation. Note how the model successfully reduces intake manifold pressure noise without introducing a time lag. Also, the intake manifold temperature dynamics is important for CAC estimation (Chevalier and Müller, 2000) and it is described by the model. This fast dynamics is important as it is not captured by the measurements due to the slow temperature sensor. However, even though the model estimates the required states, the estimate of for example the intake manifold pressure is biased. To
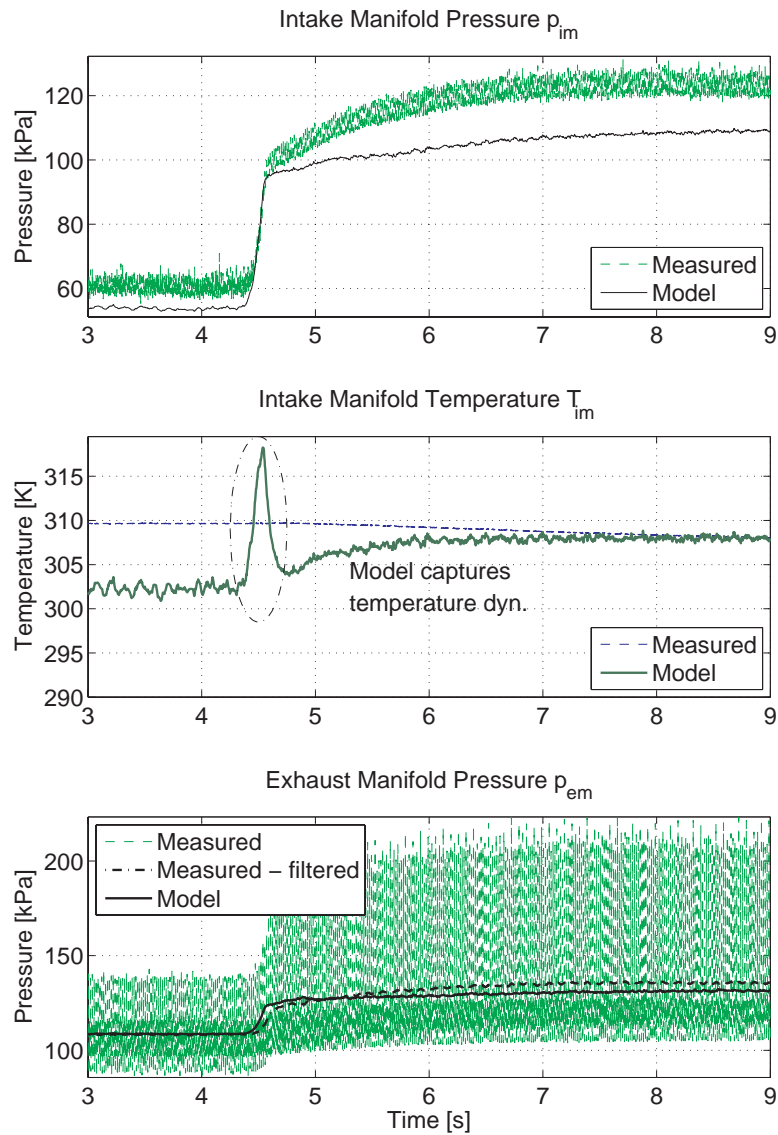
Figure 8.1: Model compared to measured data during a very rapid throttle step at constant speed at 1800 RPM. *Top:* The model reduces noise in the intake manifold pressure signal. *Center:* Transient behavior of the intake manifold temperature is captured by the model but it suffers from a bias before the transient as heat transfer to the gas in the intake manifold is not modeled. *Bottom:* Measured exhaust manifold pressure compared to modeled. There is a bias in the estimated mean exhaust manifold pressure.

reduce the state biases and thus improve the CAC estimates it is *necessary* to introduce feedback from measured signals y_m.

An observer is to be designed using the known inputs u, measured outputs y_m, and the non-linear process model $\dot{x} = f(x, u)$ given by Eq. (8.1). In the observer, the observed states are called $\hat{x}$ and the dynamics of $\hat{x}$ are described by the non-linear system dynamics $f(\hat{x}, u)$ together with feedback from the difference between the measured signals y_m and the modeled measurement signals $\hat{y}$. The observer structure used in this chapter is thus:

$$\begin{aligned}
\dot{\hat{x}} &= f(\hat{x}, u) + K(\hat{x}, u)\,(y_m - \hat{y}) \\
\hat{y} &= g(\hat{x}, u)
\end{aligned}$$

As the estimation error $y_m - \hat{y}$ is amplified through K, a compromise is required as a high K means that the observer relies more on the measurements and the noise that comes with the measurements. A low K on the other hand means that the observer relies more on the model but also on the model errors.

8.2   Observer Design

As K is a compromise between relying on the model or on the measurements, the next step is to investigate the quality of the model and the measurements over the operating region of the engine. When studying the quality of the model it is clear that the model errors, shown in Figure 6.24, are not equal over the entire operating region. Further, the level of noise on the measured signals used for observer feedback also depends on the operating point. Thus, it is desirable to have different observer gains depending on the operating point.

A challenge when several gains are to be designed over the entire operating region is that there is a large number of gains to determine. A simple example is given to illustrate that it is not reasonable to manually determine all the gains. Assume that there are thirteen states, two feedback signals, and the gains are determined in 50 operating points (10 speeds and 5 different intake manifold pressures for each speed). Then there are $2 \times 50 \times 13 = 1300$ gains to calculate! It would be too time-consuming to manually compute all these and therefore, a systematic design method that can be automatized is necessary.

8.2.1   Design Method Selection

For observers based on linear models there is an abundance of design methods to choose from. However, the model that forms the base of the observer is non-linear. Therefore, a variant of the constant gain extended Kalman filter (CGEKF) is chosen for observer design. It is a design method for non-linear systems presented in Safanov and Athans (1978) that has been used by several references for pressure and temperature observers (Jensen et al., 1997; Maloney and Olin, 1998). The method is chosen as the resulting feedback gain is a

weighing between only two design inputs Q and R, which describe the accuracy of the model and the measurements respectively. The design is performed in points spread across the operating region of the engine to take the varying process dynamics, varying quality of the model, and varying quality of the measurements into account.

8.2.2 Design Overview

Necessary inputs when designing an observer according to the CGEKF methodology are:

1. A non-linear plant model.

2. Measured signal(s) for observer feedback.

3. A description of the process noise variance Q (model uncertainty).

4. A description of the variance of the measured signal(s) noise R (measurement uncertainty).

The method uses theory for the linear stationary Kalman filter to determine the feedback gain K. In order to produce an *optimal* Kalman filter the process noise and the measurement noise have to be additive, white, and gaussian. In practical applications the noises Q and R are often considered as *design parameters* as Q and R seldom are additive, white, and gaussian. In this application Q and R are not known and it is also not known whether they are white and gaussian. Thus, they are treated as design parameters that describe the quality or uncertainty of the model and the measurements. In the following text, Q is referred to as *model uncertainty* and R as *measurement uncertainty*. In Section 8.2.5 and Section 8.2.6, a method is developed to systematically assign values to them over the operating region of TC SI-engines.

The observer design starts by selecting signals for observer feedback, which is described in Section 8.2.3. When signals for observer feedback have been determined, the proposed systematic method is applied to determine the design parameters model- and measurement uncertainty. Then the observer gains are determined for each design point. A design point is here determined by the engine speed, air-mass flow, and the pressure before the throttle. In Section 8.2.4 the selection of design points are described. Given a design point, the gain calculation can be summarized as:

1. Find the stationary point of the *model* in the design point. The stationary point is defined by values of the states x_0 and inputs u_0 such that $f(x_0, u_0) = 0$. See Section 8.2.4 for more details.

2. Linearize the model in the stationary point (x_0, u_0), see Section 8.2.4.

3. Determine the observer design parameters Q (model uncertainty) and R (measurement uncertainty) using the systematic method described in Section 8.2.5 and Section 8.2.6.

4. Design the feedback gains, see Section 8.2.8.

5. Store the calculated feedback gains in a look up table.

8.2.3   Observer Feedback Selection

As the system is locally structural observable from an arbitrarily measured state according to Chapter 7, this design method can be applied to a wide variety of measurement signals. To illustrate the observer design in this chapter two pressure signals are chosen for observer feedback: Intake manifold pressure and pressure before the throttle. These signals are chosen as they are measured using fast sensors and are available on most production engines. If for example a temperature would have been considered for observer feedback, then the model have had to be augmented with sensor dynamics as the temperature sensors are considerably slower than the system dynamics. Further, on the engine in the research laboratory there are several additional sensors available that could be used for observer feedback. One can then argue that all available sensors should be used, but this will conceal one of the observer advantages of estimating non-measured states or signals. In addition, the automotive industry is very cost sensitive and every extra sensor increases the cost of the engine.

8.2.4   Design Point Selection and Model Linearization

The observer design is carried out in stationary points determined by design points. The design points should be chosen in such way that they reflect the non-linear dynamics of the model and describe the input u_0 of the model necessary to determine the stationary point x_0. As the model consists of control volumes, whose dynamics depend on the air-mass flows; it is natural to choose the linearization points across the range of air-mass flow through the engine. The air-mass flow is basically determined by multiplying the engine speed N by the intake manifold pressure p_{im}. An excellent candidate to describe the design points is therefore an engine map as it is commonly measured for different engine speeds and different intake manifold pressures. The engine map is also used when the engine model is tuned and/or validated.

In the engine map all necessary inputs in u_0 are measured except for the wastegate angle. However, as the air-mass flow is used to describe the design point, the measured throttle angle can not be used due to small throttle model errors. Instead, the throttle angle and wastegate setting will be determined by simulating the model as described in the stationary validation in Section 6.10.1. Two controllers are used to determine the stationary point: one faster that governs the air-mass flow by adjusting the throttle angle and a second slower controller that governs the wastegate setting to achieve the same pressure before the throttle as in the measurements. The process of determining the stationary point can be summarized as:

1. Read the current design point from the engine map, that is the following values: $N, W_\mathrm{a}, p_\mathrm{ic}$

2. Determine the stationary point (x_0, u_0) by controlling the system to the design point in terms of $N, W_\mathrm{a}, p_\mathrm{ic}$.

3. Store the resulting design point (x_0, u_0) in a table for later use in the linearization.

Repeat the process for all remaining entries in the engine map.

Model Linearization

The stationary point of the model were determined in the previous section and stored in a table according to step 3. Now, for every stationary point (x_0, u_0), the model is linearized:

$$A = f_x(x_0, u_0) \qquad\qquad B = f_u(x_0, u_0)$$
$$C = g_x(x_0, u_0) \qquad\qquad D = g_u(x_0, u_0)$$

Above, the notation $f_x(x_0, u_0)$ refers to the Jacobian of $f(x, u)$ with respect to the states x evaluated in (x_0, u_0). The linearized model is in Section 8.2.8 when the Kalman gains are determined.

8.2.5 Measurement Uncertainty R

The purpose of the measurement uncertainty R is to describe the deviations from the desired measurement and here only measurements from the physical process will be used when R is determined; that is the measurement uncertainty is independent of the process model. The measurement uncertainty should be determined in the design points where the desired measured signal would be the *mean value* of the signal. However, in practice there are disturbances caused by non-modeled effects, electrical disturbances, and so on. Therefore, all *deviations* from the measured mean value of the signals are considered as measurement uncertainty R. To measure the deviations from the mean value of the measured signal, the variance of the signal is used. In practice, this requires that the engine map is extended with the *variance* of the signals considered for observer feedback in each design point. That is calculate and store the variance of the signals in each design point in addition to the mean values of the measured signals. Note that it is sufficient to have the variance for the signals that will be used in the feedback.

An example of this measurement uncertainty definition is shown in Figure 8.2. Here the non-modeled engine pumpings in the intake manifold pressure signal are considered as measurement uncertainty. As the data is sampled, the
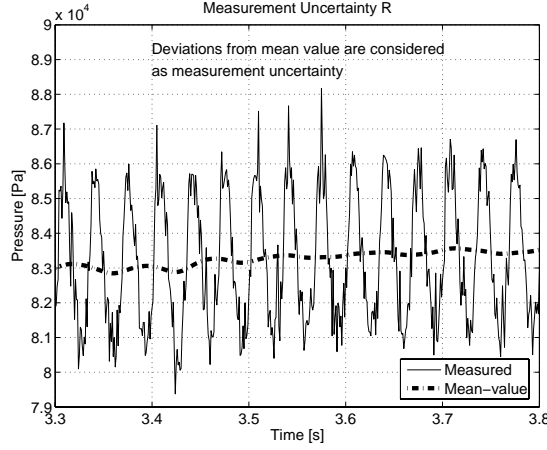
Figure 8.2: The measurement uncertainty R describes deviations from the desired measurement which is the mean value. The measurements are considered as independent of the process and here the measurement uncertainty R is defined as the variance of the measured signal. The variances of the measured signals are preferably stored during the engine mapping.

measurement uncertainty can be calculated from measurements as:

$$R_i = \frac{1}{N-1} \sum_{n=1}^{N} \left(\overline{y}_{\text{meas}_i} - y_{\text{meas}_i}[n] \right)^2$$

where i is the i:th measured signal. The uncertainties of the measured signals are assumed to be independent, which results in a diagonal R matrix.

Further, the matrix R must be positive definite and therefore the elements are bounded from below to make sure that the matrix is not singular. The threshold is individually set for each signal to one of the lower measured values. Examples of thresholds used are: $R_{p_{\text{im}}} \geq 2 \cdot 10^5$ and $R_{p_{\text{ic}}} \geq 10^4$.

8.2.6   Model Uncertainty Q

The objective is to find a description of the model's uncertainty, and the basic idea is to use the design points to extract this information. By assuming that there are no sensor biases, which is reasonable when calibrated sensors are used, a simple and straightforward method to assess the model uncertainty is to use the stationary model error. For each design point, the stationary value of the modeled state i is $\overline{x}_{\text{state}_i}$ and the value of the measured state i is $\overline{x}_{\text{meas}_i}$. The model uncertainty Q_i is then defined as:

$$Q_i = \left(\overline{x}_{\text{meas}_i} - \overline{x}_{\text{state}_i} \right)^2$$

This error was also calculated in the stationary model validation in Section 6.10.1. Thus, Q is diagonal as no knowledge of dependencies of other model equations
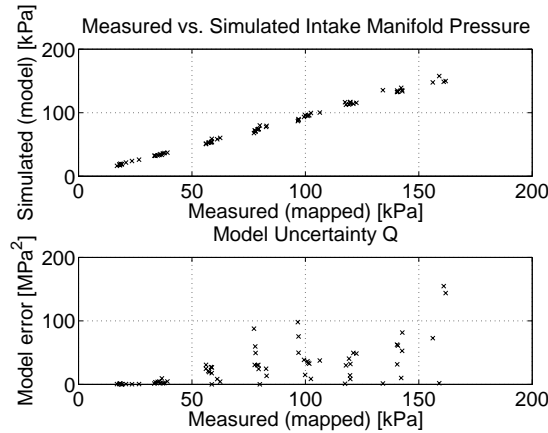
Figure 8.3: An example illustrating how the model uncertainty parameter is determined for stationary operating points. *Top:* Here the measured intake manifold pressure and the modeled intake manifold pressure is shown. *Bottom:* The resulting model uncertainty $Q_{p_{\mathrm{im}}} = (\overline{p_{\mathrm{im}}}_{\mathrm{meas}} - \overline{p_{\mathrm{im}}})^2$ is shown.

are present. If a description of dependencies between model uncertainty in the equations is available, then it can be easily included in the framework.

Using this definition the model quality is reflected in the selected operating points and an illustration of this model uncertainty definition for the intake manifold pressure is shown in Figure 8.3.

8.2.7 Alternative Measures of the Model and Measurement Uncertainty Definitions

Several other methods to estimate the covariance matrices Q and R have been proposed in the literature and here two methods are mentioned. None of these methods have been tested as the proposed method gave good results.

In Jensen et al. (1997) Q is also set diagonal, but instead of using the model error as model uncertainty the power of the pumpings in e.g. the intake manifold pressure where used as $Q_{p_{\mathrm{im}}}$. They used the measured noise on the sensor signals when the engine is not running, but the electronics is switched on, as measurement uncertainty.

Chevalier et al. (2000) develop a predicting observer for a NA-engine is developed. There the process noise is estimated using a different structure of Q where also some of the off-diagonal elements are non-zero with good results.

Another method is proposed in Bos et al. (2005) that does not rely on known covariance information. There, measured data is also used to estimate the covariance matrices based on an estimated autocovariance of the measured signals.

8.2.8   Observer Gain Calculation and Gain Switching

Now there exists a linearized model, a method to determine the design parameters Q and R, which mean that the stationary Kalman gain K in the design point can be calculated (Levine, 1996, p. 608).

$$K \quad = \quad PCR^{-1} \tag{8.2}$$

P is the *stationary* error covariance matrix, which is determined by solving an algebraic Riccatti equation (Levine, 1996, p. 608).

$$\dot{P} = 0 = AP + PA^T - PC^T R^{-1} CP + Q$$

Observer feedback gains can now be pre-computed offline for each design point given by the engine map. Later, when the observer is run, a simple table look-up of the closest feedback gain is used. Look-up keys in the gain switching are engine speed and intake manifold pressure, as these two are important parameters for the system dynamics.

8.2.9   Stability Investigations

It is hard to prove stability of extended Kalman filters especially for high order systems. Instead, two other tests are performed. First an observer non-divergence test is made and then extensive tests using measured data. The non-divergence test is presented for CGEKF in Safanov and Athans (1978). Non-divergence means that a mean-square bounded disturbance produces a mean-square bounded estimate error. The non-divergence test was applied as in Safanov and Athans (1978) in all design points and the conditions were satisfied.

The second stability test is more pragmatic than stringent: Extensive testing using different operating conditions. Here 20 different step response experiments were tested; they were 16 steps in throttle, 2 steps in engine speed, and 2 steps in wastegate setting. In neither of the cases did the observer diverge which indicates that the system is stable. Further it has not diverged during real-time tests either, which gives additional support to the stability of the observer.

8.2.10   Discussion of Design Choices

Here the extended Kalman filter theory is used to design the observer gains. The Kalman theory requires that the noise intensities (uncertainties) of the model Q and measurements R originate from additive white gaussian noise processes. To identify the corresponding values of Q and R, according to the theory, would require substantial more effort. Here two of the objectives are ease of use and that it should be easy to obtain the necessary inputs for the observer design. The proposed method to select the model and measurement uncertainties is not aimed at being general; instead it is customized for the use in TC SI-engines. Using the proposed definitions of model and measurement uncertainties, it is

sufficient to use an engine map that has been extended with the variance of the measurement signals that are considered for observer feedback. This design choice is supported by the fact that it has been tested on two different engines and no manual tuning of the resulting gains has been necessary, which supports that the method as suitable for its purpose.

Below, an example is given that shows a potential drawback of the proposed method to select the model uncertainty. In models where the state equations have strong dependencies on surrounding states, the use of a diagonal Q causes the selected uncertainty measure to propagate errors in one state equation to the surrounding equations. This is illustrated in the following synthetic example, where there is no error in the x_1 state equation but there may be an error present in the x_2 state equation:

$$
\begin{aligned}
\dot{x}_1 &= -x_1 + k_1 x_2 \\
\dot{x}_2 &= -(k_2 + \Delta k_2)x_2 + u
\end{aligned}
$$

Given that there is no model error, i.e. $\Delta k_2 = 0$, the stationary point will be u_0 and $x_0 = \left(\frac{k_1}{k_2}u_0, \frac{u_0}{k_2} \right)$. When the model error Δk_2 is non-zero the stationary point will be:

$$
u = u_0, \qquad x_{0_{\Delta k_2}} = \left(\frac{k_1}{k_2 + \Delta k_2}u_0, \frac{1}{k_2 + \Delta k_2}u_0 \right)
$$

Using the definition of the design parameter model uncertainty Q, this is defined as:

$$
Q = \mathrm{diag}(x_0 - x_{0_{\Delta k_2}})^2 = \left(\begin{array}{cc} q_{11} & 0 \\ 0 & q_{22} \end{array} \right) = \left(\begin{array}{cc} k_1^2 \frac{u_0^2 \Delta k_2^2}{k_2^2(k_2+\Delta k_2)^2} & 0 \\ 0 & \frac{u_0^2 \Delta k_2^2}{k_2^2(k_2+\Delta k_2)^2} \end{array} \right)
$$

An important observation is that the error in the x_2 state equation *propagates* to the first state x_1 as $q_{11} = k_1^2 q_{22}$ and if $|k_1| > 1$, the error is amplified! Fortunately this effect is reduced, in this engine application, as the design points are selected in such manner that the air-mass flow is the same as measured through the model and the pressure before the throttle is close to measured for all points were the wastegate is opened. This means that the effect of error propagation is most pronounced for low engine loads. The basic design proposed above has produced good designs for the feedback gain for the two engines investigated here. However, as the discussion above highlights, there are no guarantees for receiving good designs for all cases and systems. Therefore, as a fall back solution, if the results is not satisfying after the basic design, there is always the possibility to manually fine tune the gains.

8.3 Design Example

The method to select the design parameters Q and R has been applied to design an observer given the two signals that were selected for observer feedback in

Section 8.2.3, the pressure after the intercooler and the intake manifold pressure. Given these signals, the observer gains were determined in 67 design points spread across the operating region of the engine.

First properties of some selected feedback gains are discussed followed by an observer evaluation using measured engine data. The evaluation shows how the observer estimates the necessary states in the CAC model and as an example estimates of the not normally measured turbocharger speed is shown.

8.3.1   Resulting Feedback Gains

As there are 13 states and 2 feedback signals there are 26 feedback gains for each of the 67 design points. Four different gains have been selected to illustrate that the design method achieves a weighing between model uncertainty and measurement uncertainty. In Figure 8.4 these gains are shown and a description of what the figure shows is given below:

Feedback gains from measured p_{ic} to $\hat{p}_{ic}$ and $\hat{p}_{im}$ In the top left corner of Figure 8.4, it can be seen that the gain is initially increasing for air-mass flows up to 40 g/s and then stabilize at a lower level. Recall that the model uncertainty in the intercooler pressure state is higher for low air-mass flows, which was seen in Figure 6.24. For low air-mass flows, the measured p_{ic} shows low measurement uncertainty. The combination of model and measurement uncertainty results in high feedback gains to the p_{ic} state itself for low air-mass flows. For higher air-mass flows, above 40 g/s the model uncertainty is lower as the wastegate opens; the observer therefore relies more on the model and as a result the gain stabilizes at a lower level. Also, the feedback from p_{ic} do influence p_{im} through the cross coupling to the p_{im} state. This is shown in the bottom left corner, where the feedback from p_{ic} to p_{im} increases for mass-flows up to 40 g/s as the model quality is less good for these low mass-flows where the wastegate is inactive.

Feedback gains from measured p_{im} to $\hat{p}_{im}$ Measured p_{im} is subjected to more pumping fluctuations compared to the measured p_{ic}, which results in lower feedback gains compared to the feedback gains from p_{ic} (top right).

Feedback gains from measured p_{ic} to $\hat{\omega}_{tc}$ In the bottom right corner it is shown how the measured p_{ic} is used to improve other states that is not directly related to the measured signal such as the turbocharger speed.

With the proposed method to determine the model and measurement uncertainty, the resulting observer feedback gains can be applied without any manual tuning. This is not always the case, Jensen et al. (1997) reports that using a different definition of model Q and measurement uncertainties R the resulting observer gains had to be manually reduced.
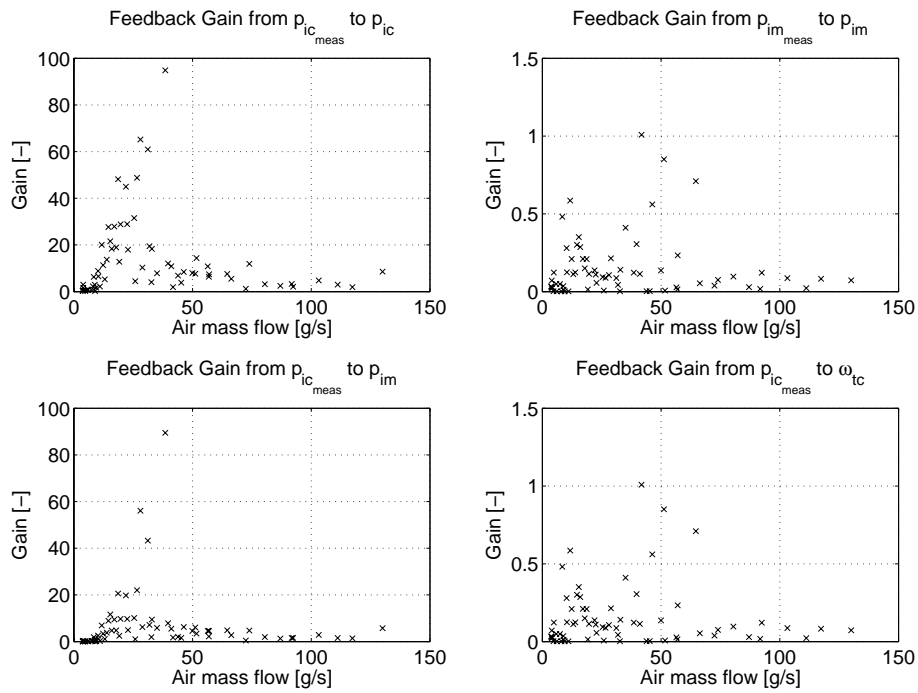
Figure 8.4: Four feedback gains have been selected to illustrate how the resulting gains reflect the weighing of model and measurement uncertainty for the design example. The gains are shown as a function of air-mass flow. *Top left*: The gain from measured p_{ic} is higher for mass-flows less than 40 g/s where the model errors are larger. *Top right*: The gain from measured intake manifold pressure is lower as the measured signal $p_{im_{meas}}$ is noisier than $p_{ic_{meas}}$. *Bottom left*: Here the coupling between feedback signals and other states is shown. The observer tries to increase intake manifold pressure when the estimated pressure after the intercooler is too low. *Bottom right*: Here it is shown how the observer uses pressure measurements to improve the turbocharger speed state estimate.

8.3.2 Evaluation using Measured Data

Measured data from a turbocharged SAAB 9^5-engine (B235R) is used to test the observer. The measurement setup is described in Appendix E. The evaluation focuses on states that are important for CAC estimation.

To show that the introduction of feedback improves state estimates, it is first tested using the same step in throttle position at 1800 RPM, which was used in Figure 8.1. The results using the observer is shown in Figure 8.5. It is clear that the model's noise attenuation property for p_{ic}, p_{im}, and p_{em} is preserved. In addition, the observer is able to reduce the stationary errors of the exhaust manifold pressure, turbocharger speed, and pressure before the throttle very well compared to the open loop simulation (model). However, the observer is not able to fully eliminate the stationary error for low intake manifold pressures.

Feedback and Stationary Errors in the Presence of Model Errors

In the previous example, it was seen that even though feedback was used from the measured intake manifold pressure, a small stationary error remained. One of the causes is that there are model errors that introduce biases in the state estimates. This effect was described in Section 3.3.2. If it is crucial to reach stationary correct values a remedy is suggested in Chapter 3 where the model is augmented with an additional state that e.g. scales a parameter in the CAC model. In this way it was possible to cancel stationary errors in the p_{im} state that also was measured.

8.4 Stationary – Non Stationary Observer

The suggested observer is based on the assumption that a stationary Kalman filter is sufficient. To verify this assumption, a non-stationary Kalman was implemented. First the resulting gains and then the state estimates are compared to the stationary Kalman filter.

The observer gain K is a function of (P, R), see Eq. (8.2), and thus to implement the non-stationary filter it is necessary to determine (P, R) in runtime. The dynamics of the error covariance P is (Levine, 1996, p. 608):

$$\dot{P} = AP + PA^T - PC^T R^{-1} CP + Q \tag{8.3}$$

Measurements of the state uncertainty Q and the measurement uncertainty R exist only for discrete points described by an engine map. Therefore these were assumed to be the nearest of the known given by the engine map. Here nearest means the closest point in terms of intake manifold pressure and engine speed, like in the selection of stationary gain. The A and C matrices are however determined by linearizing the system in the current operating point.

For comparison, the stationary and non-stationary filters were designed with feedback from measured intake manifold pressure and pressure after the inter-
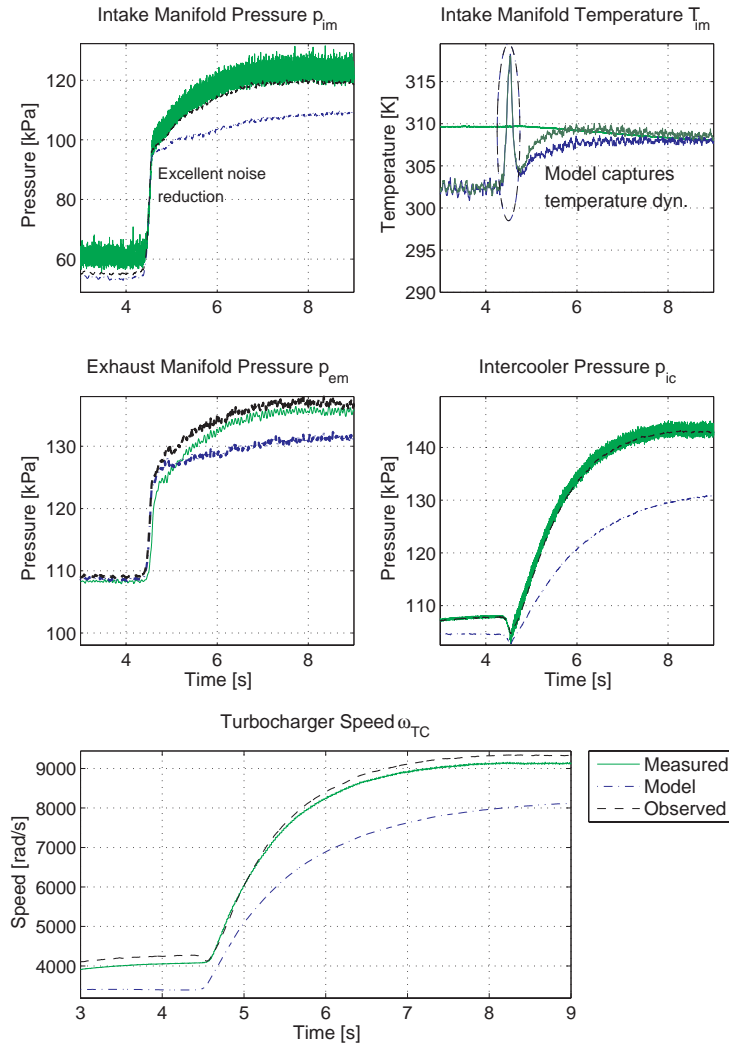
Figure 8.5: Observed and measured states during a throttle tip-in at constant engine speed of 1800 RPM. Note that the legend shown in the bottom plot applies to all plots. *Top left:* The observer reduces pumping noise. *Top right:* The intake manifold temperature is only slightly improved as the model lacks heat transfer to the gas in the intake manifold. *Center:* The observer reduces the stationary errors in p_{em} and p_{ic}. Here the measured p_{em} has been zero-phase low pass filtered to improve clarity. Compare it to Figure 8.1. *Bottom:* Observed turbocharger speed ω_{TC} is very close to the measured compared to the open loop simulation.
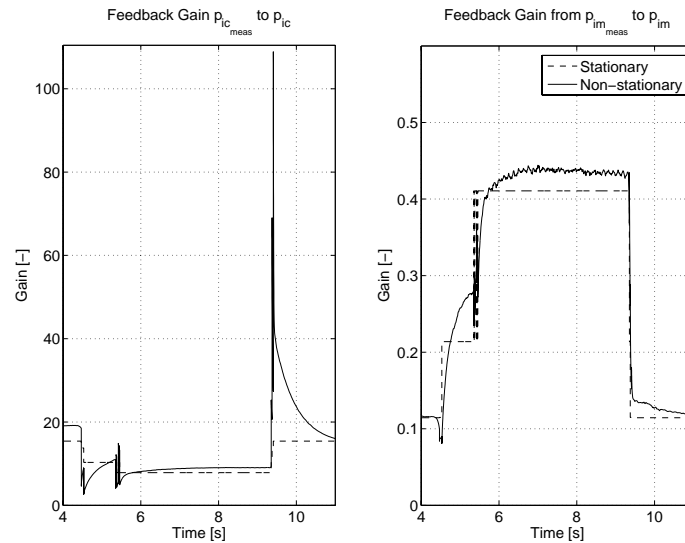
Figure 8.6: Kalman feedback gains for the stationary and non-stationary Kalman filter during a throttle transient at constant speed. When the non-stationary observer feedback gains have converged, they are in the same magnitude as the stationary feedback gain.

cooler, which is the same as used in the previous design example. The filters are evaluated using a step in throttle at constant speed.

First, selected feedback gains from the stationary and non-stationary Kalman-filters are discussed. Selected feedback gains are: the gain from measured intake manifold pressure to the intake manifold pressure state and the feedback gain from measured pressure after the intercooler to the intercooler pressure state. These gains are shown in Figure 8.6. At a first glance, it may seem like that there are large differences in feedback gains for the pressure after the intercooler state, but the gains converge to values close to the stationary in a few seconds. It can be seen that the non-stationary Kalman gains change like step responses when the stationary feedback gain switches. This as the measurement and state uncertainties only are available for discrete operating points given by the engine map. When the stationary observer switches to another feedback gain, the non-stationary observer starts to use different model and measurement uncertainties that influence the resulting feedback gain. In addition, the gains for the non-stationary filter did not converge to the same value as the stationary gains as the system is not linearized in the same operating points. The stationary filter is linearized in discrete points given by the engine map while the non-stationary system is linearized in the *current* operating point that results in a slightly different A-matrix. As the A-matrix is differs the resulting feedback gain $K_{\text{non stat}}$ will be different from K_{stat} which is seen in Figure 8.6.

Second, hardly any differences are visible in the state estimates, shown in

the top of Figure 8.7. Therefore, the differences between them are shown at the bottom of the figure. For the pressure after the intercooler, the maximum pressure difference is less than 1.5%. The maximum difference between the intake manifold pressure state estimates is less than 2.5%. As the differences between the stationary and non-stationary Kalman filter are small this is good motivation for the assumption of stationary error covariance P.

8.5 Using Different Signals for Observer Feedback

One advantage of the mean value engine model used is that it includes a description of both the intake and the exhaust side, which enables a wide variety of signals to be used for observer feedback. This property is being used here, where three combinations of different observer feedbacks are tested with three different applications in mind. The applications are described and motivated below:

$p_{\mathbf{ic}}$, $p_{\mathbf{im}}$ A standard configuration were two commonly available pressure sensors are used for observer feedback.

$p_{\mathbf{im}}$ This setup is shown to indicate that the observer can be used for diagnosis of in this case p_{ic}. For diagnosis it is necessary to create redundant information that does not rely on the signals that should be diagnosed. Here the observer *estimates* the pressure after the intercooler p_{ic} only using feedback from measured intake manifold pressure.

$\omega_{\mathbf{TC}}$ This example shows how the turbocharger speed, which is a not normally measured signal, can be used to improve both the port air-mass flow and estimated pressures.

Three different test cases are used: A modest throttle transient at 2500 RPM, a large throttle transient at 2000 RPM, and an engine speed transient at part load. Results of the different feedback combinations are shown for each test case in Figure 8.8, Figure 8.9, and Figure 8.10. The results for each observer are summarized below:

- The standard configuration with feedback from p_{ic} and p_{im} estimates the pressures, air-mass flows, and also the turbocharger speed well for all test cases.

- To diagnose sensors it is necessary to provide redundant information. Using only the measured intake manifold pressure for observer feedback, it can be seen in Figure 8.9 that the observer estimates p_{ic} accurately for
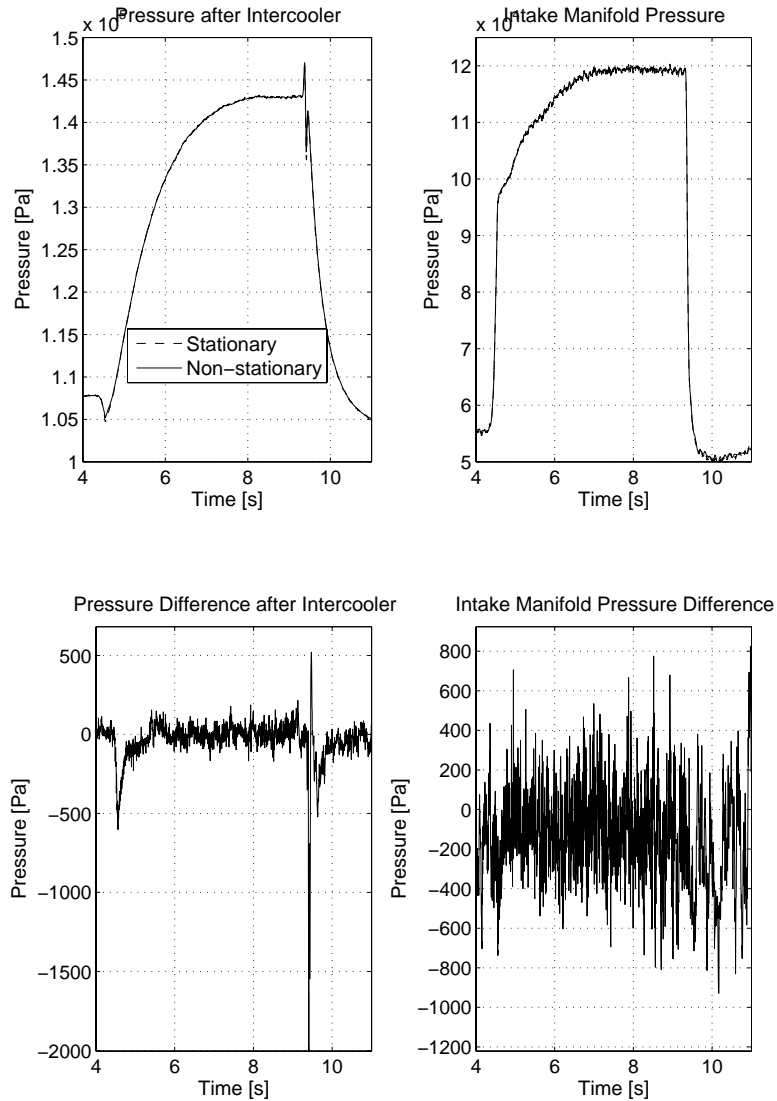
Figure 8.7: State estimates compared from a stationary and non-stationary Kalman filter during a throttle transient at constant speed. The legend in the top left also applies to the top right plot. There are no differences that can be detected by visual inspection between the state estimates provided by the stationary and non-stationary observer. *Bottom:* State estimate differences between stationary and non-stationary. During the transients there are small differences of less than 2.5%.

higher loads. For lower loads, such as in Figure 8.8 and the speed transient in Figure 8.10 the feedback from measured intake manifold pressure alone is insufficient to create accurate estimates of p_{ic} and also of ω_{TC}. This indicates that when the observer is to be used for diagnosis it is necessary to select an operating region where the observer gives accurate estimates. Here the observer can be used to create redundant information for diagnosis of, in this case, the pressure after the intercooler sensor for conditions such as in Figure 8.9.

- When the turbocharger speed is used for observer feedback, it gives a nice illustration of how the observer is able to extract information of the system state from a normally non-measured signal. However, during the engine speed transient, it makes a slight overestimate of the pressure after the intercooler, the intake manifold pressure, and of the the turbocharger speed itself.

In addition, it can be seen that using any of the observers, the estimated air-mass flow at the air-filter is close to the measured. This indicates that it might be possible to replace the air-mass flow sensor by the observer and thereby achieve a cost reduction. The port air-mass flow estimates W_{cyl} are also close to each other regardless of observer feedback. For stationary conditions, W_{cyl} can be compared to the measured W_{af} and it can be seen that the difference between them are small. This shows that the observers estimate CAC well.
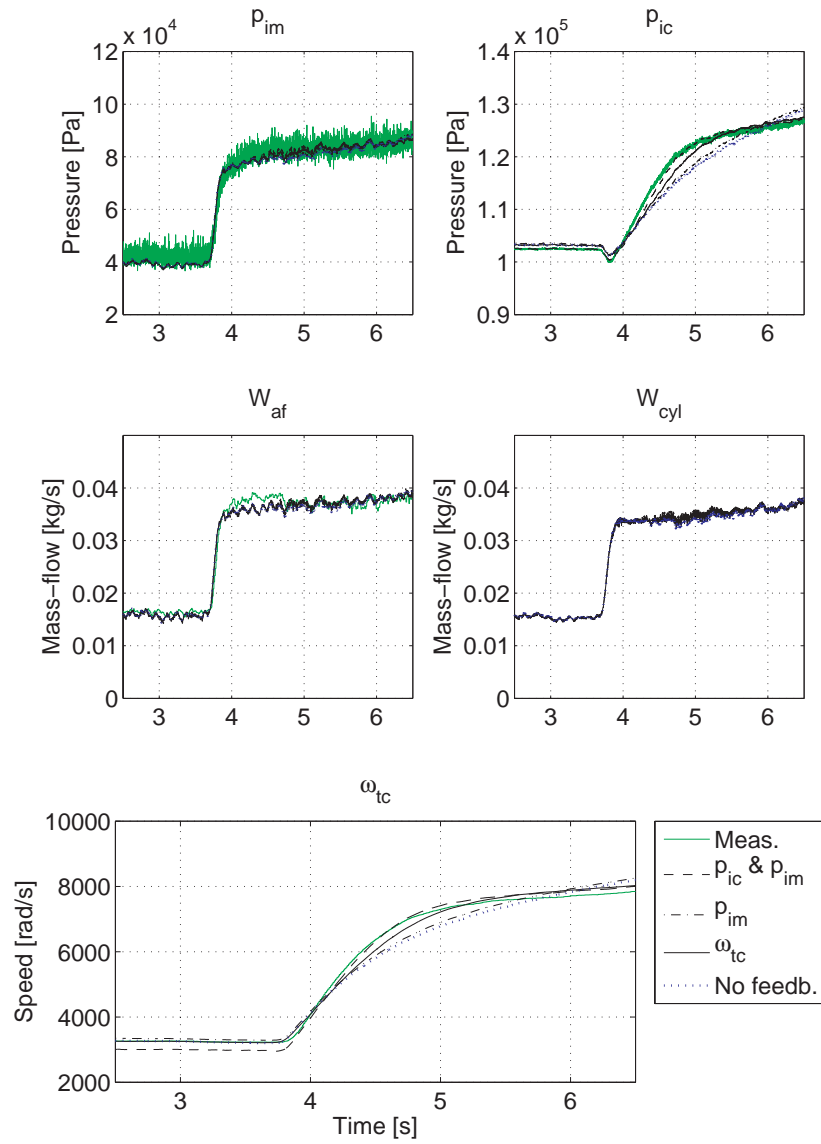
Figure 8.8: A modest throttle transient at a constant speed of 2500 RPM. The legend applies to all plots. In this case the intake manifold pressure alone is not sufficient to describe neither the turbocharger speed ω_{TC} nor the p_{ic} accurately.
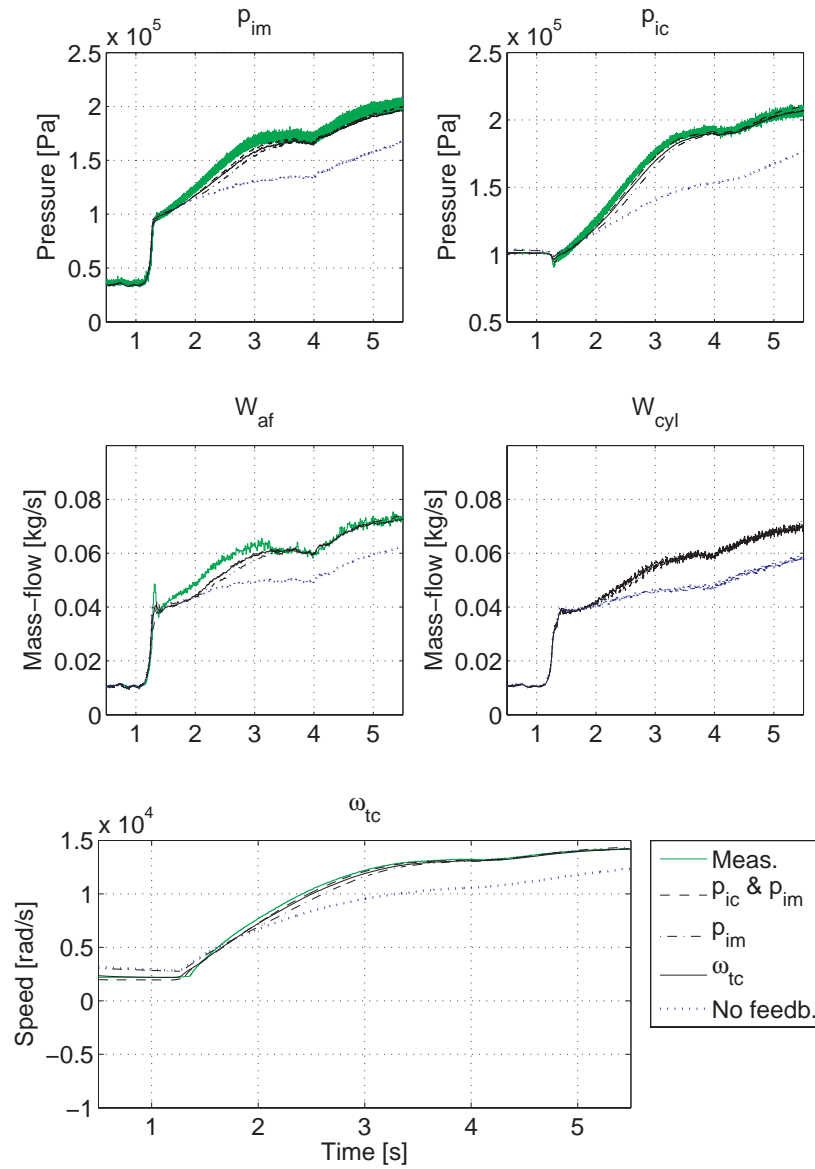
Figure 8.9: A large throttle transient at a constant speed of 2000 RPM. The legend applies to all plots. All tested signals are well described regardless of observer feedback.
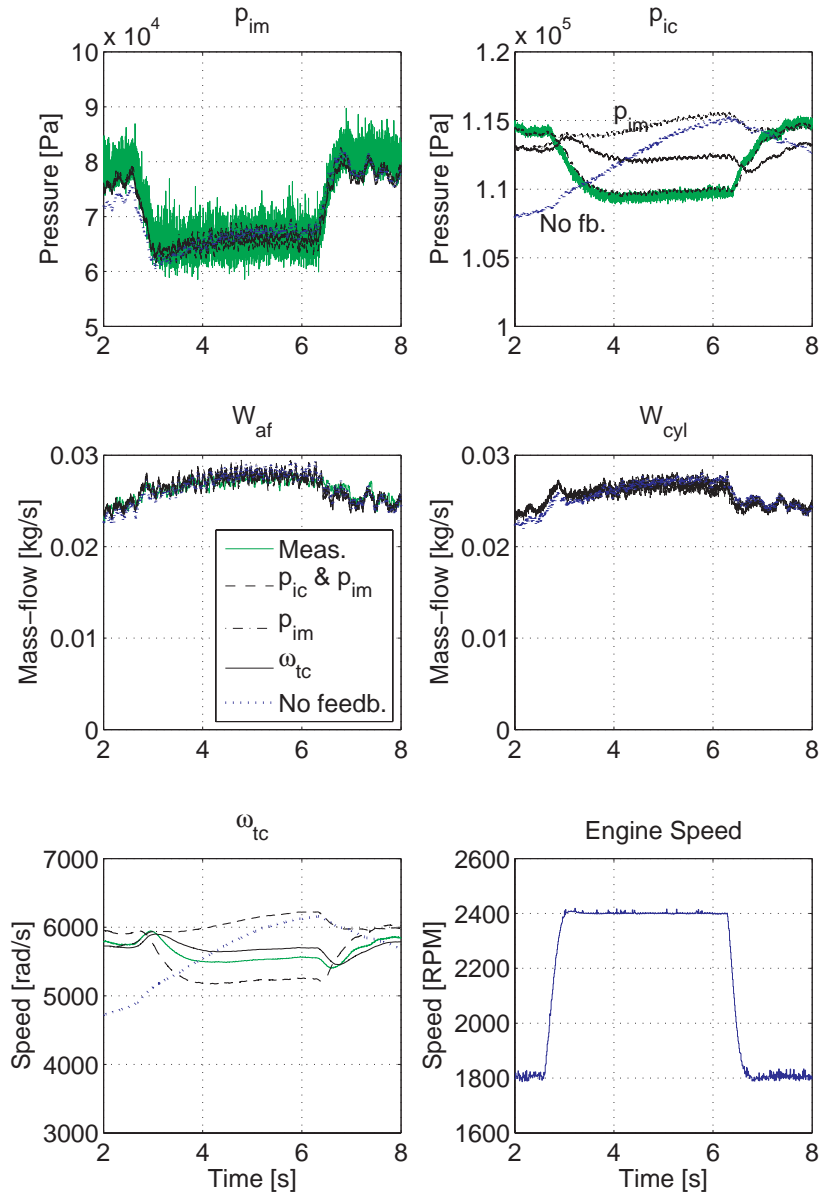
Figure 8.10: An engine speed transient at part load. The legend applies to all plots. Here it can be seen that the observer relying only on the intake manifold pressure feedback is not able to accurately describe neither the turbocharger speed nor the pressure after the intercooler. For the other cases the observer dynamics is correct but there are stationary biases in p_{ic} when p_{im} or ω_{TC} are used for observer feedback.

8.6 Results

A systematic and automatic method is proposed for a basic TC SI observer design. The observer relies on a mean value engine model and the observer is designed using the CGEKF framework. Here the contribution is a systematic method to select the design parameters model and measurement uncertainty for the CGEKF framework.

The purpose of the model uncertainty is to describe the accuracy of the model in each design point. Here the stationary error of the model in each design point is used to quantify the model uncertainty. The measurement uncertainty is given by the variance of the measured signals that are considered for observer feedback. As input to the design method, it is sufficient to supply an engine map that has been extended with the variance of the signals considered for observer feedback. A benefit of the proposed design parameter selection method is that the resulting CGEKF gains can be applied without any manual tuning. Thus the method results in a good basic observer design.

Design examples are used to illustrate the benefits of the observer. It is shown how the observer is suitable for its primary objective of estimating air-mass flow to the cylinder for air/fuel ratio control as it provides excellent noise suppression and does not introduce a large phase shift. Other possible applications are:

- Estimate non-measured signals such as for example turbocharger speed, exhaust manifold pressure, and port air-mass flow.

- Diagnosis of sensors as it can observe signals that also can be measured. Here it has been illustrated how the observer can estimate the pressure after the intercooler using only feedback from measured intake manifold pressure. Thus it creates redundant information that is necessary for diagnosis.

- Reduction of sensors as measured signals can be replaced by observed values. In several different observer designs, it is shown how the air-mass flow at the air-filter can be accurately estimated. This indicates that the air-mass flow sensor can be replaced by observed values.

Observer Based Feedforward Air-Fuel Ratio Control

In spark ignited (SI) engines it is essential to provide accurate air-fuel ratio control to successfully reduce emissions using a three way catalyst (Heywood, 1988; Bauer et al., 1996; Kiencke and Nielsen, 2000; Mondt, 2000). As the desired air is basically determined by the driver through the accelerator pedal the attention is given to the fuel. The mass of injected fuel is determined by the opening time of the fuel injectors. An Electronic Control Unit (ECU) determines the injection time by estimating the air-mass (CAC) in the cylinder at intake valve closing. Therefore, *precise cylinder air charge estimates are crucial* for accurate air-fuel ratio control. An air charge estimation challenge in TC engines is that both intake and exhaust systems are coupled through the turbo. More details on this were given in Chapter 4 where it was shown that CAC estimates are improved when the exhaust manifold pressure is included. In the proposed CAC model, Eq. (9.1), the coupling between the intake- and exhaust side is represented by the pressure ratio dependent term $\frac{p_{\mathrm{em}}}{p_{\mathrm{im}}}$:

$$\mathrm{CAC} = \frac{p_{\mathrm{im}} C_1 V_{\mathrm{d}} \left(r_c - \left(\frac{p_{\mathrm{em}}}{p_{\mathrm{im}}} \right)^{\frac{1}{\gamma_e}} \right)}{\left(1 + \frac{1}{\lambda \left(\frac{A}{F} \right)_s} \right) (r_c - 1) R_{\mathrm{im}} \left(T_{\mathrm{im}} - C_2 \frac{1 - \lambda^2}{\lambda^2} \right)} \tag{9.1}$$

The cylinder air charge (CAC) estimates thus depend on the following signals: p_{im}, T_{im}, p_{em}, and λ. However, as only stoichiometric operation is considered in this chapter, λ can be regarded as a constant.

Cylinder air charge estimation using Eq. (9.1) poses several challenges:

- The intake manifold pressure p_{im} is subjected to noise as seen in Figure 9.1. Most of the noise originates from the deterministic engine pumpings which can be suppressed by a filter with a cut-off frequency selected in such way that the pumpings are suppressed at idle. A side-effect is the non-negligible filter lag which in the example in Figure 9.1 results in a more than 5% error in the CAC estimate.

- The intake manifold temperature can be measured using a sensor, but temperature sensors dynamics is so slow that they miss the 5% to 10% temperature transient. This is illustrated in the bottom of Figure 2.3.

- CAC depends on exhaust backpressure as shown in Chapter 4 but the exhaust manifold pressure is not normally measured due to the harsh conditions on the exhaust side and thus has to be estimated.

- To achieve low hydrocarbon emissions the injection has to be finished around intake valve opening. That is, the CAC at intake valve closing has to be predicted more than half a revolution in advance.
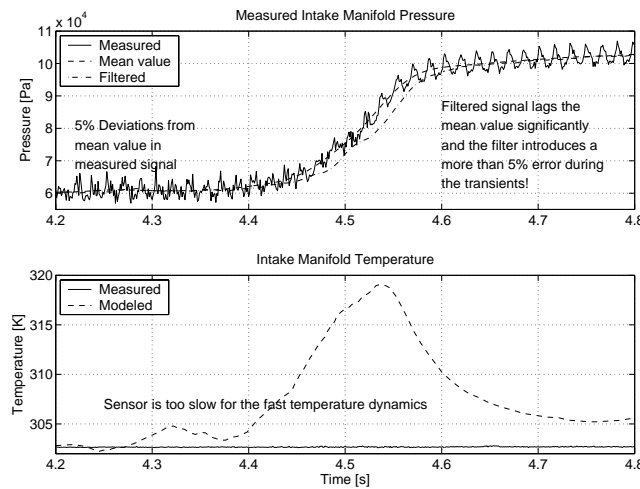
Figure 9.1: Rapid tip-in at a constant speed of 1800 RPM. *Top:* Measured intake manifold pressure is subjected to noise caused by engine pumping and electronics. Noise attenuation using a causal filter results in a significant lag compared to the mean-value. *Bottom:* Measured and modeled intake manifold temperature during the transient. As the sensor has a time constant of approximately 20 seconds, it misses the fast temperature rise captured by the model.

To illustrate the importance of prediction an example is given of how large errors in λ that can be expected if no prediction is made.

Example 9.1

Assume that the necessary prediction time is the sum of the following events:

- The induction stroke corresponds to half a revolution.
- The time to inject the fuel is between one millisecond and up to fully open injectors. Typical injections last a few milliseconds.
- The time necessary to calculate the fuel injection time.
- Communication delays are present when the computations are performed on external hardware.

This sums up to approximately the time of one revolution.

In Figure 9.2, a measured step in throttle at constant speed shows that the expected error in λ is approximately 15%. Here ideal prediction was simulated by translating the modeled port air-mass flow in time corresponding to the time of one revolution. By taking the ratio of the curves, an estimate of the expected error in λ is available.
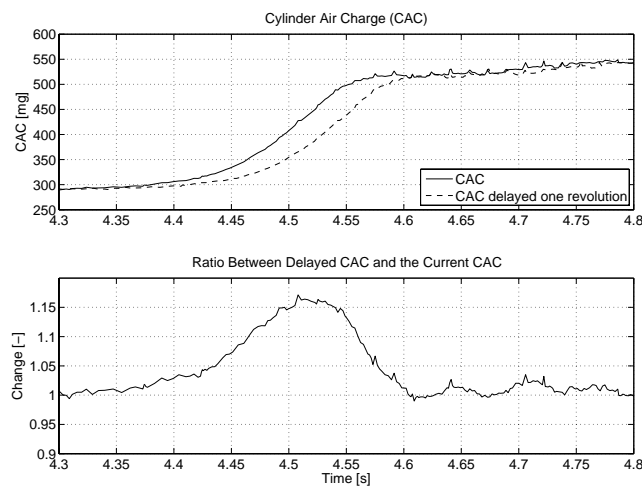
Figure 9.2: A measured step in throttle at constant engine speed 1800 RPM where the port air mass flow (solid) is compared to a translated, corresponding to perfect prediction one revolution ahead, port air-mass flow. The difference between the curves is the resulting error if no prediction is used when the fuel mass is determined and in this case it would result in a 15% error in λ.

Thus for accurate air-fuel ratio control during transients it is necessary to provide the following capabilities: filtering, estimation, and prediction. One solution that provides the desired filtering, prediction and estimation of non-measured signals are observers, which has been successfully used for CAC estimation on naturally aspirated engines (Powell et al., 1998b; Choi and Hedrick, 1998). A good result using a predicting controller is presented in Chevalier
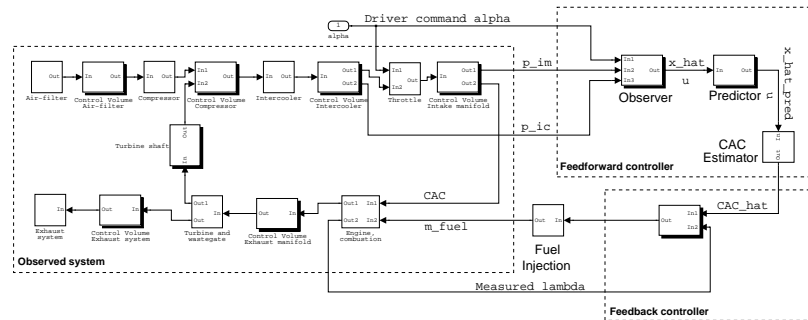
Figure 9.3: An overview of a turbocharged SI-engine where the couplings between the intake and exhaust side are explicitly shown through the connecting shaft and the cylinder air charge (CAC). The observer estimates an initial condition to the predictor which estimates the system state one revolution ahead. The predicted state is used to estimate CAC (feedforward). Measured air-fuel ratio λ is used as feedback to remove stationary errors. In the figure the letters CV means control volume, which represents a volume that connects two components. The control volume have states for pressure and temperature.

et al. (2000) for NA engines. But here turbocharged (TC) engines are considered, which have a more complex air-system where the turbocharger connects the intake side to the exhaust side through the turbine shaft and the CAC has a dependency on the exhaust back-pressure. Therefore, a more sophisticated controller, and observer, is necessary.

For TC-engines, a traditional control structure is suggested, with one feedforward part for transient control and one slower feedback controller. The feedback controller maintains $\lambda = 1$ at stationary conditions using a PI-controller with feedback from a wide-band oxygen-sensor. This chapter focuses on design of the advanced feedforward controller that predicts CAC at intake valve closing. An overview of the controller is shown in Figure 9.3.

9.1   Model of the System Dynamics

A description of the system dynamics is necessary for the feedforward controller to estimate the behavior during rapid transients. Here the system dynamics is described by a mean value engine model of the intake and exhaust system. The modeling methodology of restrictions in series with adiabatic control volumes is applied; see Chapter 6 for a full description of the model.

In the model there are thirteen states and the state derivatives are described by nonlinear functions of states and inputs, see Eq. (9.2). Inputs to the model are: Throttle plate angle α, engine speed N, wastegate opening u_{wg}, normalized air-fuel ratio λ, and ambient conditions (pressure p_a and temperature T_a). Outputs are states and signals that can be derived from the estimated states such as air-mass flows. A summary of the model equations is given in Eq. (9.2).

Please consult Appendix A for more nomenclature details.

$$
\underbrace{\begin{bmatrix}
\dot{p}_{\mathrm{af}} \\
\dot{T}_{\mathrm{af}} \\
\dot{p}_{\mathrm{comp}} \\
\dot{T}_{\mathrm{comp}} \\
\dot{p}_{\mathrm{ic}} \\
\dot{T}_{\mathrm{ic}} \\
\dot{p}_{\mathrm{im}} \\
\dot{T}_{\mathrm{im}} \\
\dot{p}_{\mathrm{em}} \\
\dot{T}_{\mathrm{em}} \\
\dot{p}_{\mathrm{t}} \\
\dot{T}_{\mathrm{t}} \\
\dot{\omega}_{\mathrm{tc}}
\end{bmatrix}}_{\dot{x}}
=
\underbrace{\begin{bmatrix}
f_{p_{\mathrm{af}}}(p_{\mathrm{af}}, T_{\mathrm{af}}, p_{\mathrm{comp}}, \omega_{\mathrm{TC}}, p_{\mathrm{a}}, T_{\mathrm{a}}) \\
f_{T_{\mathrm{af}}}(p_{\mathrm{af}}, T_{\mathrm{af}}, p_{\mathrm{comp}}, \omega_{\mathrm{TC}}, p_{\mathrm{a}}, T_{\mathrm{a}}) \\
f_{p_{\mathrm{comp}}}(p_{\mathrm{af}}, T_{\mathrm{af}}, p_{\mathrm{comp}}, T_{\mathrm{comp}}, p_{\mathrm{ic}}, \omega_{\mathrm{TC}}) \\
f_{T_{\mathrm{comp}}}(p_{\mathrm{af}}, T_{\mathrm{af}}, p_{\mathrm{comp}}, T_{\mathrm{comp}}, p_{\mathrm{ic}}, \omega_{\mathrm{TC}}) \\
f_{p_{\mathrm{ic}}}(p_{\mathrm{comp}}, T_{\mathrm{comp}}, p_{\mathrm{ic}}, T_{\mathrm{ic}}, p_{\mathrm{im}}, \alpha) \\
f_{T_{\mathrm{ic}}}(p_{\mathrm{comp}}, T_{\mathrm{comp}}, p_{\mathrm{ic}}, T_{\mathrm{ic}}, p_{\mathrm{im}}, \alpha) \\
f_{p_{\mathrm{im}}}(p_{\mathrm{ic}}, T_{\mathrm{ic}}, T_{\mathrm{im}}, p_{\mathrm{im}}, p_{\mathrm{em}}, N, \alpha, \lambda) \\
f_{T_{\mathrm{im}}}(p_{\mathrm{ic}}, T_{\mathrm{ic}}, T_{\mathrm{im}}, p_{\mathrm{im}}, p_{\mathrm{em}}, N, \alpha, \lambda) \\
f_{p_{\mathrm{em}}}(p_{\mathrm{im}}, T_{\mathrm{im}}, p_{\mathrm{em}}, T_{\mathrm{em}}, p_{\mathrm{t}}, N, \lambda, u_{\mathrm{wg}}, T_{\mathrm{a}}) \\
f_{T_{\mathrm{em}}}(p_{\mathrm{im}}, T_{\mathrm{im}}, p_{\mathrm{em}}, T_{\mathrm{em}}, p_{\mathrm{t}}, N, \lambda, u_{\mathrm{wg}}, T_{\mathrm{a}}) \\
f_{p_{\mathrm{t}}}(p_{\mathrm{em}}, T_{\mathrm{em}}, p_{\mathrm{t}}, T_{\mathrm{t}}, \omega_{\mathrm{TC}}, u_{\mathrm{wg}}, p_{\mathrm{a}}) \\
f_{T_{\mathrm{t}}}(p_{\mathrm{em}}, T_{\mathrm{em}}, p_{\mathrm{t}}, T_{\mathrm{t}}, \omega_{\mathrm{TC}}, u_{\mathrm{wg}}, p_{\mathrm{a}}) \\
f_{\omega_{\mathrm{TC}}}(p_{\mathrm{af}}, T_{\mathrm{af}}, p_{\mathrm{comp}}, p_{\mathrm{em}}, T_{\mathrm{em}}, p_{\mathrm{t}}, \omega_{\mathrm{TC}})
\end{bmatrix}}_{f(x,u)}
\tag{9.2}
$$

9.2 Air-Fuel Ratio Controller Design

The control objective is to maintain the normalized air-fuel ratio λ close to one. During transients, the challenge is the fast dynamics in the intake manifold requiring prediction of the CAC as shown in Figure 9.2. Here the air-fuel ratio control problem is partitioned into two parts, one feedforward controller to deal with the fast transients and one feedback controller to cancel stationary errors, see Figure 9.3. This division is standard in air-fuel ratio control (Guzzella, 1995; Powell et al., 1998b; Chevalier et al., 2000).

9.2.1 Observer Based Predicting Feedforward Control

The CAC depends on three states: $p_{\mathrm{im}}, T_{\mathrm{im}}$, and p_{em}. For accurate CAC estimation, it is necessary to predict or guess these states approximately one revolution ahead. The prediction is implemented in two steps: First the system state is estimated using an observer. A predictor then estimates the system states given the observed state and an assumption of constant inputs during the prediction. Using the predicted states, the future CAC can be estimated. Thus, the first step is to design the state observer.

State Observer Design

An observer,

$$\dot{\hat{x}} = f\left(\hat{x}, u\right) + K\left(y - g\left(\hat{x}, u\right)\right)$$

with the measured outputs is $y = g\left(x, u\right)$, is developed. As the observer objective is to estimate the current system state $\hat{x}$ it is important to make sure that the system is observable from the selected feedback signals. In Chapter 7 it

Figure 9.4: A Simulink diagram of the implemented state observer.

is shown that the system is locally structurally observable using feedback from arbitrary state(s). Therefore, the selection is based on which sensors that is available. On the engine in the laboratory of Vehicular systems the following sensors are available: Air-mass flow after the air filter, pressure in the intake manifold, pressure before the throttle, and intake manifold temperature. Pressure sensors are preferred for their fast dynamics and the following two sensors are chosen as feedback sources: Pressure after the intercooler p_{ic} and intake manifold pressure p_{im}.

The observer gains are then generated offline using the systematic design method in Chapter 8 and gain switching is then performed online to select a pre-computed K. This means that the online computational power demand is low. The gains were determined in 45 different stationary points for engine speeds between 1200 RPM and 4700 RPM and intake manifold pressures between 40 kPa up to 160 kPa.

In Figure 9.4 a schematic of the implemented state observer is shown. Further, Chapter 8 shows how this observer is able to reduce the noise in the intake manifold pressure, estimate the intake manifold temperature, and estimate the non-measured exhaust manifold pressure. Next, it is described how the estimated states $\hat{x}(t)$ are used in the predictor.

Compression   Expansion   Exhaust   Intake

180 deg   180 deg   180 deg   180 deg

Injection (duration can vary)

CAN transport (fix in time)

Fuel calculation (fix in time)

Figure 9.5: The duration of the injection depends on the inducted cylinder air charge. Prediction is necessary as the injection has to be finished before the induction stroke starts. The required prediction time is the sum of the injection time and the time for the fuel calculation and in this case the transport delay on the CAN-bus.

Predictor Design

Prediction is implemented by simulating the dynamic system $f(x, u)$ using a numerical integration method.

$$\hat{x}(t_{\mathrm{pred}}) = \int_{t_0}^{t_{\mathrm{pred}}} f(x, u(t_0)) \mathrm{d}t$$

This type of problem is referred to an initial value problem (Ascher and Petzold, 1998). To solve initial value problems (IVP), it is necessary to provide a description of the system dynamics and initial values of the states. Here, the system dynamics is described by Eq. (9.2) that also is used for the observer and the initial state values are given by the observer. Also, the simulation requires knowledge of future inputs but here this is replaced by setting the inputs constant to the value at t_0. Next, the prediction end time t_{pred}, integration method, and integration step size are chosen.

First, the prediction horizon t_{pred} has to be selected. It is determined by the sum of the computation time, injection time, and the time of the intake stroke. In the tests performed here the injection time is shorter than half a revolution (between 3 and 12 ms), the intake stroke is half a revolution, and the computation time $\frac{1}{400}$ as the controller is run at 400 Hz. Additionally, in this implementation the computations are performed on an external PC which means that the transfer time over the CAN bus has to added. The PC sends the calculated injection time with 400 Hz and the ECU reads the CAN-bus every $\frac{1}{160}$ seconds. The timing diagram is shown in Figure 9.5 and the total prediction time is:

$$t_{\mathrm{pred}} - t_0 = \frac{1}{2} \frac{60}{N} + \frac{1}{400} + \frac{1}{160} + t_{\mathrm{inj}}$$

In Figure 9.6 the delays in the crank angle domain are shown for the injection, computation, and transmission. As the injection time depends on the inducted CAC which is not known means that the injection time is not known either. One method is to iterate and solve for the prediction time or use a worst case scenario based on the longest possible injection time. Instead a compromise is made by taking a mean value of the minimum delay and maximum delay for the
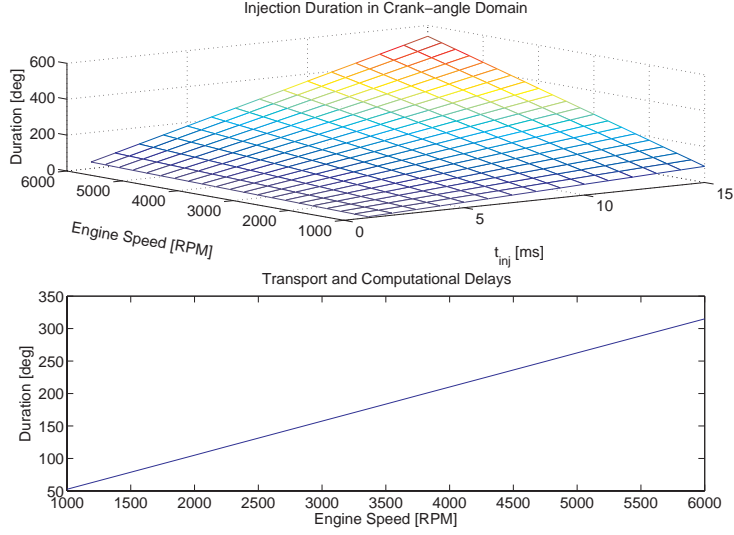
Figure 9.6: Crank angle duration of the injection and the computation and transmission delays. For engine speeds between 1500 and 3000 RPM the sum of the delays are between 90 to 360 degrees.

studied operating regime. For engine speeds between 1500 and 3000 RPM the required prediction time is between 270 and 540 degrees and the mean of those is approximately the time of one revolution. The prediction time is therefore fixed to the time of one revolution. Given the required prediction time, the state at t_{pred} can be determined by simulating $\dot{\hat{x}} = f(\hat{x}, u)$ with the assumption that the input u is constant between t_0 and t_{pred}.

Second, a numerical integration method have to be selected and here an explicit one step method, Runge-Kutta 4 (RK4), was chosen with an integration step size of step size of $\frac{1}{400}$.

Given the predicted states $\hat{x}(t_{\mathrm{pred}})$, the CAC at t_{pred} is estimated:

$$\widehat{\mathrm{CAC}}(t_{\mathrm{pred}}) = \frac{\hat{p}_{\mathrm{im}}(t_{\mathrm{pred}})C_1 V_{\mathrm{d}}\left(r_c - \left(\frac{\hat{p}_{\mathrm{em}}(t_{\mathrm{pred}})}{\hat{p}_{\mathrm{im}}(t_{\mathrm{pred}})}\right)^{\frac{1}{\gamma_e}}\right)}{\left(1 + \frac{1}{\lambda\left(\frac{A}{F}\right)_s}\right)(r_c - 1)R_{\mathrm{im}}\left(\hat{T}_{\mathrm{im}}(t_{\mathrm{pred}}) - C_2\frac{1-\lambda^2}{\lambda^2}\right)}$$

9.2.2 λ-Feedback Control

The purpose of the feedback controller is to compensate for stationary errors and it is implemented as a PI-style controller:

$$e = (\lambda - \lambda_{\mathrm{ref}}) \tag{9.3a}$$

$$y = K_{\mathrm{FB}}(e + \int \frac{1}{T_I} e \, \mathrm{d}t) \tag{9.3b}$$
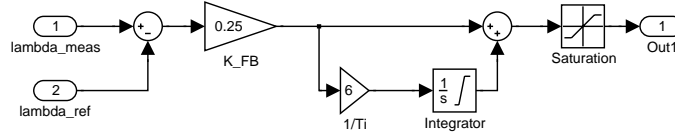
Figure 9.7: Simulink diagram of the implemented feedback controller.

In this case the output y is limited and also the integrator is limited in order to avoid wind-up. The selection of K_{FB} and $\frac{1}{T_I}$ are not crucial and the following values were chosen using step response experiments: $K_{\mathrm{FB}} = 0.25$ and $\frac{1}{T_I} = 6$. Figure 9.7 shows the Simulink implementation, note that the output has been limited to 1 ± 0.5. From Figure 9.3 it can be seen that the output of the controller is multiplicative, which is standard in air-fuel ratio control as most errors are multiplicative.

9.2.3 Total Controller

The combined controller, with $\lambda_{\mathrm{ref}} = 1$, has the following appearance:

$$m_f = \underbrace{\frac{\widehat{\mathrm{CAC}(t_{\mathrm{pred}})}}{\left(\frac{A}{F}\right)_s}}_{\text{Feedforward}} \times \underbrace{K_{\mathrm{FB}}\left((\lambda - 1) + \int \frac{1}{T_I}(\lambda - 1)\mathrm{d}t\right)}_{\text{Feedback}} \qquad (9.4)$$

9.3 Experimental Setup

The suggested controller has been tested in the research laboratory of Vehicular Systems on a 2-liter SAAB turbocharged SI-engine and the experimental setup is shown in Figure 9.8. The engine is controlled by an engine control unit (ECU) that communicates with a personal computer (PC) over a CAN-bus. More details on the laboratory setup are given in Appendix E.

The observer and predictor is run in the PC and Eq. (9.4) is implemented in MathWorks RealTime Workshop using Linux and RTAI 3.2 (Quaranta and Mantegazza, 2001; Rosenquist, 2003). In the PC it is also possible to measure analog signals. Here the PC measures the following signals using analog inputs: throttle angle, intake manifold pressure (Kistler), pressure before the throttle (Kistler), and the air-fuel ratio λ from a wideband sensor (Bosch LSU4). The wastegate position is not measurable and the engine is therefore initially run in conditions were the wastegate is closed. The engine speed is measured over the CAN-bus together with the intake manifold temperature (production sensor). Using the measurements, the PC estimates the system state, predicts the CAC one revolution ahead, runs the feedback controller, and finally sends the desired injection time to the ECU over the CAN-bus. During run-time it is possible to enable/disable the prediction part and the feedback controller.

In the implementation the state observer and feedback controller is run at a step size of $\frac{1}{400}$ and the Simulink solver was set to ode4 (Runge-Kutta).
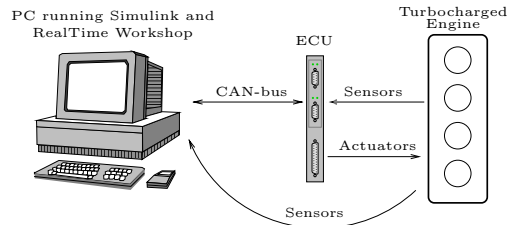
Figure 9.8: The PC is running a realtime operating system (Linux with the RTAI patch) and communicates with the ECU over a CAN-bus. The ECU is responsible for sending sensor readings to the PC and also to inject the determined amount of fuel.

9.4 Experimental Results

The performed experiment is a rapid step in engine load at a constant speed of 2000 RPM. The same step has been repeated using four different controller configurations. In each case the measured air-fuel ratio λ is used to evaluate the controller. Following four test cases have been used:

Experiment 1 *Purpose:* Show the necessity of observer and predictor.
Method: Use a conventional speed-density feedforward controller, Eq. (9.5), and the λ-feedback controller, Eq. (9.3).

Experiment 2 *Purpose:* Show that significant improvements are made by the introduction of the observer.
Method: The observer is run with the predictor step disabled. The λ-feedback enabled.

Experiment 3 *Purpose:* Verify that prediction improves air-fuel ratio.
Method: Run the controller with prediction and λ-feedback enabled.

Experiment 4 *Purpose:* Estimate prediction errors.
Method: Disable λ-feedback but enable the observer and predictor.

In all experiments, the engine has first been warmed up to operating temperature. An advantage of performing the experiments in an engine test cell is the high repeatability of the experiments as shown in Figure 9.9. In the top plot it can be seen that the throttle moves very repeatable and in the center the intake manifold pressure traces have been low pass filtered to show that engine behaves the same in the different experiments. In the bottom plot it is shown that the dynamometer performs the same during the experiments with only a modest overshoot of 60 RPM. The high repeatability of the engine, throttle controller, and dynamometer ensures that differences in measured λ originates from the air-fuel controller.
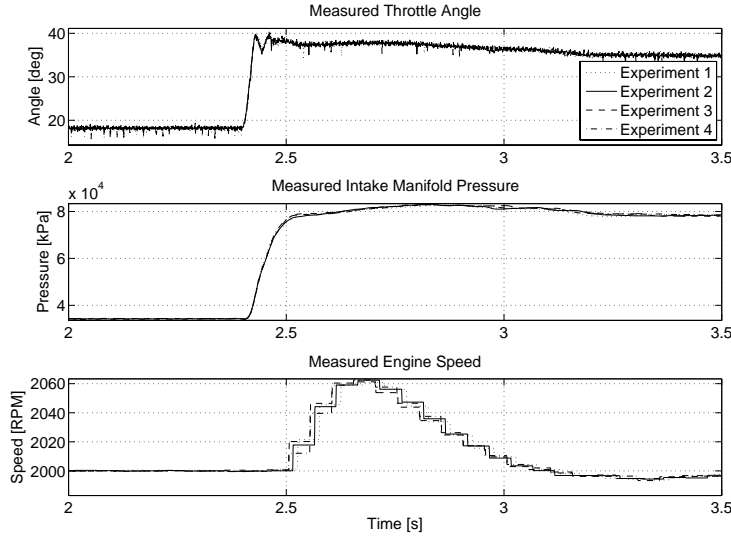
Figure 9.9: Here the high repeatability of the engine test cell is shown. The repeatability is excellent as it is hard to distinguish any differences between the four measurements.

9.4.1 Conventional Speed-density

To compare the proposed feedforward controller a conventional speed-density method is implemented, where the CAC is estimated as:

$$\text{CAC} = \underbrace{(a_0 p_{\text{im}} + a_1)}_{\eta_{\text{vol}} p_{\text{im}}} \frac{V_d}{R_{\text{im}} T_{\text{im}}} \tag{9.5}$$

which is suggested in Hendricks et al. (1996). To reduce noise in the measured intake manifold pressure signal due to engine pumpings, it is low-pass filtered using a fourth order butterworth filter. The cut-off frequency of the filter is chosen in such way that it is able to reduce the pumpings at engine idle. To reduce the pumpings at idle, 800 RPM, the filter has to damp the two pumpings per revolutions which results in a cut off-frequency of $\frac{2 \cdot 800}{60} \approx 25$ Hz.

Using the speed-density controller the resulting λ-excursions are higher than 25%, which can be seen as a dashed line in Figure 9.10. The controller was also tested with the intake manifold pressure low-pass filter disabled, which reduced the error in λ to only 14%. However, the variance of the injection time was 3 times higher and results in unnecessary cycle-to-cycle variations. Further experiments are therefore performed with the low-pass filter enabled.

9.4.2 Observer without Prediction

Here the CAC is estimated from the current state provided by the observer. Using this CAC estimate the dash-dotted line in Figure 9.10 shows the resulting

λ for the throttle transient. Compared to the baseline speed-density method the error is reduced to only 10%, which is even better than the speed-density method with disabled low-pass filter. The remaining error is mainly a result of that the fuel is injected based on a CAC estimate at t=IVO minus the injection time and computation time. λ-excursions during transients are mainly caused by the substantial CAC change between the time of the fuel calculation and intake valve closing, as shown in for example Figure 9.2.

9.4.3   Observer and Prediction

Using the observer a considerable part of the remaining error in λ originates from the lack of prediction. When the prediction step is enabled the transient error in λ almost disappears as the solid line in Figure 9.10 is close to $\lambda = 1$.
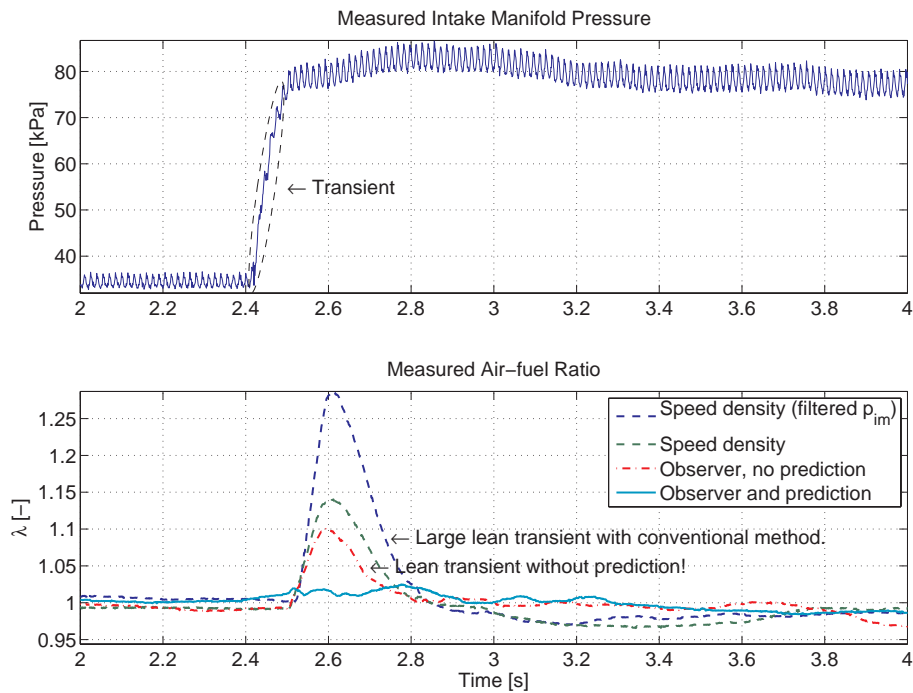
Figure 9.10: *Top*: Intake manifold pressure. *Bottom*: Conventional speed density control, with filtered intake manifold pressure, results in a 27% error. With a disabled low-pass filter the error was still 14%. Using the observer without prediction reduces the error to a 10% lean transient in λ, shown as a dash-dotted line. When the suggested observer is used together with prediction of the CAC one revolution ahead, the error decreases to approximately 3%.

9.4.4 Validation

Above, the controller was been tested at 2000 RPM in one operating point. To validate the controller for a larger operating region, the following tests have been done:

1. Test the same rapid medium load step at 1500 RPM and 3000 RPM. This shows that the controller is able to control the air-fuel ratio accurately at different speeds without modifications.

2. A larger throttle step, where the wastegate opens has also been made for three different speeds: 1500, 2000, and 3000 RPM.

Medium Load Transient at Different Engine Speeds

Here the observer based predicting feedforward controller was run at 1500 RPM and then the speed was doubled to 3000 RPM. The purpose is to test whether it is sufficient to use the fix prediction horizon of one revolution or if a more sophisticated calculation of the prediction horizon is necessary. Figure 9.11 shows the result in λ for both transients. For both engine speeds, the maximum error is limited to 7%. A large portion of this error is related to a stationary model error which is described in Section 9.4.5 and Figure 9.15.

As the controller is able track $\lambda = 1$ using prediction one revolution ahead even when the engine speed is doubled, which changes the required prediction time, shows that the strategy of a fix prediction horizon in the crank angle domain is sufficient. The remaining error in λ shows one similarity between the experiments: At the tip-in there is a lean transient and the cause of this is further investigated in Section 9.4.5.

Large Load Transient at Different Engine Speeds

The controller is now tested for a larger load step at three different engine speeds: 1500, 2000, and 3000 RPM. In this case a rapid load step in intake manifold pressure from 40 kPa up to 120 kPa and here the wastegate will open. Thus, a PI-style wastegate controller is introduced in the observer to determine u_{wg}. The wastegate controller operates in such manner that the pressure after the intercooler is the same as the measured pressure after the intercooler. In Figure 9.12 the implemented controller is shown. The PI-controller parameters were tuned manually.

Figure 9.13 shows the step in intake manifold pressure for the three different engine speeds. Note the step in intake manifold pressure consists of two phases: First a rapid increase up to ambient pressure and then a slower increase while the turbocharger spins up and supplies boost pressure. In the resulting λ-traces, the first transient is mostly pronounced. Here three different controllers were tested, the speed-density, the observer based, and the observer and predictor. Figure 9.14 shows the results of the different controllers. As in the previous tests,
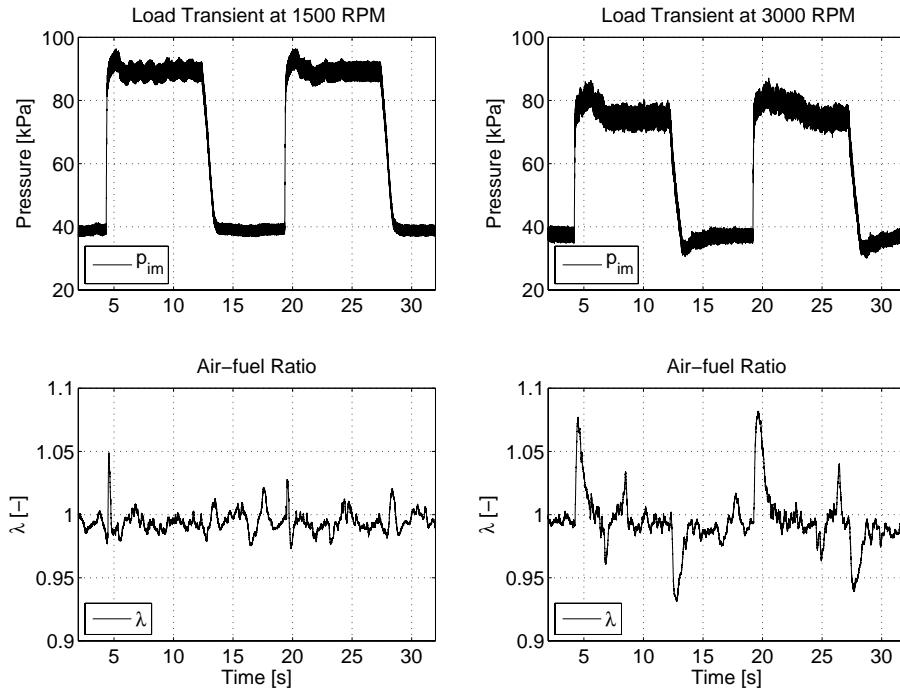
Figure 9.11: Rapid load transients at 1500 RPM and 3000 RPM with the suggested observer based controller. *Top*: Intake manifold pressure. *Bottom*: Measured air-fuel ratio. During transients the resulting errors in λ are less than 7% for both operating points.
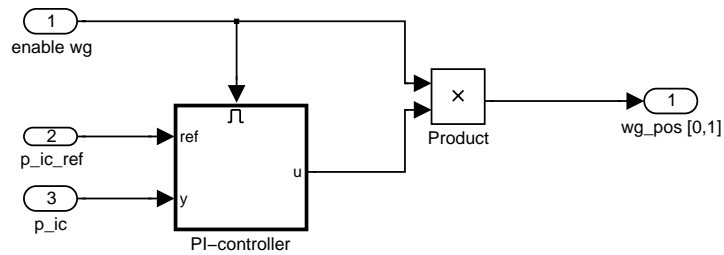
Figure 9.12: The wastegate controller is of a PI-type with $K = 5 \cdot 10^{-5}$ and $\frac{1}{T_I} = 10$. The controller opens the wastegate when the observed pressure after the intercooler is higher than the measured. There is also an on/off functionality to make sure that the wastegate is closed for low boost pressures.
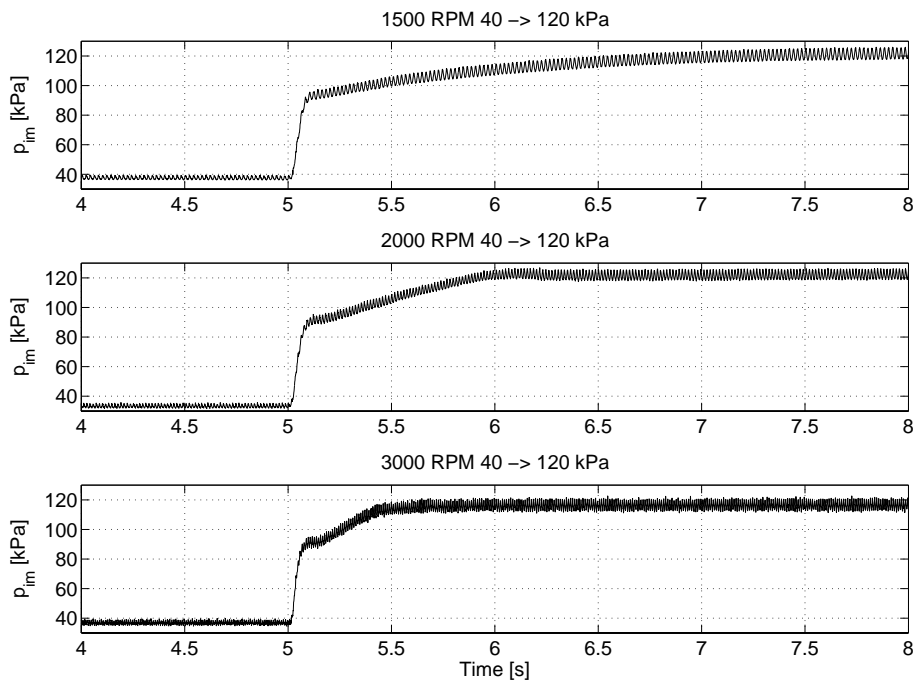
Figure 9.13: A larger load step at constant engine speed. In all cases the transient consists of two parts. First the rapid increase in intake manifold pressure up to ambient which takes approximately 2 to 4 revolutions. It is followed by a slower increase in pressure that depends on the time required for the turbocharger to reach sufficient boost pressure.

most of the reduction of the error in λ originates from the introduction of the observer. When the prediction is added to the observer a further reduction of the maximum error is possible and did not reach more than 6% in the transients..

9.4.5 Remaining Error Sources

There are primarily five sources to the air-fuel ratio error:

- Model errors.

- Prediction is made with the assumption of constant inputs that they are not.

- No fuel dynamics included. However this effect is mostly pronounced at cold engine operation which is not considered here (Fozo and Aquino, 1988).

- The prediction time has a dependency on the injection time, but in the tested load and speed range this effect is small. For higher engine speeds, above 3500 RPM, and high loads this effect is no longer negligible.
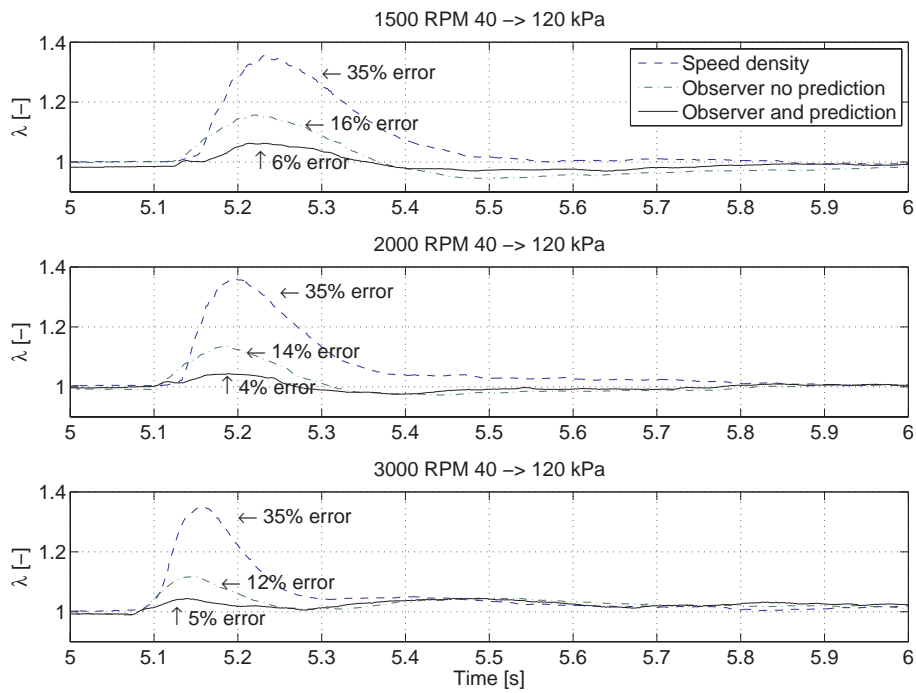
Figure 9.14: Measured λ for three different controllers using a large rapid load transient at three different speeds. The legend shown in the top plot applies to all plots. For all speeds there is a lean transient in λ. As in the previous tests the introduction of the observer is able to reduce the error in λ with 50% compared to pure speed-density CAC estimation. When the predicting step is enabled a further reduction is possible and the maximum error is reduced to 6%.

- The effect of the fuel pressure regulator settling time. Depending on type this can vary between a few milliseconds up to 0.5 second (Hubbard, 2002).

The three first items are discussed next.

Model Errors

As CAC is only measurable for stationary conditions a test of the feedforward component, observer with prediction, was made by disabling the λ-feedback controller. The result is shown in Figure 9.15 and note that regardless of engine speed there is a small lean transient after each tip-in. This transient error can be caused by several phenomenon such as:

- Incorrect volume of the intake manifold.

- The prediction time should vary with the injection time, but here a fix prediction of one revolution is used.

- The throttle angle is not constant during the prediction time.

- There may be unmodeled dynamics such as fuel dynamics.

Another contributing factor to the shape of the transient response in λ is differences in stationary model error between operating points. Figure 9.15 shows the model's stationary description of the cylinder air charge. For the load transients at 1500 RPM and 2000 RPM, the stationary error before and after the transient is only a few percent. Recall that for 3000 RPM there was a larger transient error in λ, see Figure 9.11. This larger transient error is explained by the large difference in stationary model error that is present at 3000 RPM. To compensate for the error in λ, the feedback controller has to integrate the error and this takes time. This integration is clearly visible after each transient in the lower right corner of Figure 9.11.

Unknown Inputs During Prediction

There are mainly two inputs that change during transients: Engine speed and throttle position. In addition, the wastegate setting can change during transients. Normally the engine speed changes slowly which makes the assumption of constant speed during the prediction time valid. In this experiment the engine speed changes less than 3%. The throttle on the other hand moves rapidly during the prediction horizon; in Figure 9.16 the change during the prediction is shown and this rapid change contributes to a portion of the measured error in air-fuel ratio. Without future knowledge of the throttle position, this kind of error is *unavoidable*. Fortunately, the intake manifold acts as a low pass filter and the port-air mass flow is therefore less influenced by the rapid change in throttle area which is seen in the lower right corner of Figure 9.16. One method to reduce the error would be to model the throttle servo and use
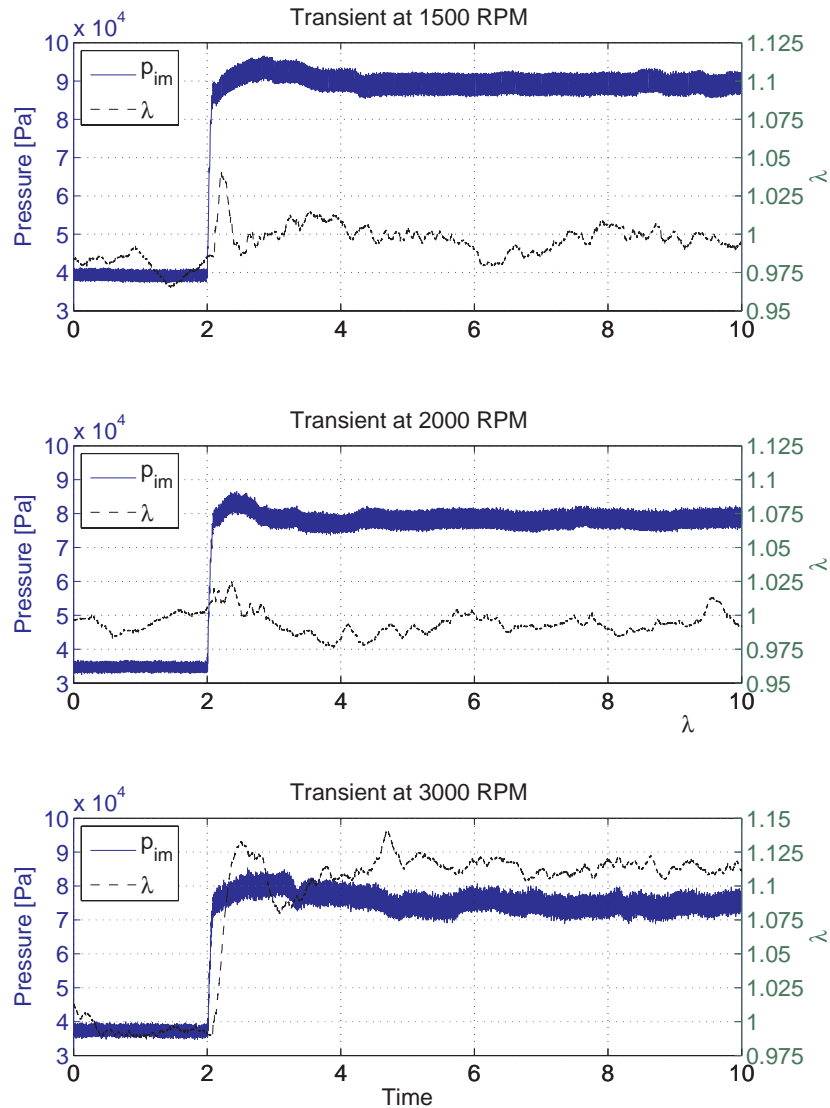
Figure 9.15: Measured data with prediction enabled but with the feedback controller disabled for three different speeds. The accuracy of the model is measured using the difference between λ before the step and λ at the end of the step. The important result here is that the stationary error of the model is small at 1500 and 2000 RPM. For 3000 RPM there is a large difference in stationary, approximately 10%, error before and after the step that have to dealt with by the λ-feedback controller. Finally, note that there is a lean transient after each tip-in.

the requested throttle area as input instead. As no model of the throttle servo was available, this approach has not been implemented. Another approach was applied in Chevalier et al. (2000) where the throttle actuation was delayed in order to know the throttle position in advance. This was not followed here as it introduces an undesirable torque delay.

The expected error in λ from the assumption of a constant throttle area during the prediction is that there would be a lean transient during tip-ins and a rich transient during tip-outs. In Figure 9.11, there are systematic lean transients during tip-ins and small rich transients during the tip-outs. However, these can also be caused by fuel dynamics, which is the next topic.
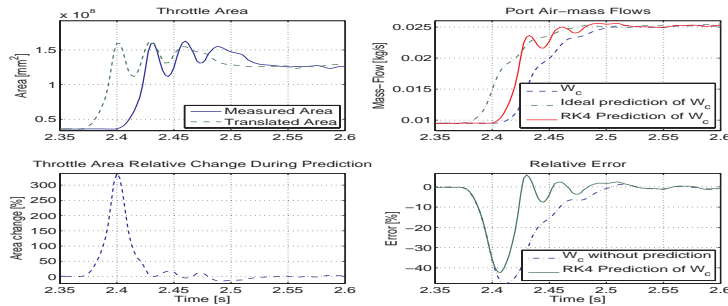
Figure 9.16: The prediction is carried out with the assumption of fix throttle area and the prediction time corresponds to one revolution or 30 ms at 2000 RPM. *Left column:* Here the magnitude of the area change is shown for a tip-in. The constant area assumption results in a short error of up to 300%. *Right column:* Estimated port air-mass flows. The predicted mass-flow using RK4 and the constant area assumption results in a short error of up to 40% which is considerably smaller than the throttle area error!

Fuel Dynamics

Fuel dynamics is related to that not all fuel vaporizes during injection as a fraction of the injected fuel χ_{fp} forms a liquid film on the intake manifold wall. Fuel dynamics is therefore commonly modeled as a "puddle" which mass is modeled using one state m_{fp} and Eq. (9.6). This film evaporates with a time constant of τ_{fp} and then enters the cylinder as vapor together with the fuel that was not deposited in the puddle, Eq. (9.7).

$$\frac{\mathrm{d}m_{\mathrm{fp}}}{\mathrm{d}t} = \chi_{\mathrm{fp}}W_{\mathrm{f_{inj}}} - \frac{1}{\tau_{\mathrm{fp}}}m_{\mathrm{fp}} \tag{9.6}$$

$$W_{\mathrm{fc}} = (1 - \chi_{\mathrm{fp}})W_{\mathrm{f_{inj}}} + \frac{1}{\tau_{\mathrm{fp}}}m_{\mathrm{fp}} \tag{9.7}$$

This phenomena has been studied and for port injected engines in for example Fozo and Aquino (1988) where the effect is most pronounced for cold engines. According to Fozo and Aquino (1988) the effect is around 5% during a slow load

transient and warmed up engine but others claim higher values. An example is shown in Guzzella and Onder (2004, p. 55) where the identified χ_{fp} for a fully warmed up 1.8 dm^3 engine can reach values close to 50% for high loads. The time constant τ_{fp} varies between 0.2 seconds and up to 0.5 seconds according to the same reference for the 1.8 dm^3 engine. Similar values are described in Simons et al. (1998). The parameters are engine dependent and the values shown here is only a guideline.

The effect of fuel dynamics would be a lean transient during the tip-in and a rich transient during the tip-out. In the measured data, there are systematic lean and rich transients at tip-ins and tip-outs respectively *but* this is the same effect that can be expected by the unknown inputs during the prediction. Hence, the effect of fuel dynamics can not be excluded and it is possible that the introduction of fuel dynamics can improve the air-fuel ratio control further.

9.5   Results

TC SI engines have a complex air-system that makes precise air-fuel ratio control a challenging task. Accurate air-fuel ratio control relies on precise cylinder air charge estimates. To estimate the CAC, knowledge is necessary of the intake manifold pressure and temperature together with the exhaust pressure. Especially transient control requires the fast intake manifold dynamics to be taken into account. Therefore an observer based feedforward control structure is proposed.

Two controllers are used, one feedforward and one feedback. The feedback controller cancels stationary errors using feedback from measured λ. The feedforward controller consists of an observer and a predictor that both are based on a mean value engine model. The observer estimates the system state using feedback from measured pressure after the intercooler and intake manifold pressure. The estimated system state is used as an initial condition to the predictor, which then estimates the system state one revolution ahead. Given the predicted system state it is now easy to estimate the CAC. In engine experiments, the deviation from stoichiometric is reduced from almost 30% down to less than 7% over a wide range of engine speeds. Most of the improvement originates from the introduction of a model-based observer.

10

CONCLUSIONS

Turbocharged (TC) spark-ignited (SI) engines are popular as they combine high power output with good fuel economy. In addition, the emissions can be successfully reduced using a three way catalyst (TWC) provided that the air-fuel ratio is precisely controlled. As the air-fuel ratio depends on the precision of the air charge estimate, this thesis is devoted to systematically improve cylinder air charge (CAC) estimation on TC SI engines. The result is a predicting observer based feedforward controller, which shows very good result in engine tests.

In the first part the attention is turned to stationary effects. TC SI engines pose additional challenges for the CAC estimation and these are pointed out in Chapter 3. TC SI engines are equipped with a wastegate that influences the exhaust manifold pressure and as a side effect the cylinder air charge. A new observer that estimates the stationary correct CAC is proposed and evaluated.

The exhaust manifold pressure has a non-negligible effect on the CAC and Chapter 4 focuses on finding a suitable model for CAC estimation that cover the engine's entire operating region. It is concluded, using the resulting model, that the CAC is most sensitive to exhaust manifold pressure changes at part load; a result that is independent of tuned engine parameters. Further, TC SI engines commonly use fuel enrichment at high loads and the additional fuel cools the air charge as it evaporates. A new CAC model that includes exhaust back-pressure and charge cooling is therefore proposed. It reduces the stationary CAC errors from 10% down to only 3% for rich of stoichiometric operating points at high loads. Finally in part 1, Chapter 5 proposes an estimation method for the normally non-measured exhaust manifold pressure, using only sensors on the intake side.

In the second part, the attention is turned to the dynamic behavior of TC SI engines air- and exhaust system. First, a parameterized component based model of the engine's intake system and exhaust system including the turbocharger and wastegate is compiled in Chapter 6. The systematic modeling methodology of control volumes between restrictions was successfully applied. Benefits are that components can be separately identified and it is easy to reuse identical components such as control volumes and various restrictions. This modeling methodology was tested on two different engines where the only modification was the inputs to the parameter tuning method. Using the model, all pressures and temperatures are successfully described including those necessary for CAC estimation.

An observer is then used to improve the state estimates. It compensates for model errors and engine aging as well as address issues such as filtering of the intake manifold pressure and intake manifold temperature estimation. Additionally, the use of an observer enables more information to be extracted from available sensors and it is thus suitable for sensor and actuator diagnosis.

When an observer is designed, it is important that the system is observable from the measured signals. Therefore, an observability analysis is performed in Chapter 7. The result is that the system locally structurally observable from an arbitrary measured state or mass-flow. This result is valid for all TC SI-engine models of the same structure. As the system is observable, the next step is to design the observer. Nonlinearities and the limited computational power of engine control systems make observer design a complex task. Here, a well-known and tested observer design methodology for NA SI-engines is adopted for TC SI engines in Chapter 8: The gain switched extended Kalman filter. In the design process, it is necessary to supply the noise variances of the process and the measurement(s). These noise variances are design parameters and a systematic and automatic method is proposed for determining them. Inputs to the systematic method are an engine map that is extended with measured variance on the signals considered for observer feedback. The resulting observer was tested using measured engine data and was found to estimate the system state well. In addition, examples are shown how it accurately estimates normally non-measured signals such as turbocharger speed using only feedback from two measured pressures on the intake side.

Finally the result of the proposed methodology is evaluated, in Chapter 9, where the CAC model is used together with the designed observer and a model-based predictor to achieve observer based feedforward control of the estimated cylinder air charge. Engine test results show that the air-fuel ratio is controlled to within 7% for very rapid load steps between 1500 RPM and 3000 RPM.

REFERENCES

California's OBD-II regulation. (section 1968.1, Title 13, California Code of Regulations), Resolution 93-40, July 9, 1993.

Per Andersson and Lars Eriksson. Air-to-Cylinder Observer on a Turbocharged SI-Engine with Wastegate. In *Electronic Engine Controls*, SP-1585, pages 33–40. SAE 2001 World Congress, March 2001, Detroit, MI, USA, March 2001. SAE Technical Paper No. 2001-01-0262.

Per Andersson and Lars Eriksson. Detection of Exhaust Manifold Leaks on a Turbocharged SI-engine with Wastegate. In *Electronic Engine Controls*, SP-1704, 2002. SAE Technical Paper No. 2002-01-0844.

Per Andersson and Lars Eriksson. Cylinder Air Charge Estimator in Turbocharged SI-Engines. Society of Automotive Engineers, 2004. SAE Technical Paper No. 2004-01-1366.

C. F. Aquino. Transient A/F Control Characteristics of the 5 Litre Central Fuel Injection System. SP-487, 1981. SAE Technical Paper No. 810494.

I. Arsie, F. De Franceschi, C. Pianese, and G. Rizzo. O.D.E.C.S. - A Computer Code for the Optimal Design of S.I. Engine Control Strategie. SP-1168, pages 195–207, 1996. SAE Technical Paper No. 960359.

U.M Ascher and L.R Petzold. *Computer Methods for Ordinary Differential Equations and Differential-Algebraic Equations.* siam, 1998. ISBN 0-89871-412-5.

Theophil Auckenthaler. *Modelling and Control of Three-Way Catalytic Converters*. PhD thesis, SWISS FEDERAL INSTITUTE OF TECHNOLOGY ZURICH, 2003.

Theophil S. Auckenthaler, Christopher H. Onder, and Hans P. Geering. Modelling of a Solid-Electrolyte Oxygen Sensor. 2002. SAE Technical Paper No. 2002-01-1293.

Mario Balenovic, Jerome Edwards, and Ton Backx. Vehicle Application of Model-Based Catalyst Control. In *Proceedings Preprints IFAC Symposium on Advances in Automotive Control*, pages 351–356, 2004.

Horst Bauer, Arne Cypra, Anton Beer, and Hans Bauer, editors. *Bosch Automotive Handbook*. Robert Bosch Gmbh, 4 edition, 1996.

Johan Bergström and Jan Brugård. Modeling of a turbo charged spark ignited engine. Master's thesis, Linköping, 1999. URL `http://www.fs.isy.liu.se/Publications/`. LiTH-ISY-EX-2081.

Gordon P. Blair. *DESIGN and SIMULATION of FOUR-STROKE ENGINES*. SAE International, 1999. ISBN 0-7680-0440-3.

Robert Bos, Xavier Bobois, and Paul M. J. Van den Hof. Designing a kalman filter when no noise covariance information is present. Prague, 2005. IFAC World Congress.

Robert Bouza and Jon Caserta. Effects of Injection Timing on Exhaust Emissions of a Fuel Injected Spark Ignition Engine. Technical report, Dept. of Mechanical Engineering, University of Michigan-Dearborn, 2003.

Erich P. Brandt, Yanying Wang, and Jessy W. Grizzle. Dynamic Modeling of a Three-Way Catalyst for SI Engine Exhaust Emission Control. *IEEE Transactions on Control Systems Technology*, 8(5):767–776, September 2000.

Yunus A. Cengel. *Heat Transfer – A Practical Approach*. McGraw-Hill, second edition, 2003. ISBN 0-07-115150-8.

Chen-Fang Chang, Nicholas P. Fekete, and J. David Powell. Engine Air-Fuel Ratio Control Using an Event-Based Observer. 1993. SAE Technical Paper No. 930766.

Alain Chevalier and Martin Müller. On the Validity of Mean Value Engine Models During Transient Operation. In *Modeling of SI Engines*, SP-1511, 2000. SAE Technical Paper No. 2000-01-1261.

Alain Chevalier, Christian Winge Vigild, and Elbert Hendricks. Predicting the Port Air Mass Flow of SI engines in Air/Fuel Ratio Control Applications. In *Electronic Engine Controls*, SP-1500, 2000. SAE Technical Paper No. 2000-01-0260.

Yuen-Kwon Chin and Francis E. Coats. Engine dynamics: Time-based versus crank-angle based. SP-653, 1986. SAE Technical Paper No. 860412.

Y. Cho, C. Kim, D. Kim, J. Lee, S. Lee, K. Myung, and J. Choo. Prediction of Exhaust Gas Temperature at the Inlet of an Underbody Catalytic Converter During FTP-75 Test. 1997. SAE Technical Paper No. 972913.

Seibum B. Choi and J. Karl Hedrick. An Observer-Based Controller Design Method for Improving Air/Fuel Characteristics of Spark Ignition Engines. *IEEE Transactions on Control Systems Technology*, 8(3):325–334, May 1998.

C Lyle Cummins, Jr. *Internal Fire*. dba Carnot Press, third edition, 2000. ISBN 0-917308-05-0.

S. L. Dixion. *Fluid Mechanics and Thermodynamics of Turbomachinery*. Butterworth-Heinemann, 4 edition, 1998.

I. Ekroth and E. Granryd. *Tillämpad termodynamik*. KTH, 1991.

Lars Eriksson. Mean value models for exhaust system temperatures. In *Modeling of SI engines*, SP-1702, 2002. SAE Technical Paper No. 2002-01-0374.

Lars Eriksson, Lars Nielsen, Jan Brugård, Johan Bergström, Fredrik Pettersson, and Per Andersson. Modeling of a Turbocharged Spark Ignited Engine with Waste Gate. In *IFAC Workshop - Advances in Automotive Control; Karlsruhe, Germany*, pages 379–388, March 2001.

Lars Eriksson, Simon Frei, Christopher Onder, and Lino Guzzella. Control and Optimization of Turbo Charged Spark Ignited Engines. IFAC world congress, Barcelona, Spain, 2002a.

Lars Eriksson, Lars Nielsen, Jan Brugård, Johan Bergström, Fredrik Pettersson, and Per Andersson. Modeling of a Turbocharged SI Engine. *Annual Reviews in Control*, 26(1):129–137, October 2002b.

N.P Fekete, U. Nester, I. Gruden, and J.D. Powell. Model-based air-fuel ratio control of a lean multi-cylinder engine. 1995. SAE Technical Paper No. 950846.

Michael Fons, Martin Muller, Alain Chevalier, Christian Vigild, Elbert Hedricks, and Spencer C. Sorenson. Mean Value Modelling of an SI Engine with EGR. In *SI Engine Modeling*, SP-1451, pages 323–330, 1999. SAE Technical Paper No. 1999-01-0909.

Jonathan W. Fox, Wai K. Cheng, and John B. Heywood. A Model for Predicting Residual Gas Fraction in Spark-Ignition Engines. 1993. SAE Technical Paper No. 931025.

S. Robert Fozo and Charles F. Aquino. Transient A/F Characteristics for Cold Operation of a 1.6 Liter Engine With Sequential Fuel Injection. 1988. SAE Technical Paper No. 880691.

Simon Frei. *Performance and Driveability Optimization of Turbocharged Engine Systems*. PhD thesis, Swiss Federal Institute Of Technology Zurich, 2005.

Simon Frei and Lars Eriksson. Modelling of a Turbocharged SI Engine. Technical Report Mot 4–01, Measurement and Control Laboratory, ETH, IMRT, October 2001.

J.W. Grizzle, J.A. Cook, and W.P. Milam. Improved Cylinder Air Charge Estimation for Transient Fuel Ratio Control. In *Proceedings of the American Control Conference*, pages 1568–1573, Baltimore, June 1994.

L. Guzzella, U. Wenger, and R. Martin. IC-Engine Downsizing and Pressure-Wave Supercharging for Fuel Economy. 2000. SAE Technical Paper No. 2000-01-1019.

Lino Guzzella. Models and Modelbased Control of IC-Engines – A Nonlinear Approach. 1995. SAE Technical Paper No. 950844.

Lino Guzzella and Alois Amstutz. Control of diesel engines. *IEEE Control Systems*, pages 53–71, October 1998.

Lino Guzzella and Christopher Onder. *Introduction to Modeling and Control of Internal Combustion Engine Systems*. Springer-Verlag, 2004.

Martin Hart, Michael Ziegler, and Otmar Loffeld. Adaptive Estimation of Cylinder Air Mass Using the Combustion Pressure. In *Electronic Engine Controls*, pages 117–122, 1998. SAE Technical Paper No. 980791.

Heinz Heisler. *Advanced engine technology*. Arnold, Hodder Headline Group, 1997.

E. Hendricks and S. C. Sorensen. Mean Value Modelling of Spark Ignition Engines. 1990. SAE Technical Paper No. 900616.

E. Hendricks, T. Vesterholm, and S. C. Sorensen. Nonlinear, Closed Loop, SI Engine Control Observers. 1992. SAE Technical Paper No. 920237.

Elbert Hendricks, Micahel Jensen, Alain Chevalier, and Thomas Vesterholm. Conventional event based engine control. SP-1029, 1994. SAE Technical Paper No. 940377.

Elbert Hendricks, Alain Chevalier, Michael Jensen, and Spencer C. Sorenson. Modelling of the Intake Manifold Filling Dynamics. 1996. SAE Technical Paper No. 960037.

Tomas Henriksson and Lars Nielsen. Modeling effects due to varying command signal timing. In *IFAC Workshop – Advances in Automotive Control (Preprints)*, 1998.

John B. Heywood. *Internal Combustion Engine Fundamentals*. McGraw-Hill International Editions, 1988.

J. P. Holman. *Heat Transfer*. McGraw-Hill, seventh edition edition, 1992. ISBN 0-07-112644-9.

Mont Hubbard. Effects of Diaphragm Compliance on Spring-Diaphragm Pressure Regulator Dynamics. *Journal of Dynamic Systems, Measurement, and Control*, 124:290–296, 2002.

Mrdjan Jankovic and Steve W. Magner. Air-charge estimation and prediction in spark ignition internal combustion engines. In *Proceedings of the American Control Conference*, pages 217–221, San Diego, California, June 1999.

J.P. Jensen, Kristensen A.F, S.C Sorenson, N. Houbak, and E. Hendricks. Mean Value Modeling of a Small Turbocharged Diesel Engine. 1991. SAE Technical Paper No. 910070.

Per B. Jensen, Mads B. Olsen, Jannik Poulsen, Elbert Hendricks, Michael Fons, and Christian Jepsen. A New Family of Nonlinear Observers for SI Engine Air/Fuel Ratio Control. In *Electronic Engine Controls*, SP-1236, pages 91–101, 1997. SAE Technical Paper No. 970615.

James C. Peyton Jones. Modeling Combined Catalyst Oxygen Storage and Reversible Deactivation for Improved Emissions Prediction. 2003. SAE Technical Paper No. 2003-01-0999.

James C. Peyton Jones, Richard A. Jackson, J. Brian Roberts, and Pierre Bernard. A simplified model for the dynamics of a three-way catalytic converter. In *Exhaust Aftertreatment Modeling and Gasoline Direct Injection Aftertreatment*, SP-1533, 2000. SAE Technical Paper No. 2000-01-0652.

Thomas Kailath. *Linear Systems*. Prentice-Hall, 1980. ISBN 0-13-536961-4.

Uwe Kiencke and Lars Nielsen. *Automotive Control Systems. For Engine, Driveline, and Vehicle*. Springer-Verlag, 2000. ISBN 3-540-66922-1.

Allan J. Kotwick and John D. Russell. An algorithm to compensate for air charge prediction errors. In *Electronic Engine Controls 2000*, SP-1500, 2000. SAE Technical Paper No. 2000-01-258.

Allan J. Kotwick, John D. Russell, Ross Pursifull, and Don Lewis. An air meter based cylinder air charge estimator. In *Electronic Engine Controls 1999*, SP-1419, pages 81–90, 1999. SAE Technical Paper No. 1999-01-0856.

Pressure Transmitter 42xxA. . . -43xxA. . . . Kristall Instrumente AG, a 4.10e edition, 7 1997. Product specification.

Mattias Krysander. Luftflödet förbi en trottel. Master's thesis, Linköping University, SE-581 83 Linköping, 2000. URL `http://www.fs.isy.liu.se/Publications/`.

W. S. Levine, editor. *The Control Handbook*. CRC Press and IEEE Press, 1996. ISBN 0-8493-8570-9.

Ching-Tai Lin. Structural controllability. *IEEE Transactions on Automatic Control*, 19(3):201–208, June 1974.

Marzio Locatelli, Ezio Alfieri, Christopher H. Onder, and Hans P. Geering. Identification of the Relevant Parameters of the Wall-Wetting System by Extended Kalman Filtering. In *Proceedings Preprints IFAC Symposium on Advances in Automotive Control*, pages 326–331, 2004.

Peter J. Maloney and Peter M. Olin. Pneumatic and Thermal State Estimators for Production Engine Control and Diagnostics. In *Diagnostics and Control*, SP-1357, pages 53–64, 1998. SAE Technical Paper No. 980517.

Kouji Miyamoto, Hiroyouki Takebayashi, Takahisa Ishihara, Hiroyuki Kido, and Koichi Hatamura. Measurement of Oxygen Storage Capacity of Three Way Catalyst and Optimization of a/f Perturbation Control to Its Characteristics. In *Emissions Modeling and General Emissions*, SP-1676, 2002. SAE Technical Paper No. 2002-01-1094.

Michael Mladek. *Cylinder pressure for control purposes of spark ignition engines*. PhD thesis, ETH Zürich, 2003.

J.R. Mondt. *Cleaner Cars. The History and Technoloby of Emission Control Since the 1960s*. SAE International, 2000. ISBN 0-7680-0222-2.

Paul Moraal and Ilya Kolmanovsky. Turbocharger Modeling for Automotive Control Applications. In *SI Engine Modeling*, SP-1451, pages 309–322, SAE 1999 World Congress, Detroit, MI, USA, March 1999. SAE Technical Paper No. 1999-01-0908.

Martin Müller, Elbert Hendricks, and Spencer C. Sorenson. Mean Value Modelling of Turbocharged Spark Ignition Engines. In *Modeling of SI and Diesel Engines*, SP-1330, 1998. SAE Technical Paper No. 980784.

Mattias Nyberg. Model Based Diagnosis of Both Sensor-Faults and Leakage in the Air-Intake System of an SI-engine. 1999. SAE Technical Paper No. 1999-01-0860.

Mattias Nyberg and Lars Nielsen. Model Based Diagnosis for the Air Intake System of the SI-engine. 1997. SAE Technical Paper No. 970209.

Christopher Onder, Michael Simons, and Hans P. Geering. Wall-wetting parameters over the operating region of a sequential fuel-injected si engine. 1998. SAE Technical Paper No. 980792.

Christopher H. Onder and Hans P. Geering. Model-Based Multivariable Speed and Air-to-Fuel Ratio Control of an SI Engine. In *Electronic Engine Controls*, volume SP-955, pages 69–80, 1993. SAE Technical Paper No. 930859.

Christopher H. Onder, Christian A. Roduner, and Hans P. Geering. Model Idenfication for the A/F Path of an SI Engine. In *Electronic Engine Controls SP-1236*, number 970612. Society of Automtive Engineers, 1997.

Fredrik Pettersson. Simulation of a Turbo Charged Spark Ignited Engine. Master's thesis, Linköping University, SE-581 83 Linköping, 2000. URL `http://www.fs.isy.liu.se/Publications/`.

J. David Powell. Engine Control Using Cylinder Pressure: Past, Present, and Future. *Journal of Dynamic Systems, Measurements, and Control*, 115:343–350, June 1993.

J. David Powell, N. P. Fekete, and Chen-Fang Chang. Observer-Based Air-Fuel Ratio Control. *IEEE Control Systems*, 1998a. 0272-1708/98.

J. David Powell, N.P Fekete, and Chen-Fang Chang. Observer-based air-fuel control. *Control Systems Magazine*, vol. 18(no. 5):pages 72–83, October 1998b.

Ross Pursifull, Allan J. Kotwick, and Sulgi Kong. Throttle Flow Characterization. In *Modeling of SI Engines*, SP-1511, pages 149–161, 2000. SAE Technical Paper No. 2000-01-0571.

G. Quaranta and P. Mantegazza. Using MATLAB-Simulink RTW to Build Real Time Control Applications in User Space with RTAI-LXRT. Milano, 2001. Realtime Linux Workshop.

Christer Rosenquist. Hard realtime rapid prototyping development platform. Master's thesis, Linköpings Universitet, SE-581 83 Linköping, 2003. LiTH-ISY-EX-3377-2003.

Michael G. Safanov and Michael Athans. Robustness and computational aspects of nonlinear stochastic estimators and regulators. *IEEE Transactions on Automatic Control*, AC-23(4):717–725, August 1978.

Hamid B. Servati and Robert G. DeLosh. A Regression Model for Volumetric Efficiency. 1986. SAE Technical Paper No. 860328.

R.W. Shields and J.B. Pearson. Structural Controllability of Multiinput Linear Systems. *IEEE Transactions on Automatic Control*, 21(2):203–212, 1976.

Yaojung Shio and John J. Moskwa. Model-based cylinder-by-cylinder air-fuel ratio control for SI engines using sliding observers. In *Proceedings of the 1996 IEEE International Conference on Control Applications*, pages 347–354, Dearborne, MI, September 1996.

Michael R. Simons, Esfandiar Shafai, and Hans P. Geering. On-line Identification Scheme for Various Wall-Wetting Models. In *Electronic Engine Controls*, pages 133–140, 1998. SAE Technical Paper No. 980793.

L A Smith, T Fickenscher, and R P Osborne. Engine Breathing – Steady Speed Volumetric Efficiency and its Validity Under Transient Engine Operation. 1999. SAE Technical Paper No. 1999-01-0212.

Patric Soltic. *Part-Load Optimized SI Engine Systems*. PhD thesis, Swiss Federal Institute of Technology Zürich, 2000.

Charles Fayette Taylor. *The Internal-Combustion Engine in Theory and Practice*, volume 1. The M.I.T. Press, 2 edition, 1994.

William J. Terrell. Local Observability of Nonlinear Differential-Algebraic Equations (DAEs) From the Linearization Along a Trajectory. *IEEE Transactions on Automatic Control*, 46(12), 2001.

Tung-Cing Tseng and Wai K. Cheng. An adaptive air/fuel ratio controller for SI engine throttle transients. In *Electronic Engine Controls 1999 (SP-1419)*, pages 37–48, 1999. SAE Technical Paper No. 1999-01-0552.

N. Watson and M.S. Janota. *Turbocharging the Internal Combustion Engine*. The Macmillan Press Ltd, 1982. ISBN 0-333-24290-4.

Robert W. Weeks and John J. Moskwa. Transient Air Flow Rate Estimations in a Natural Gas Engine Using a Nonlinear Observer. 1994. SAE Technical Paper No. 940759.

Nicholas Wickström and Stefan Byttner. Robust Tuning of Individual Cylinders AFR in SI Engines with the Ion Current. In *Electronic Engine Controls 2005*, SP-1975, 2005. SAE Technical Paper No. 2005-01-0020.

Yuji Yasui, Shusuke Akazaki, Masaki Uenzo, and Yoshihisa Iwaki. Secondary O_2 Feedback Using Prediction and Identification Type Sliding Mode Control. In *Electronic Engine Controls*, SP-1501, pages 169–178, 2000. SAE Technical Paper No. 2000-01-0936.

A

NOMENCLATURE

A variable specifying the type (presser, temperature, etc.) and subscript are used to describe the location. Example: p_{af} refers to the pressure after the air-filter.

Variable	Symbol
Pressure	p
Temperature	T
Mass-flow	W
Efficiency	η
Pressure ratio	Π
Angle	α
Torque	Tq
Diameter	D
Volume	V
MAss	m

Subscripts are used in the following way to indicate the location of the described variable:

Location	Subscript
Ambient or air	a
Exhaust gas	eg
Air-filter	af
Compressor	comp
Intercooler	ic
Intake manifold	im
Cylinder	cyl
Exhaust manifold	em
Turbine	t
Wastegate	wg
Crank shaft	cs
Displacement	d
Before	before
After	after

All pressures are assumed to be static pressures and all temperatures are assumed to be stagnation temperatures as this is the output of the sensors used (Ekroth and Granryd, 1991).

Other symbols used are:

Symbol	Description
$A(\alpha)$	Throttle area
$A_{\mathrm{eff}}(\alpha)$	A fitted function to the measured product of area and discharge coefficient
$\left(\frac{A}{F}\right)_s$	Stoichiometric air/fuel ratio
$C_d(\alpha)$	Discharge coefficient for the throttle
c_v	Specific heat at constant volume
k_1	Constant in polynomial for nominal exhaust manifold pressure
k_2	Constant in polynomial for nominal exhaust manifold pressure
k	Scaling factor to calculate air and fuel mass given air mass, $k = 1 + \frac{1}{\lambda\left(\frac{A}{F}\right)_s}$
K_e	Constant in equation for exhaust manifold pressure difference
K_{im}	Filling/emptying constant $K_{\mathrm{im}} = \frac{R_{\mathrm{im}} T_{\mathrm{im}}}{V_{\mathrm{im}}}$ for the intake manifold
K_{inj}	Maximum delivered fuel mass per second
K_{obs}	Feed-back gain from pressure estimation error in observer using proportional feed-back to the $\hat{p}_{\mathrm{im}}$ state
K_1	Feed-back gain from pressure estimation error in the 2-state observer to the $\hat{p}_{\mathrm{im}}$ state
K_2	Feed-back gain from pressure estimation error in the 2-state observer to the $\widehat{\Delta\mathrm{CAC}}$ state

	continued from previous page
Symbol	**Description**
L_1	Time constant in (Tseng and Cheng, 1999)
$\mathcal{M}$	Molar mass
$\mathcal{M}_a$	Molar mass of air
$\mathcal{M}_f$	Molar mass of fuel
CAC	Mass of air the cylinder
m_f	Mass of fuel the cylinder
m_r	Residual gas mass
ΔCAC	In-cylinder air-mass offset
$\widehat{\Delta\text{CAC}}$	Estimated in-cylinder air-mass offset
n_r	Number of revolutions per cycle
N	Engine speed i revolutions per second or revolutions per minute.
$\tilde{R}$	Gas constant, 8.31 $[\frac{J}{\text{mole}\cdot K}]$
$p_{\text{em}_{\text{nom}}}$	Nominal exhaust manifold pressure
p_{em_Δ}	Exhaust manifold pressure difference from nominal pressure
$\overline{p_{\text{em}_\Delta}}$	Mean of exhaust manifold pressure difference from nominal pressure
$\hat{p}_{\text{im}}$	Estimated intake manifold pressure
r_c	Compression ratio of the engine
R_c	Specific in cylinder gas constant at intake valve closing
R_{im}	Specific gas constant in the intake manifold
T_1	Temperature of charge (air, fuel, and residual gases) at start of compression
T_r	Temperature of residual gases
t_0	Time in seconds for the injector needle lift or start of prediction time
t_{inj}	Time in seconds where the injector is open
V_c	Clearance volume
V_r	Volume of residual gases
W_a	Measured air-mass-flow
W_{cyl}	Air-mass-flow to cylinder
$W_{\text{cyl}_{\text{std}}}$	Air mass flow to cylinder using mapped volumetric efficiency
$W_{\text{cyl}_{\text{ts}}}$	Air mass flow to cylinder using mapped volumetric efficiency with estimated offset $\Delta\eta_{\text{vol}}$
x_r	Residual gas fraction
α	Throttle angle
γ	Ratio of specific heats $\frac{c_p}{c_v}$
η_{vol}	Volumetric efficiency
$\Delta\eta_{\text{vol}}$	Offset in volumetric efficiency
$\Delta\hat{\eta}_{\text{vol}}$	Estimated offset in volumetric efficiency

continued from previous page	
Symbol	**Description**
λ	Normalized air/fuel ratio $\frac{m_a}{m_f\left(\frac{A}{F}\right)_s}$
σ_v	Standard deviaion of noise
$\left(\frac{A}{F}\right)_s$	Stoichiometric air/fuel ratio = 14.5
mps	Mean piston speed
BMEP	Brake mean effective pressure
PMEP	Pump mean effective pressure
FMEP	Friction mean effective pressure

DEFINITION OF AIR-FUEL RATIO

Air-fuel ratio is the composition, on mass basis, of air and fuel in the cylinder when the intake valve has closed. Denote the mass of air by m_a, the mass of fuel by m_f, and the air-fuel ratio is then $\frac{m_a}{m_f}$. In most cases the normalized air-fuel ratio is used, that is the air-fuel ratio divided by the stoichiometric ratio. The stoichiometric air-fuel ratio $\left(\frac{A}{F}\right)_s$ describes the ratio of air and fuel, on mass basis, where it is just enough air to fully oxidize the fuel. A typical stoichiometric reaction of air and a fuel is shown below.

$$\underbrace{\underbrace{C_aH_bO_c}_{\text{Fuel}} + \underbrace{\left(a + \frac{b}{4} - \frac{c}{2}\right)(O_2 + 3.77N_2)}_{\text{Air}}}_{\text{Reactants}} \longrightarrow$$

$$\underbrace{aCO_2 + \frac{b}{2}H_2O + \left(a + \frac{b}{4} - \frac{c}{2}\right)3.77N_2}_{\text{Products}}$$
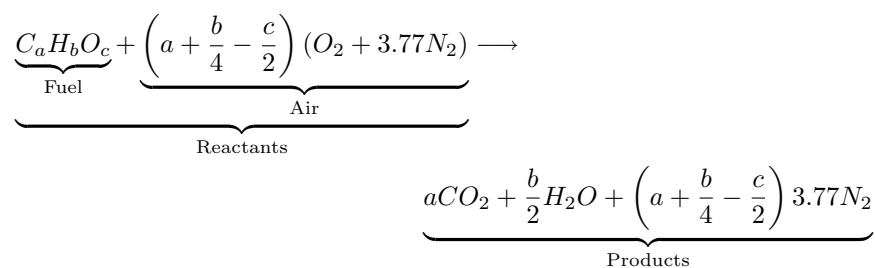
Now the stoichiometric air-fuel ratio is defined as

$$\left(\frac{A}{F}\right)_s = \frac{\left(a + \frac{b}{4} - \frac{c}{2}\right)\mathcal{M}_{air}}{\mathcal{M}_{fuel}} \approx \frac{\left(a + \frac{b}{4} - \frac{c}{2}\right)(32 + 3.77 \cdot 28)}{12a + b + 16c}$$

For isooctane C_8H_{18} this evaluates to $\left(\frac{A}{F}\right)_s \approx 15.1$ and for commercial gasoline the value of 14.7 is commonly used. In the following text the air-fuel ratio is

used as a synonymous to the normalized air-fuel ratio λ

$$\lambda = \frac{m_a}{m_f \left(\frac{A}{F}\right)_s}$$

Two other common definitions are lean and rich mixture. For lean mixtures there are excess air, $\lambda > 1$, and in rich mixtures there are more fuel than the available air can oxidize, $\lambda < 1$. At stoichiometric conditions the normalized air-fuel ratio λ is one.

Derivation of p_{EM} Dependent CAC Model

Instead of using energy balance as in (Taylor, 1994, pp. 510), which lacks parameters that can be tuned for a specific engine, the volume of inducted air V_{a} is estimated (Eriksson et al., 2002a) and the CAC is hence:

$$\text{CAC} = \frac{p_{\text{im}} V_{\text{a}}}{R_{\text{im}} T_{\text{im}}} \tag{C.1}$$

Using the fact that the ideal gas law can be expressed like

$$V = \frac{nRT}{p} = (n_1 + \cdots + n_n)\frac{RT}{p}$$

$$(V_1 + \cdots + V_n) = (n_1 + \cdots + n_n)\frac{RT}{p}$$

$$V_i = n_i \frac{RT}{p} \quad 1 \leq i \leq n$$

This results in that the gases in the cylinder can be divided into volumes of air, fuel, and residual gases, which is illustrated to the right of Figure 4.8.

The volume of air V_{a} and evaporated fuel V_{f} is simply estimated by subtracting the volume that the residual gases occupies at intake valve closing (IVC) from the total volume.

$$\underbrace{V_{\text{a}} + V_{\text{f}}}_{\text{Volume of air and fuel}} = \underbrace{V_{\text{d}} + V_{\text{c}}}_{\text{Total cylinder volume}} -V_{\text{r}}$$

Residual gas volume at IVC is estimated by isentropic expansion of the residual gases from the conditions at exhaust valve closing (EVC). That is they expand

from volume V_{c} which gases occupies at exhaust manifold pressure p_{em} to the volume V_{r} which they occupy at IVC and intake manifold pressure p_{im}:

$$V_{\mathrm{r}} = \left(\frac{p_{\mathrm{em}}}{p_{\mathrm{im}}}\right)^{\frac{1}{\gamma}} V_{\mathrm{c}}$$

Here the residual gas volume at EVC is assumed to be constant and equal to the clearance volume V_{c}. This is reasonable as the engine is not equipped with any cam phasing device and also by the fact that volumes change only slightly around TDC. The remaining volume, after the expansion of the residual gases to intake manifold pressure, is then compensated for the volume of the fuel vapor (all fuel is assumed to enter the cylinder as vapor). The volume of inducted air is then V_a:

$$V_{\mathrm{af}} = \left(\frac{r_c - \left(\frac{p_{\mathrm{em}}}{p_{\mathrm{im}}}\right)^{\frac{1}{\gamma}}}{r_c - 1}\right) V_{\mathrm{d}}$$

$$V_{\mathrm{a}} = \frac{1}{1 + \frac{1}{\lambda\left(\frac{A}{F}\right)_s}} V_{\mathrm{af}}$$

In the Equations above the following identities have been used: $V_{\mathrm{d}} + V_{\mathrm{c}} = r_c V_{\mathrm{c}}$ and $V_{\mathrm{c}} = \frac{V_{\mathrm{d}}}{r_c - 1}$.

To describe the pumping capabilities of the engine one tunable gain parameter $C_{\eta_{\mathrm{vol}}}$ is introduced and inserted into Eq. (C.1), and the final CAC model becomes:

$$\mathrm{CAC} = \frac{p_{\mathrm{im}} C_{\eta_{\mathrm{vol}}} \overbrace{\frac{1}{1 + \frac{1}{\lambda\left(\frac{A}{F}\right)_s}} \left(\frac{r_c - \left(\frac{p_{\mathrm{em}}}{p_{\mathrm{im}}}\right)^{\frac{1}{\gamma}}}{r_c - 1}\right) V_{\mathrm{d}}}^{V_{\mathrm{a}}}}{R_{\mathrm{im}} T_{\mathrm{im}}} \qquad (\mathrm{C.2})$$

ALTERNATIVE DERIVATION OF p_{EM_Δ}

D.1 p_{em_Δ} Derivation Based on a Simplified Thermodynamical Model

The calculated $\Delta\mathrm{CAC}$ will be used in the derivation of p_{em_Δ}, which starts by considering a simplified gas exchange process. In the simplified gas exchange process, it is assumed that there are no valve overlap and no heat transfer to/from the gas. The assumption of small overlap is motivated for turbocharged engines in Fox et al. (1993). Furthermore, it is assumed that the gases are ideal and that the thermodynamic properties c_{p}, c_{v}, and R are the same for unburned and burned gases. This is a standard assumption for simplified thermodynamic models (Heywood, 1988, p. 102). The mass of gas inside the cylinder at intake valve closing is denoted m and it consists of the mass of air m_a[1] and air-fuel m_{af} and residual gas mass m_r. Now, according to the first law of thermodynamics, the internal energy of the mixture is conserved:

$$m c_v T_{\mathrm{cyl}} \quad = \quad m_{\mathrm{af}} c_v T_{\mathrm{af}} + m_r c_v T_r \tag{D.1a}$$

$$m_{\mathrm{af}} \quad = \quad m_a + m_f = m_a \underbrace{\left(1 + \frac{1}{\lambda \left(\frac{A}{F}\right)_s}\right)}_{k} \tag{D.1b}$$

Here it will also be assumed that the fresh mixture of air and fuel T_{af} has

---

[1]Here m_a denotes the *measured* CAC. This is a deviation from the standard nomenclature to keep the notation in the energy balance consistent.

the temperature given by Eq. (4.8).

Now, the ideal gas law gives the total in-cylinder mass m which is required by Eq. (D.1a):

$$m = \frac{p_{\mathrm{cyl}}\,(V_c + V_d)}{RT_{\mathrm{cyl}}} \tag{D.2}$$

In Eq. (D.2) the in-cylinder pressure at intake valve closing is needed to determine m. As this is not measured it is instead approximated by the mean intake manifold pressure, that is $p_{\mathrm{cyl}} = p_{\mathrm{im}}$. Further, the ideal gas law also gives the mass of residual gases m_r:

$$m_r = \frac{p_{\mathrm{em}} V_r}{RT_r} \tag{D.3}$$

The mass of air inside the cylinder during stationary conditions is described by Eq. (5.3):

$$m_a = \eta_{\mathrm{vol}}\,(N, p_{\mathrm{im}})\,\frac{p_{\mathrm{im}} V_d}{RT_{\mathrm{af}}} + \Delta \mathrm{CAC} \tag{D.4}$$

Insert Equations (5.1, D.1b, D.2, D.3, D.4) into Eq. (D.1a) which cancels T_{cyl}, c_v, and T_r:

$$\frac{p_{\mathrm{im}}\,(V_c + V_d)}{R} = \eta_{\mathrm{vol}}\,(N, p_{\mathrm{im}})\,\frac{p_{\mathrm{im}} V_d}{R}k + \Delta \mathrm{CAC} \cdot T_{\mathrm{af}}k + \frac{(p_{\mathrm{em_{nom}}} + p_{\mathrm{em_\Delta}})\,V_r}{R} \tag{D.5}$$

The change in exhaust pressure $p_{\mathrm{em_\Delta}}$ that resulted in the air-mass-offset $\Delta \mathrm{CAC}$ can now be expressed as

$$\frac{p_{\mathrm{em_\Delta}} V_r}{R} = \frac{p_{\mathrm{im}}\,(V_c + V_d)}{R} - \eta_{\mathrm{vol}}\,(N, p_{\mathrm{im}})\,\frac{p_{\mathrm{im}} V_d}{R}k - \Delta \mathrm{CAC} \cdot T_{\mathrm{af}}k - \frac{p_{\mathrm{em_{nom}}} V_r}{R} \tag{D.6a}$$

$$p_{\mathrm{em_\Delta}} = \underbrace{p_{\mathrm{im}} \left(\frac{(V_c + V_d)}{V_r} - \eta_{\mathrm{vol}}\,(N, p_{\mathrm{im}})\,\frac{V_d}{V_r}k \right)}_{\text{When } \Delta \mathrm{CAC} = 0 \text{ then } p_{\mathrm{em_\Delta}} = 0 \text{ and this term must equal } p_{\mathrm{em_{nom}}}} -$$
$$p_{\mathrm{em_{nom}}} - \Delta \mathrm{CAC} \cdot T_{\mathrm{af}}k\frac{R}{V_r} \tag{D.6b}$$

given the volume of the residual gases is V_r. As the term to the left of $p_{\mathrm{em_{nom}}}$ in Eq. (D.6b) is linear in p_{im} and changes in p_{im} are small when the exhaust manifold pressure changes, these terms cancel each other which results in:

$$p_{\mathrm{em_\Delta}} = -\Delta \mathrm{CAC} \cdot T_{\mathrm{af}} \underbrace{\left(1 + \frac{1}{\lambda \left(\frac{A}{F} \right)_s} \right)}_{k} \underbrace{\frac{R}{V_r}}_{K_e} \tag{D.7}$$

For a motivation of the small change in p_{im} when the wastegate is opened see for example Figure 5.4. In the equations above V_r is constant as the engine

does not have variable valve timing. For an ideal otto cycle $V_r = V_c$ but a real engine has valve overlap and heat transfer, therefore V_r is not necessarily equal to V_c. In the final exhaust manifold pressure model, the parameters V_r and R are lumped together to K_e. K_e is determined from measured wastegate steps and in the studied region, from 1800 to 3100 RPM and brake mean effective pressures from 5 to 12 bar, a fixed $K_e \approx 2.4 \cdot 10^3 \ \frac{\text{Pa}}{\text{kg} \cdot \text{K}}$ was used.

Further support for the assumption of constant K_e is given when the CAC sensitivity to changes in exhaust manifold pressure, Eq. (4.12), is studied. In Figure D.1, the sensitivity is shown for operating points with nominal wastegate setting over the entire operating region. The result is plotted as a function of intake manifold pressure and it is clear that the sensitivity is small (-0.2 to -0.1) for intake manifold pressures above 50 kPa.
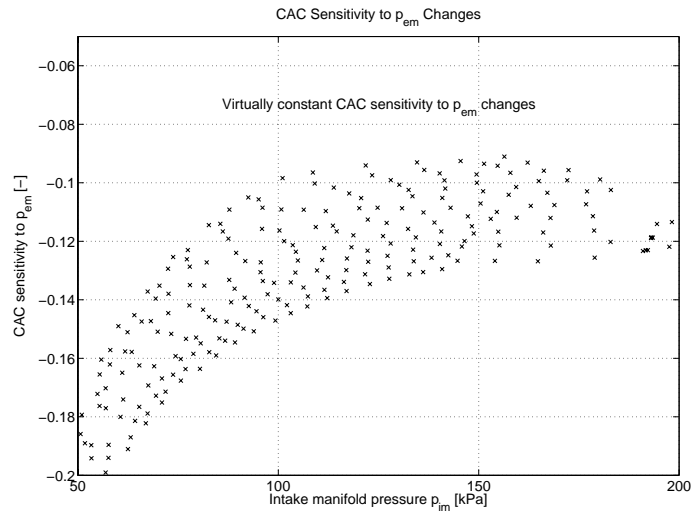
Figure D.1: Sensitivity to exhaust manifold pressure changes are small over the operating region of the engine. However for low intake manifold pressures the magnitude of the sensitivity increases which suggest that the exhaust pressure estimation can be improved by incorporating the intake manifold pressure.

D.2 Summary of Exhaust Pressure Calculation Process

First the temperature of the air-fuel mixture is calculated according to Eq. (4.8) and then the air-mass offset ΔCAC, Eq. (5.3), is calculated. The nominal exhaust pressure is determined by Eq. (5.2), the exhaust manifold pressure

offset by Eq. (D.7) and finally inserted into Eq. (5.1) which yields p_{em}.

$$
T_{\text{af}}(T_{\text{im}}, \lambda) \quad = \quad T_{\text{im}} - C_1 \left(\frac{1 - \lambda^2}{\lambda^2} \right)
$$

$$
\Delta \text{CAC}\left(W_{\text{a}}, N, p_{\text{im}}, T_{\text{im}}, \lambda\right) \quad = \quad W_{\text{at}} \frac{n_r}{N} - \frac{\overbrace{\left(a_1 p_{\text{im}} + a_0\right)}^{\eta_{\text{vol}} p_{\text{im}}} V_d}{R T_{\text{af}}(T_{\text{im}}, \lambda)}
$$

$$
p_{\text{em}_{\text{nom}}}(W_{\text{a}}) \quad = \quad p_{\text{a}} + k_1 W_{\text{a}} + k_2
$$

$$
k \quad = \quad 1 + \frac{1}{\lambda \left(\frac{A}{F} \right)_s}
$$

$$
p_{\text{em}}\left(W_{\text{a}}, \Delta \text{CAC}, k, T_{\text{im}}\right) \quad = \quad p_{\text{em}_{\text{nom}}}(W_{\text{a}}) - K_e k T_{\text{im}} \Delta \text{CAC}
$$

Important second order effects, such as heat transfer, and valve overlap etc. are taken into account by $p_{\text{em}_{\text{nom}}}$.

Experimental Setup

The research laboratory at Vehicular Systems consists of a control room and an engine test cell. A schematic of the experimental setup is shown in Figure E.1.

E.1 Engine Test Cell

During the project two different engines were used:

1. Initially a SAAB B235R was used for the wastegate experiments, to develop the mean value engine model, and the observer design methodology.

2. A modified SAAB B207R, was used for the real-time control experiments.

Next the engines, sensors, and dynamometers are described.

E.1.1 SAAB 235R Engine and Sensors

This is a 2.3 dm^3 turbocharged SAAB 9^5 engine with wastegate. Compared to a production engine, this engine has additional holes drilled in the intake and exhaust system to allow extra sensors. Further, the engine was equipped with a device (handle) to enable manual steps in wastegate and for safety reasons it was only possible to open the wastegate using this device. During the first part of the project this engine was neither equipped with a compressor by-pass valve nor a closed crank-case ventilation. The engine data is listed in Table E.1.
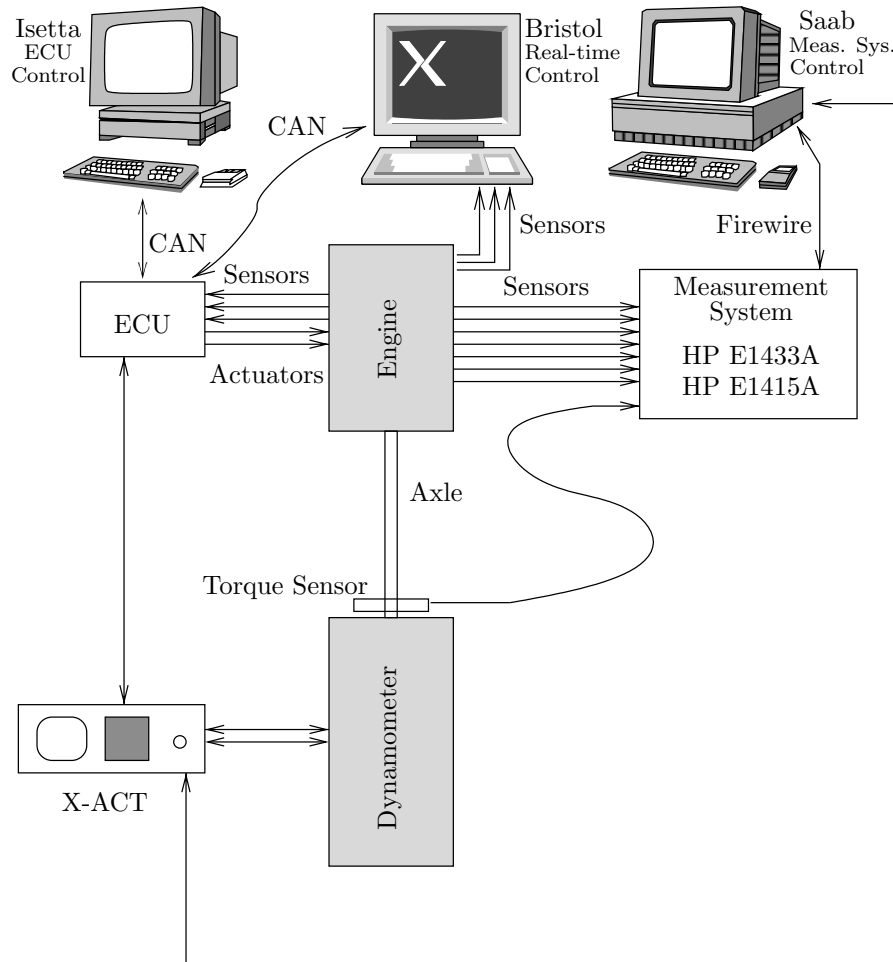
Figure E.1: Experimental setup. The two computers, measurement system and X-ACT are located in the control room. The engine, dynamometer and engine control system (ECU) are in the engine test cell.

Manufacturer	SAAB Automobile
Model	B235R
Displacement Volume	2.3 dm^3
Compression ratio	9.3
Maximum Power	170 kW @ 6200 RPM
Maximum torque	350 Nm @ 1900 RPM

Table E.1: B235 Engine data

Available Sensor Signals

The additional temperature sensors are listed in Table E.2 and the additional pressure sensors are listed in Table E.3. Further sensor signals are listed in Table E.4. Note that the laminar air-mass flow sensor is not always connected. The approximate location of the sensors are shown in Figure E.2.

Nr	Location	Designation	Type
1	Air-filter entry	T_a	Thermocouple
2	After compressor	T_comp	PT200
3	After intercooler	T_ic	PT200
4	In intake manifold	T_im	PT200
5	Exhaust manifold	T_em	Thermocouple
6	After turbine	T_t	Thermocouple

Table E.2: Available temperature sensors. The thermocouples are of type K.

Nr	Location	Designation
1	Ambient pressure	p_a
2	Before compressor	p_af
3	After compressor	p_comp
4	After intercooler	p_ic
5	Intake manifold	p_im
6	Exhaust manifold	p_em
7	After Turbine	p_t

Table E.3: Available pressure sensors. All sensors except for the ambient pressure are high performance Kistler Kristall sensors (Kri, 1997). The ambient pressure is measured through the laminar flow meter LFE3, which is equipped with an ambient pressure sensor.

Dynamometer

An asynchronous Schenck Dynas$_2$ 220 dynamometer is fitted to the engine. With this type of dynamometer it is possible to either brake or supply torque to the engine. The later is used to start the engine and gives the possibility to simulate downhill driving.

The dynamometer is controlled via a user interface called X-ACT. From X-ACT the engine speed and engine throttle position are controlled. It is also possible to control the engine speed and throttle position from a computer via a serial interface (RS-232). This is done during for example the engine mapping. Dynamometer data are listed in Table E.5.

Nr	Location	Designation	Type
1	Air-mass flow	W_{af}	
2	Air-mass flow	$W_{af_{LFE\ 3}}$	
3	Injection time	t_{inj}	Cylinder 1
4	Air-fuel ratio	λ	NTK UEGO TC-6000
5	Throttle angle	α	-
6	Engine speed	N	Leine&Linde 540
7	Turbine speed	N_t	Gready ES-DA 1
8	Torque	T_q	X-ACT

Table E.4: Miscellaneous sensors. The second air-mass flow sensor is a laminar air-mass flow sensor.
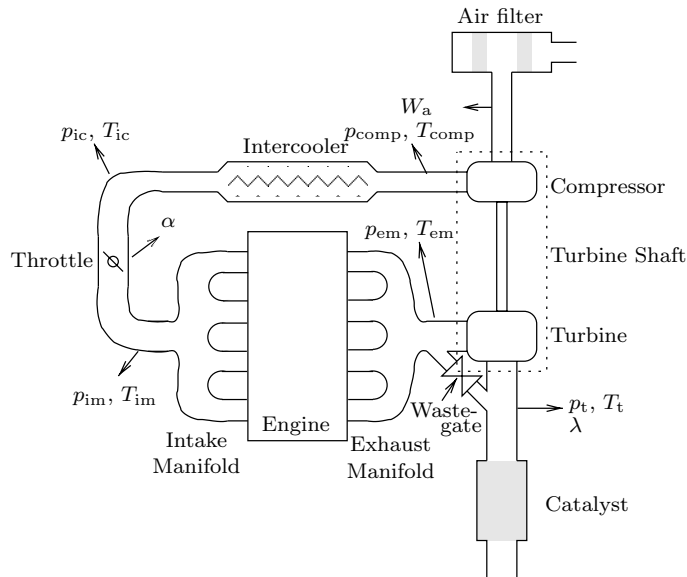
Figure E.2: Engine schematic with approximate sensor locations. Note that the wastegate position is not measurable.

Manufacturer	Schenck
Model	$Dynas_2$ 220
Maximum power	220 kW
Maximum torque	450 Nm
Max speed	9500 RPM

Table E.5: Dynamometer $Dynas_2$ data.

E.1.2 SAAB 207R Engine and Sensors

This is a 2.0 dm^3 turbocharged SAAB 9^3 Sport Sedan engine with wastegate. Compared to the original engine, it has several holes drilled for sensors, and it is equipped with a modified cylinder head. The ECU is a prototype engine control system where functionality has been added to allow external controllers to override the built-in controllers.

This engine was only mapped for between engine speeds 1000 and 3000 RPM and for intake manifold pressures below ambient.

Available Sensor Signals

The additional temperature sensors are listed in Table E.6 and the additional pressure sensors in Table E.7. Further sensor signals are listed in Table E.8. The approximate location of the sensors are shown in Figure E.2.

Nr	Location	Designation	Type
1	Air-filter entry	T_{af}	Thermocouple
2	After compressor	T_{comp}	Thermocouple
3	After intercooler	T_{ic}	Thermocouple
4	In intake manifold	T_{im}	Thermocouple
5	Exhaust manifold	T_{em}	Thermocouple
6	After turbine	T_{t}	Thermocouple
7	Ambient	T_{a}	Thermocouple

Table E.6: B207R: Available temperature sensors. The thermocouples are of type K and 3 mm in diameter.

Nr	Location	Designation
1	Ambient pressure	p_{a}
2	Before compressor	p_{af}
3	After compressor	p_{comp}
4	After intercooler	p_{ic}
5	Intake manifold	p_{im}
6	Exhaust manifold	p_{em}
7	After Turbine	p_{t}

Table E.7: B207R: Available pressure sensors. All sensors except for the ambient pressure are high performance Kistler Kristall sensors (Kri, 1997).

Dynamometer

An asynchronous Schenck Dynas$_3$ 250 dynamometer is fitted to the engine. With this type of dynamometer it is possible to either brake or supply torque

Nr	Location	Designation	Type
1	Air-mass flow	W_{af}	-
2	Injection time	t_{inj}	Cylinder 1
3	Air-fuel ratio	λ	ETAS LA3
4	Throttle angle	α	-
5	Engine speed	N	Leine&Linde 540
6	Turbine speed	N_t	Acam Picoturn
7	Torque	T_q	X-ACT

Table E.8: B207R: Miscellaneous sensors.

to the engine. The later is used to start the engine and gives the possibility to simulate downhill driving.

The dynamometer is controlled via a user interface called X-ACT. From X-ACT the engine speed and engine throttle position are controlled. It is also possible to control the engine speed and throttle position from a computer via a serial interface (RS-232). This is done during for example the engine mapping. Dynamometer data are listed in Table E.9.

Manufacturer	Schenck
Model	$Dynas_3$ 250
Maximum power	250 kW
Maximum torque	480 Nm
Max speed	10000 RPM

Table E.9: Dynamometer $Dynas_3$ data

E.2   Control Room

From the control room, the engine and dynamometer are controlled. In the control room there are three computers with specific tasks. As computers at Vehicular Systems are named after car brands they are listed by their "names":

Isetta Communicates with the ECU over a CAN-bus. From Isetta it is possible to set and read data in the ECU. Isetta is used mainly during the real-time experiments to enable/disable controllers within the ECU.

Saab Controls the measurement system and the dynamometer. See Section E.2.1.

Bristol Executes controllers in real-time with possibility to measure analog signals, and to interact with the ECU over a private CAN-bus. See Section E.2.2.

E.2.1 Measurment System

There are two high quality VXI-measurement instruments from Hewlett-Packard, E1415A and E1433A, which are controlled by the computer "Saab". Custom software have been developed in order to make all measurements from Matlab. LabWindows/CVI from NationalInstruments was used to development the measurement software.

HP E1415A

E1415A can measure up to 64 channels with a maximum sampling frequency of 2000 Hz and it features a built-in self calibration. The raw measurement signals are adapted to the instrument through signal conditioning hardware. This instrument can be equipped with up to eight different signal conditioning modules, where each covers a maximum of eight channels. The installed signal conditioning modules are listed in Table E.10.

Module	Description	Nr. of channels
HP E1503A	Number of voltage channels	3×8=24
HP E1505	Number of current source channels	8
HP E1538A	Number of frequency, PWM channels	8

Table E.10: Signal conditioning modules in HP E1415.

To measure the resistance over the PT200 elements the current source module is used and the voltage over the element is measured using the so called 4-wire principle. As the voltage and the current are known it is easy to calculate the resistance and hence the temperature.

HP E1433A

This instrument can measure eight channels simultaneously using *separate* A/D converters at a sampling frequency of up to 196 kHz. It can further perform measurements in the crank angle domain. Here E1433A is used to measure the noise levels which are used in the observer design in Section 8.2.

E.2.2 Real-Time Engine Control

It is possible to control the engine in hard real-time using models/controllers designed in Simulink's Real-time Workshop. The injection time is controlled in this way from the remote computer "Bristol", in Chapter 9. To enable hard real-time on a desktop computer, the operating system has to support this functionality. Here a hard real-time extension to the Linux kernel, called Real-Time Application Interface (RTAI), is used. This environment was carefully setup and tested in Rosenquist (2003). In RTAI a port to Matlab/Simulink is included through RTAI-Lab (Quaranta and Mantegazza, 2001) and an interface
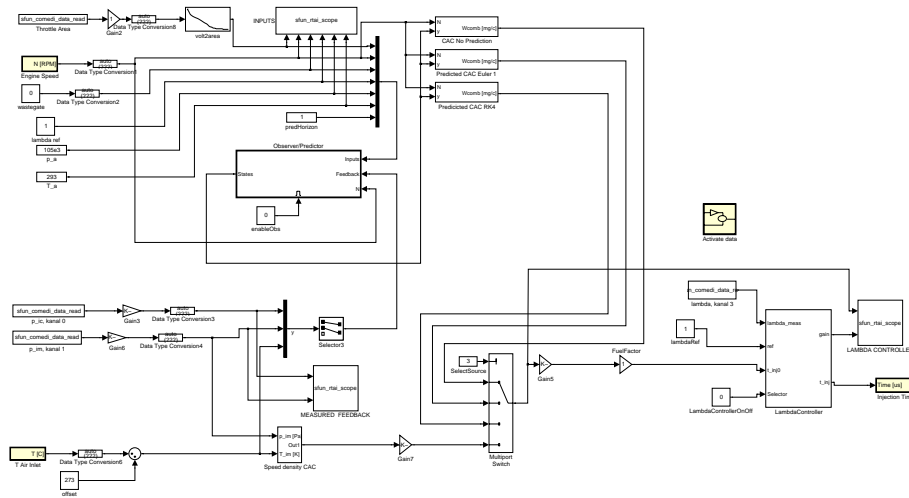
Figure E.3: The implemented Simulink schematic that was compiled and run in hard real-time on Bristol.

to a data acquisition card is also supported through the Comedi project. Compared to the initial implementation from Rosenquist (2003), the environment was updated to use RTAI 3.1 and also the ability to communicate with the ECU over a CAN-bus was added. To access the ECU additional Simulink-blocks were developed, and an example of a simulink schematic used for control is shown in Figure E.3. For details on the system, please see Table E.11.

CPU	AMD Athlon 1900+
Linux Distribution	Fedora Core 1 (`fedora.redhat.com`)
Kernel	2.4.27 (`www.kernel.org`)
Kernel patch	ADEOS (`www.adeos.org`)
RTAI version	3.2 (`www.rtai.org`)
DAQ-card	National Instruments PCI-6035E
Comedi driver version	0.7.69 (`www.comedi.org`)
CAN interface	PEAK-System Technik PCAN-PCI ISO
PCAN driver version	3.6 (`www.peak-system.com`)
Matlab/Simulink	7.1

Table E.11: Real-time computer "Bristol".

E.2.3   Measurements

In this thesis two kinds of measurements have been performed:

1. Stationary measurements (engine mapping)

2. Transient measurements (step response experiments)

Engine Mapping

The engine mapping is an automated process where the engine speed and throttle position are controlled by the computer "Saab". When the engine has run a pre-determined time in each point, the measurement is started and the signals are measured for 5 to 10 seconds and then the mean values are stored in a table. Three engine maps were measured:

1. An engine map of the B235R with 343 points is measured between 800 and 4300 RPM. These measurements are used for tuning of the mean-value models.

2. A small engine map of the B235R with different fix throttle areas. The pressure ratio over the throttle was varied by changing the engine speed. These measurements are used when the parameter(s) in the compressible flow model in Section 6.3.1 are determined.

3. An engine map of the B235R in 69 points for validation of the mean value model. This map is also used in the observer design in Chapter 8. In the observer design methodology it is also necessary to supply signal noise data. Therefore, an additional time-based measurement is performed immediately after the mean-value measurement. There the instrument is re-initiated to take a fast measurement at 1000 Hz on all channels. The duration of the noise measurement corresponds to 100 cycles. The map covers engine speeds from 1000 to 6000 RPM.

4. An engine map of the B207R in 45 points including noise measurements. These data are used to tune the engine model and in the observer design in Chapter 9.

Transient Experiments

In the transient experiments, signals are measured over time with a fix sampling frequency. The dynamic experiments are performed with four different objectives:

1. Measurements to study how the intake side is influenced by changes in exhaust manifold pressure caused by an opening of the wastegate. A sampling frequency of up to 1000 Hz is used and the alias filters were disabled to reduce the phase lag. This measured data is mainly used in Chapter 3.

2. Measurements using steps in wastegate are made to study how information on the intake side can be used to estimate the exhaust manifold pressure in Chapter 5. As the stationary behavior is most interesting here the data is sampled at 10 Hz.

3. Several steps in load (throttle) at constant speed are performed to model the inertia of the turbocharger and also to tune the turbine friction parameter. This data is also used to validate the designed model in Chapter 6 and the observer in Chapter 8. These data were measured at 1000 Hz and with the alias filters disabled.

4. Measurements of steps in engine speed to validate the engine model for dynamic conditions.

INDEX